Slamming of High-Speed Craft: A Machine Learning & Parametric Study of Slamming Events

Mark W. Shepheard

Thesis submitted to the Faculty of the

Virginia Polytechnic Institute and State University

in partial fulfillment of the requirements for the degree of

Master of Science

in

Ocean Engineering

Christine Gilbert, Chair

Stefano Brizzolara

Craig Woolsey

April 26, 2022

Blacksburg, Virginia

Keywords: High-Speed Craft, Slamming, Machine Learning

Slamming of High-Speed Craft: A Machine Learning & Parametric Study of Slamming Events

Mark W. Shepheard

ABSTRACT

Slamming loads are the critical structural design load for high-speed craft. In addition to damaging the hull structure, payload, and injuring personnel, slamming events can also significantly limit operating envelopes and decrease performance. To better characterize slamming events and the factors affecting their severity, a parametric study will be carried out in the Virginia Tech Hydroelasticity Lab. This thesis provides the groundwork for this longitudinal project through meticulous analysis of irregular wave tow tank experiments. Through the modification of machine learning techniques and taking inspiration from facial recognition algorithms, key parameters were identified to form an experimental matrix which captures intricacies of the complex interdependent relation of variables in the slamming problem. The independent effects of parameters to be evaluated include hull flexural rigidity, LCG location, heave and surge velocity, and impact trim, angular velocity and acceleration. In preparation for this parametric study, an innovative experimental setup was designed to simulate the impact of a deep-vee planing hull into waves, through a controlled motion slam into calm water. To provide a baseline to compare data from future controlled motion experiments to, a model drop experiment was completed to characterize the relationships of impact velocity and trim to slamming event severity. During this experiment, the position, acceleration, strain, and pressure were measured. These measurements illustrated a decrease in peak acceleration, pressure, and strain magnitude with an increase in impact trim. Additionally, as trim was increased a delay in the time of peak magnitude for all

measurements was observed. These results are attributed to the change in buoyancy with the change in impact angle. At non-zero angles of trim, a pitching moment was generated by the misalignment of the longitudinal center of buoyancy and center of gravity. This moment caused racking in the setup which was observed in the acceleration time histories immediately after impact. This finding furthers the need to investigate the angular velocity and acceleration of the model at impact, through the proposed series of experiments, as they are crucial naturally occurring motions inherent to slamming events.

Slamming of High-Speed Craft: A Machine Learning & Parametric Study of Slamming Events

Mark W. Shepheard

GENERAL AUDIENCE ABSTRACT

Slamming loads are the critical structural design load for high-speed craft. Slamming events occur when a boat or ship impacts the water. This impact causes high peak pressures and accelerations. In addition to damaging the hull structure, payload, and injuring personnel, slamming events can also significantly limit operating envelopes and decrease performance. To better characterize slamming events and the factors affecting their severity, a parametric study will be carried out in the Virginia Tech Hydroelasticity Lab. This thesis provides the groundwork for this longitudinal project through meticulous analysis of irregular wave tow tank experiments, which mimic actual conditions in a sea way. Through the modification of machine learning techniques and taking inspiration from facial recognition algorithms, key parameters were identified to form an experimental matrix which captures intricacies of the complex interdependent relation of variables in the slamming problem. The independent effects of parameters to be evaluated include hull structural stiffness, location of the longitudinal center of gravity, vertical and forward velocity at impact, and impact angle, angular velocity and angular acceleration. In preparation for this parametric study, an innovative experimental setup was designed to simulate the impact of a generic high-speed boat into waves, through prescribing a motion path to the boat as it slams into calm water. To provide a baseline to compare data from future controlled motion experiments to, a precursor experiment dropping a boat into calm water was completed to characterize the relationships

of impact velocity and trim to slamming event severity. During this experiment, the position, acceleration, strain, and pressure were measured. These measurements illustrated a decrease in peak acceleration, pressure, and strain magnitude with an increase in impact trim. Additionally, as trim was increased a delay in the time of peak magnitude for all measurements was observed. These results are attributed to the change in buoyancy with the change in impact angle. At non-zero angles of trim, a pitching moment was generated by the misalignment of the longitudinal center of buoyancy and center of gravity. This moment caused racking in the setup which was observed in the acceleration time histories immediately after impact. This finding furthers the need to investigate the angular velocity and acceleration of the model at impact, through the proposed series of experiments, as they are crucial naturally occurring motions inherent to slamming events.

Dedication

To my grandpa who always fostered my curiosity and made sure that I never forgot that you can learn something from everyone. Thank you.

Acknowledgments

A special thank you is given to Dr. Javad Javaherian, Nicholas Scianna, & James Duval for their physical and moral support during many late nights in the lab.

I would like to thank my family that has supported me in pursuit of all things

I would like to thank Dr. Christine Gilbert for being a great advisor and mentor who helped me navigate this project, and for always pushing me to do better.

Additional appreciation is extended towards our partners at DLBA and Ediburgh Designs. I would specifically like to thank Don Rickerson & Tyler Jenkins for their collaboration on the construction of the Vertical Planar Motion Mechanism (VPMM).

Finally I would like to acknowledge the support and funding from the Office of Naval Research Grant #s N00014-16-1-3188 & N00014-20-1-2254.

Contents

List of Figures

List of Tables

List of Abbreviations

α	Angular Acceleration
β	Deadrise Angle
Δ	Displacement
ν	Poisson's Ratio
ω	Angular Velocity
ρ	Water Density
τ	Trim Angle
e_0	Categorization Tolerance
Fn_B	Beam Froude Number
Fn_L	Length Froude Number
L_{OA}	Overall Length
V_0	Impact Velocity
X_{sp}	Spray root location
B	Beam
CFD	Computational Fluid Dynamics
D	Flexural Rigidity

DAQ	Data Acquisition System
E	Young's Modulus
g	Gravitational Acceleration
GPPH	Generic Prismatic Planing Hull
L	Length
LCG	Longitudinal Center of Gravity
p	Pressure
S-DIC	Stereoscopic Digital Image Correlation
SVD	Singular Value Decomposition
T	Draft
t	Thickness
t	Time
USNA	U.S. Naval Academy
V	Velocity
VCG	Vertical Center of Gravity
VPMM	Vertical Planar Motion Mechanism
X	Transverse location
z	Depth of submergence

Chapter 1

Introduction

Slamming loads are the critical structural design load for small high-speed craft. In addition to damaging the hull structure, payload, and cargo, slamming events can cause passenger discomfort and injury. Not only can slamming events damage the craft, but they can also significantly decrease performance and operating envelopes. The typical approach for analyzing slamming events involves analyzing the root mean square value of the acceleration peaks. The values for the average third, tenth, hundredth, etc… highest accelerations are then reported. These values are used by the designer for structural design in given sea states. Small high-speed craft frequently undergo slamming events when traveling at high speeds. The high frequency of slamming events means that high speed craft will often see the highest end of these statistical predictions. Further understanding of the physics of slamming events can be used to mitigate severe slamming events and reduce their impacts on performance and operating envelopes. To better characterize slamming events and the factors affecting their severity, a parametric study will be carried out in the Virginia Tech Hydroelasticity Lab. This thesis lays the foundation for this longitudinal project through meticulous analysis of irregular wave tow tank experiments. Through the modification of machine learning and facial recognition algorithms, key parameters were identified to form an experimental matrix which captures intricacies of the complex interdependent relation of variables in the slamming problem. In providing the ground work for the larger project, a innovative experimental setup was designed to simulate the impact of a deep-vee planing hull into waves, through a controlled motion slam into calm water. To provide a baseline to compare data from future controlled motion experiments to, a model drop experiment was completed to characterize the relationships of impact velocity and trim to slamming event severity.

The performance of hull forms is typically evaluated through the use of model tests. Ikeda & Judge (2014) performed free-to-heave-and-pitch tow tank experiments with a generic prismatic planing hull (GPPH) [6]. A deterministic approach was taken, where each slamming event was analyzed individually, rather than statistically. Through the duration of the analysis both point pressure sensors and pressure pads were used and their results were compared. In comparison of the point pressure sensors and pressure pads, it was noted that the point pressure sensors have a higher temporal resolution, whereas the pressure pads have a higher spatial resolution. Attention was further drawn to the ability of these sensors to accurately resolve the pressure on the hull during a slamming event. The pressure pad had a shift in both peak time and magnitude and showed different behavior than the point sensors. The data collected during this study is used to determine the key parameters and develop the experimental matrix for this study, which is discussed further in the following section.

Judge (2020 pt I and pt II) compared experiments and simulations in a computational fluid dynamics (CFD) verification and validation study for small high speed craft [1, 7]. Like Ikeda & Judge (2014) a wide array of data was collected at high accuracy and sampling frequency. Comparisons of experimental and simulation results were performed in calm water, regular waves, and irregular waves. Experiments were performed, using the GPPH, at both USNA and NSWC Carderock at different times of the year and the results showed good agreement. When comparing the results of the simulations to the results of the experiments, the calm water resistance and trim was not validated at all speeds, with the Fn average error being less than 4%. The sinkage was validated for high speeds, but not for low speeds, with the Fn average error being less than 3%. Part II of Judge (2020) details the regular and irregular wave comparisons of the CFD verification and validation study. Judge identified that the most severe slams corresponded with short steep waves. In addition, both simulations and experiments confirmed peak pressures on the hull when the hull is re-entering and emerging from the water. The pressure distributions can be seen in the CFD simulations shown in Fig. 1.1. The work presented in Judge part I and II expands upon the work presented in Ikeda & Judge (2014).The experimental results from Judge (2020 ptI) will be used for model verification of the new Virginia Tech GPPH model constructed for the purposes of this study. The results of Judge (2020 ptII) will be used to further verify the experimental results of the upcoming series of controlled motion slamming experiments in the Virginia Tech Advanced Towing Facility. [1, 6, 7]

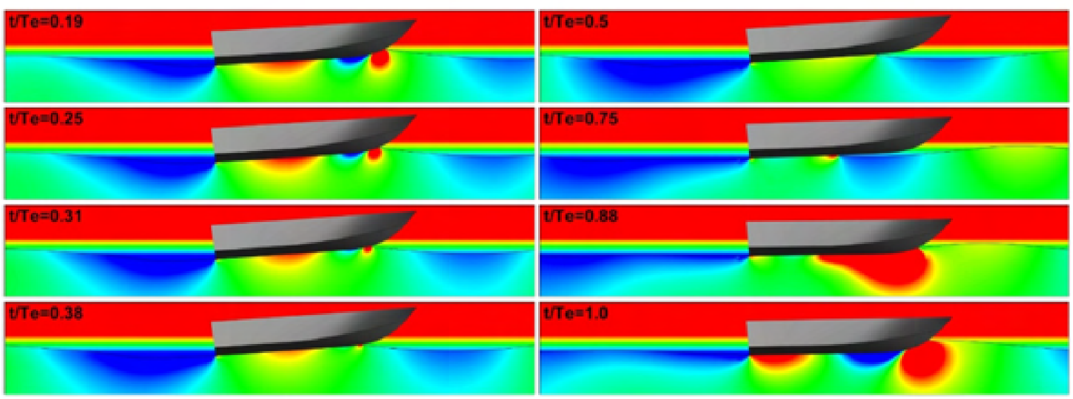

Figure 1.1: CFD results showing re-entering (left) and emerging slams (right) from [1] (used with permission).

A significant amount of effort has been placed on characterizing the response of planning craft in both regular and irregular waves. Fridsma (1969) determined the independent effects of speed, significant wave height, deadrise, trim, load and length-to-beam ratio, and bow shape on craft motions in irregular waves [8]. Fridsma (1969) concluded that as the boat progresses from displacement speeds to planing speeds, the boat movement transitions from following the waveforms to skimming across the crests of the waves. Although the overall vessel motions are reduced at high speeds, slamming accelerations are increased, the motions becoming more rapid and violent. It was found that higher significant wave heights correspond to a decrease in performance measured through added resistance, peak accelerations, and vessel motion magnitudes. The parametric study performed by Fridsma characterizes the general effects of many of the parameters to be studied in this investigation. Fridsma took a statistical approach, analyzing the peak accelerations and motions. The work in this thesis will investigate similar parameters, but take a more controlled and deterministic approach analyzing each slamming event individually.

Husser, Judge, Brizzolara (2021) determined the capability of RANSE CFD to predict the forces on a planing hull undergoing a forced heaving motion. This series of simulations and comparison to experiments showed the RANSE CFD, although having some discrepancy to experimental values, had very good general agreement.[9]

In analyzing acceleration time history of full scale high-speed craft, Riley et al. (2010, 2012, 2017) noted that the response of the craft stabilizes between distinct slamming events [2, 10, 11]. Since the vessel response stabilizes between the slamming events, each slamming event can be analyzed individually. Through the analysis of acceleration time histories of full scale craft in seaways, Riley et al. proposed three categories of slamming events: alpha, bravo, and charlie. The type alpha event is characterized by a freefall with a stern first landing, which causes a bow down pitching motion, resulting in the highest peak accelerations of all of the categories. Type bravo is similar to type alpha, however, the stern can stay in the water and the vessel has no bow down pitching motion. For both types alpha and bravo, a loss of thrust is possible due to propeller emergence. Type charlie, on the other hand, differs from the other two types, where rather than landing on the wave, the vessel runs into the wave. As a result, the vessel experiences a rapid bow up pitching motion. The first section of the slamming event is primarily governed by the initial conditions of the vessel, often determined by the previous slamming event. The second phase of the event includes

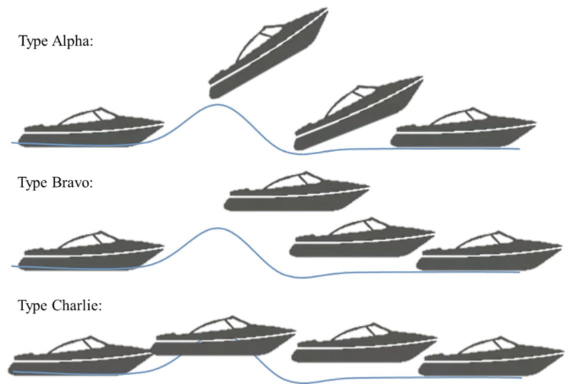

Figure 1.2: Cartoons of slamming rigid body motions (based on [2])

.

the rapid spike in vertical acceleration governed by the wave impact. After the vessel impacts the wave, buoyancy plays a key role in determining the vessel motion. Riley proposes that although peak acceleration provides a good first order evaluation of slamming events, it does not provide a complete picture of the severity of the impulse caused by the slamming event. Riley et al's analysis determined that the impulse durations for slamming loads typically last 100 - 400 milliseconds. As the peak acceleration increases, the duration of the impulse decreases asymptotically to 100 milliseconds. The duration of the impulse in combination with the magnitude of the peak acceleration both play key roles in structural loads, vessel performance, and human factors. Riley concluded with remarks on the limitations of full scale trials to measure the cause effect relationship in slamming events. In addition, the availability of weather conditions and other factors which cannot be controlled at full scale, provide additional complexities to using full scale trials to study the details of slamming. This gives further reason for the use of model tests and the continued development of CFD speed and accuracy for further investigations into the cause-effect relationship of slamming. Riley et al. also cautions that the ability to deterministically analyze slamming events should not be at the expense of statistical knowledge.

The slamming fluid-structure interaction problem is very complex. To simplify this problem the complexities of hull geometry are often removed from the equation. Prismatic wedges, which represent a cross section of the hull, are frequently used to study slamming. Javaherian et al (2020) analyzes slamming events through both the lenses of wedge drop and tow tank experiments. The wedge drop experiments, reported in Javaherian et al (2020, 2019) and Ren et al (2019a, 2019b), found that with increasing hull bottom flexibility, there was a significant reduction in peak pressure [12, 13, 14, 15]. In addition, a delay in the time of peak pressure was also observed. Through spray root visualization on the bottom of the wedge, it was found that the peak pressure lags slightly behind the spray root. Moreover, as the flexural rigidity of the panel decreases, the spray root velocity is decreased at ebay stages of penetration. This reduction is attributed to the deflection of the panel and corresponding additional distance that the spray root must travel. Through the analysis of tow tank experiments in regular waves performed at USNA, it was shown that the vertical heave velocity is not a function of the towing speed, and merely a function of the incoming wave characteristics. The kinematics of individual slamming events were shown to be repeatable through the comparison on multiple runs in regular waves. The combination of these two conclusions provides validity to the use of wege drop experiments as a tool to more closely study the fluid-structure interaction, which occurs during slamming events. Similar experimental and data analysis techniques to those in Javaherian et al(2020) and Javaherian et al (2019) will be used in this experimental study. As the series of controlled motion slamming experiments are continued in the Virginia Tech Advanced Towing Facility, the effects of hull flexibility on model scale planing craft will be evaluated and eventually extrapolated to full scale.

Bhardwaj, Javaherian, Husser, Brizzolara (2021) employed simulations of wedge water entry experiments to characterize 3D effects as a function of aspect ratio. The results of this study both demonstrate current simulation capabilities and can be used for experimental design to ensure pressure at the center of the model is accurately captured.[16]

Honey et al. (2021) compared tow tank and wedge drop experiments to quantify how well the wedge drop experiments act as simplification of the slamming problem [17]. Honey found that the use of a beam Froude number for similarity between tow tank and wedge drop experiments allowed for good agreement of impact velocity and peak acceleration. However, Honey highlighted multiple discrepancies between the tow tank and wedge drop experiments. These discrepancies occur in the velocity and position time histories. The tow tank experiments had shorter freefall durations and longer pulse widths in comparison to the wedge drop experiments. Honey attributed this disagreement to the waves in the tow tank experiments. Honey's experiments point out key findings, which will be used in the development of the model drop experiments presented in this thesis and upcoming controlled motion experiments. This series of experiments combines aspects of both tow tank and wedge drop experiments.

Multiple methods have been developed to predict the hull pressure and vessel kinematics for prismatic sections of deep-vee hulls. Initial theoretical models were developed by Wagner (1931) for the landing of seaplanes [18]. The location of the spray root:

$$X_{sp} = \frac{\pi}{2} \frac{z}{\tan\beta} \tag{1.1}$$

is a key piece of information in all of the pressure prediction models. Knowing the instantaneous velocity of the section and the spray root location the Wagner defined the pressure distribution along the bottom of the hull as:

$$p(X) = \frac{1}{2}\rho V^2 [\frac{\pi}{\tan\beta} \frac{X_{sp}}{\sqrt{X_{sp}^2 - X^2}} - \cos^2\beta \frac{X_{sp}^2}{X_{sp}^2 - X^2} - \sin^2\beta + 2 - \pi] \tag{1.2}$$

Wagner's formulation has been further expanded upon and improved by multiple researchers, including Vorus (1996), and Armand & Cointe (1986) [19, 20]. These theories can be expanded from nominal vee-shaped wedges and be applied to planing hulls using methods such as 2D+t, described in Zarnik (1978) [21]. The 2D+t approach models a vessel in a seaway as a series of discrete wedges at different stages of impact. Solving for the hydrodynamic loading of each 2D wedge section and integrating across the length provides a prediction for the overall load on the vessel. With the hydrodynamic force, the equations of motion can be solved and the corresponding vessel motions estimated. The capabilities of empirical prediction methods allows for fast first order approximations and evaluations of hull shapes and loading conditions. These theoretical prediction methods will be used as comparisons for the experimentally resolved hull bottom pressures during both controlled motion and model drop experiments.

This thesis develops the blueprint for a longitudinal parametric study of slamming events. The objective of the overarching project is to evaluate the differences in kinematics, pressure, and structural loading between traditional wedge drop experiments and full model slamming experiments. Through the analysis of pre-existing tow tank experiments from the US Naval Academy (USNA), key parameters affecting the severity of slamming events are identified. The ranges of these parameters were sampled to develop an experimental matrix. The first stages of these experiments will be performed in calm water. In order to account for impacting waves, the parameters are transformed based on wave characteristics to propose an experimental matrix for calm water slamming events. In the near future, the Hydroelasticity Lab will be conducting controlled motion slamming experiments based on the proposed experimental matrix using a vertical planar motion mechanism (VPMM) in the recently renovated Virginia Tech Advanced Towing Facility. In the meantime, to gain insight into the expected experimental results and assist in finalizing the instrumentation suite and experimental matrix for the upcoming experiments, a series of drop tests were performed.

The drop tests were performed using the generic prismatic planing hull (GPPH). The drop experiments cover a small portion of the experimental matrix and are free to heave and fixed in all other degrees of freedom. After presenting the results of the model drop experiments, conclusions will be made with modifications and comments regarding the proposed experimental matrix. The conclusions will be followed by a future work section which outlines future experiments and their strengths and weaknesses at modeling the performance and loading of planing hulls in a seaway.

Chapter 2

Irregular Wave Tow Tank Slamming Analysis [1]

Before developing the experimental matrix for the controlled motion slamming tests, the key parameters that play a role in the kinematics and severity of the slamming events had to be determined. To accomplish this goal, data from tow tank tests performed on a generic prismatic planing hull (GPPH) in waves by Ikeda & Judge (2014), Judge and Ikeda (2014), and Judge (2020 ptII) is presented and analyzed [1, 3, 23]. In this thesis, rather than using the typical approach of manually comparing the acceleration time histories or producing the statistics of the highest peak accelerations, a novel approach is taken and slamming events are categorized using a nearest neighbor machine learning method. Should this novel approach be employed in the future it will save researchers a significant amount of time with respect to manually comparing the acceleration time histories. Principal dimensions for the GPPH model used in these experiments can be found in Table 1, with a lines drawing in Fig. 3.4, in which pressure and acceleration data were recorded at the bow, the longitudinal center of gravity, and a midpoint between the two, in addition to the pitch and heave motions. The locations of these sensors are shown in Fig. 2.1. During each run, the general prismatic planing hull underwent multiple slamming events. Model tests were conducted in both regular and irregular waves. For further details regarding the experimental set up

[1] This Chapter contains previously published work used with permission with minor modifications and additions from Shepheard (2021) [22]

and instrumentation, please see Ikeda & Judge (2014), Judge and Ikeda (2014), or Judge (2020 ptII) [1, 3, 23]. This data set was chosen because of the large amount of data collected during the experiments, including wave height, vertical acceleration and pressure at several point, and high-speed footage of the entire run. The plethora of available data allowed for analysis of any features of interest throughout the investigation.

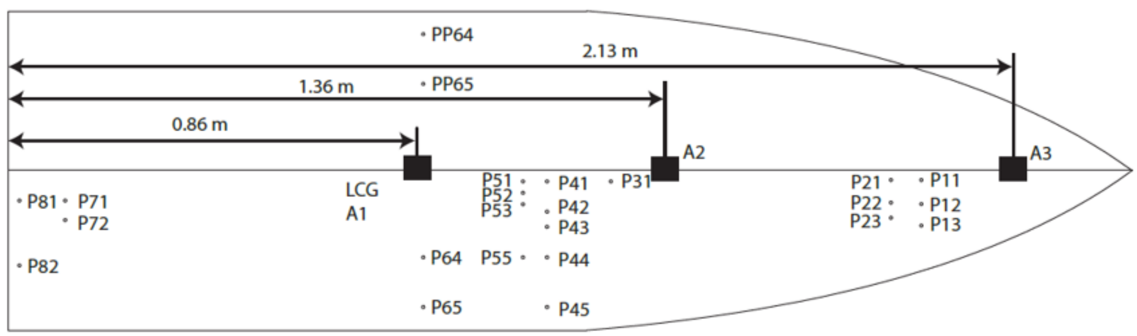

Figure 2.1: The above figure shows the body plan and sensor locations for the generic prismatic planning hull (GPPH) (Ikeda & Judge (2014), used with permission [3]).

The method used will be laid out in greater detail in the following section, followed by an analysis of the categories resulting from the method applied to sensor data, with a focus on how change in categorization tolerance alters the "narrowness" of the categories. Through this investigation the usefulness of the proposed categorization method will be evaluated and alterations to the method will be proposed to increase confidence in the results. After discussing the results, some conclusions will be made followed by the development of the experimental matrix for the controlled motion slamming experiments.

2.1 Methodology

Widespread classification of slamming events enables the use of deterministic and statistical approaches. To enable more refined classification of slamming events, inspiration was taken from image/data processing methods such as facial recognition. The goal of the facial recognition problem is to determine if an image of a face is included within a set of recognized faces or if the face is unrecognized. The three basic steps of the facial recognition problem are to normalize the image to a given size and contrast range. The method will then determine the similarity of an image to a set of known images. The final step is to classify the face as either one of the known images or as an unknown image.

Zeng (2006) proposed a method for fast and robust facial recognition using the singular value decomposition, which functions like a nearest neighbor machine learning method [24]. In this study, sensor data from a towing tank experiment is used to generate a matrix of values to perform the categorization. The method, shown in a flow chart in Fig. 2.2, works by creating a "face space" which is a subspace spanned by a set of known "base faces." An unknown face is then classified as a known face, an unknown face, or not a face at all. A face is considered a known face if it falls on the face space and the distance between the projection of the face onto the face space is less than a specified error, e_0, from a known face. A face is classified as an unknown face if it falls on the face space and the distance of the projection is greater than the specified error. The advantage of this methodology is that it enables the simultaneous classification of faces and the addition of faces to the base set. This method allows for a relatively small base set of slamming events to begin the classification, which can be further developed into a large set of base slamming events. Once all events are classified, the method is repeated until the average event for each category converges. This is done because as events are added to each category, the average event for that category moves. By adding a convergence step this ensures that the averages for each category have settled and all events that have been grouped together still belong together.

In order to validate the categories produced by the algorithm, multiple features were extracted from each slamming event. These features include the magnitude of the peak vertical

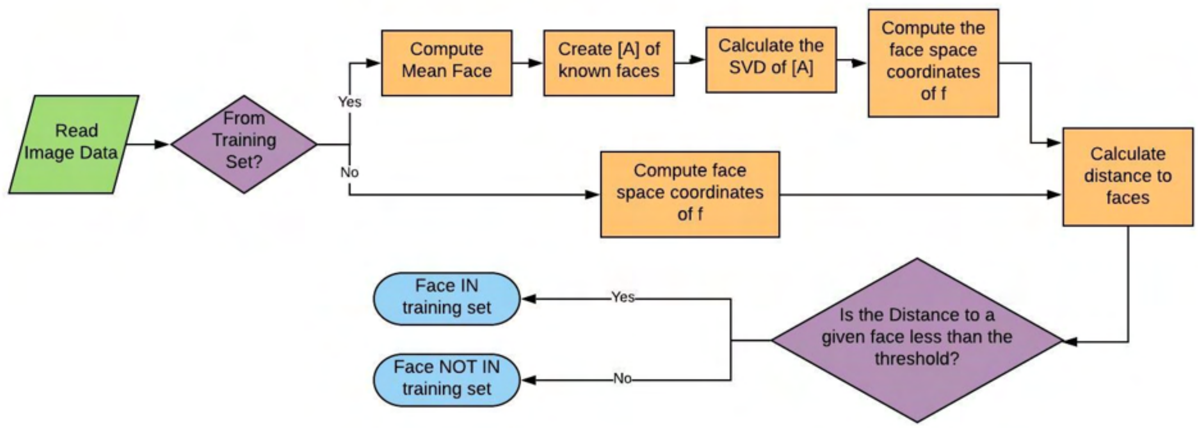

Figure 2.2: Flow chart of Zeng's method for facial recognition using the singular value decomposition. (Adapted from Cao (2006) [4]).

bow acceleration, the magnitude of the peak vertical LCG acceleration, the delay between the peak bow acceleration and peak LCG acceleration, the pitch at the peak bow acceleration, and the vertical bow acceleration 0.05 s before the peak bow acceleration. The vertical bow acceleration just before the peak bow acceleration gives insight as to whether or not the vessel was in free-fall prior to the slamming event. These features were plotted against each other in order to judge the quality of the nearest neighbor machine learning model, which can be used to solve both classification and regression problems. Classic nearest neighbor machine learning models use a series of known features to categorize events. For this study, the features are extracted from the measured signals for each slamming event. Scatter plots are used to determine the effectiveness of the categories identified using Zeng's Method. Fig. 2.3, from Harrison (2021), illustrates how points which can be categorized together typically lie close together when key features are plotted against one another [5]. A good nearest neighbor model shows close clustering activity with minimal outliers from the clustered boundaries. The shaded regions in Fig. 2.3 show the areas where a point in question would be classified with a given category; red, blue, green. The colored points correspond to the original data points and their given categories. This means that the model fits the

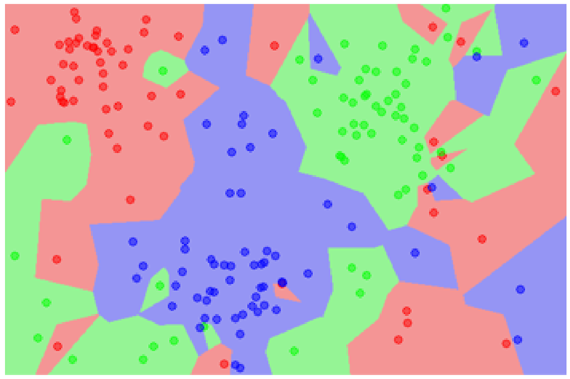

Figure 2.3: Example of a nearest neighbor machine learning model [5].

data set relatively well.

Prior to implementing Zeng's method, there must be a fundamental understanding of the singular value decomposition. Since an image is, in essence, a large matrix composed of values relating to the color of each pixel, it can be decomposed into their four fundamental subspaces: the column space, the row space, the null space, and the left null space. The following, Eq. (1) to Eq. (8) detail the singular value decomposition and the "image" matrix used to categorize the slamming events [4, 24, 25].

Suppose $\mathbf{A} \in \mathbb{R}^{m \times n}$ and has rank$(\mathbf{A}) = r$. Then, matrix $\mathbf{A}$ can be written as:

$$\mathbf{A} = \mathbf{U}\ \mathbf{V}^{\mathbf{T}}, \tag{2.1}$$

where the columns $\mathbf{U} \in \mathbb{R}^{m \times m}$ and $\mathbf{V} \in \mathbb{R}^{n \times n}$ are orthonormal, such that

$$\mathbf{U}^{\mathbf{T}}\mathbf{U} = \mathbf{I} \in \mathbb{R}^{\mathbf{m \times m}}, \text{ and } \mathbf{V}^{\mathbf{T}}\mathbf{V} = \mathbf{I} \in \mathbb{R}^{\mathbf{n \times n}}, \tag{2.2}$$

and the first r columns of $\mathbf{U}$ and $\mathbf{V}$ form orthonormal basis for the column and row space

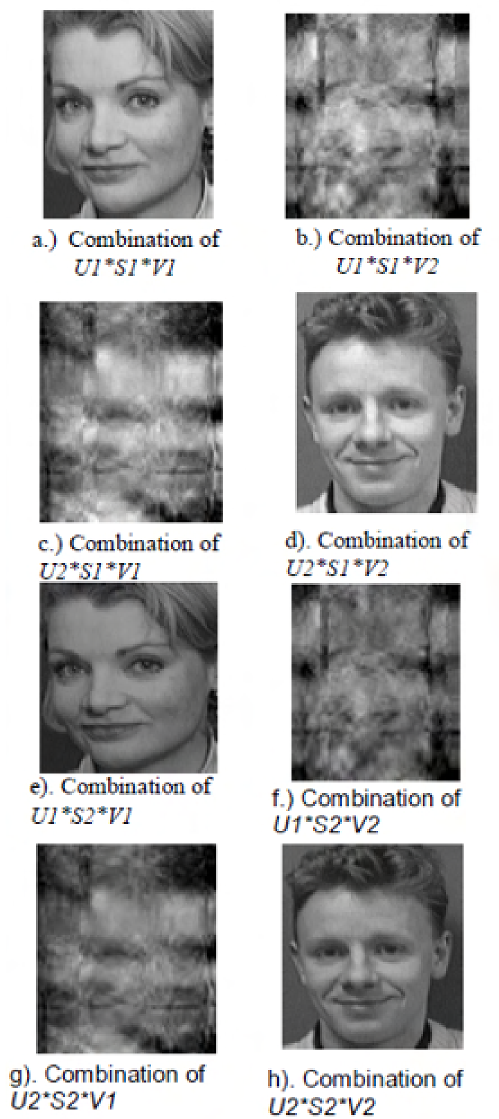

Figure 2.4: Example of image reconstruction with singular value decomposition from Cao (2006) [4]

and the remaining columns form a basis for the left null space and the null space respectively.

$$\mathcal{R}(\mathbf{A}) = span\{\mathbf{u_1}, ..., \mathbf{u_r}\} \tag{2.3}$$

$$\mathcal{N}(\mathbf{A}^T) = span\{\mathbf{u_{r+1}}, ..., \mathbf{u_m}\} \tag{2.4}$$

$$\mathcal{R}(\mathbf{A}^T) = span\{\mathbf{v_1}, ..., \mathbf{v_r}\} \tag{2.5}$$

$$\mathcal{N}(\mathbf{A}) = span\{\mathbf{v_{r+1}}, ..., \mathbf{v_n}\} \tag{2.6}$$

and $\in \mathbb{R}^{m \times n}$ is zero everywhere but the main diagonal for entry (j, j) are the singular values and

$$\sigma_1 \geq \sigma_2 \geq ... \geq \sigma_r > \sigma_{r+1} = ... = \sigma_{min\{m,n\}} = 0 \tag{2.7}$$

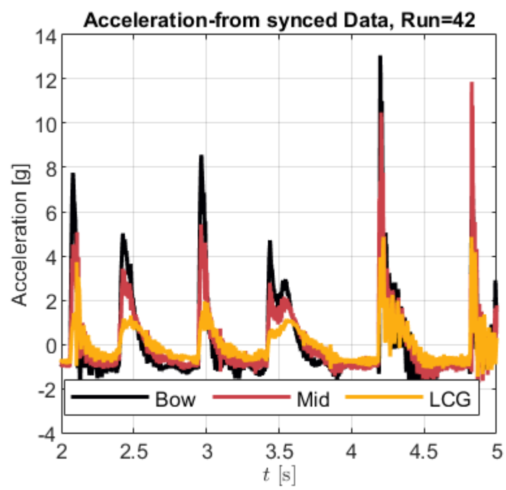

(a)

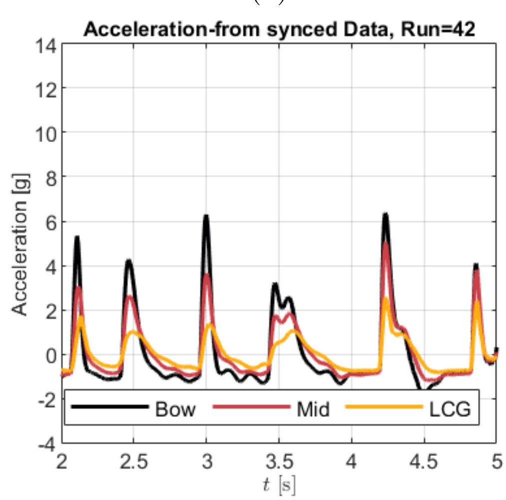

(b)

Figure 2.5: (a) Raw vertical acceleration time-histories and (b) filtered vertical acceleration data with a low pass filter with a cutoff frequency of 20 Hz.

Singular Value Decomposition can be thought of as a prescribed set of linear transformations [5]. The **V** matrix holds the direction of the transformations, while the **U** matrix holds lengths of the projections onto **V**, normalized by the singular values. The large singular

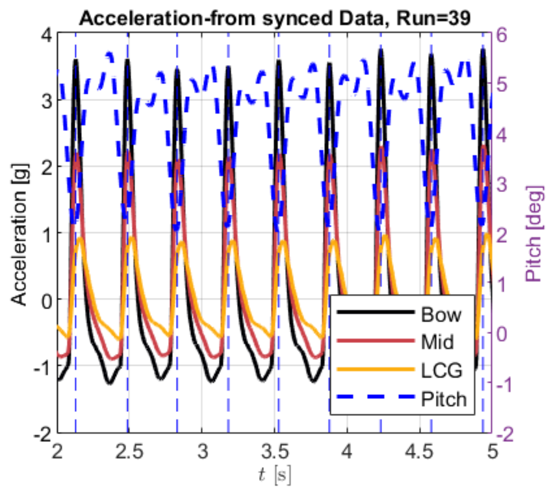

Figure 2.6: Individual events identified, with dashed light blue line, based on peak bow acceleration

values give insight to the main features of a matrix. The details of a matrix are held within the left and right singular vectors contained in the **U** and **V** matrices [24]. This can be shown through the example in Fig. 2.4 from Cao (2006) [4]. Using the original picture displayed in image a and image h, the image is completely changed by manipulating only one set of singular vectors. However, if both sets of singular vectors are swapped, the image also changes, as seen in images d and e.

For the analysis of the slamming event, the individual event matrix, E, is composed of columns of data acquired during the individual slamming event,

$$E = [a_{bow}, a_{mid}, a_{LCG}, a_{surge}, \theta_{pitch}], \tag{2.8}$$

which will be considered our image that will enter into the facial recognition algorithm.

First, the data was filtered to remove any high-frequency noise, which could possibly affect the singular value decomposition, and interrogation windows for individual slamming events were established. High-frequency noise, from structural vibration and the electrical power source, was eliminated using a low-pass Butterworth filter with two poles. The cutoff frequency for the filter was determined through spectral analysis, of all signals, as 20 Hz. The high-amplitude content of the signals had diminished at frequencies greater than 20 Hz. The data before and after filtering has been plotted in Fig. 2.5 for three acceleration signals as an example. As expected, the peak heights have been reduced along with the random noise after filtering.

In order to analyze individual slamming events, an interrogation window needed to be defined to identify the relevant time history prior to, during, and after the slamming event. The interrogation window for individual slamming events was identified based on the peaks in the vertical bow acceleration, which are most prominent due to its distance from the longitudinal center of gravity (LCG). Once a peak in the bow acceleration was identified, the interrogation window was centered with the vertical bow acceleration peak at zero with 0.125 seconds of data on either side of the peak. An example of these peaks identified can be seen in Fig. 2.6. Once these interrogation windows are collected, data for individual slamming events are formed into the event matrix defined in Eq. (8).

Fig. 2.7 shows the orientation of the vessel at three instants of time during the slamming event. For this slamming event, there is a significant bow down motion, that can be seen in both the plot and in the frames of the high speed footage, as the bow of the boat slams down onto an incoming wave.

2.2 Results & Discussion

The results for an initial categorization of sensor data will be discussed for two different cases. The difference between the two cases corresponds to a different categorization tolerance. The categorization tolerance is a key factor in determining the size and refinement of the

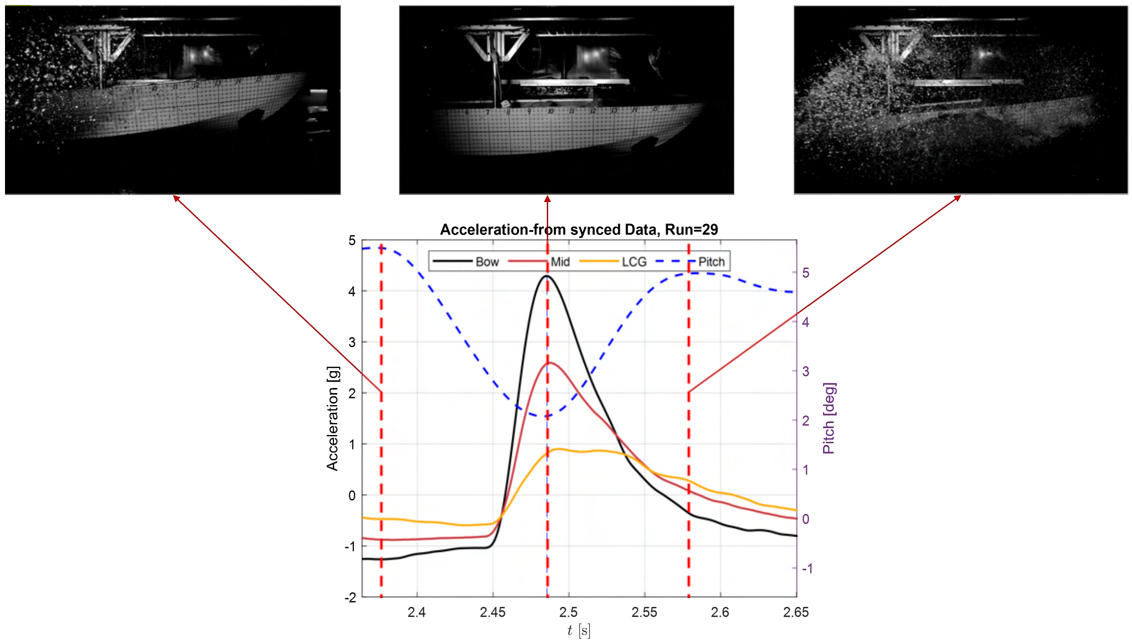

Figure 2.7: Frames selected from the high-speed video are marked by red dashed lines.

generated categories. The categorization tolerance, e_0, is a unitless parameter. It is defined as the maximum distance from the average event of a given category to which an uncategorized event must lie within in order to be considered part of that category. The following discussion investigates the resulting trends and categories produced by using two different categorization tolerances, $e_0 = 100$ and $e_0 = 75$. It is important to note that this method of categorization is done purely mathematically without taking into account the physical aspects of different slamming events directly.

The results of the Zeng's method for each categorization tolerance will be evaluated using scatter plots of features extracted from the slamming event time history, including the magnitude of the peak vertical bow acceleration, the magnitude of the peak vertical LCG acceleration, the delay between the peak bow acceleration and peak LCG acceleration, the pitch at the peak bow acceleration, and the vertical bow acceleration 0.05 s before the peak bow acceleration. The scatter plots provide a mapping of the categories within the slam-

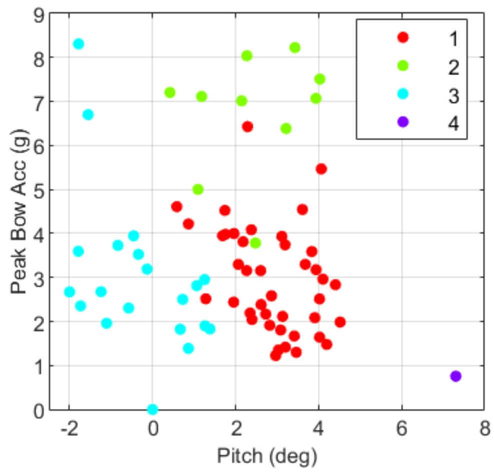

Figure 2.8: A scatter plot of the identified slamming categories, for a categorization tolerance of 100, and what ranges of pitch and peak bow acceleration they span.

ming space to uncover trends. If the events for the resulting categories are clustered closely together, the method worked effectively based on the feature which are believed to be important in the categorization. In the following scatter plots, events in each category are shown as colored dots. The legend corresponds the dot color to the category number.

Fig. 2.30h shows the results of the $e_0 = 100$ categories and the corresponding ranges of peak-bow-acceleration and pitch. Using this categorization tolerance, four categories are found. The first category, shown in red, roughly spans pitch angles greater than two degrees with peak bow accelerations for the most part less than $5g$. The following Fig. 2.9 depicts the magnitudes of the peak bow acceleration and the peak LCG acceleration. There is an apparent linear correlation between the peak bow and LCG accelerations, with the peak bow acceleration having a magnitude approximately four times larger than the peak LCG acceleration. However, there are a significant number of events in category two, which do not comply with this trend. A reason for this discrepancy could lie in the rigid body motion of category two. Although showing many trends, this plot gives little indication of the clustering of the categories and how they span the space.

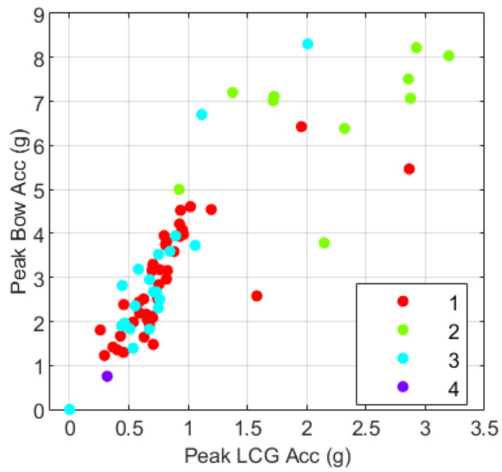

Figure 2.9: A scatter plot of the identified slamming categories, for a categorization tolerance of 100, and how their peak bow accelerations and LCG accelerations are correlated.

Fig. 2.10 displays the average acceleration of each slamming event identified in category one. The average event is used to gain an overall perspective of the acceleration time history of the events in the category since this data is not viewed directly in processing. These events are characterized by a negative $1g$ freefall event prior to the slamming event. Within the events identified in this category, the model lands with no downwards pitching motion. This is why events in category one have relatively low peak bow accelerations compared to those in category two. Overall this prominent category corresponds with the category Bravo event identified in Riley et al. (2010) [2].

The vertical acceleration time history for the second category is displayed in Fig. 2.11. Like the first category, the second category is defined by a $1g$ freefall event. However, category two also has a bow down moment, which causes higher peak bow accelerations. This motion could also cause the variation in the ratio of peak bow to peak LCG accelerations seen in category two in Fig. 2.9. This second category corresponds well with the category Alpha slams identified in Riley et al. (2010) [2].

The third category average acceleration time-history is shown in Fig. 2.12. Although the

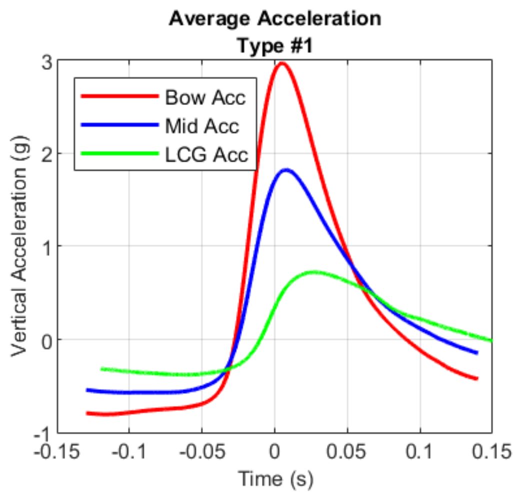

Figure 2.10: Average bow, mid, and LCG accelerations in category 1 for a tolerance of 100.

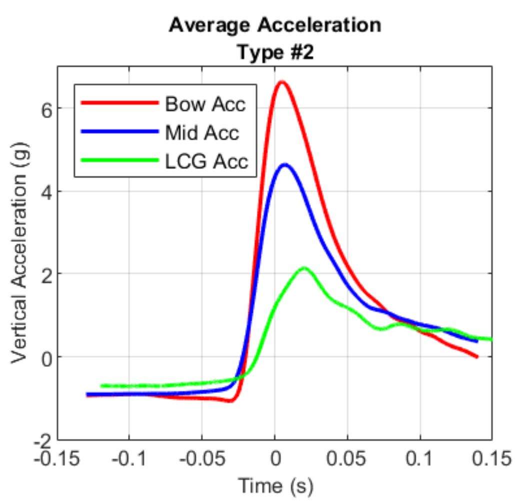

Figure 2.11: Average bow, mid, and LCG accelerations in category 2 for a tolerance of 100.

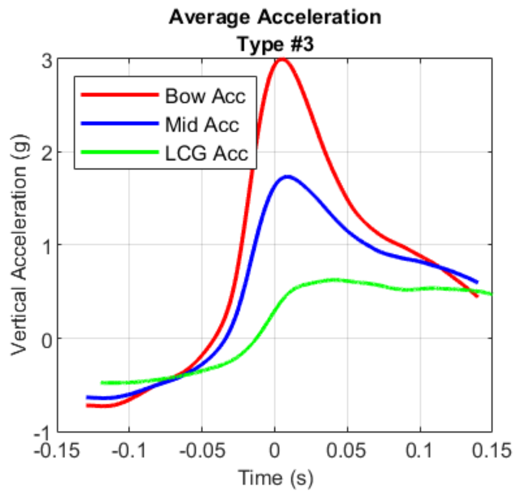

Figure 2.12: Average bow, mid, and LCG accelerations for category 3, for tolerance of 100.

acceleration signal appears to have the same shape and trend as other categories average events, the composite plot, Fig. 2.13 showing the acceleration time-history of all of the events in the category have a significant spread in amplitude and peak time duration. However, all the events within category three do not drop back to zero as rapidly as the acceleration signals in categories one and two. For comparison, Fig. 2.14 is shown for category two, which shows slamming events with less spread in the acceleration signals.

Similar analysis was carried out for a categorization tolerance of $e_0 = 75$. The main distinction for this smaller value of e_0 is that a greater number of categories has been identified. There is less clustering of the categories and more overlap in their respective ranges of peak-bow-acceleration and pitch. This overlap in categories when inspecting their key features means that the categories are less linearly independent and do not span the slamming space as well as the categories generated with $e_0 = 100$. Fig. 2.15, like Fig. 2.30h, best illustrates how the slamming categories are defined by peak-bow-acceleration and pitch. It appears as though each of the larger categories identified in the $e_0 = 100$ case have been further divided and categorized by more subtle differences.

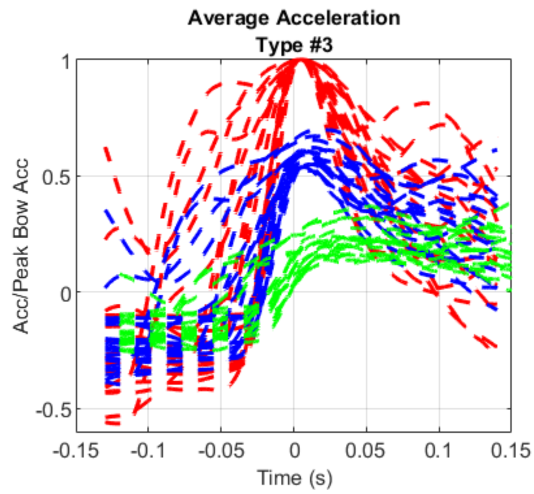

Figure 2.13: Composite plot of the bow, mid, and LCG accelerations for all events in category 3, for tolerance of 100.

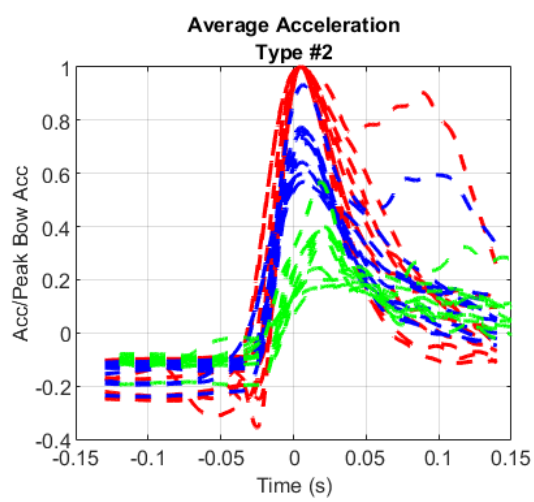

Figure 2.14: Composite plot of the bow, mid, and LCG accelerations for all events in category 2, for tolerance of 100.

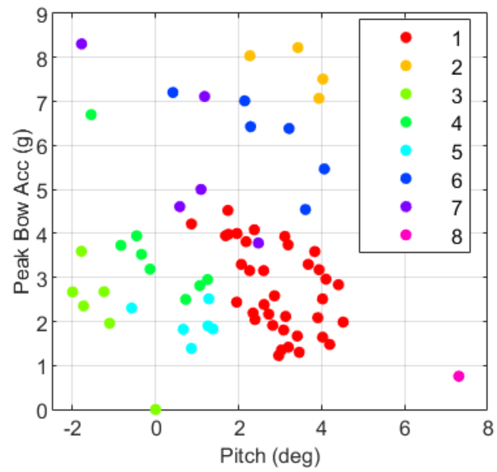

Figure 2.15: A scatter plot of the identified slamming categories, for a categorization tolerance of 75 and what ranges of pitch and peak bow acceleration they span.

The following discussion of the individual categories will be focused on categories two, three, four, and seven.

Category two, seen in Fig. 2.16, is characterized by a freefall event with a bow down motion. This smaller category consists of the highest peak vertical accelerations as seen in Fig. 2.15. This is consistent with the category alpha slam results from Riley et al. (2010) [2]. Categories three and four, $e_0 = 75$, have a significant delay between the peak bow and peak LCG accelerations. While most of the observed slamming events have a delay of approximately 25 milliseconds, a delay closer to 125 milliseconds is seen in category three and four slams. Category seven is interesting as it spans a large range of peak bow and LCG accelerations and pitches, but all have a negative $1g$ acceleration just before the peak bow acceleration. The remaining categories are not discussed because they did not have features that were interesting or distinct from the other categories.

In Fig. 2.17, beyond the intersecting and relatively chaotic clusters in the bottom left, there is a tight cluster of category two events that is composed of events with the greatest peak bow and LCG vertical accelerations. This cluster of events is significantly tighter than the other

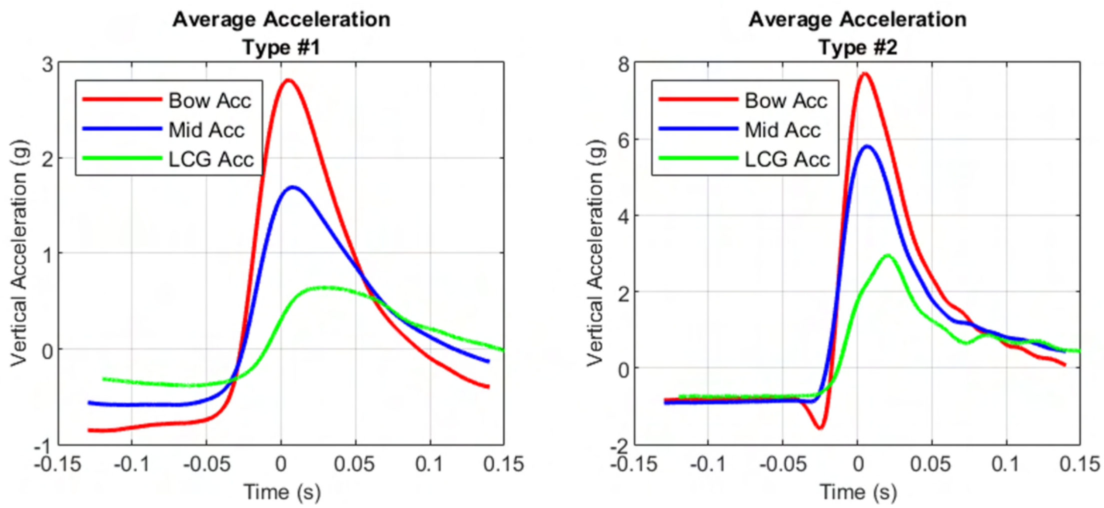

Figure 2.16: Average bow, mid, and LCG accelerations for category 1 and 2 and tolerance of 75.

clusters identified and proposes the highest likelihood of causing damage and discomfort aboard a vessel.

The category three and four events, shown in Fig. 2.18, were of interest in the scatter plots due to the increased delay between the peak bow and peak LCG accelerations with respect to the other categories. These events have relatively low peak accelerations. In contrast to other categories, category three and four have lingering high vertical accelerations after the slamming event that slowly decrease to zero. Categories 3 and 4 are differentiated by the steepness of the vertical acceleration upon initial impact. Category 3 has a relatively gradual slope and an average peak-bow-acceleration of $2g$. Meanwhile, category 4 has a steep initial vertical acceleration with an average peak-bow-acceleration of $3.5g$.

Category seven, shown in Fig. 2.20, like categories 3 and 4 also has lingering acceleration after the peak. However, its initial vertical acceleration is steep and has a higher average peak-bow-acceleration of $5g$. Overall, categories generated using a categorization tolerance of $e_0 = 100$ provide more insight into the categorization of slamming events, since the categories have less overlap and better defined boundaries.

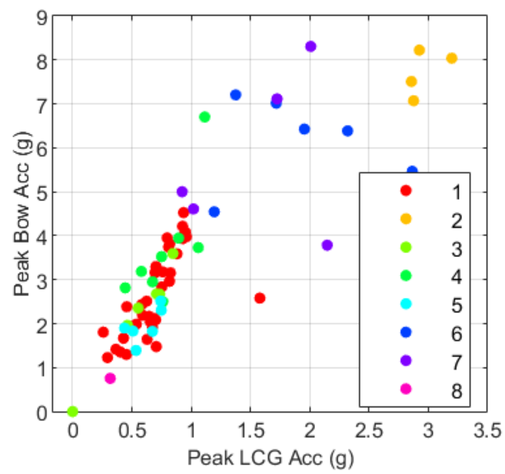

Figure 2.17: A scatter plot of the identified slamming categories, for a categorization tolerance of 75, and how their peak bow accelerations and LCG accelerations are correlated.

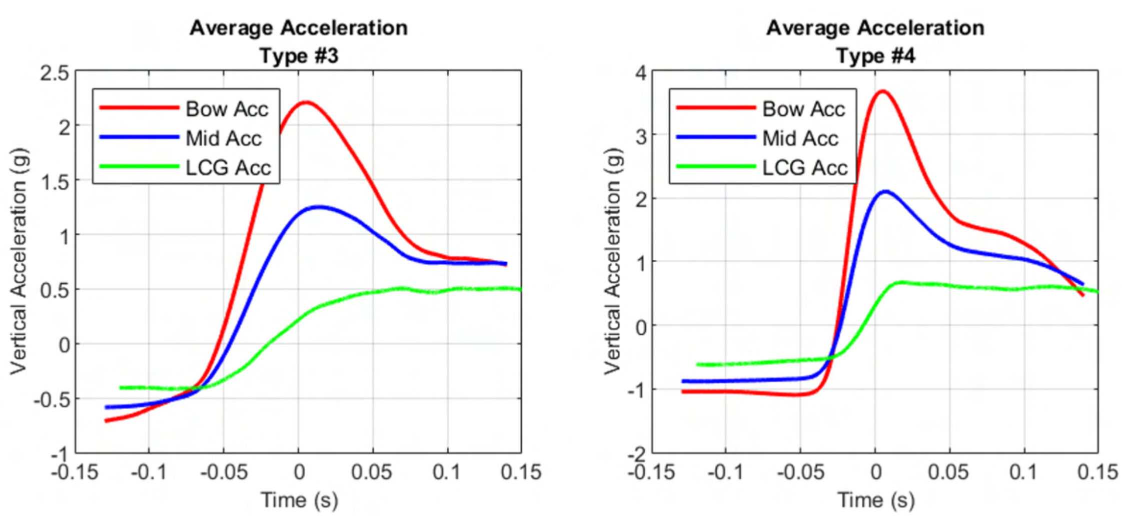

Figure 2.18: Average bow, mid, and LCG acceleration for category 3 and 4 and a tolerance of 75

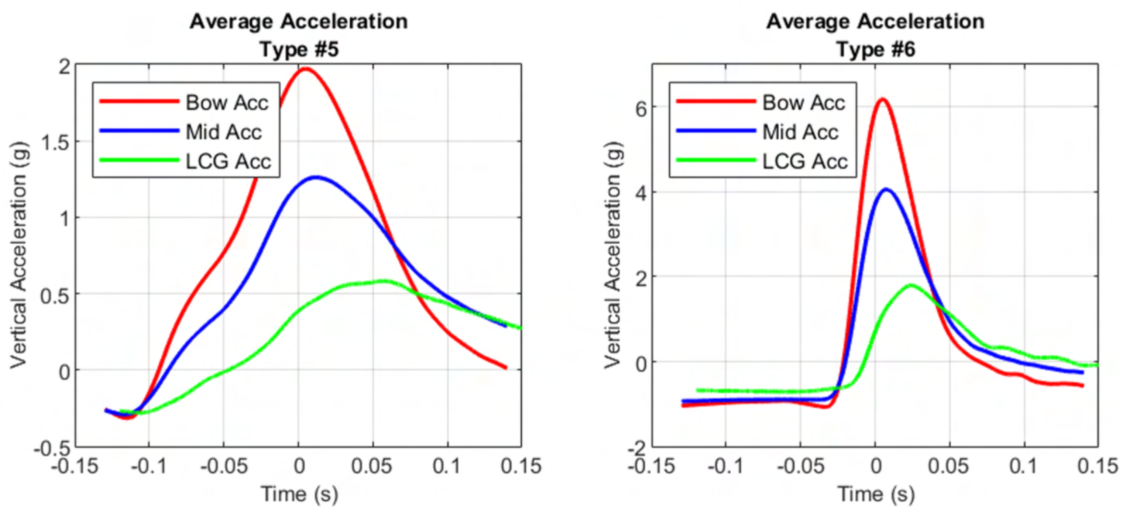

Figure 2.19: Average bow, mid, and LCG acceleration for category 5 and 6 and a tolerance of 75.

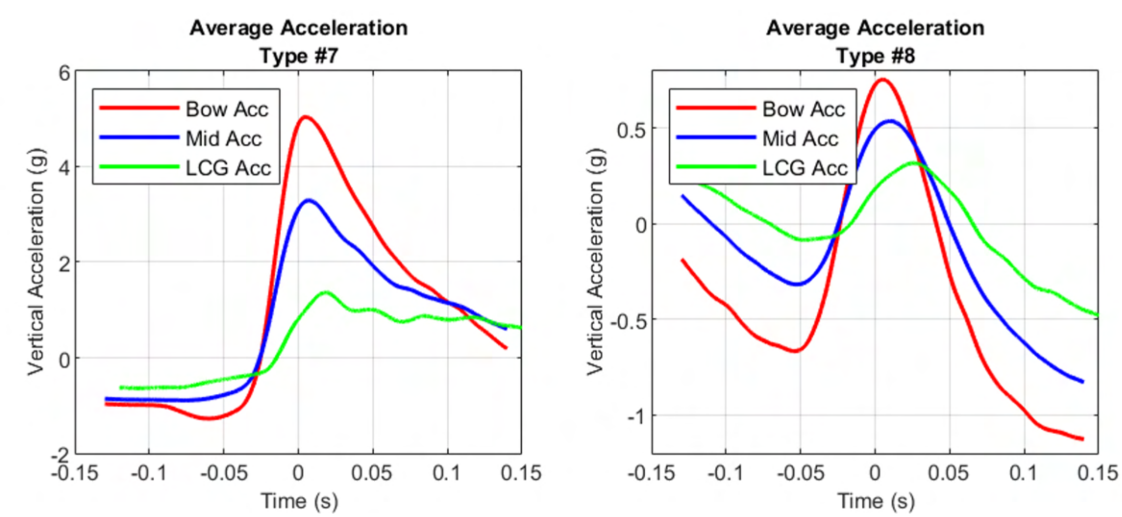

Figure 2.20: Average bow, mid, and LCG acceleration for category 7 and 8 and a tolerance of 75.

Through the investigations outlined, the proposed method inspired by facial recognition has shown promise in the ability to categorize slamming events based on the acceleration and pitch data. Although the clusters are not completely distinct, the majority of data within a given category lies within the bounds of a cluster. The scatter plots from the initial categorization identified that there is an increasing density of high peak acceleration events as impact pitch increases. This trend prompted investigation into the angular parameters in the whole vessel slamming problem, including impact trim, angular velocity, and angular acceleration.

2.3 Angular Parameter Investigation

This prompted a second categorization that incorporates angular velocity and angular acceleration. This modification is easily implemented by numerically deriving the pitch time-history using a simple forward difference scheme,

$$\omega_{\mathbf{i}} = \frac{\tau_{\mathbf{i+1}} - \tau_{\mathbf{i}}}{\mathbf{t}_{\mathbf{i+1}} - \mathbf{t}_{\mathbf{i}}}, \qquad \alpha_{\mathbf{i}} = \frac{\omega_{\mathbf{i+1}} - \omega_{\mathbf{i}}}{\mathbf{t}_{\mathbf{i+1}} - \mathbf{t}_{\mathbf{i}}} \tag{2.9}$$

where τ is the pitch angle, t is the time, ω is the angular velocity, and α is the angular acceleration. Since the variables in the categorization were altered, an adequate categorization tolerance, e_0, had to be determined again. A categorization tolerance, e_0, of 12,225 was selected. This value was determined by using a bracketing interval and iterating on the categorization tolerance until the algorithm identified the same number of categories as defined in the initial categorization for a tolerance of $e_0 = 100$. The value is significantly larger tolerance value makes sense since the values of angular velocity and acceleration are significantly larger and there are more data sources in the method. This makes our previously five dimensional slamming space to a seven dimensional space.

The scatter plots generated for this categorization are identical to the previous analysis but with the addition of the angular velocity and angular acceleration at impact as identified by the dramatic change in slope of the bow acceleration. An example of the impact moment identification can be seen in Fig. 2.21. The identification of the impact moment accurately captures the rapid change in slope. The identification of the impact moment was visually verified across all of the slamming events.

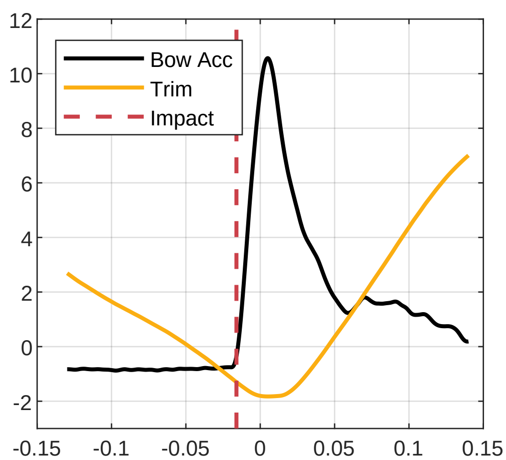

Figure 2.21: Single slamming event bow acceleration and pitch time histories, with the slope change marked by a vertical line

After adding in the angular components, there are significantly fewer events falling into the type 3 category and there is still no significant differentiation among categories by peak accelerations or the ratio of peak bow acceleration to peak LCG acceleration, as shown in Fig. 2.22.

In comparison to the prior categorization, there is less stratification based on the trim at impact and than the categorization based on peak bow acceleration, as seen in Fig. 2.23. The impact trim ranges from -1 degrees to just over 6 degrees. Here it can be seen that the peak bow acceleration has an impact on the categorization algorithm. There is still a significant overlap in categories. In general the events in category 1 typically have lower peak

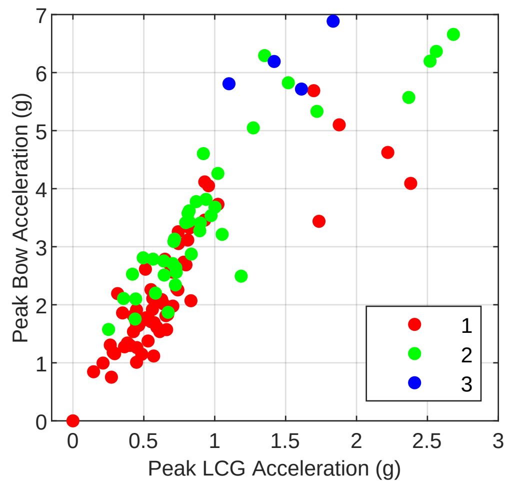

Figure 2.22: Peak Bow Acceleration vs Peak LCG Acceleration for angular categorization

accelerations and the events in category three all have higher peak accelerations, while the events in category two spans both of these groups. There does not seem to be any significant trends correlating the peak bow acceleration to the impact trim.

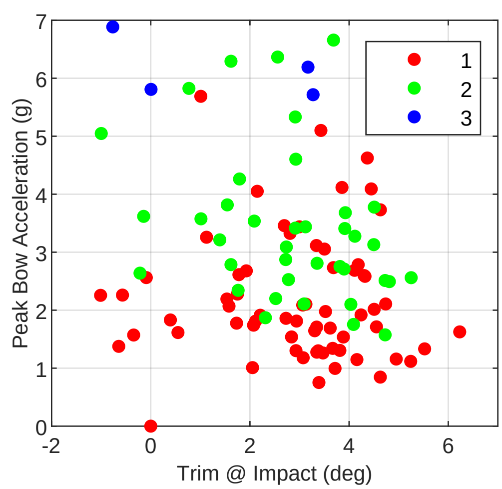

Figure 2.23: Peak Bow Acceleration vs Trim at Impact for angular categorization

The general trend shown in Fig. 2.24 is that as the angular velocity decreases the peak bow acceleration increases. Thus as the bow down angular velocity is increasing, the slamming impact severity increases. All the events with bow up, positive, angular velocities at impact have low peak bow accelerations. This makes physical sense as the bow will have a decreased relative vertical velocity in comparison to the LCG as it impacts the water. In this plot it is apparent that category three events all have high bow down angular velocities at the moment of impact. The majority of events have angular velocities that lie between -60 and 20 deg/s.

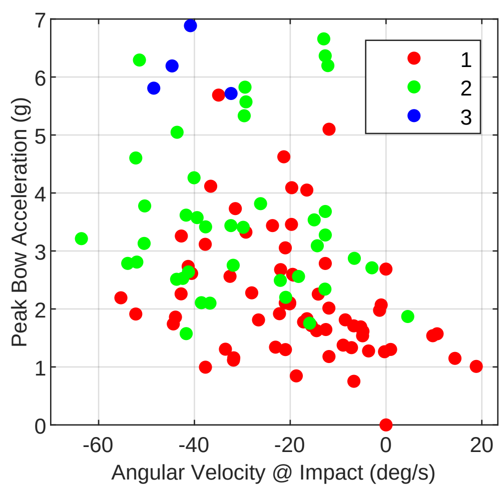

Figure 2.24: Peak Bow Acceleration vs Angular Velocity at Impact

As the angular acceleration at impact is decreasing the peak bow acceleration increases, seen in Fig. 2.25. The angular acceleration at impact ranges from -800 $^\circ/s^2$ to $800^\circ/s^2$. There is no apparent distinction of categories one and two based on the angular acceleration at impact. However, category three appears to all have high bow down angular acceleration at impact.

The above analysis has shown general trends in slamming behavior and severity relating to angular parameters. From here the correlation between impact velocity and peak acceleration investigated to determine how both forward and vertical motion affect slamming severity and what the primary component to focus on is in oblique impacts.

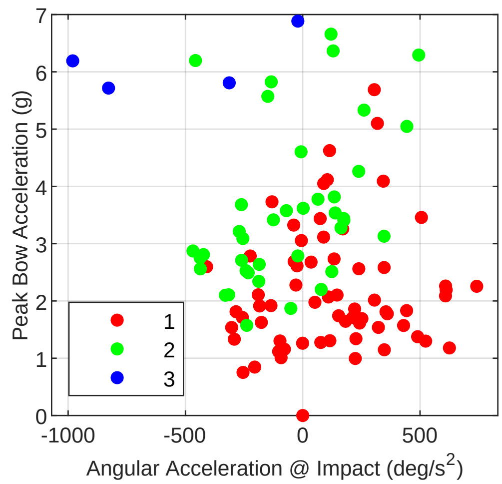

Figure 2.25: Peak Bow Acceleration vs Angular Acceleration at Impact

2.4 Heave Velocity & Total Velocity Investigation

To include the heave velocity into the analysis of the tow tank results, it was first derived from the record position data, with a first order forward Euler method. Since the main goal of this investigation was to look at trends in the data set and develop ranges for heave velocity and total velocity for the experimental matrix, the categorization of the data including these parameters was forgone. However, these parameters can be easily included in the algorithm via the same method as the angular parameters.

Fig. 2.26 shows a scatter plot of the heave velocity at the impact moment versus the peak bow acceleration. A linear trend can be seen in the data. As the downward heave velocity increases the peak bow acceleration also increases. The heave velocity in the USNA data set ranges from 0 to 7 ft/s, with the majority of the slamming events in a model scale sea state 3 occurring between 0 and 4 ft/s.

When the forward motion is accounted for, calculating the total velocity yields Fig. 2.27. The two different tow speeds of 29.5 ft/s and 25 ft/s form very distinct near vertical lines.

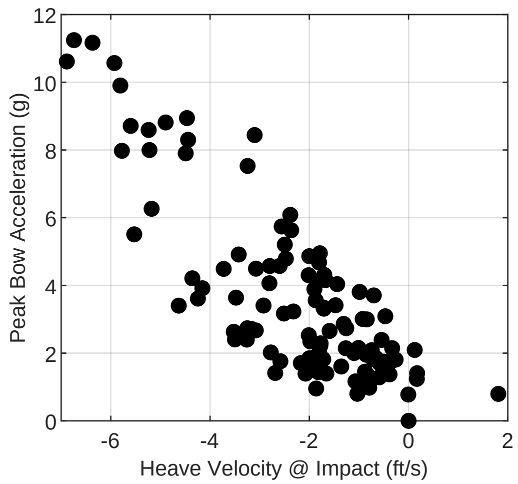

Figure 2.26: Peak Bow Acceleration vs Heave Velocity at Impact

Both of the tow speeds show the high peak bow accelerations, with the higher tow speed of 29.5 ft/s generating a couple slamming events with higher peak bow accelerations. Fig. 2.27 makes it apparent that the surge component of the velocity does not have as much of an impact on the peak bow acceleration as the heave velocity.

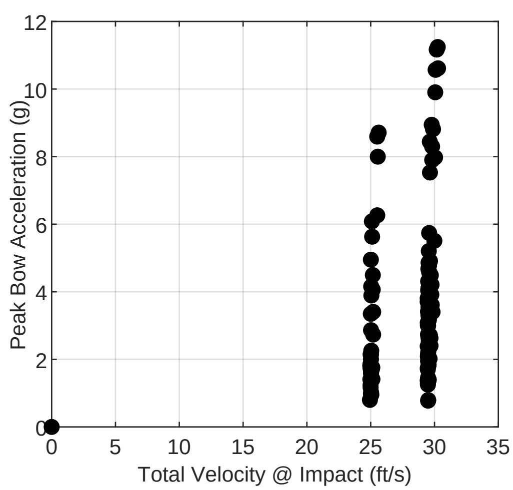

Figure 2.27: Peak Bow Acceleration vs Total Velocity at Impact

The results of Fig. 2.27 prompted the calculation of the velocity angle, which is the angle of the velocity vector to the horizontal. The results of this calculation are displayed in

Fig. 2.28. The same general pattern as seen in the heave velocity scatter plot, Fig. 2.26, is seen in the velocity angle data. The results of the heave velocity and total velocity plots combined suggest that the surge velocity plays a smaller role in slamming events compared to the heave velocity. This conclusion is supported in literature by Javaherian (2020) [12]. ***This conclusion is very impactful since it supports the validity of simplifying the complete slamming problem from the complete six degrees of freedom to two degrees of freedom, heave and pitch.***

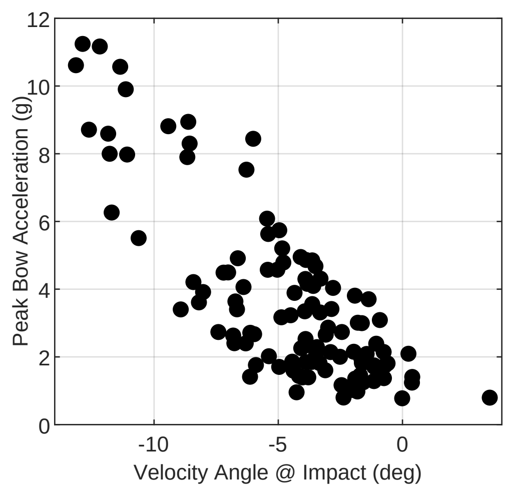

Figure 2.28: Peak Bow Acceleration vs Velocity Angle

2.5 High-Speed Video Analysis

To evaluate how the waveform changes the relative impact angle and velocity of the model, snapshots of the high speed video were taken at the impact moment. The snapshot where first sorted through manually to select representative figures for the extremes of different slamming types, Fig. 2.29.

An approximate outline of the waveform has been drawn on the selected frames and can be seen in Fig. 2.30. Using the representative snapshots the relative angle of the hull to the

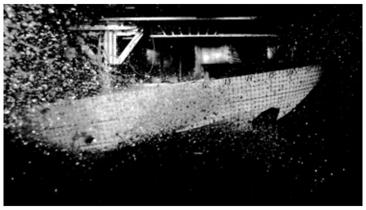

(a) Event 1

(b) Event 2

(c) Event 6

(d) Event 7

(e) Event 8

(f) Event 10

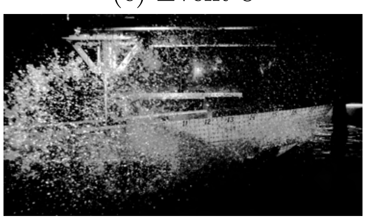

(g) Event 12

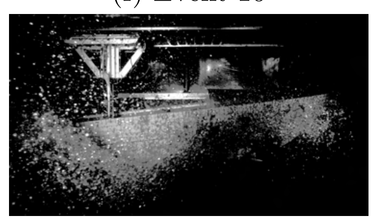

(h) Event 14

Figure 2.29: a) 16cm Drop height position time-histories for all angles b) 5cm Drop height position time-histories for all angles

wave was roughly measured. This range of relative impact angles was then compared to the range of impact angles from the data analysis.

From the frames in Fig. 2.30, it was seen that for type alpha and bravo slamming events, the wave acted to decrease the relative impact angle from the measured angle when the boat landed on the leading side of the wave and increased the angle when landing on the back side of the wave. On the contrary, for type charlie events, the relative impact angle is increased from the measured angle. As the model is running into the wave the trim is

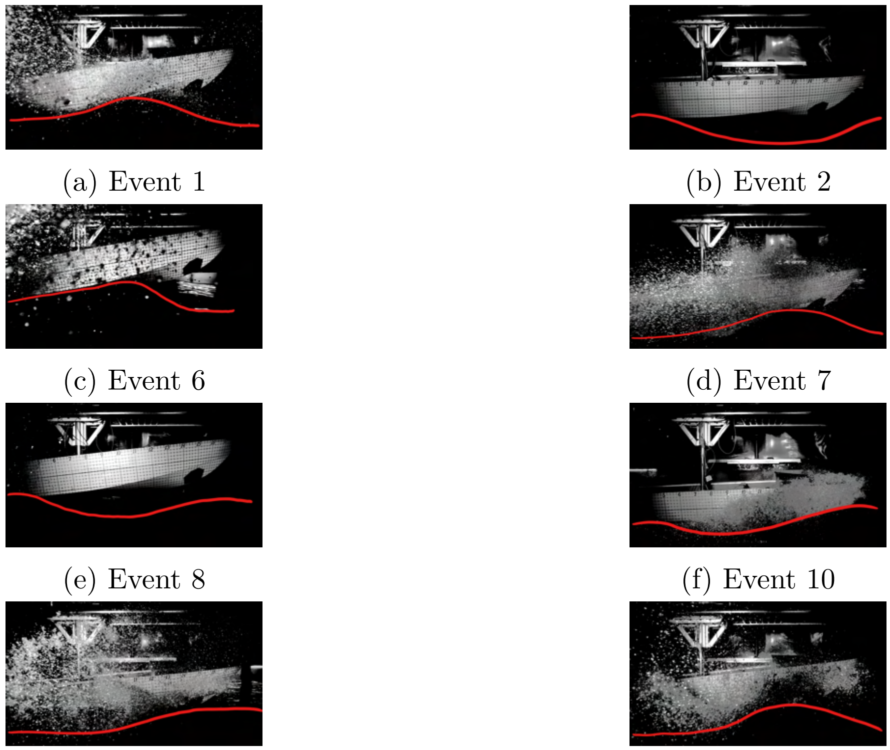

(a) Event 1 (b) Event 2 (c) Event 6 (d) Event 7 (e) Event 8 (f) Event 10 (g) Event 12 (h) Event 14

Figure 2.30: a) 16cm Drop height position time-histories for all angles b) 5cm Drop height position time-histories for all angles

relatively low before the rapid bow up pitching motion. For type alpha and bravo events the impact angles ranged from 0-6 degrees which is comparable to the range of measured impact angles. For the type charlie events, the relative impact angle of the bow was negative and could be greater than 10 degrees bow down.

2.6 Study Conclusions

The work presented in this section illustrates how a singular value decomposition technique can be used to categorize slamming events. This analysis was performed on an existing data set from the U.S. Naval Academy. It was found, as expected, that by decreasing the categorization tolerance, the number of categories increased. With a higher number of categories, the visual boundaries between categories overlap more, which was shown in the scatter plots. It was also found that when low peak bow accelerations occur, there is a strong linear correlation between the magnitude of the peak bow acceleration and peak LCG accelerations. However, at higher peak accelerations, this trend begins to break down, especially in category two events. Using Zeng's method,we were able to distinguish different categories of slamming events based on the time histories of data collected from tow tank experiments. The generated categories showed clustering behaviors especially for higher categorization tolerances. The implementation of modified facial recognition and machine learning techniques have shown promise in its ability to categorize slamming events. This can be seen by the fact that using a categorization tolerance of $e_0 = 100$ was able to identify two traditionally identified slamming events. After the addition of angular parameters to the algorithm, it was shown that for the majority of events, high peak accelerations can occur for all values of angular parameters. Zeng's method uses purely mathematical analysis to determine categories without regard for the physics of the problem. Coupling this method along with the physics of the slamming events identified will allow for a better and more meaningful categorization of slamming events. It was also shown that the heave velocity is directly related to the severity of the slamming event and the peak bow acceleration. This conclusion coupled with the two tow speeds both generating a wide and overlapping range of peak bow accelerations led to the conclusion that the surge velocity has minimal impact on the peak bow acceleration in comparison to the heave velocity. This conclusion supports the simplification of the slamming problem from the complete six degrees of freedom to two degrees of freedom, heave and pitch. This study resulted in the identification of several key factors that warrant further parametric investigation, such as impact trim, angular velocity, angular acceleration, and impact velocity.

2.7 Determining Key Parameters

Based on common knowledge and the wealth of research provided by Wagner, Vorus, and others, impact velocity is known to be a key factor in slamming loads and severity. This work identified that there is an increasing density of high peak acceleration events as impact pitch increases. This trend prompted investigation into angular parameters and impact velocity in the whole vessel slamming problem, including impact trim, angular velocity, angular acceleration, heave velocity and total velocity, as discussed in Sec. 2.3 & 2.4. Outside of kinematic parameters discussed in the above sections multiple other key parameters in the slamming problem have been identified in literature. Javaherian et al (2019, 2020) and Ren et al (2019a, 2019b) demonstrated the effects of hull flexural rigidity. Finding that decreased flexural rigidity, and the inclusion of flexibility into the design process has been shown to reduce the pressure loading on the hull, and peak accelerations [12, 13]. The location of the LCG plays an important role in the dynamics of high speed craft in calm water and waves, and as such is expected to be a key factor in the slamming kinematics and the resulting loads on the hull structure [8, 26]. The aforementioned parameters highlight a few of the many variables which affect the severity of slamming events. In an attempt to further understand and characterize the slamming problem and experimental matrix is proposed, which samples this space of variables

2.8 Proposed Experimental Matrix

Based on the analysis presented in this section, a large experimental matrix has been developed. The experimental matrix presented in Table 2.1 lays the foundation for a longitudinal project investigating the slamming of high-speed craft. Each column of Table 2.1 lists a single variable in the parametric study and the points to be sampled for that parameter. If data is collected at each possible combinations of parameters there will be 14,400 distinct experimental data points.

Table 2.1: Experimental matrix for VPMM experiments

Flexural Rigidity	Rigid	Transitional	Semi-Flexible	Flexible	-	-	-	-
LCG Location	-10%	0	10%	-	-	-	-	-
Heave Velocity (Fn_B)	0.525	0.942	-	-	-	-	-	-
Surge Velocity (Fn_L)	0	1.84	1.56	-	-	-	-	-
Trim	-20°	-16°	-12°	-6°	0°	2°	4°	6°
Angular Velocity ($°/s$)	-60	-40	-20	0	20	-	-	-
Angular Acceleration ($°/s^2$)	-600	-300	0	300	600	-	-	-

The key experimental parameter will be the hull flexural rigidity. The flexural rigidity of the hull will be matched to that of the wedge drop experiments described in Javaherian (2020) based on the hydroelasticity factor,

$$R = \frac{\tan\beta}{V_0}\sqrt{\frac{D}{\rho L^3}}, \qquad \text{where} \qquad D = \frac{Et^3}{12(1-\nu^2)} \tag{2.10}$$

which provides a measure of the relative stiffness of a structure undergoing a water entry [12]. Four hull stiffnesses will be evaluated, as listed in Table 2.1. The rigid bottom is defined as having a hydroelasticity factor greater than two along the entire hull at all impact speeds. The transitional bottom is defined as acting rigid along the entire hull at low impact velocities and flexible at higher impact velocities. The semi-flexible hull is defined as the condition when the hydroelasticity factor is less than 2 but close to 2 for all impact velocities along the entire hull. The flexible hull is defined as having a hydroelasticity factor significantly less than 2 for all impact velocities along the entire hull.

The LCG location will act as the center of rotation for during the controlled motion experiments. The primary location will be the true LCG for the GPPH. The LCG will then be shifted 10% of the L_{OA} forward and aft. The +/- 10% shift spans the range of LCG shift that a high-speed craft may experience in operation. By varying the LCG the results can give vital information to designers and operators as to how the LCG affects slamming loads, furthering its importance in the design of high speed craft.

The two impact heave velocities were selected based on the heave impact velocities observed in the USNA tow tank experiments, which had a range of 0-6 ft/s. To ensure that the results could be compared to the wedge drop experiments performed in the Virginia Tech Hydroelasticity lab, beam Froude number similarity

$$Fn_{B_{Wedge}} = Fn_{B_{GPPH}} \tag{2.11}$$

$$\frac{V_{Wedge}}{\sqrt{gB_{Wedge}}} = \frac{V_{GPPH}}{\sqrt{gB_{GPPH}}} \tag{2.12}$$

$$V_{GPPH} = V_{Wedge}\sqrt{\frac{B_{GPPH}}{gB_{Wedge}}} \tag{2.13}$$

was used to calculate the impact velocities for the GPPH that correspond to wedge drop experiment impact velocities. The parameters for the wedge can be seen in Table 2.2.

Based on this analysis, beam Froude numbers of 0.52 & 0.94 were chosen. The selected Froude numbers correspond to impact velocities of 3.24 ft/s and 5.81 ft/s for the GPPH model.

The relative bow up impact trim observed in the USNA experiments varied from 0°-6°. The bow up range of relative impact trims was sampled at 0, 2, 4, & 6 degrees to provide adequate coverage of the model behavior. The relative impact angle for type charlie events is closer

Table 2.2: GPPH Principle Characteristics

Characteristics	
Length Overall/L_{OA} (cm)	63.5
Max Beam/B (cm)	57.27
Displacement/Δ (kg)	40.6
Deadrise/β (°)	20

to 10°- 15°bow down. However, in order to accurately model these events, a bow up angular velocity must be present, otherwise the model will swamp. For experiments that are fixed in pitch, and have no bow up angular velocity or acceleration, the bow down angle must be limited. For experiments with pitching motion, the bow up pitching motion over the course of the slamming event will allow for higher bow down impact angles to be safely tested without risk of submerging the model. For these experiments impact angles will be added at -12, -16, and -20 degrees, with a corresponding bow up motion to safely and realistically model type charlie slamming events.

Based on the slamming events analyzed, the angular velocity at impact ranged from -60 to 20 deg/s. The impact angular acceleration was found to range between -1000 and 800 deg/s^2. However the majority of events lie within angular accelerations of -600 and 600 deg/s^2. Five samples will be taken from both of these ranges at regular intervals. The specific values of angular velocity and acceleration to be tested are listed in Table 2.1.

Chapter 3

Experimental Setup

3.1 Apparatus

3.1.1 Tow Tank & Carriage

The Virginia Tech Advanced Towing Facility is 98 ft long, 6 ft wide and 5ft deep. This facility has recently been upgraded. The old carriage has been replaced with a brand new carriage, designed and built by Edinburgh Designs in collaboration with Donald L. Blount Associates (DLBA). The carriage is capable of a maximum velocity of 23 ft/s (7 m/s) for a 1 s data window. The new carriage has many functions and all associated procedures and safety protocol have been documented in detail in Appendix **??**. The carriage is propelled with a belt driven system with one large electric motor on each of the two rails. The brakes are electromagnetic to provide enough braking force for the high acceleration and deceleration loads. The carriage is capable of 5m/s^2 and 20m/s^3 both accelerating and decelerating. The main structure of the carriage is constructed using ITEM aluminum extrusions, in combination with large custom aluminum parts. These extrusions allow for the easy construction and modification of experimental set ups.

3.1.2 Vertical Planar Motion Mechanism (VPMM)

The Vertical Planar Motion Mechanism (VPMM) works to move the model in heave and pitch. The VPMM uses two linear actuators, which enables the mechanism to move the model in heave up to a rate of 65 cm/s and pitch at a rate of 54°/s , with a maximum range of 60 cm of heave and +/-28°of pitch. The VPMM was designed by DLBA and constructed by the author based on a delivered parts list and 3D model. A 3D rendering of the VPMM mounted to the towing carriage is included in Fig. 3.1. DLBA's delivered bill of materials can be found in Appendix C. Additional drawings by the author used to machine components at Virginia Tech are also included in Appendix C.

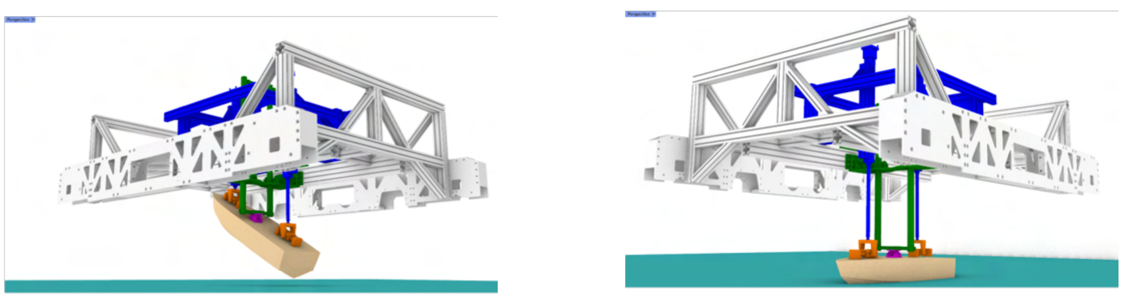

(a) Model in raised bow up position

(b) Model in normal floating condition

Figure 3.1: The above images show the VPMM in both a raised bow up position, (a), and a lowered zero trim position, (b). Images of the VPMM are used with permission of DLBA.

3.1.3 Slamming Tank & Drop Rig

The slamming tank is located in the Virginia Tech Hydroelasticity lab. The tank is 14' 5" (4.4 m) long, 7' 10" (2.4 m) wide, and has a depth of 3' 11" (1.2 m), and is constructed from 3" (76.2 mm) acrylic panels with a steel frame. The tank is raised above the ground by 26.5" (0.673 m) to allow for placement of high speed cameras to observe the bottom of objects as they enter the water. On top of the steel tank structure, T-slot aluminum extrusions support the experimental set up to drop models into the tank. Much care has been taken to ensure the the guide rails are level and square so the the model enters perpendicular to the calm water surface and can be used as reference surfaces for measurements.

The T-slot framing for this specific model drop experiment mimics the VPMM set up. The model was attached to the testing rig via two linear bearings on the centerline which allows the pitch angle of the model to be set without changing the length of the experimental set up for each pitch angle tested. When the pitch angle is set, the angle is locked and is fixed through the duration of the drop. The linear bearings are connected to a t-slot frame which slides inside of the static frame. These frames are connected using four linear bearings to prevent the setup from racking and to reduce the mechanical friction of the system to achieve as close to gravitational acceleration as possible. The pitch of the model can be changed between drops by adjusting the relative heights of the posts connected to the model. Moving the forward post up will cause a bow up pitch and moving it down will cause a bow down trim.

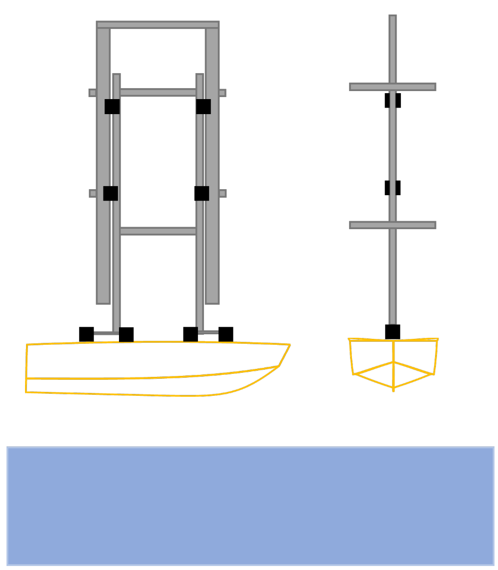

Figure 3.2: Drawing of experimental drop setup *Not to scale*

(a) Model trimmed up

(b) Model in even keel floating position

Figure 3.3: The above images show the model drop rig with the GPPH model trimmed up (a) and at even keel (b)

3.1.4 Generic Prismatic Planing Hull (GPPH)

The Generic Prismatic Planing Hull (GPPH) Model was used as the test model for this study to provide similarity to the Ikeda & Judge (2014) experiments which were used to develop the experimental matrix. The majority of the experiments performed at USNA were completed using an 8' model GPPH. To ensure this model would work in the Virginia Tech tank, which is significantly smaller, both the maximum velocity and wake reflection were taken into account. The calculations for wave reflection confirm that the bow wave will not intercept the hull of the model. However, the maximum speed of the carriage is 23 ft/s (7m/s) and the highest tested speed for the 8' model at USNA is 27.5 ft/s. Since these speeds will not be reached due to facility limitations, the 4' model was chosen. This model was manufactured by taking a mold off of the USNA's 4' model. This fiberglass negative mold was then used to create the final model. The layup schedule was based on the original USNA model's with the addition of some additional layers for added rigidity. Further details of the model construction can be found in Appendix A. A lines drawing and table of principle characteristics for the GPPH can be found in Fig. 3.4 and Table 3.1

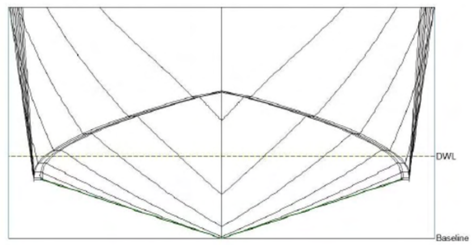

Figure 3.4: Body plan of the GPPH model (Ikeda & Judge (2014), used with permission[3])

Table 3.1: GPPH Principle Characteristics

Characteristic	Full-Scale	Model
Length Overall/L_{OA} (m)	13.0	1.22
Max Beam/B (m)	4.0	0.36
Draft/T (m)	0.77	0.0721
Displacement/Δ (tons)	15.9	0.013
LCG (m)	4.6	0.4298
VCG (m)	1.5	0.1372
Deadrise/β (°)	18	18

3.2 Instrumentation

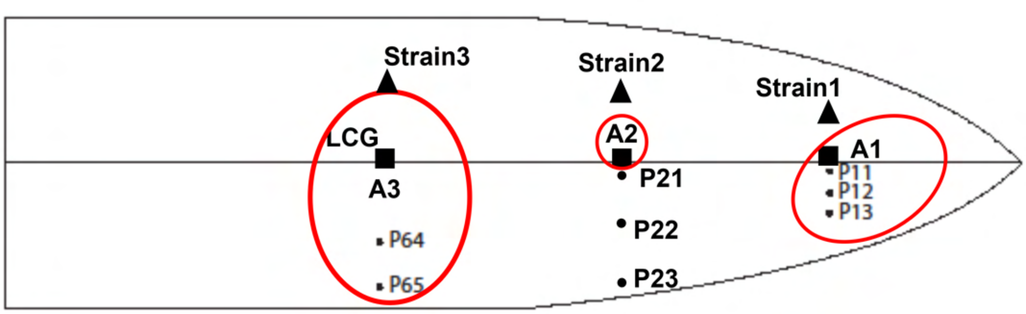

Figure 3.5: GPPH Sensor Configuration

The GPPH model was instrumented with a wide array of sensors including accelerometers, pressure sensors, strain gauges, and a potentiometer. All of these sensors will provide key data for analysis of fluid structure interaction and expanding the experimental wedge drop results to a hull geometry. The diagram in Fig. 3.5 shows the sensor configuration in the

GPPH model. The locations of the pressure sensors are denoted by a 'P' and the accelerometers by an 'A'.

3.2.1 Data Acquisition System (DAQ)

A PIXIe 1082 was used for data acquisition in the model drop experiment. Two NI PCIe-4492 modules for analog input were used, which take input from pressure sensors, accelerometers, and the potentiometer. A specific NI TB-4330 8 Ch Bridge Input module is employed to take readings from strain gauges.

3.2.2 Strain Gauges/LiDAR

Micro-Measurements quarter bridge strain gauges were adhered to the interior of port side of the hull at the same longitudinal locations as the pressure sensor rows. The port side of the hull has no pressure sensors or aluminum mounts which act to stiffen the composite hull structure. The strain gauges were oriented transversely to measure the strain from the keel to the chine. The strain gauges will confirm the assumptions made in the model design and fabrication process, ensuring the model is rigid, or demonstrate that the model is not behaving rigidly. The quarter bridge strain gauges have a resistance of 350Ω and a gauge factor of 2.070 at 24°C. The strain gauges were sampled at 1000 Hz, which provided enough time resolution to gain an accurate picture of the structural characteristics of the model. When the move from rigid to flexible panels is made in future experiments, the addition of a sensitive LiDAR will measure the panel deflection. The LiDAR will be rigidly mounted to the model and a triaxial AC-accelerometer will be mounted to the frame to account for any vibration in the setup and reduce the corresponding error in the measurement.

3.2.3 Pressure Sensors

PCB Model 102B18 ICP Pressure Sensors were placed along the bottom of the hull on the starboard side, with one sensor on the port side to verify model symmetry. These sensors were surface-treated with a thermal ablative coating to mitigate any changes in temperature. The pressures measured during slamming events occur very rapidly and generate high peak pressures. These sensors have a measurement range of 50 psi (344.7 kPa) for +/-5V output. This wide measurement range is complemented by a +/-15% sensitivity of 100mV/psi (14.5 mV/kPa) for highly precise measurements. The pressure sensors were sampled at 200 kHz. This high sampling rate allows the peak of the pressure wave to be accurately captured as it propagates along the hull. For the best measurements the probes require a mounting torque of 5-8 ft*lbs. To achieve this mounting torque on the fiberglass hull, aluminum cylinders were manufactured and epoxied to the hull to provide the threading and required thickness and structure. A drawing of these mounting cylinders can be found in Fig. 3.6.

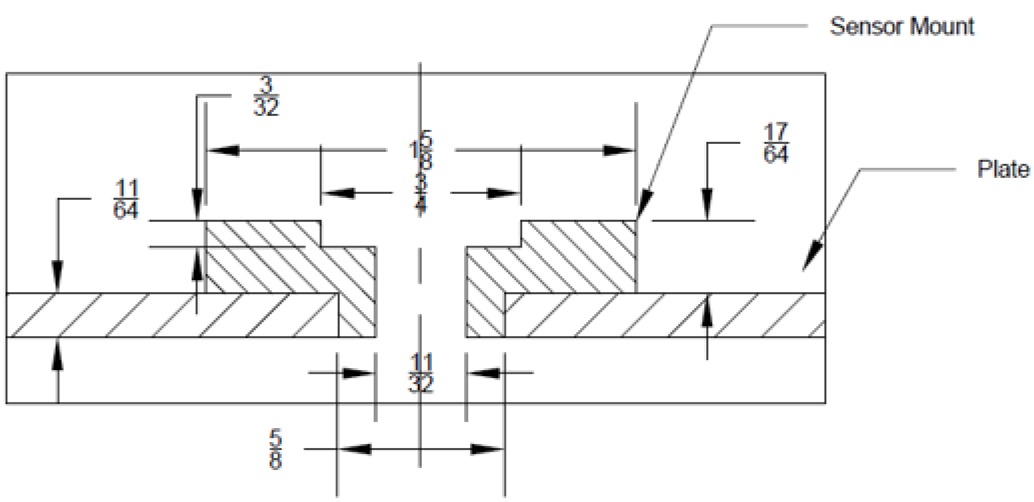

Figure 3.6: Pressure Sensor Mount drawing

3.2.4 Accelerometers

There are two main phases for acceleration during drop type experiments: freefall prior to impact and response post impact. To accurately measure both the freefall and response phases, multiple types of accelerometers are required. For the VPMM experiments, although the accelerations will be programmed, the accelerometers will act to verify that the actual acceleration matches the prescribed acceleration.

DC Accelerometer

DC accelerometers perform well at measuring low frequency accelerations. Thus, a PCB model 3741F122G DC accelerometer is mounted at the LCG to measure the freefall phase of the experiment. The DC accelerometer was sampled at 2000 Hz. This high sampling rate allows the freefall phase of the drop to be adequately captured. Knowing the acceleration of the model prior to impact is important in verifying the setup and quantifying how closely the experiment is modeling the physical phenomenon. Ideally the accelerometer should read gravitational acceleration during the entirety of the freefall phase. However, there is friction in the system, the possibility of racking, and a variety of other factors that can alter the acceleration during the freefall phase of the experiment. Using the measured freefall acceleration, adjustments can be made to the testing rig during experiments to produce accelerations closer to true freefall. After the freefall phase is the slamming response phase of the experiment. During this phase, the acceleration is not constant and in fact changes very rapidly. In this case DC accelerometers perform poorly. The DC accelerometer has a sensitivity of 1350 mV/g and a +/-2 g measurement range. The DC accelerometer gives off a continuous DC signal and thus the sampling frequency is limited by the DAQ rather than by the sensor.

AC Accelerometers

In order to measure the slamming response accelerations accurately, PCB model 352A24 AC accelerometers were mounted at both the bow and the LCG. AC accelerometers perform well at capturing time varying responses, but perform poorly at recording constant accelerations. So they cannot be used for both phases of the slamming event. The AC accelerometers recording the response will give insight to the severity of the slamming event. The AC accelerometers have a sensitivity of 100 mV/g and a measurement range of +/-50 g. The AC accelerometers were sampled at 2000 Hz which is enough to accurately capture the response phase of the slamming event.

3.2.5 Inclinometer

A SQ-GIX-2022 GravityGyro inclinometer was mounted at the LCG to record the pitch of the model. In the drop experiments the inclinometer will verify that the pitch is constant as the model enters the water, and in the VPMM experiments it will verify that the mechanism is performing the programmed motions properly. The inclinometer has a range of +/- 75 deg in elevation and +/-180 deg in roll. The static tilt accuracy of the sensor is 0.1 deg and the dynamic tilt accuracy is 0.5 deg of RMS error. The sensor also has a high shock tolerance, with a 1000g ½ sin 0.1 ms 3x in any axis. This value is significantly higher than any shock expected to occur during this series of experiments. Within the expected operating conditions the additional error due to vibration, shock, and acceleration is 0.5 deg RMS error. The sensor has IP67 rated protection which makes the inclinometer suitable for model mounted use in a wet environment. The inclinometer has an analog update rate of 125 Hz which although is significantly lower than the other instruments being used, the pulse width of the pitch motions from the USNA data set are at a lower frequency and have less defined peaks. The longer pulse width and smoother peak behavior make this lower sampling rate acceptable.

3.2.6 Potentiometer

A SGD-120-3 string pot potentiometer will be attached to the model at the LCG. The potentiometer will measure the heave of the model and show the position as it impacts the water. Using the potentiometer in combination with the inclinometer, the position of the entire model relative to calm water level can be determined. Although in the VPMM experiments, this motion will be prescribed, again the potentiometer acts to verify that the actual movement pattern matches the programmed movement pattern. The potentiometer has a maximum range of 120 in (3048 mm) and is a DC instrument giving off a continuous signal. Thus the resolution of the potentiometer measurement is limited by the DAQ and not by the sensor. This signal was sampled at 2000 Hz which is more than enough to capture the dynamic position of the model, and is consistent with the sampling rate of the accelerometers. The potentiometer has a 0.3% FS accuracy. In addition, the potentiometer has an IP67 rating. Although it is not expected that the potentiometer gets wet this protection has added comfort for incidental splashes and other risks that are posed by working in a wet environment.

3.3 High-Speed Cameras

Two Phantom VEO 710S high-speed cameras were placed underneath the set up to observe how the spray root travels across the bottom of the model and how the wetted surface and spray root velocity changes with the drop height and impact trim of the model. The cameras can capture at a resolution of one megapixel up to 7000 fps. These cameras were synced, and captured the slamming event at 2000 fps.

3.4 Model Drop Experimental Matrix

A portion of the experimental matrix described in Sec. 2.8 has been completed using the model drop setup, and will be discussed in the remainder of this thesis. The model drop experiments will use a rigid model to evaluate the effects of impact trim and heave velocity on slamming severity. The experimental matrix for this subset of experiments is depicted in Table 3.2. Not all bow down angles of impact could be tested since the drop set up does not have the capability to provide angular velocity. The maximum bow down angle of -6°was determined over the course of the experiment by gradually increasing the bow down impact angle until increasing the angle any more would have an unacceptable amount of risk of submerging the model.

Table 3.2: Experimental matrix for model drop experiments

Trim Angle	Drop Height (cm)	
τ	5	16
-6°	✓	✓
0°	✓	✓
2°	✓	✓
4°	✓	✓
6°	✓	✓

3.5 Data Filtering

Although best practices were used to minimize the amount of noise in measurement signals there was still noise present in multiple of the signals. The potentiometer and strain gauge measurements had very little noise and did not require filters. To reduce noise in the data, a low pass butterworth was applied in post-processing to the data to smooth the curves. Care was taken during this process to ensure that data peaks were not erroneously eliminated and all of the key features and trends in the data before filtering are still present after filtering.

The first step in the filter design process was to employ a fast Fourier transform to determine frequencies present in the data signal. From there, frequencies consistent with the physics of the event are distinguised from possible noise sources and a reasonable cutoff frequency can be determined. The process was completed for all instruments on several runs. Since each run generated similar results, a single run was used for the remaining duration of the filter design. The resulting spectral analysis can be seen in Fig. 4.1 below.

The spectral analysis of the DC accelerometer signal, in Fig. 4.1a, shows a large spike in the signal magnitude below 20 Hz. This is the frequency range where the signal is strongest. Since the signal reduced significantly after 20 Hz, and stays at a low magnitude, a cutoff frequency for the DC accelerometer has been set at 100 Hz to keep the signal while eliminating all of the noise from 100 Hz to the sampling frequency of 2000 Hz. Fig. 4.2a shows a plot of the filtered DC accelerometer signal on top of the unfiltered signal. The filtered signal here matches the trends of the unfiltered signal reasonably well, capturing the increase in acceleration from the release of the model to stabilizing at gravitational acceleration.

The spectral analysis of the A1 AC accelerometer, in Fig. 4.1b, has significant signal magnitudes across a wider range of frequencies in comparison to the DC accelerometer. The magnitude of the signal has decreased substantially around 40 Hz. A cutoff frequency of 100

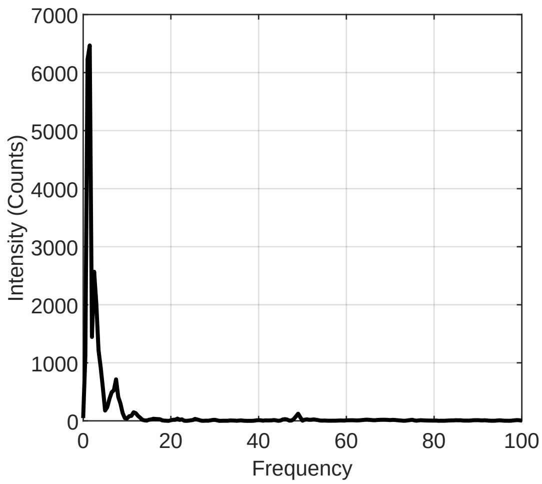

(a) DC Spectral Analysis

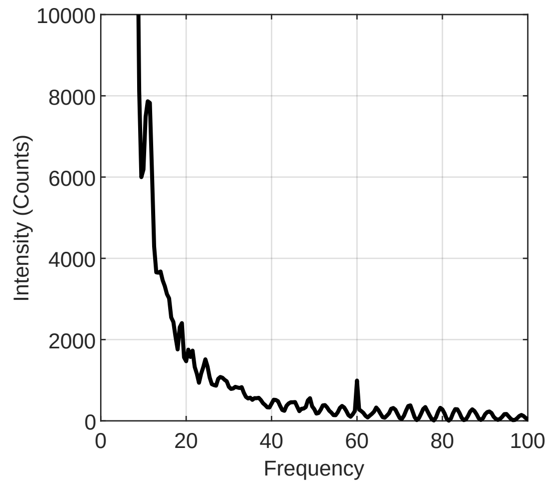

(b) A1 Spectral Analysis

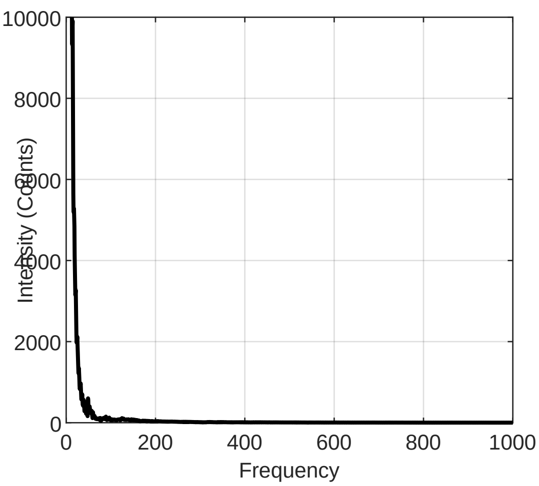

(c) P31 Spectral Analysis

Figure 3.7: The above graphs show the results of the fast Fourier transform. (a) Depicts the spectral for the DC accelerometer (b) & (c) show the spectral analysis for the A1 accelerometer and the P31 pressure sensor respectively as representative examples for the the AC accelerometers and the pressure sensors

Hz was also applied to the AC accelerometers, which preserves the low frequency content of the signal and removes the higher frequency components. The filtered signal is compared to the unfiltered signal in Fig. 4.2b, which demonstrates the filtered signal still captures the trends in the data, with a small temporal shift in the signal after filtering the data.

The pressure sensors used in the experiment had relatively low levels of noise. The spectral analysis for the P31 sensor can be seen Fig. 4.1c. The magnitude of the signal is sufficiently decreased by 200 Hz. However, since the signal is so clean, and sampled at a high frequency of 200 kHz, a filter was applied at 2000 Hz. This filter decreased the magnitude of high magnitude data spikes, as seen in Fig. 4.2c. Yet the filtered data still follows the unfiltered signal very closely.

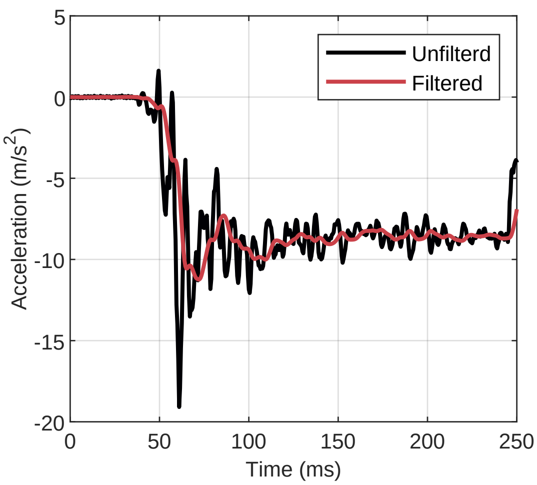

(a) DC Filter Comparison

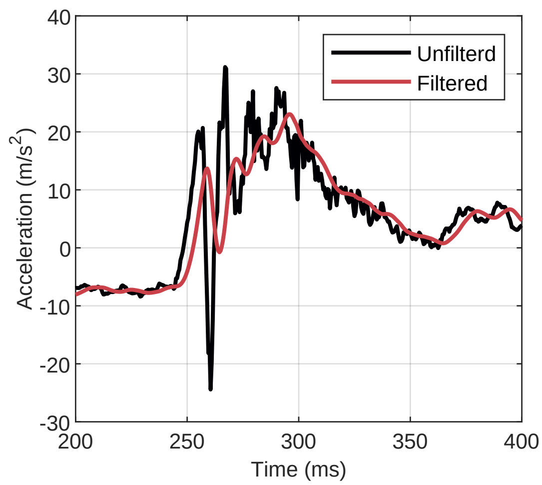

(b) A1 Filter Comparison

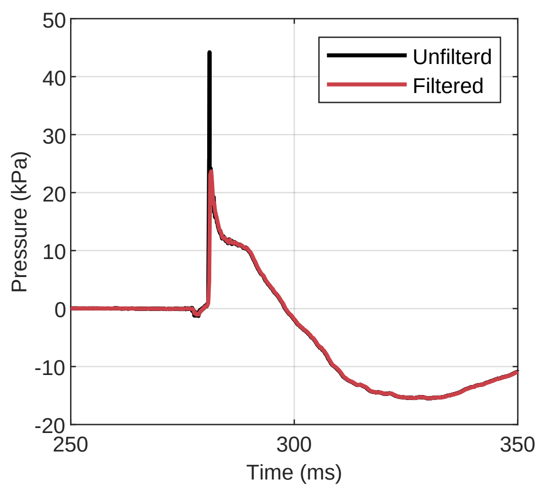

(c) P31 Filter Comparison

Figure 3.8: Comparison of data before and after filtering

Chapter 4

Analysis

4.1 Data Filtering

Although best practices were used to minimize the amount of noise in measurement signals there was still noise present in multiple of the signals. The potentiometer and strain gauge measurements had very little noise and did not require filters. To reduce noise in the data, a low pass butterworth was applied in post-processing to the data to smooth the curves. Care was taken during this process to ensure that data peaks were not erroneously eliminated and all of the key features and trends in the data before filtering are still present after filtering.

The first step in the filter design process was to employ a fast Fourier transform to determine frequencies present in the data signal. From there, frequencies consistent with the physics of the event are distinguised from possible noise sources and a reasonable cutoff frequency can be determined. The process was completed for all instruments on several runs. Since each run generated similar results, a single run was used for the remaining duration of the filter design. The resulting spectral analysis can be seen in Fig. 4.1 below.

The spectral analysis of the DC accelerometer signal, in Fig. 4.1a, shows a large spike in the signal magnitude below 20 Hz. This is the frequency range where the signal is strongest. Since the signal reduced significantly after 20 Hz, and stays at a low magnitude, a cutoff frequency for the DC accelerometer has been set at 100 Hz to keep the signal while eliminating

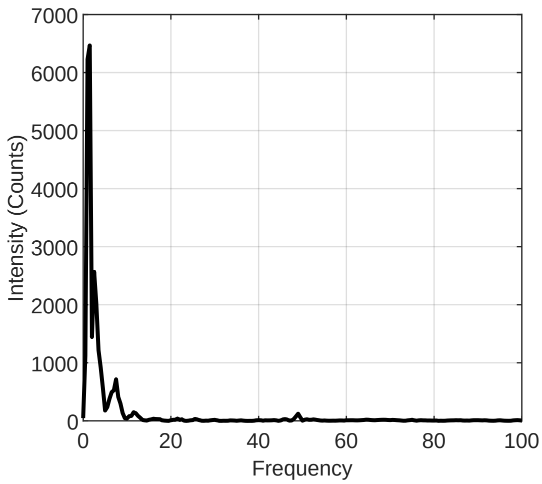

(a) DC Spectral Analysis

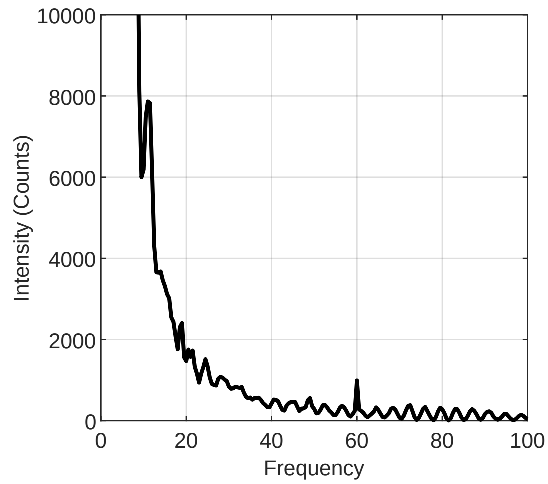

(b) A1 Spectral Analysis

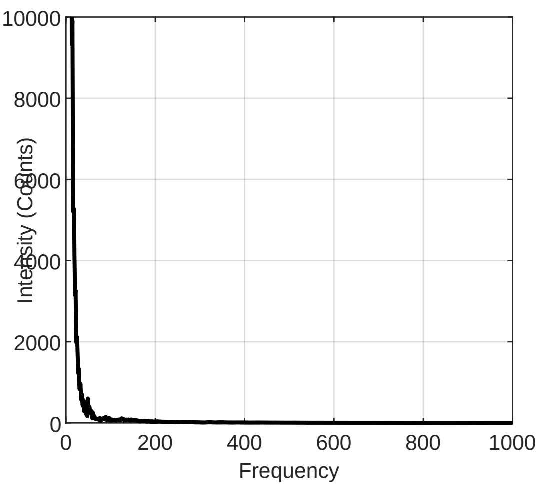

(c) P31 Spectral Analysis

Figure 4.1: The above graphs show the results of the fast Fourier transform. (a) Depicts the spectral for the DC accelerometer (b) & (c) show the spectral analysis for the A1 accelerometer and the P31 pressure sensor respectively as representative examples for the the AC accelerometers and the pressure sensors

all of the noise from 100 Hz to the sampling frequency of 2000 Hz. Fig. 4.2a shows a plot of the filtered DC accelerometer signal on top of the unfiltered signal. The filtered signal here matches the trends of the unfiltered signal reasonably well, capturing the increase in acceleration from the release of the model to stabilizing at gravitational acceleration.

The spectral analysis of the A1 AC accelerometer, in Fig. 4.1b, has significant signal magnitudes across a wider range of frequencies in comparison to the DC accelerometer. The magnitude of the signal has decreased substantially around 40 Hz. A cutoff frequency of 100 Hz was also applied to the AC accelerometers, which preserves the low frequency content of the signal and removes the higher frequency components. The filtered signal is compared to the unfiltered signal in Fig. 4.2b, which demonstrates the filtered signal still captures the trends in the data, with a small temporal shift in the signal after filtering the data.

The pressure sensors used in the experiment had relatively low levels of noise. The spectral analysis for the P31 sensor can be seen Fig. 4.1c. The magnitude of the signal is sufficiently decreased by 200 Hz. However, since the signal is so clean, and sampled at a high frequency of 200 kHz, a filter was applied at 2000 Hz. This filter decreased the magnitude of high magnitude data spikes, as seen in Fig. 4.2c. Yet the filtered data still follows the unfiltered signal very closely.

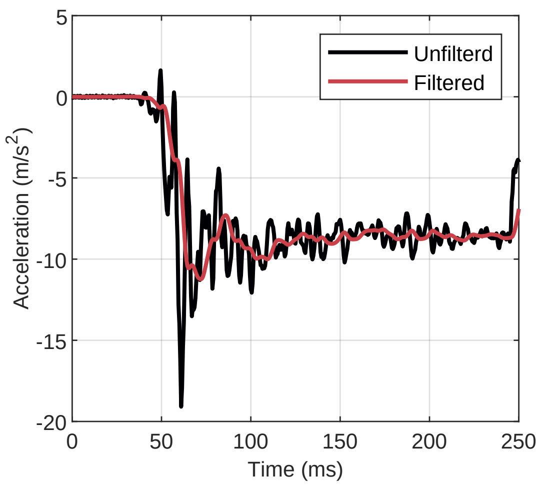

(a) DC Filter Comparison

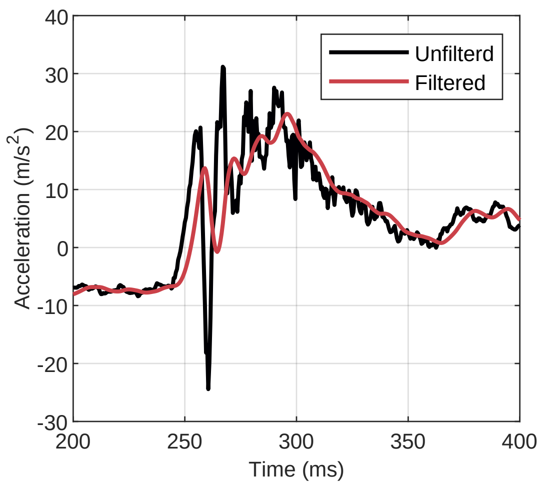

(b) A1 Filter Comparison

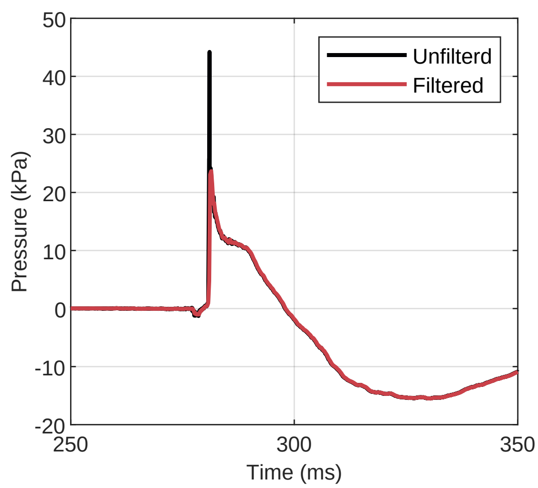

(c) P31 Filter Comparison

Figure 4.2: Comparison of data before and after filtering

Chapter 5

Model Resistance Verification

Chapter 6

Results & Discussion

The model drop experiments gave further insight to the slamming problem and the relationship between impact trim angle and slamming event severity. The experiments characterized this relationship based on strain, pressure, and acceleration measurements. These measurements, in combination with high speed footage of the bottom of the hull, provide further understanding of how the hull shape and operating parameters alter and expand upon the crucial results and theoretical formulations developed for prismatic wedges. A discussion of how model kinematics, spray root propagation, and slamming severity change with trim will be presented.

6.1 Model Kinematics

The first phase of the model drop experiment is a freefall period. During this period, the model is falling at gravitational acceleration. Due to friction in the system, or air cushioning effects at small drop heights, the true acceleration reached by the model will be slightly reduced from 9.81 $\mathrm{m/s^2}$. Fig. 6.1 shows the mean position, velocity, and acceleration of the model for a drop height of 16 cm and a trim angle of zero degrees. After a 30 ms delay, power to the magnets is cut and the model is released. This time corresponds to the first 30 ms of data, where the acceleration and position are constant. The true average acceleration reached by the model is 9.25 $\mathrm{m/s^2}$, Fig. 6.1c. This is indicative of friction in the system,

Table 6.1: Linestyle Legend

Location	Angle (deg)	Line
Bow	-6	
	0	
	2	
	4	
	6	
Mid	-6	
	0	
	2	
	4	
	6	
LCG	-6	
	0	
	2	
	4	
	6	

and possibly a small amount of misalignment. The decreased acceleration leads to a small decrease in the anticipated impact velocity. The discrepancy between the predicted and actual impact velocities is acceptable. The true impact velocity still lies within the range of impact velocities recorded in the 2014 USNA tow tank experiments. After the model impacts the surface, there is an immediate peak in acceleration. This can be seen in the position reading, as a slight change in curvature. The model continues to travel downwards, decelerating until it reaches its deepest point where the model begins to rebound. After rebounding, the model reaches a steady state, which corresponds to the draft of the model. The drop rig including the model is assumed to be rigid and thus the acceleration time histories from both the A1 and A2 accelerometers should match closely, as seen in Fig. 6.1c.

For each condition, the mean position of three repeated runs is plotted in Fig. 6.2. Fig. 6.2a shows the position for the 16cm drop height and Fig. 6.2b, for the 5cm drop height. For both drop heights, as the trim angle increases, the model submerges deeper into the water.

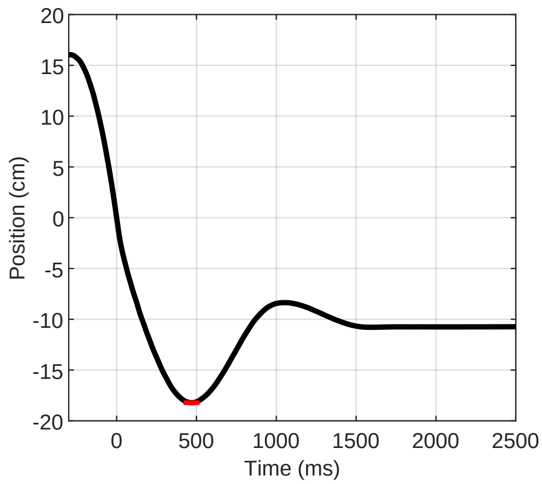

(a) 0-deg 16 cm Drop Position

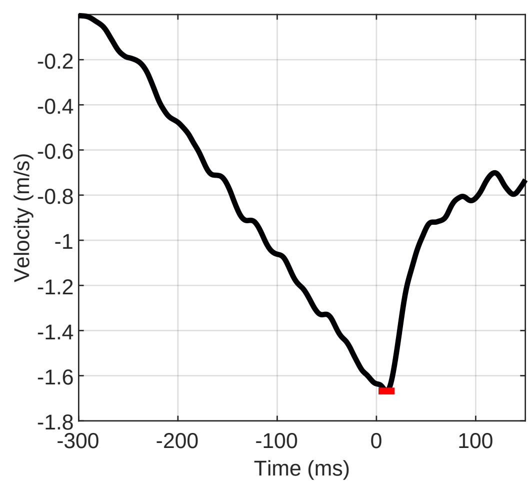

(b) 0-deg 16 cm Drop Velocity

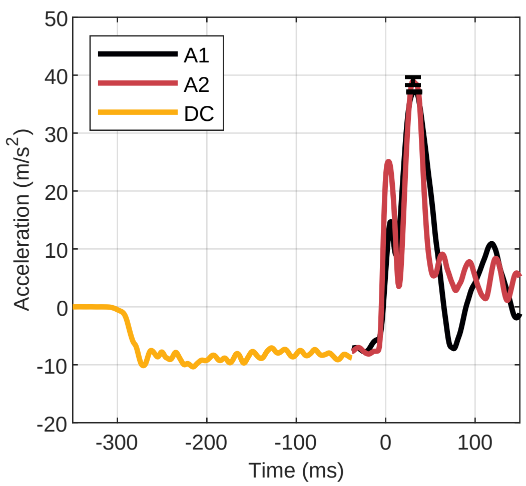

(c) 0-deg 16 cm Drop Acceleration

Figure 6.1: (a) 16cm drop height position time-history for a 0°impact angle (b) 16cm drop height velocity time-history for a 0°impact angle (c) 16cm drop height acceleration time-history for a 0°impact angle

This is expected, since the buoyancy of the model increases more gradually at greater angles (both positive and negative), whereas for a zero degree impact, the rate that the buoyant force increases is significantly higher.

The effects of buoyancy are reflected in the acceleration data, Fig. 6.3 at the 5cm drop height. Fig. 6.3 shows the mean acceleration time-history for each trim angle tested. Fig. 6.3a depicts

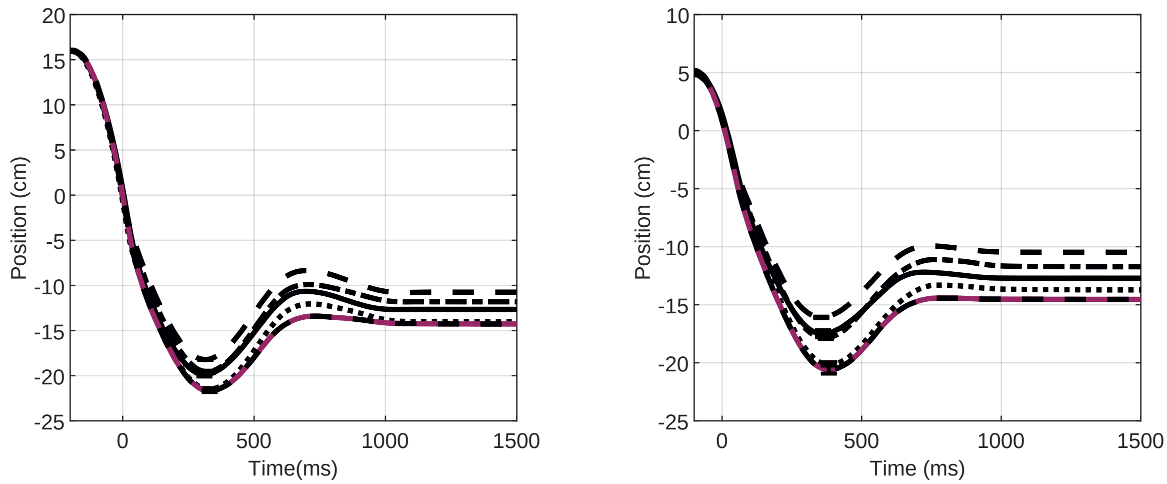

(a) 16 cm Drop Height

(b) 5 cm Drop Height

Figure 6.2: Position time history for all impact trim angles at 16cm, (a), and 5cm, (b).

the acceleration time-histories for the 16 cm drop heights and Fig. 6.3b, for the 5 cm drop heights. At slight bow up trim angles of two and four degrees, there is an increase in acceleration compared to the zero degree case. The increase occurs since the stern on a planing hull is fuller than the bow. Thus the small increase in trim increases the rate of increase in buoyancy. The peak acceleration is delayed from the zero degree case since the steady state sinkage is deeper, as seen in Fig. 6.3b. The steady state sinkage corresponds to the position at which the model begins to accelerate upwards. Since this location is deeper for higher trim angles it requires a longer time to reach. However, as the angle increases, the midbody does not submerge as rapidly, thus decreasing the rate of increase in buoyancy. Higher angles of trim correspond to decreases in peak acceleration and increasing delays in peak time, as seen in Fig. 6.4. The decreased peak acceleration and delayed peak time is due to the decrease in the rate of increase of buoyancy. As expected, the acceleration time histories for both the A1 and A2 accelerometers match fairly closely, for the 5 cm drop height, as evident in the peak time and magnitude scatter plots. However, at the 16cm drop height, the acceleration time histories and peak magnitudes do not match well, Fig. 6.3a and

Fig. 6.4 respectively. As the trim angle increases, the peak bow acceleration, A1, increases and the peak LCG acceleration, A2, decreases. This is believed to be an effect of the bow down moment caused when the stern impacts the water first. When the model enters the water at an angle, the longitudinal center buoyancy and the hydrodynamic forces is shifted aft. The misalignment between the forces acting on the model and the center of gravity generate a bow down moment. This bow down moment presses the guide rails forward and results in a significant increase in friction. This motion causes racking in the setup and allows for a small, but violent pitching motion in the drop set up. This jerking motion leads to a small rapid change in trim angle, which increases the bow, A1, acceleration and decreases the LCG, A2, acceleration. In comparison to the acceleration results at the 5cm drop height, all of the peak accelerations at the 16cm drop height have greater peak accelerations. In addition, there are similar characteristics in the time delay of the acceleration peak at 16cm drop height, as compared to the 5cm drop height.

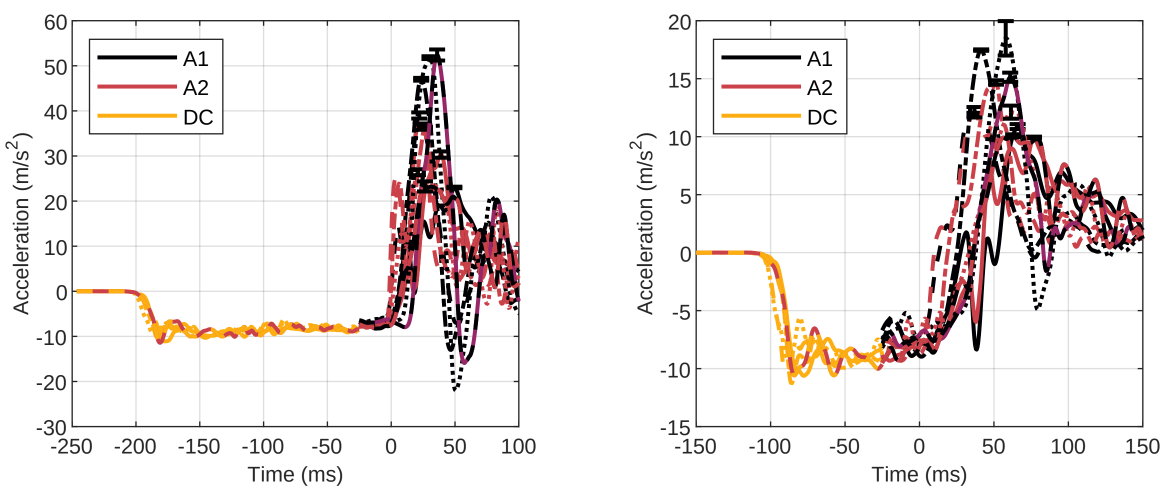

(a) 16 cm Drop Height

(b) 5 cm Drop Height

Figure 6.3: Acceleration time history for all impact trim angles at 16cm, (a), and 5cm, (b).

The velocity time history plotted in Fig. 6.5 and is derived from the position data. The 0-degree impact has the steepest slope after reaching the maximum velocity. This indicates

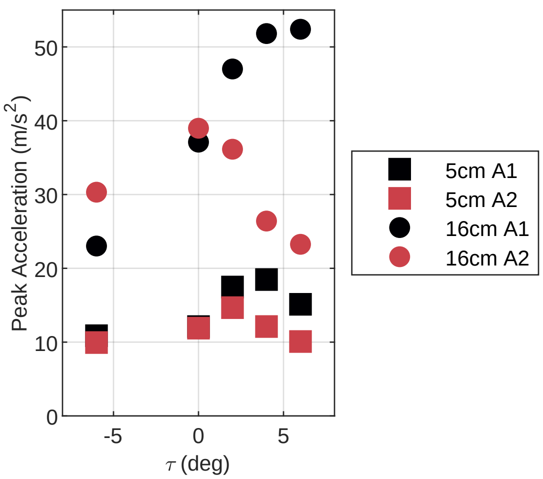

(a) Peak Acceleration vs Impact Trim Angle

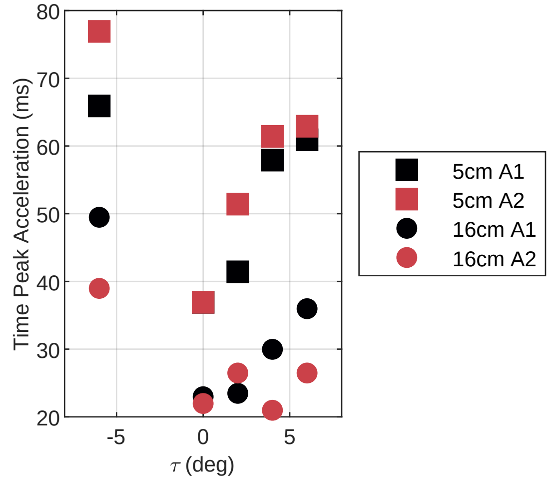

(b) Acceleration Peak Time vs Impact Trim Angle

Figure 6.4: Scatter plots illustrating how the acceleration peak amplitude, (a) and time, (b), vary with impact angle

that it is accelerating the most rapidly of all of the impact angles. As the absolute value of the impact angle increases, the slope of the velocity decreases, indicating decreased upwards acceleration.

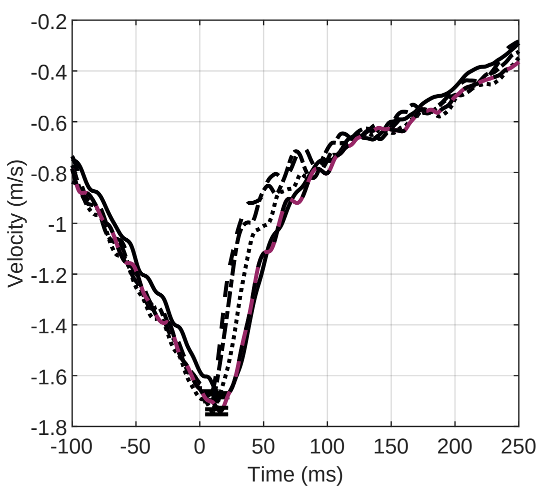

(a) 16 cm Drop Height

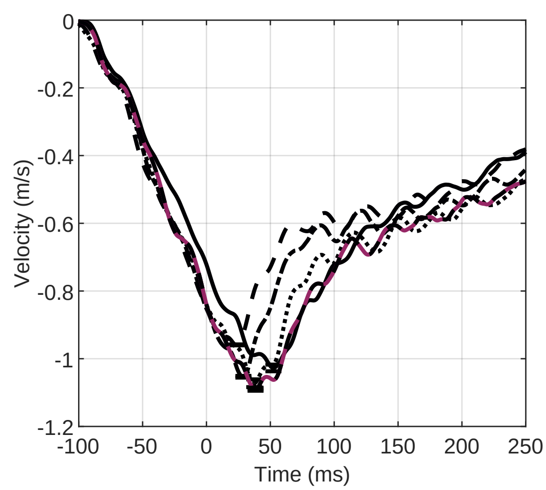

(b) 5 cm Drop Height

Figure 6.5: Velocity time history for all impact trim angles at 16cm, (a), and 5cm, (b).

6.2 Pressure

Pressure measurements for the 16cm drop height at a zero degree trim angle, can be seen in Fig. 6.6. The typical trend in pressure time history from wedge drop experiments is displayed very well in the P2 & P3 pressure sensor rows. The P2 & P3 pressure sensor row exhibit this trend well since they are on a fairly prismatic portion of the model. The P1 row of pressure sensors at the bow do not exhibit this trend as clearly since the bow is less prismatic and has a higher deadrise. Upon impact, as the spray root and corresponding pressure wave propagate along the bottom of the hull, from keel to chine, the peak pressure follows. The propagation of the pressure wave is seen in Fig. 6.6. The pressure sensors closer to the chine experience the pressure peak after the sensors closer to the keel. After the pressure wave passes a pressure sensor, the pressure at that point gradually drops, which is seen clearly in the time histories of the P31 and P32 sensors as well as the P21 and P22 sensors, Fig. 6.6. The apparent trend in the zero degree case, is that the peak pressure is greatest at the LCG and decreases towards the bow. This trend corresponds with the increase in deadrise angle and the presence of 3D effects, which has been shown by Chuang (1966) to decrease peak pressure [27]. The other interesting feature of the zero degree data in comparison to classic wedge drop experiments is that at the bow there is an increase in pressure at the sensor farthest from the keel. This pressure increase occurs prior to the other two sensors in the P1 row which are closer to the keel measuring any pressure. Since this increase has a small magnitude of just over 2 kPa, it is currently thought to be caused by spray on the sensor. Further investigation is required to pin point the true source of this peak.

The mean pressure time histories for each trim angle are plotted in Fig. 6.7 & Fig. 6.8 for the 16 cm and 5 cm drop heights respectively. Two features occur in the pressure time history as the trim angle increases. First, there is a delay in the peak pressure time with respect to the zero degree impact. This delay is present since as the angle increases the first point to

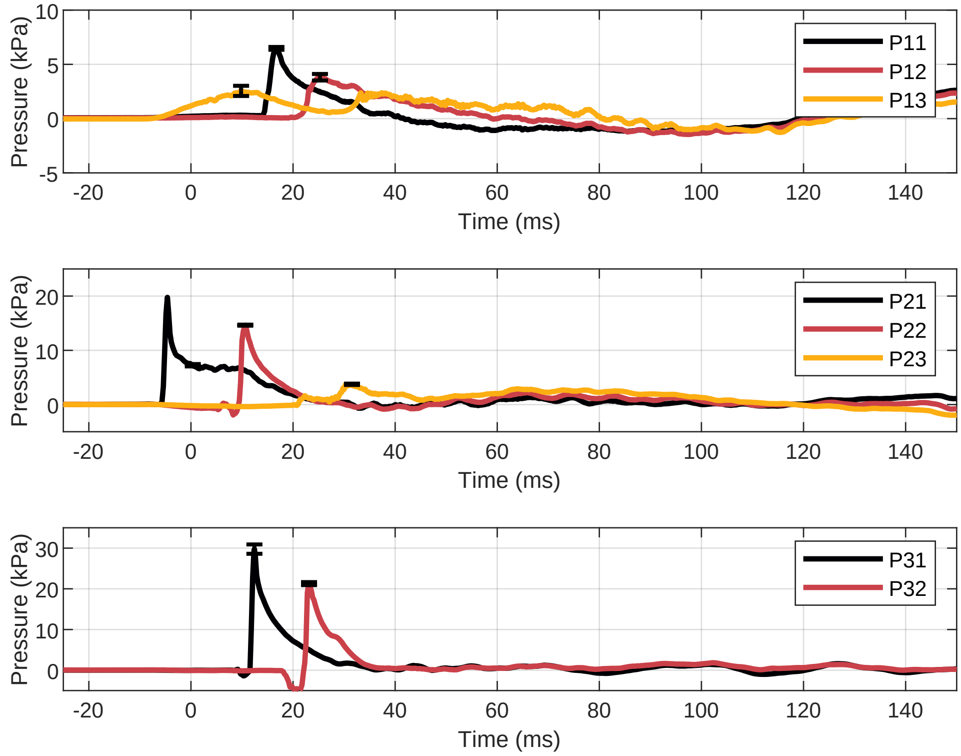

Figure 6.6: 0-deg 16 cm Pressure

impact the water is the keel and thus the spray root must travel farther to reach the pressure sensors. Second, the magnitude of the peak pressure decreases as the trim angle increases.

This trend is more apparent in the 16cm drop through the scatter plots in Fig. 6.11 and when only the time history of the first row is plotted, as shown in Fig. 6.9 and Fig. 6.10. As was shown through the kinematics displayed in Fig. 6.4, the peak acceleration of the model decreases as the trim angle of the model increases. These two findings corroborate each other and increase the confidence in the experimental results.

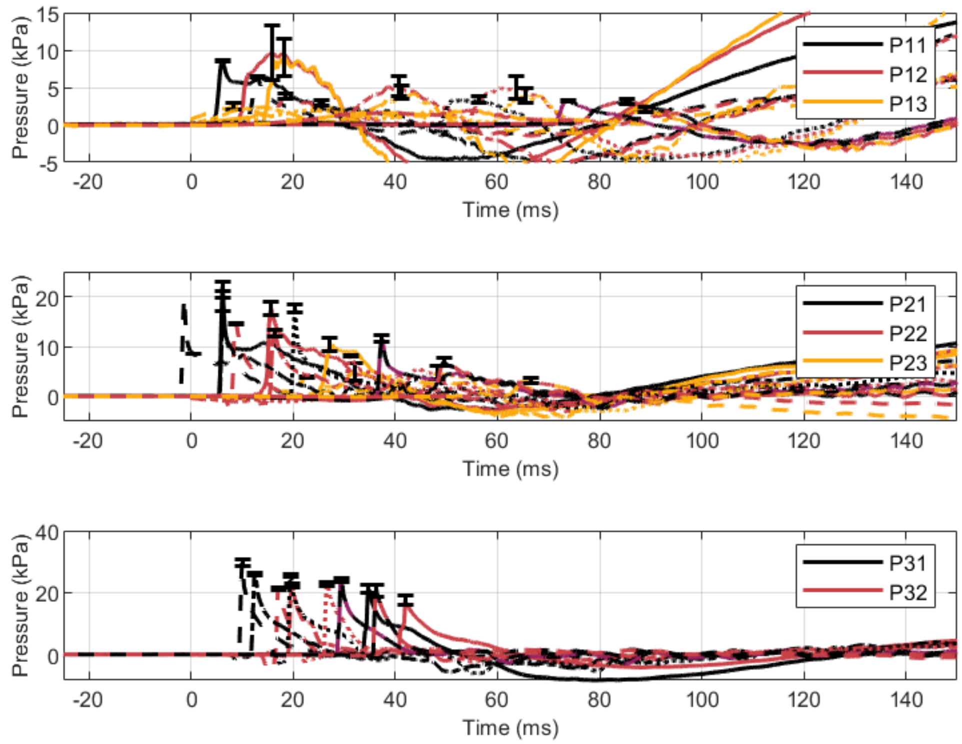

Figure 6.7: Pressure time history for all impact trim angles at 16 cm Drop Height

6.3 Strain

Strain measurements were taken to verify the model is rigid. The strain gauges are aligned transversely on the model and measure the change in deformation in the direction of the keel to the chine. The average strain measurements for the 16cm drop height at an 0-deg trim angle can be seen in Fig. 6.12. The LCG measures the highest amount of strain. This measurement is supported by the fact that the LCG is seeing the highest magnitude of peak pressure and has the largest unsupported area. Interestingly, the strain 2 gauge, located at the midpoint between the bow and LCG, is measuring lower strain than the bow gauge, even though there is significantly more unsupported area at the midpoint than the bow and

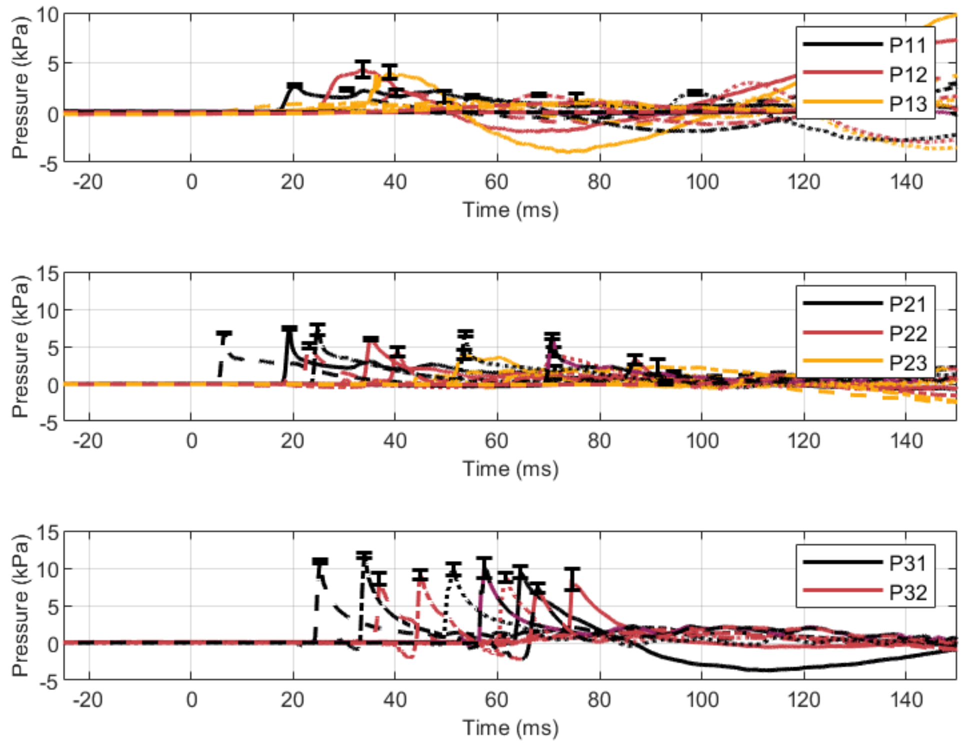

Figure 6.8: Pressure time history for all impact trim angles at 5 cm Drop Height

the midpoint experiences higher peak pressures. One possible reason that this behavior is occurring could be due to variability in composite stiffness from local variations in the fiber-matrix ratio. To further evaluate the structural behavior of the hull bottom, a technique such as stereoscopic digital image correlation (S-DIC) should be implemented to gain better spatial resolution of the hull deflection.

Although the model was instrumented with strain gauges with the intention of ensuring that the model was rigid, they produced some interesting results. The average strain for each trim angle at the 16 cm drop height is shown in Fig. 6.13. Unfortunately, for the 16 cm drop height across all trim angles, the model was not rigid along its entire length. The LCG strain gauge measured the highest strain just after impact. This corresponds with

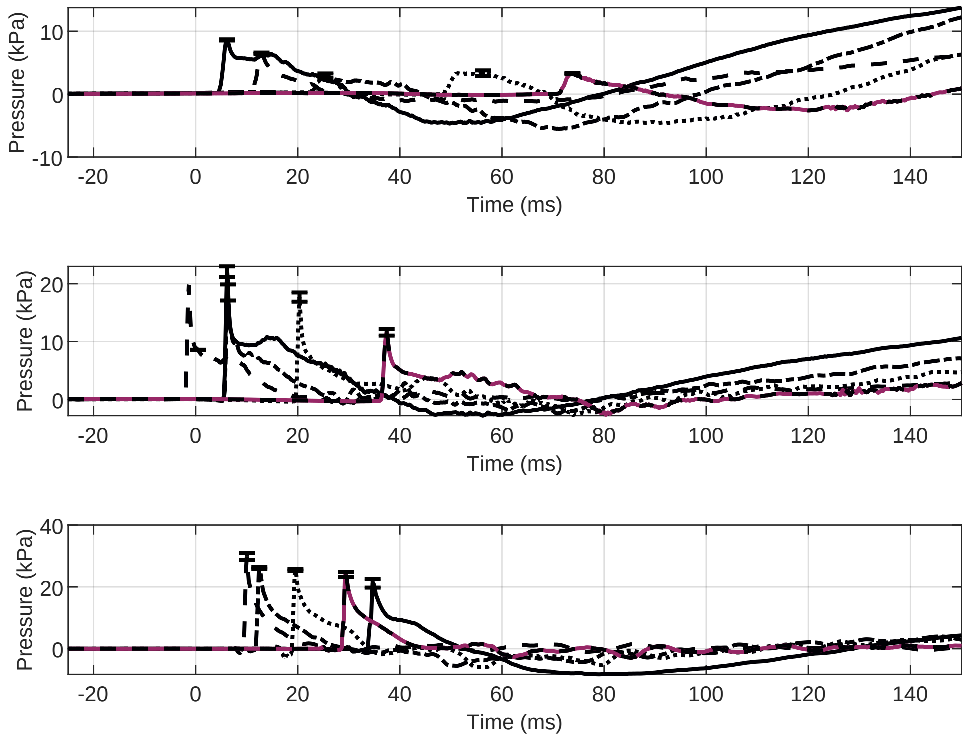

Figure 6.9: Pressure time history at the first row of pressure sensors for all impact trim angles at 16 cm Drop Height

predictions since this prismatic section of the model has the largest unsupported area. As the trim angle increases, the peak strain value at the LCG follows a linear trend. This means that as the angle increases from 0-4 degrees the impact loading at the LCG is increasing. In addition, right after impact, where the strain at the LCG and bow is increasing in tension, the midpoint is undergoing compression. This suggests that there is an interesting deformation pattern across the bottom of the hull. The same general trends are observed in the 5cm drop height strain as in the 16 cm drop height strain, except the strain for the 5cm drop height case is decreased by half, as seen in Fig. 6.14. This decrease is proportional to the decrease in impact velocity. These trends in peak strain values are best visualized in scatter plot in Fig. 6.15.

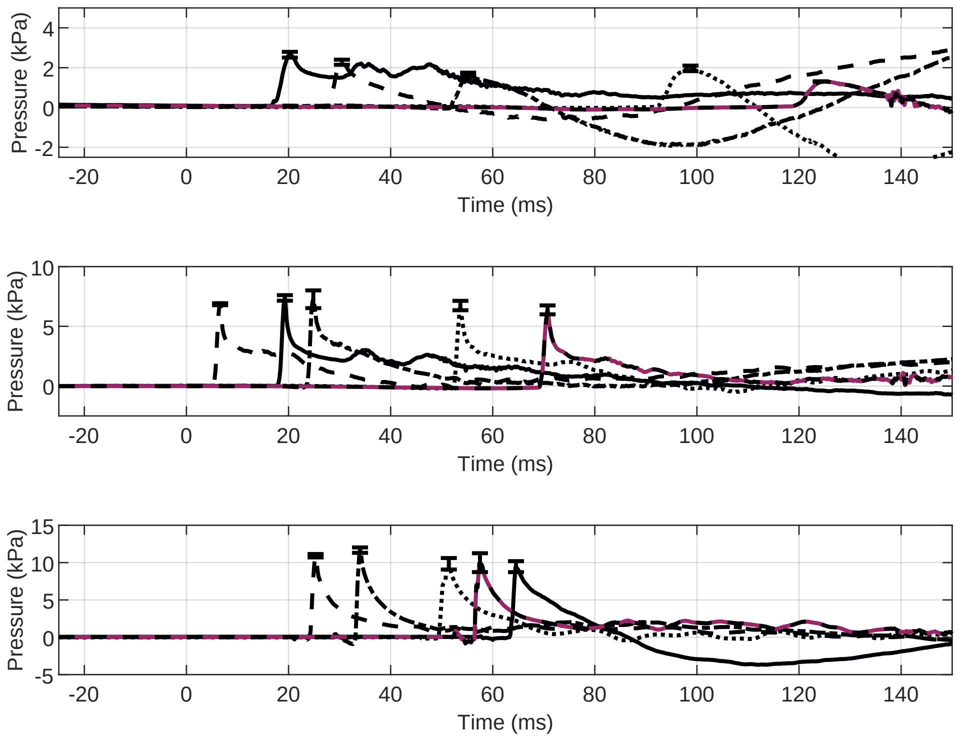

Figure 6.10: Pressure time history at the first row of pressure sensors for all impact trim angles at 5 cm Drop Height

6.4 Spray Root Visualization

The physical interpretation of the delay of the peak values can be visualized through the bottom camera videos. These videos allow the spray root to be visualized as it propagates along the bottom of the hull. In order to capture the entire length of the hull, two cameras were used. The frames from these two cameras are then stitched together using the grid pattern drawn on the bottom of the hull. The following series of frames depicts the hull at different stages of penetration during the drop event. Fig. 6.16 shows frames throughout a 0-degree angle impact, during the prismatic portion of the model the spray root propagates perpendicularly from the keel to the chine. In Fig. 6.16a immediately after impact, the

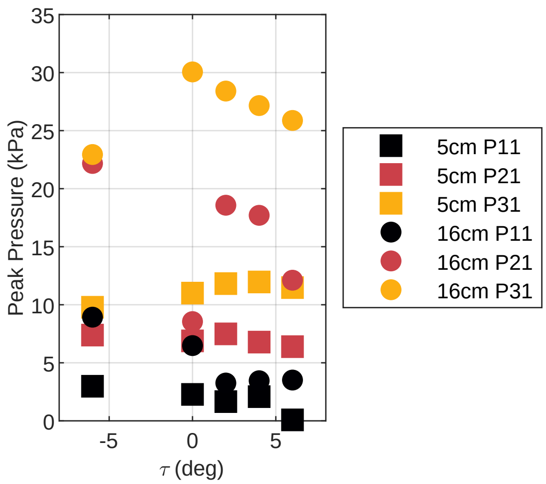

(a) Peak Pressure vs Impact Trim Angle

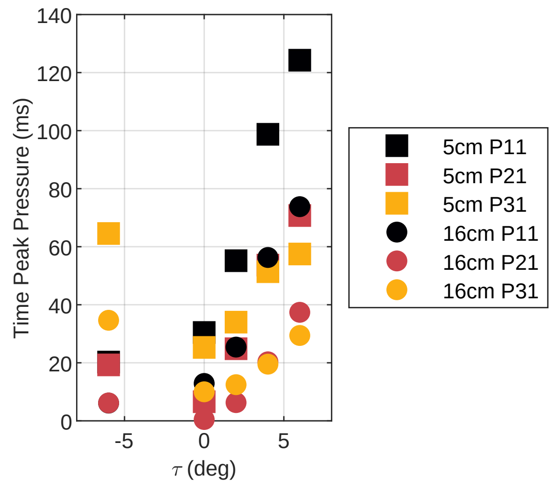

(b) Pressure Peak Time vs Impact Trim Angle

Figure 6.11: Scatter plots illustrating how the pressure peak amplitude, (a) and time, (b), vary with impact angle

majority of the keel has been wetted. This wetted area would spread to the transom, however there is a defect in the original USNA model, which has been copied in the Virginia Tech model for consistency. The slight upwards slope at the stern means that the keel at the transom will submerge later than the rest of the keel in the prismatic section. In addition, as the model continues to submerge, Fig. 6.16b - 6.16d, 3D effects can be observed at the transom. The 3D effects are identified through the slight curving of the spray root as it reaches the transom. The curvature in the spray root indicates a reduced spray root velocity. The reduction in velocity is caused by flow escaping over the transom rather than just over the chine. The escaping flow leads to a reduction in pressure. At the bow, the spray root curves in following the waterlines, and propagates in the direction of steepest ascent, perpendicular to the waterlines.

Fig. 6.17 depicts frames for the 2-deg impact at similar levels on penetration to those displayed in Fig. 6.16. In comparison of the two, it can clearly be observed that the transom impacts the water first, Fig. 6.17a. From this point, the spray root propagates in the direc-

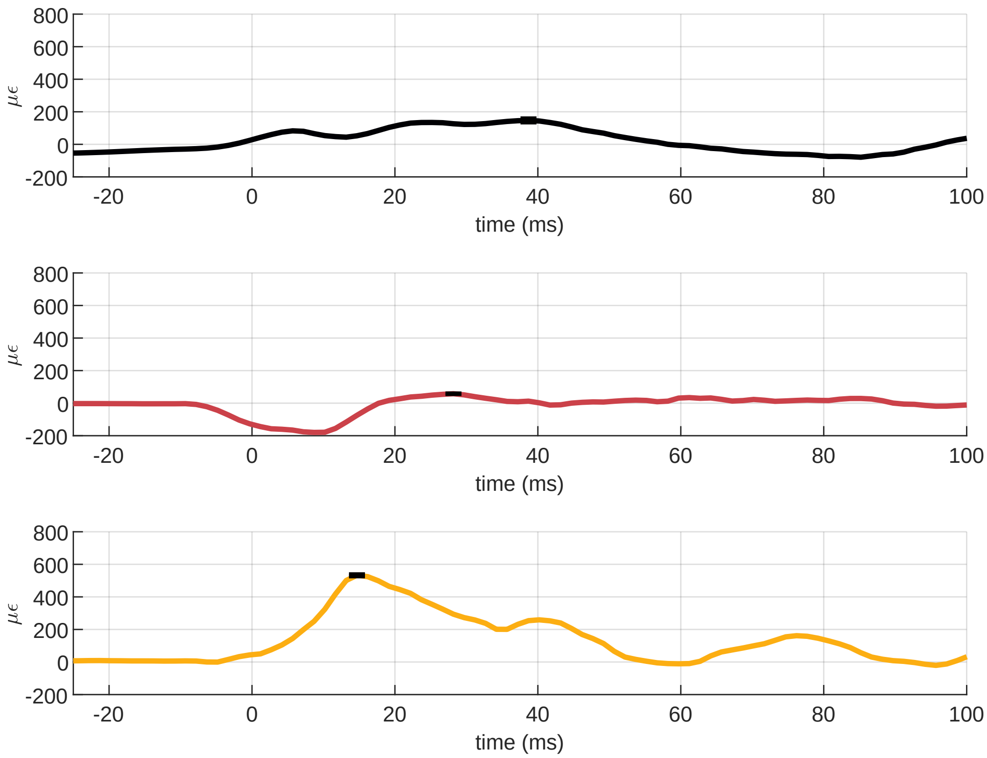

Figure 6.12: 0-deg 16 cm Strain

tion of steepest ascent, which is at an angle from the keel, rather than perpendicular from the keel to the chine Fig. 6.17b and Fig. 6.17c. As the spray root propagates forward it begins to curve in more towards the bow, Fig. 6.17d. The curving occurs due to the rise of the bow stem and the increase in deadrise near the bow.

Fig. 6.18 depicts frames for the 4-deg impact. As seen in the pressure and acceleration time delay scatter plots, Fig. 6.11 and Fig. 6.4, as the angle increases, the impact event takes longer, and the model must submerge further to meet the equilibrium condition. The lengthened period of the slamming event means that frames at similar time steps may not be selected, since they show a smaller difference. To stay comparable with the images depicted in Fig. 6.16 and Fig. 6.17, frames have been selected at similar levels of hull wetting. Take note

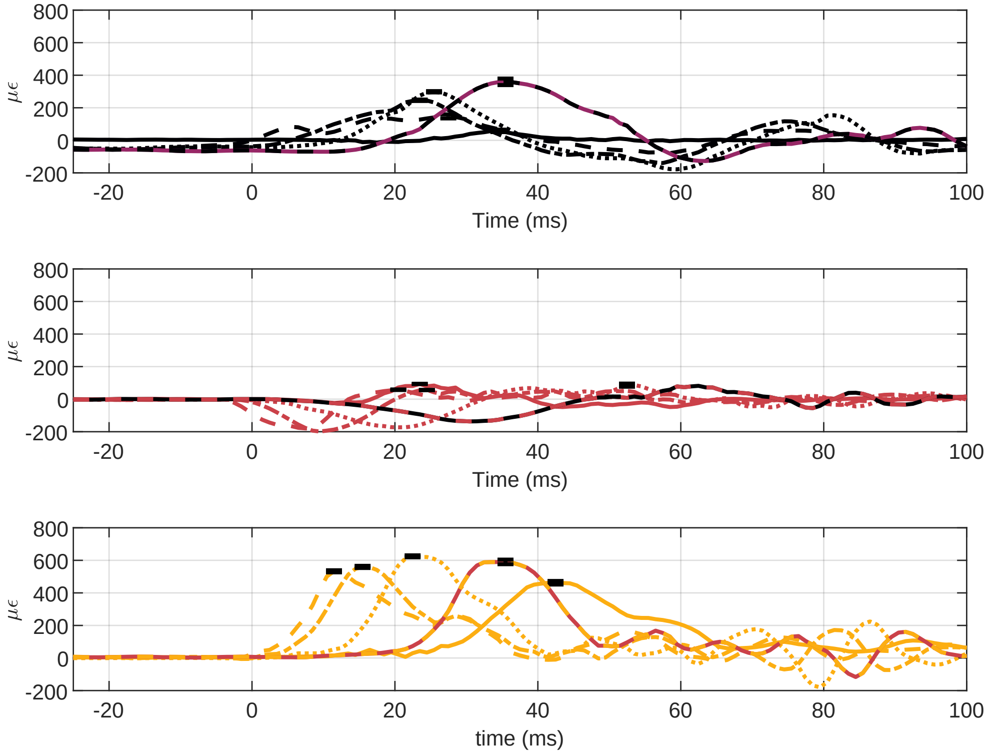

Figure 6.13: Strain time history for all impact trim angles at 16 cm Drop Height

that in comparison to the 2-deg frames, the 4-deg frames are spaced out over a significantly longer period of time. The increase in time corresponds to the decrease in peak acceleration, pressure, and increasing pulse widths. Overall, the trends of the spray root propagation identified in the 2-deg case are continued and accentuated in the 4-degree case. The angle of the spray root to the keel is greater. This is caused by the change in the direction of steepest ascent. As the model is pitched more bow up, the spray root begins to propagate more longitudinally rather than transversely. This is seen in the bottom view cameras as the angle of the spray root to the keel increases.

Fig. 6.19 depicts frames at similar points of penetration to the above series of figures for a 6 degree bow up impact. The trends that have been identified in both the 2 and 4 degree

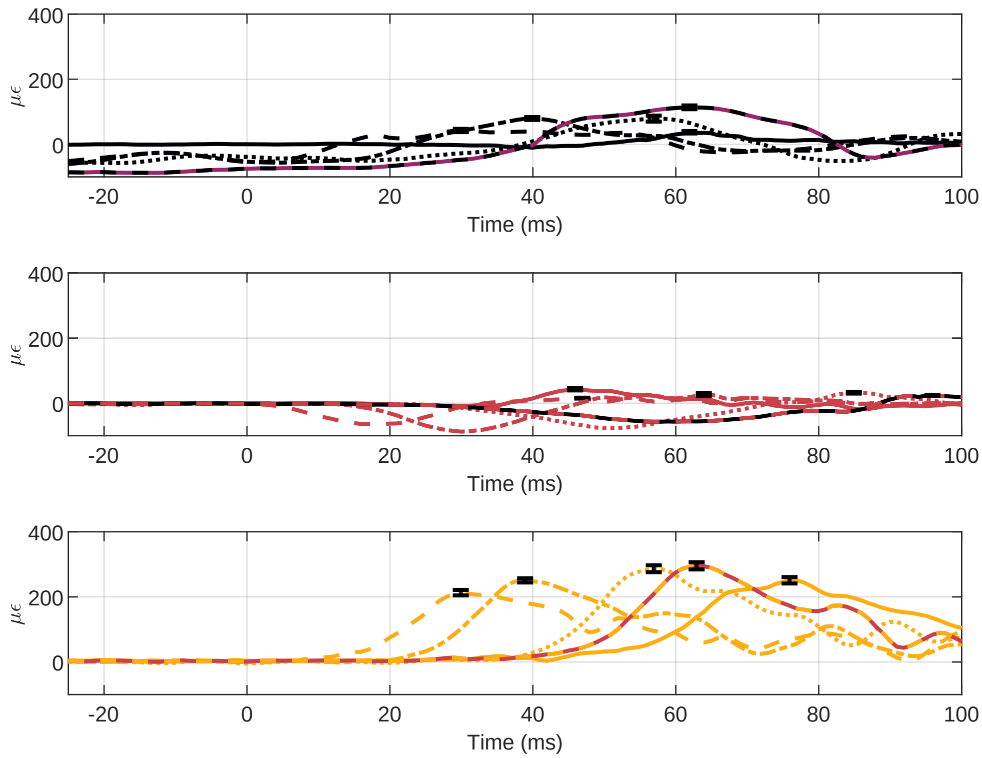

Figure 6.14: Strain time history for all impact trim angles at 5 cm Drop Height

cases continue to progress. The slamming event takes place over a longer period of time and the angle of the spray root to the keel continues to increase.

Fig. 6.20 depicts the frames for the -6 degree impact case. The duration of the impact is similar to that to the positive 6-degree bow up case. However, the propagation pattern of the spray root differs significantly from that for the bow up cases. For the bow down cases, the bow stem penetrates the water first.The spray root rapidly reaches the chine at the bow and progresses along the prismatic section at an angle similar to that of the positive 6 degree case. This symmetry is expected since the relative angle hull bottom in the prismatic section is the same for both the 6 degree bow up and bow down cases.

If the anticipated waterline is projected onto the individual frames, the 3D effects can be

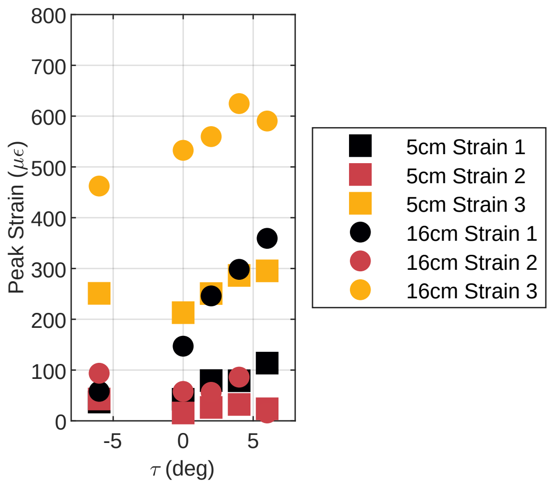

(a) Peak Strain vs Impact Trim Angle

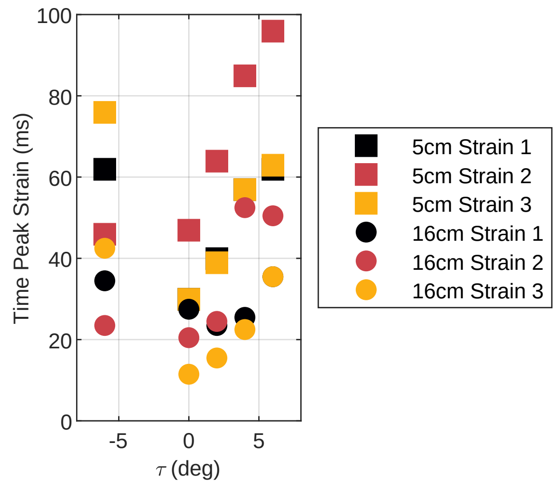

(b) Strain Peak Time vs Impact Trim Angle

Figure 6.15: Scatter plots illustrating how the strain peak amplitude, (a) and time, (b), vary with impact angle

better observed along the length of the hull. Just after the impact moment, there does not appear to be any significant 3D effects as seen in Fig. 6.21.

As the model continues to enter the water, the 3D effects become more apparent as the spray root diverges more from the anticipated waterline, seen in Fig. 6.22. Longitudinally the spray root location (seen in the pictures) matches the waterline location (slices from GPPH 3D model) well. However, transversely the spray root begins to have more curvature than the waterlines. There is more water pile up in the experiment above the waterline at the center of the model than near either end. The spray root bows out in the middle, with the forward most and aft most point of the spray root matching the waterline. The outward curvature of the spray root is caused by the spray root traveling faster near the center of the model.

These effects are further developed as the model continues to submerge deeper into the water, seen in Fig. 6.23. The curvature of the spray root in comparison to the waterline is more apparent.

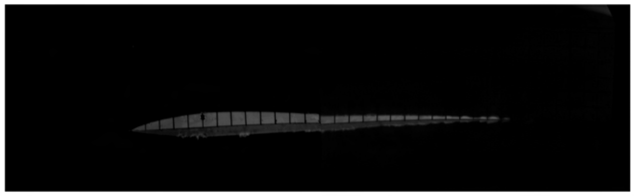

(a) 0-deg Slam 3 ms after impact

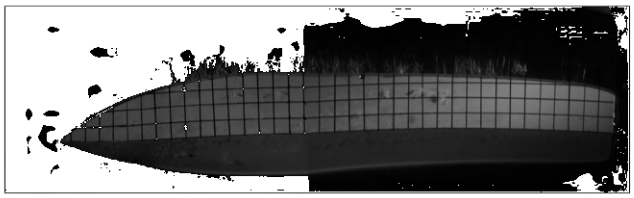

(b) 0-deg Slam 14 ms after impact

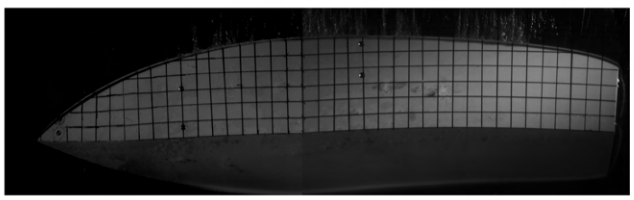

(c) 0-deg Slam 22.5 ms after impact

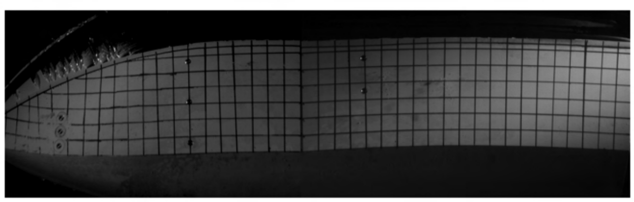

(d) 0-deg Slam 92 ms after impact

Figure 6.16: Extracted from high-speed video of 16 cm drop height for a 0-degree impact angle

6.5 Summary

The experimental measurements from this parametric study corroborate and support conclusions made from each type of measurement to form a relatively complete picture of the

(a) 2-deg Slam 7.5 ms after impact

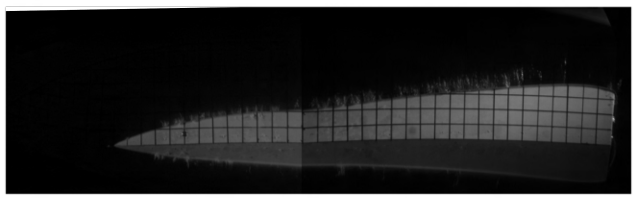

(b) 2-deg Slam 14 ms after impact

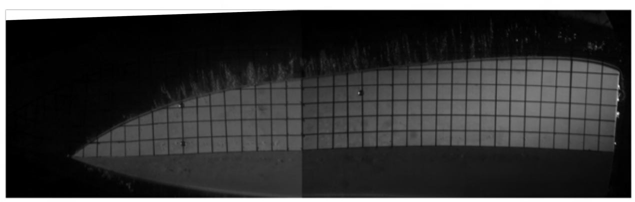

(c) 2-deg Slam 22.5 ms after impact

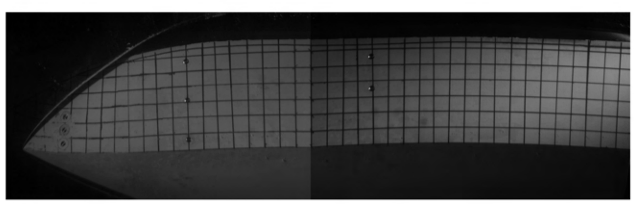

(d) 2-deg Slam 57.5 ms after impact

Figure 6.17: Extracted from high-speed video of 16 cm drop height for a 2-degree impact angle

kinematics and loading on a deep-vee prismatic planing hull as it impacts the water at different angles of trim. The results showed that as the model was trimmed bow up, the impact acceleration at first increased slightly, before beginning to decrease. This change in acceleration was attributed to a change in the rate of increase of buoyancy. Increasing trim also leads

(a) 4-deg Slam 7.5 ms after impact

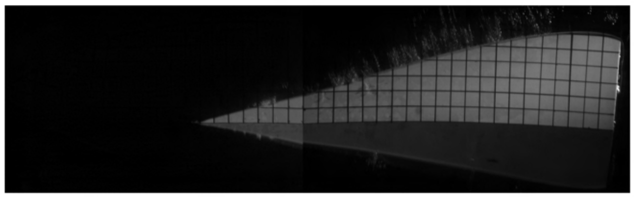

(b) 4-deg Slam 22.5 ms after impact

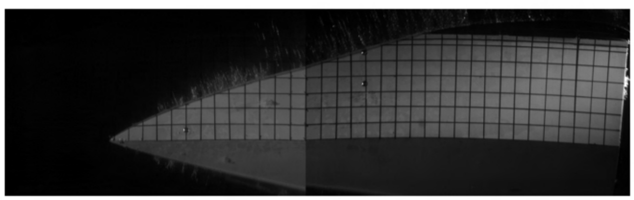

(c) 4-deg Slam 32.5 ms after impact

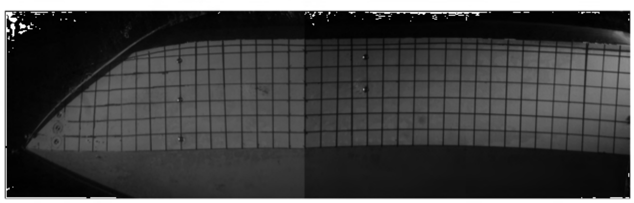

(d) 4-deg Slam 72.5 ms after impact

Figure 6.18: Extracted from high-speed video of 16 cm drop height for a 4-degree impact angle

to an increased acceleration pulse width and a delayed peak time. The delay and extended duration of the impact event was seen across the results in the pressure, strain, velocity, and position readings. In addition the delay was visually noticeable through inspection of the bottom view cameras as the spray root velocity significantly slowed. As the trim angle

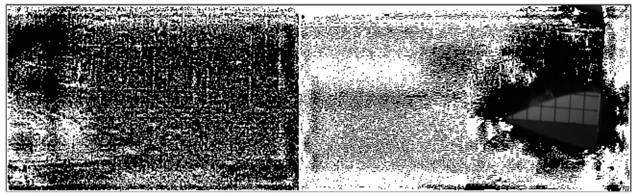

(a) 6-deg Slam 7.5 ms after impact

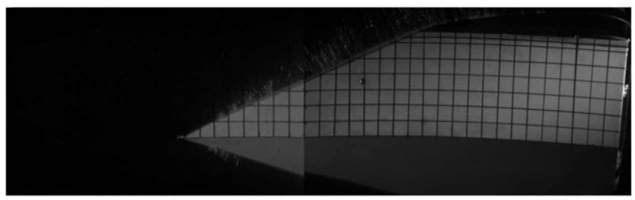

(b) 6-deg Slam 37.5 ms after impact

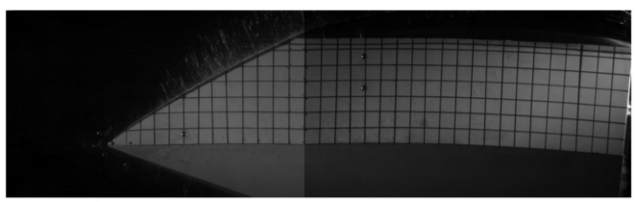

(c) 6-deg Slam 52.5 ms after impact

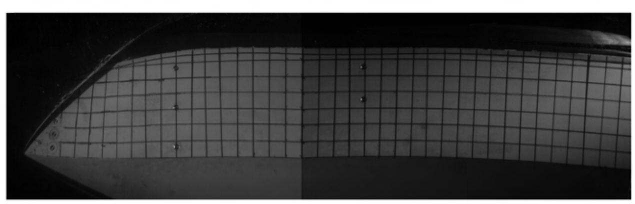

(d) 6-deg Slam 97.5 ms after impact

Figure 6.19: Extracted from high-speed video of 16 cm drop height for a 6-degree impact angle

was increased, the peak pressure magnitude had a decreasing trend, which corresponded to the increased distance that the spray root had to travel in order to reach the sensors. The strain initially showed an increase in peak magnitude as the trim angle was increased, which after reaching 4 degrees started to decrease. This was attributed to the increased loading

(a) -6-deg Slam 10 ms after impact

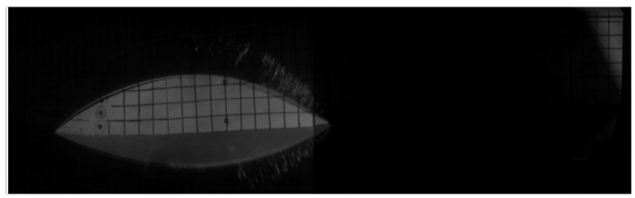

(b) -6-deg Slam 20 ms after impact

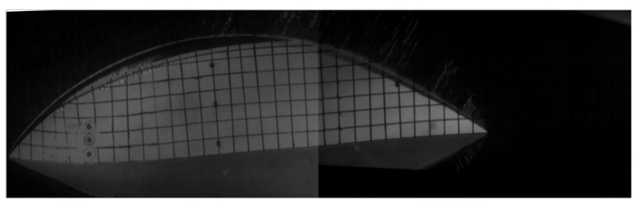

(c) -6-deg Slam 40 ms after impact

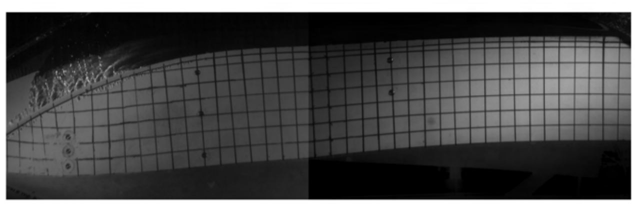

(d) -6-deg Slam 95 ms after impact

Figure 6.20: Extracted from high-speed video of 16 cm drop height for a -6-degree impact angle

on the prismatic section of the hull, since it was supporting more force more rapidly. As expected, the LCG showed the greatest strain since it had the largest unsupported area. However, instead of experiencing a decreasing peak magnitude at the midpoint and then at the bow, the midpoint peak was smaller than that of the bow. This led to the conclusion

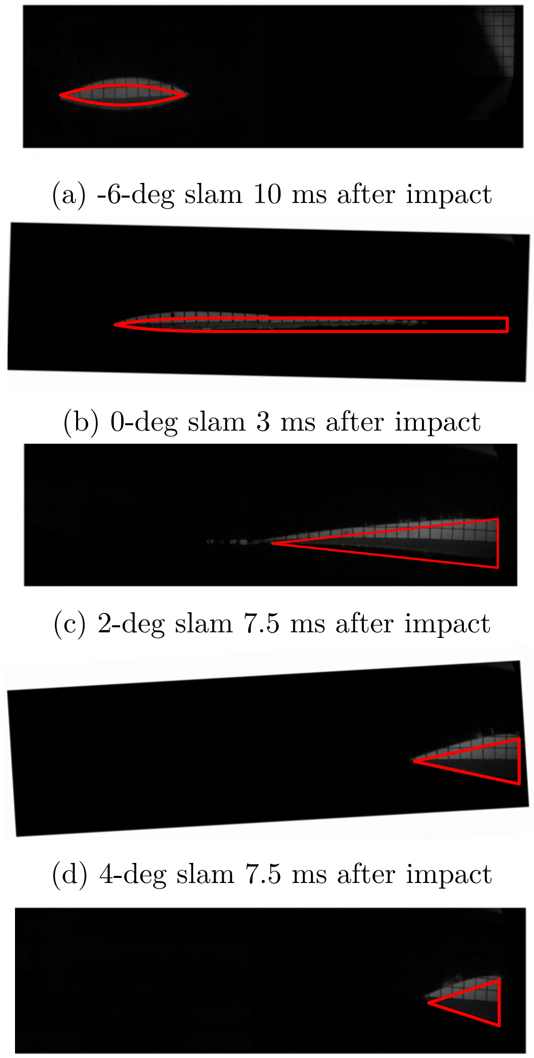

(a) -6-deg slam 10 ms after impact

(b) 0-deg slam 3 ms after impact

(c) 2-deg slam 7.5 ms after impact

(d) 4-deg slam 7.5 ms after impact

(e) 6-deg slam 7.5 ms after impact

Figure 6.21: Waterline projected onto spray root (a) frames

that the hull bottom was undergoing a complex deformation pattern. When the model was trimmed 6 degrees bow down, there was a significant change in trends. The first point of penetration was the bow stem rather than the transom. This leads to the spray root propagating in the opposite direction as the bow up cases. A delay in peak time and an increase in event duration was still observed. However, the pressure peaks at the bow occurred before the LCG, as would be expected. This change in orientation also led to an increase in bow

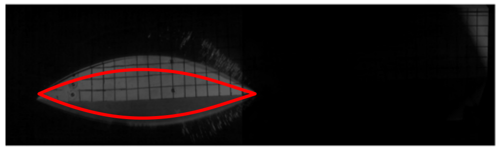

(a) -6-deg slam 20 ms after impact

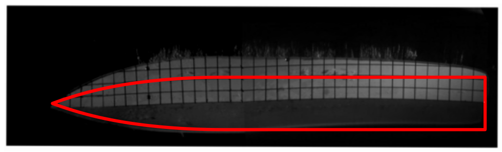

(b) 0-deg slam 14 ms after impact

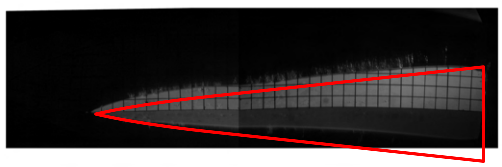

(c) 2-deg slam 14 ms after impact

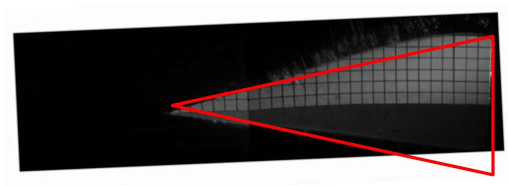

(d) 4-deg slam 22.5 ms after impact

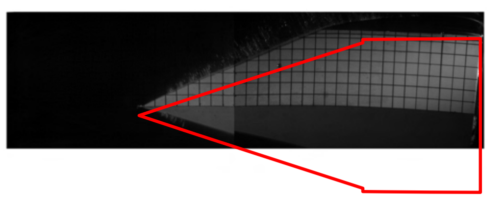

(e) 6-deg slam 37.5 ms after impact

Figure 6.22: Waterline projected onto spray root (b) frames

peak pressure magnitude and a decrease in LCG peak magnitude, which corresponds to the increased distance which the spray root had to travel to reach the pressure sensors. The agreement of the conclusions made using a wide array of sensors increases the confidence in these preliminary results and their insight to future findings through controlled motion investigations.

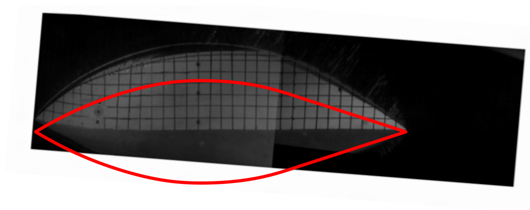

(a) -6-deg slam 40 ms after impact

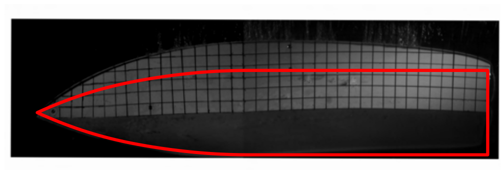

(b) 0-deg slam 22.5 ms after impact

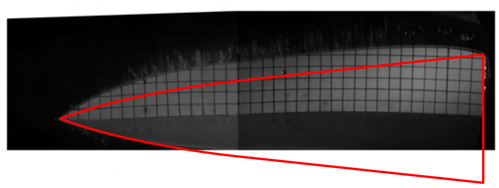

(c) 2-deg slam 22.5 ms after impact

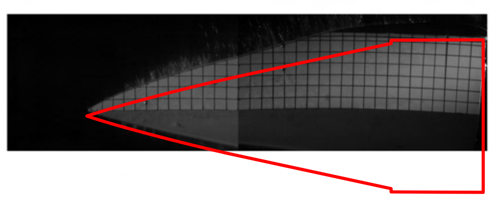

(d) 4-deg slam 32.5 ms after impact

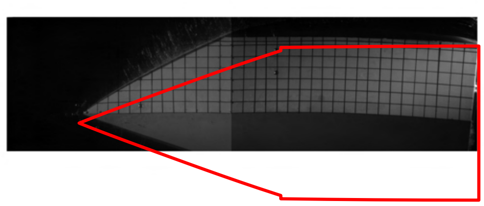

(e) 6-deg slam 52.5 ms after impact

Figure 6.23: Waterline projected onto spray root (c) frames

Chapter 7

Conclusions & Future Work

7.1 Conclusions

The body of work presented in this thesis can be broken into two main sections - analysis of tow tank experiments using machine learning and model drop experiments. The data analysis performed in the effort to develop an experimental matrix for the parametric study of slamming events was inspired by and adapted from machine learning techniques. These techniques were used to categorize slamming events based on the time history of the vessel motions in model sea state 3 irregular waves. The implemented algorithm identified three main slamming categories. The categories identified by the machine learning algorithms match closely to the type alpha, bravo, charlie slams identified by Riley et al. (2010, 2012, 2017) [2, 10, 11]. This analysis also highlighted an increasing density of high peak acceleration slamming events as impact trim increased. These results prompted investigation into the angular parameters are the impact heave and surge velocity. **The investigation into angular velocity and acceleration showed a rough trend between bow down angular velocity and increasing peak bow acceleration. The investigation into heave and surge velocity made the impactful conclusion that the heave velocity plays a significantly more influential role in slamming severity than the surge velocity.** This conclusion supported the validity of wedge and model drop experiments as applicable simplifications of the complete slamming problem.

The analysis conducted on the US Naval Academy experiments yeilded two experimental matrices. The first experimental matrix encompassed the complete parametric study to be completed using the newly renovated Virginia Tech Advanced Towing Facility and vertical planar motion mechanism (VPMM). This parametric study will test the effects of hull flexural rigidity, LCG location, impact heave and surge velocity, trim, angular velocity, and angular acceleration. If this parametric study is completed in full there will be 14400 distinct experimental data points. The experiments presented in this thesis are for a cross-section of this larger experimental matrix and performed with a simplified experimental setup. A model drop experimental setup was designed and built, which is only free to heave. Using this setup and a rigid model, experiments were performed to evaluate the effects of trim and heave velocity. The maximum bow down trim angle was constrained by the forward buoyancy of the model since no bow up angular velocity could be incorporated into the slamming event.

The results from the model drop experiment demonstrated that the increasing heave velocity increased peak acceleration, pressure, and strain on the hull. As the model was trimmed bow up, the peak acceleration was increased slightly for small trim angles, less than 2 degrees; after which, the peak acceleration began to decrease. In addition, as the impact trim angle was increased, there was an increasing discrepancy between the bow and LCG acceleration. This discrepancy was attributed to racking in the experimental setup caused by the moment generated by the model when the transom or the bow impacted the water first. These results emphasize the importance of angular velocity and acceleration in slamming of a hull geometry in comparison to a vertical wedge drop experiment. The peak pressure magnitude decreased with increases in absolute impact angle. The decreasing trend corresponds with the increased distance that the spray root must travel to reach the pressure sensors. The peak strain magnitude at the LCG exhibited a similar trend to the peak acceleration magnitude, with increasing trim the strain increased until 4 degrees, after which the peak strain magnitude decreased. The peak strain at the LCG was significantly higher than the strain at the midpoint and bow. The increased strain is due to the increased unsupported area in the prismatic section of the hull. The hypothesis was that the strain would decrease towards the bow as the unsupported area decreased. However, the strain at the bow was greater than the strain at the midpoint, which has a higher unsupported area, this intriguing result prompts the use of more advance experimental techniques to measure the deformation of the hull. A delay in peak time and increase in event duration with increase in impact trim angle was present across all measurements.

When the model was trimmed down to -6 degrees, the trends identified in the bow up cases appeared to be mirrored about an even keel impact. For bow down slams, the bow stem becomes the first point to penetrate the water surface rather than the transom, causing the spray root to propagate in the opposite direction. As would be expected, an increase in bow peak pressure was observed, with a corresponding decrease in LCG peak pressure. A decrease in peak acceleration was also experienced by the model. Again, the peak times of all signals were delayed and the duration of the slamming event increased in comparison to the even keel impact.

Through the visualization of the spray root with high-speed video of the bottom of the hull, an obvious decrease in spray root velocity was observed for higher impact trim angles as the spray root propagated along the hull. Additionally as the impact trim was increased the angle between the keel and the direction of spray root propagation decreased. This finding showed that the spray root propagated in the direction of steepest ascent.

The acceleration, pressure, and strain all demonstrated similar trends in peak magnitude and delay with variation in impact angle. The agreement of the trends across all of the measurements taken increases the confidence that the sensors are accurately capturing the physics of the experiment. The trends observed in the model drop experiments will help provide insight and inform hypotheses as the parametric study progresses with controlled motion experiments using the VPMM.

7.2 Future work

There are still many gaps in the literature regarding extrapolating the results wedge drop experiments to the design of high-speed craft. Specifically, the inclusion of flexibility into structural design so that full scale vessels may reap the benefits of lighter weight more efficient structures. The experimental results of only a subset of the complete parametric study of slamming events were presented in this thesis, as the study is still ongoing. The Hydroelasticity Lab has a substantial amount of work to be completed in performing and analyzing the results of the complete parametric study using the Virginia Tech Advanced Towing Facility and vertical planar motion mechanism (VPMM). Initial series of experiments with this setup must use the information gained from each set of experiments, in combination with a design of experiments process to inform the researcher of what data points provide the most valuable information to both academia and industry.

In order to capture and analyze the complex deformation pattern experienced by the hull, more advanced experimental techniques and sensors must be employed such as stereoscopic digital image correlation (S-DIC) or Li-DAR. These systems will likely experience a significant amount of vibration. Thus the mounting rigs for the sensors must also be instrumented to subtract any error in the measurements due to vibration and the motion of the rig.

The results of future experiments will not only provide information on how to improve the design of high-speed craft, but also their operation. Information regarding the effects of impact trim, angular acceleration and velocity will generate useful knowledge regarding the best way to impact a wave. This information can be used by academia and industry to develop active and passive control systems to mitigate the severity of slamming events by changing the operating attitude of the vessel. Operators will also benefit from this information by changing the loading and trim of the vessel to expand the safe operating envelope

Bibliography

[1] C. Judge, M. Mousaviraad, F. Stern, E. Lee, A. Fullerton, J. Geiser, C. Schleicher, C. Merrill, C. Weil, J. Morin, M. Jiang, and C. Gilbert, "Experiments and cfd of a high-speed deep-v planing hull - part ii: Slamming in waves," *Applied Ocean Research*, 2020.

[2] M. Riley, T. Coats, K. Haupt, and D. Jacobson, "The characterization of individual wave slam acceleration responses for high speed craft," *The 29th American Towing Tank Conference*, 08 2010.

[3] C. Ikeda and C. Judge, "Slamming impacts of hydrodynamically–supported craft," in *ASME 2014 33rd International Conference on Ocean, Offshore and Arctic Engineering*, pp. V08AT06A035–V08AT06A035, American Society of Mechanical Engineers, 2014.

[4] L. Cao, "Singular value decomposition applied to digital image processing," *Division of Computing Studies Arizona State University Polytechnic Campus*, 2006.

[5] O. Harrison, "Machine learning basics with the k-nearest neighbors algorithm | by onel harrison | towards data science.," 2021.

[6] C. M. Ikeda and C. Q. Judge, "Slamming Impacts of Hydrodynamically–Supported Craft," vol. Volume 8A: Ocean Engineering of *International Conference on Offshore Mechanics and Arctic Engineering*, 06 2014.

[7] C. Judge, M. Mousaviraad, F. Stern, E. Lee, A. Fullerton, J. Geiser, C. Schleicher, C. Merrill, C. Weil, J. Morin, M. Jiang, and C. Gilbert, "Experiments and cfd of a

high-speed deep-v planing hull - part i: Calm water," *Applied Ocean Research*, pp. –, 2020.

[8] G. Fridsma, "A systematic study of the rough water performance of planing boats," tech. rep., Davidson Laboratory, Stevens Institute of Technology, 1969.

[9] N. Husser, C. Judge, and S. Brizzolara, "Validation of forced heave simulations on a planing hull," 2021.

[10] M. Riley, T. Coats, K. Haupt, and D. Jacobson, "Ride severity index - a new approach to comparing wave slam acceleration responses of high-speed craft," *Ship Systems Integration and Design Department Technical Memorandum*, 11 2012.

[11] M. Riley and T. Coats, "Lessons learned from full-scale seakeeping trial acceleration data for high- speed planing craft and implications for scale model testing," *The 30th American Towing Tank Conference*, 10 2017.

[12] J. Javaherian, M., Z. Ren, C. Judge, and C. Gilbert, "Structural response due to the slamming of high-speed craft by water entry and towing tank experiments," *33rd Symposium on Naval Hydrodynamics*, 05 2020.

[13] M. J. Javaherian, Z. Ren, C. M. Gilbert, *et al.*, "Flow visualization, hydrodynamics, and structural response of a flexible wedge in water entry experiments," in *SNAME Maritime Convention*, The Society of Naval Architects and Marine Engineers, 2019.

[14] Z. Ren, Z. Wang, F. Stern, C. Judge, and C. Ikeda-Gilbert, "Vertical water entry of a flexible wedge into calm water: A fluid-structure interaction experiment," *Journal of Ship Research*, vol. 63, no. 1, pp. 41–55, 2019.

[15] Z. Ren, J. Javaherian, and C. Gilbert, "Vertical wedge drop experiments as a model for

slamming," 2019. SNAME Maritime Convention, Tacoma, WA, USA, 29 October to 1 November 2019.

[16] A. Bhardwaj, J. Javaherian, N. Husser, and S. Brizzolara, "Vertical wedge water-entry through experiments and simulation to explore three-dimensional hydrodynamic flow characteristics," 2021. International Conference on Fast Sea Transportation, Providence, RI 26-27 October 2021.

[17] L. Honey, C. Q. Judge, and C. M. Gilbert, "Slamming events of a planing hull and wedge water entry experiment: Comparisons and insights on fluid-structure interaction," in *SNAME Maritime Convention*, The Society of Naval Architects and Marine Engineers, 2021.

[18] H. Wagner, "The landing of seaplanes," Tech. Rep. Technical Note 622, 254, NACA, 1932.

[19] W. S. Vorus *et al.*, "A flat cylinder theory for vessel impact and steady planing resistance," *Journal of ship research*, vol. 40, no. 02, pp. 89–106, 1996.

[20] J. Armand and R. Cointe, "Hydrodynamic impact analysis of a cylinder," *Journal of offshore mechanics and Arctic engineering*, vol. 109, no. 3, pp. 237–243, 1987.

[21] E. Zarnick, "A nonlinear mathematical model of motions of planing boat in regular waves," Tech. Rep. DTNSRDC-78/032, David W. Taylor Naval Ship R&D Center, Carderock, MD, 1978.

[22] M. Shepheard, C. Q. Judge, and C. M. Gilbert, "Classification of slamming events in irregular waves measured through tow tank experiments," in *SNAME Maritime Convention*, The Society of Naval Architects and Marine Engineers, 2021.

[23] C. Judge and C. Ikeda, "An experimental study of planing hull wave slam events," in *30th Symposium on Naval Hydrodynamics*, 2014.

[24] G. Zeng, "Face recognition with singular value decomposition," *CISSE Proceeding*, 2006.

[25] M. Embree, *Matrix Methods for Computational Modeling and Data Analytics (Chapter 6: The Singular Value Decomposition)*, ch. 6. 2019.

[26] D. Savitsky, "Hydrodynamic design of planing hulls," *Marine Technology*, vol. 1, no. 1, 1964.

[27] S. Chuang, "Slamming of rigid wedge-shaped bodies with various deadrise angles," Tech. Rep. 2268, David Taylor Model Basin, Carderock, MD, 1966.

Appendices

Appendix A

GPPH Fabrication

USNA was gracious enough to lend Virginia Tech their 4' GPPH model. This model was used as a plug to create a female mold of the boat. This female mold was then used the fabricate the model used in the experiments. The final comparison can be seen in Fig. A.1

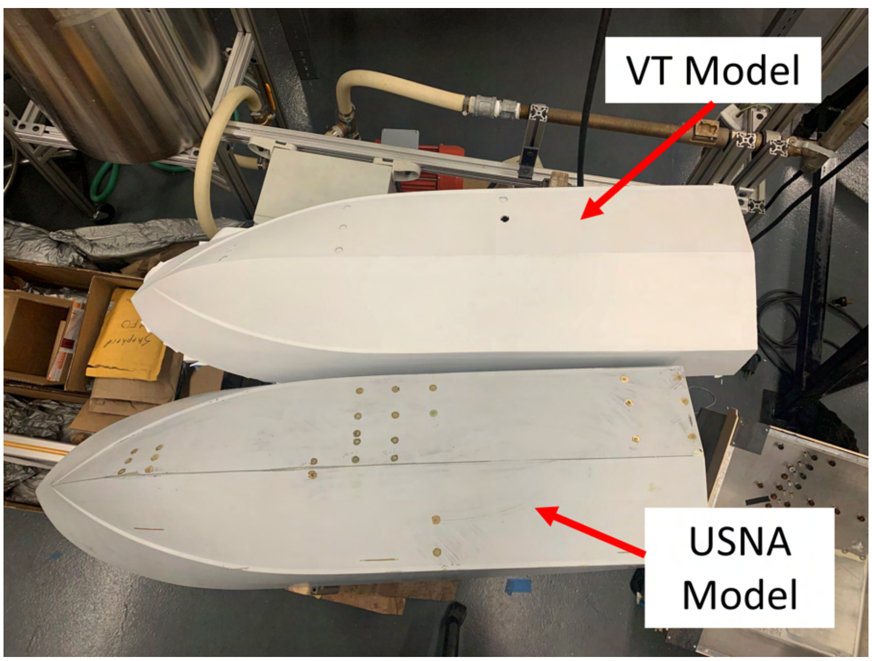

Figure A.1: Side by side of the USNA model and the recently constructed Virginia Tech Model GPPH.

A.1 Plug Preparation

The key to any good layup is good surface preparation. All tapes and markings on the

USNA model were first removed. The model was then cleaned with acetone to remove any residual adhesives etc...Once the model was clean, a few surface defects, including deep and surface scratches, chips, and dings were then repaired using an easy sanding epoxy based fairing compound. At the same time the holes from the pressure sensor mounts were also covered. It is important during this repair process to remember to work clean and only apply compound to areas that need it. It is easier to add more compound than to sand it off. The surface was prepared for fairing compound by sanding the damaged area to 120 grit to ensure good adhesion. The area was then cleaned off to remove any dust. The fairing compound was then applied and allowed to dry. Some of the deeper defects required multiple coats of fairing compound the build the surface. Between coats of fairing compound the area was lightly sanded to provide a good surface and promote a strong bond.

After repairing all surface defects, starting at 120 grit, entire model was flatted and sanded, paying close attention to areas around the chine to preserve the shape. After flatting, the model was then sanded to 800 grit. When changing grits the model was cleaned to ensure that no dust generated by the previous grit would cause scratches in the finer grit finish.

After sanding the model it was given another cleaning with acetone to ensure all dust was removed and the surface was ready to proceed to the next step. A melamine board was prepared to provide a flange area for the mold by cutting a hole in the center of the board just smaller than the model. The model was then tacked to the melamine backing board with vacuum sealant tape and clamped to the board to prevent any movement.

After the backing board and the model were joined, there is a small crease that undercuts the model between the model and the vacuum tape. This crease was filled with modeling clay, which was then fileted to provide a smooth transition between the model and the backing board. If this crease had not been filled with clay, during the layup it would have been filled with epoxy. This would make demolding a challenge as there would be a mechanical lock

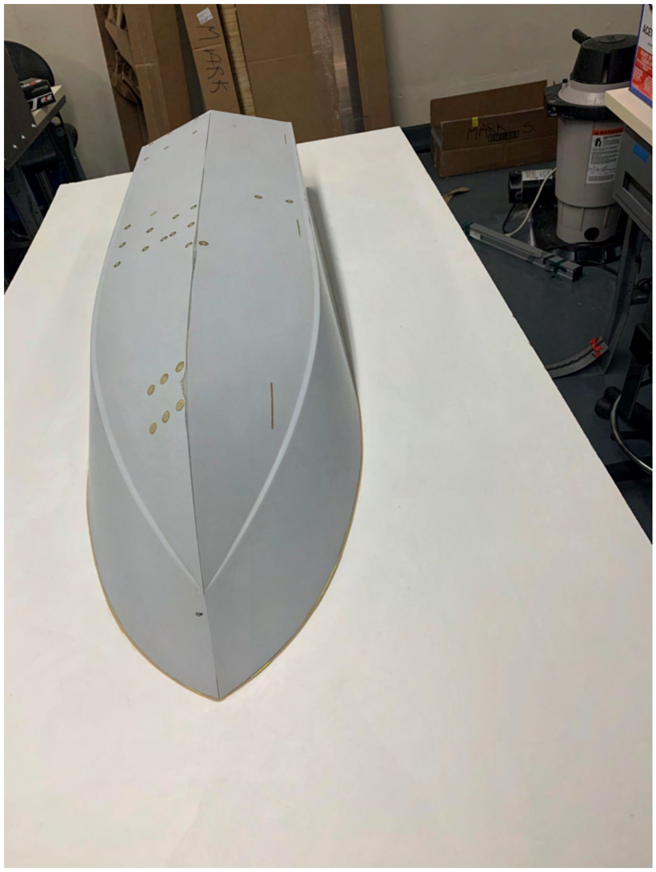

Figure A.2: USNA GPPH Model mounted to a melamine backing board

between the plug and the layup.

With the plug completely assembled, the next steps are to enhance the surface finish and ensure release. Four coats of release wax were applied to the plug. After waxing on there was approximately a five minute delay or until the wax hazed over before buffing the wax off. The waxing leaves a glossy surface, which will provide a better release and surface finish on the mold.

Figure A.3: Filling seam between backing board and USNA model with clay

A.2 Mold Fabrication

With the plug waxed, vacuum sealant tape is applied to the melamine board, and covered with painters tape BEFORE the application of release agent. If the tape is applied after release agent it will not stick. The painters tape helps to keep epoxy and fibers off of the vacuum tape. This precaution makes the vacuum bagging process go much more smoothly. After applying the sealant tape, four coats of PVA are applied within the area outlined by the vacuum tape. The first coat is a light mist or tack coat. The following three coats build a thin film green film which will ensure the release of the mold from the plug.

When the PVA is completely dry the layup can be performed. The following layup process

Figure A.4: Waxing the mold and backing board in preparation for the mold layup

described is a wet layup followed by a vacuum bag. There are multiple other options, including vacuum infusion etc… these options have their advantages and disadvantages. A wet layup with a vacuum bag was selected for these layups since it is relatively simple, does not require many additional material and produces a good surface finish and fiber-matrix ratio.

The stacking sequence for the mold layup is detailed in Table A.1. The surfacing veil conforms to the plug very well and produces a glossy class-A surface. This is backed by layers of oz twill weave to provide good adhesion to the surfacing veil and reduce print through. This is then backed by a 20oz tooling cloth which rapidly build strength and thickness. A thinner and weaker stacking sequence could be used for one off molds, but

Figure A.5: PVA release agent being applied to plug

since it is intended for this mold to have multiple uses it has been built for durability.

Table A.1: Layup Schedule for GPPH Mold

Layer #	# of Layers	Description
1	1	2oz Plain Weave Fiberglass
2	2	6oz Twill Weave Fiberglass
3	3	10oz Plain Weave Fiberglass
4	5	20oz Fiberglass Tooling Fabric

Each layer in the stacking sequence is cut to rough size before the layup and set out in order of use. The first layer is laid on top of the plug and wetted out with the epoxy from the center out. At the bow and the transom relief darts in the fabric had to be made to get the fabric to conform to the plug. As the layer is wetted out care was taken to ensure there were no bubbles of air between the fabric and the plug. This is especially important in the first few layers as they undergo the most stress during the release process and the cavities left by air bubbles significantly weaken the surface and can lead to chipping and cracking which will require future repair. Layer after layer the fabric is wetted out with epoxy, remembering to work clean and keep epoxy off of the vacuum tape.

Figure A.6: First layer of the mold being wetted out with epoxy

After all of the layers have been wetted out, a peel ply is applied on the plug, which separates the layup from the vacuum bagging materials to follow. After the peel ply, a cotton bleeder cloth is applied, which soaks up any extra resin. The ports for the vacuum are then placed on top of the bleeder fabric. Additional bleeder fabric is placed under the vacuum ports to prevent any resin from being sucked into the vacuum. After the bleeder fabric, the vacuum bag is applied. The bag must be oversized, since it needs extra material to work its way into all of the creases and crevasses in the plug and apply pressure to the composite. The additional bag is taken up by pleats in the vacuum tape. Sticking the vacuum bag to the vacuum tape requires clean and delicate work to prevent wrinkles in the bag at the tap which become leaks. Small wrinkles can often be worked out by massaging and stretching the bag into the tap. After the vacuum bag is completely sealed, small holes are cut above the vacuum ports to connect the vacuum to the bag. The vacuum tubing is then connected and the vacuum turned on. The vacuum bag should suck down onto the plug. As the bag is sucking down onto the plug, adjust the bag to make sure that it thoroughly compresses into the corners etc… A good vacuum has been achieved when the pressure gauge reads above 20 psi, perfect bags typically read between 25 - 30 psi depending on the vacuum pump. If the pressure is not above 20 psi, you have one or more leaks. To find a leak inspect the vacuum tape and ensure that there are no wrinkles in the bag or gaps at pleats or butt joints in the tape. It is generally a good idea to go around the bag and press down on all of the tape. By holding your ear to the bag you can generally hear a leak, denoted by a high pitch whistling as it sucks air into the bag. If the leak is not in the tape, check the vacuum port connections to the plug, and ensure they are tight and not leaking. Once a good vacuum is achieved, allow it to cure completely before demolding.

Once the resin is completely cured, the composite should now be hard and have no give to pushing a finger into it. The demolding process can begin by turing off the vacuum and removing the vacuum ports. The bagging materials can then all be peeled off. Now there is only the mold and the plug remaining. Start by sliding a putty knife or other thin object around the flange to release it. Then begin putting wedges under the flange and eventually between he model and model. Work around the layup slowly releasing all areas. Eventually the mold will release from the plug and you can pull it out. If the composite is still flexible

Figure A.7: Vacuum bag on mold layup

you may leave it to cure for additional time. The more rigid the composite is the easier it will be to demold since it will not be able to flex with the addition of wedges and instead will have to release from the plug.

A.3 Mold Preparation

After demolding the mold from the plug, there will be sharp edges. Trim these edges with a dremel or other cutting tool. This step will save you from many cuts and fiberglass splinters in the future. Brush the mold off of any dust and clean it with acetone. If there are any defects in the mold surface, repair the with fairing compound using the same method as

Figure A.8: Mold immediately after releasing from the plug

to repair the model surface. When the surface is defect free sand it to 220-320 grit. This light sanding will promote the adhesion of primer. Clean the mold with acetone once again to remove any fiberglass dust. Then apply an epoxy based surface primer. Many of these primers are hazardous so make sure to take all appropriate safety precautions. Since there are not adequate facilities at Virginia Tech for the scale of our model we partnered with Collision Plus in Christiansburg. They were gracious enough to donate their time and facilities to spray our mold with a Duratec Gray Surfacing primer according to the spec sheet, building up a coat of 20 mils and allow it to cure in their paint booth. After applying the surface primer, begining with 120 grit, flat and sand the mold, eventually sanding to 800 grit, remembering to clean the surface, and water if wet sanding, between each grit of sandpaper.

After sanding the surface finish should be very good and feel smooth to the touch. To get an even better surface finish polish the mold with a step one and step 2 compound to leave a glossy finish.

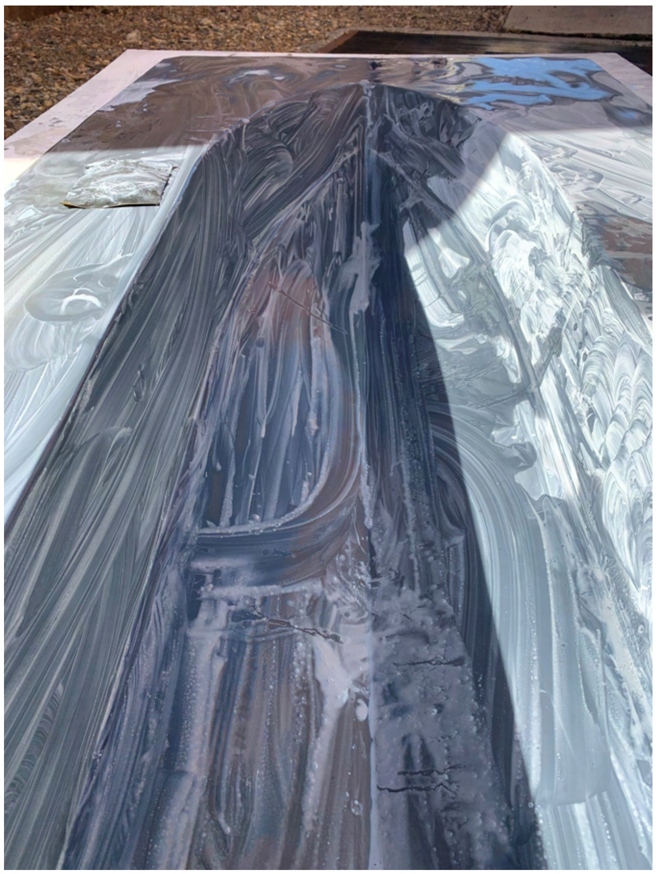

Figure A.9: Sanding the mold to create a class ”A” surface finish

A.4 Model Layup

From this point proceed with the layup steps of waxing, applying vacuum sealant tape, applying release agent, and performing the layup, and vacuum bagging as described previously for the fabrication of the mold. For the fabrication of the model the flange does not need to be large since it will be cut off of the final part. The stacking sequence for the model was

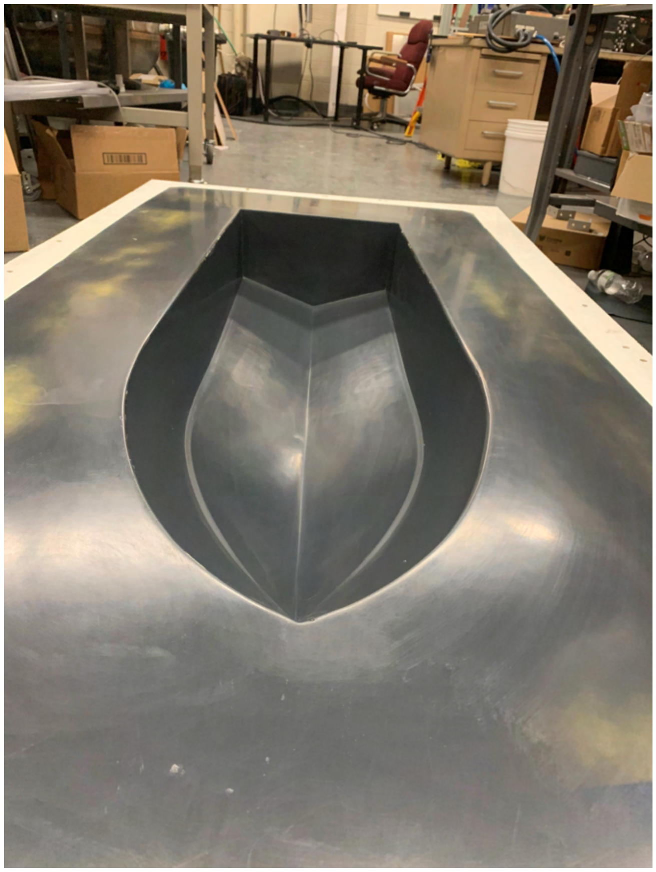

Figure A.10: Mold after buffing to a class ”A” surface finish

based on the stacking sequence of the USNA model. However, for increased stiffness and thickness, additional layers of fabric were added. The stacking sequence for both the USNA model and the Virginia Tech model are detailed below in Table A.2.

Table A.2: Layup Schedule for GPPH Model

Layer #	# of Layers	Description
1	1	2oz Plain Weave Fiberglass
2	2	8.5oz Twill Weave E-glass
3	4	20oz Fiberglass Tooling Fabric

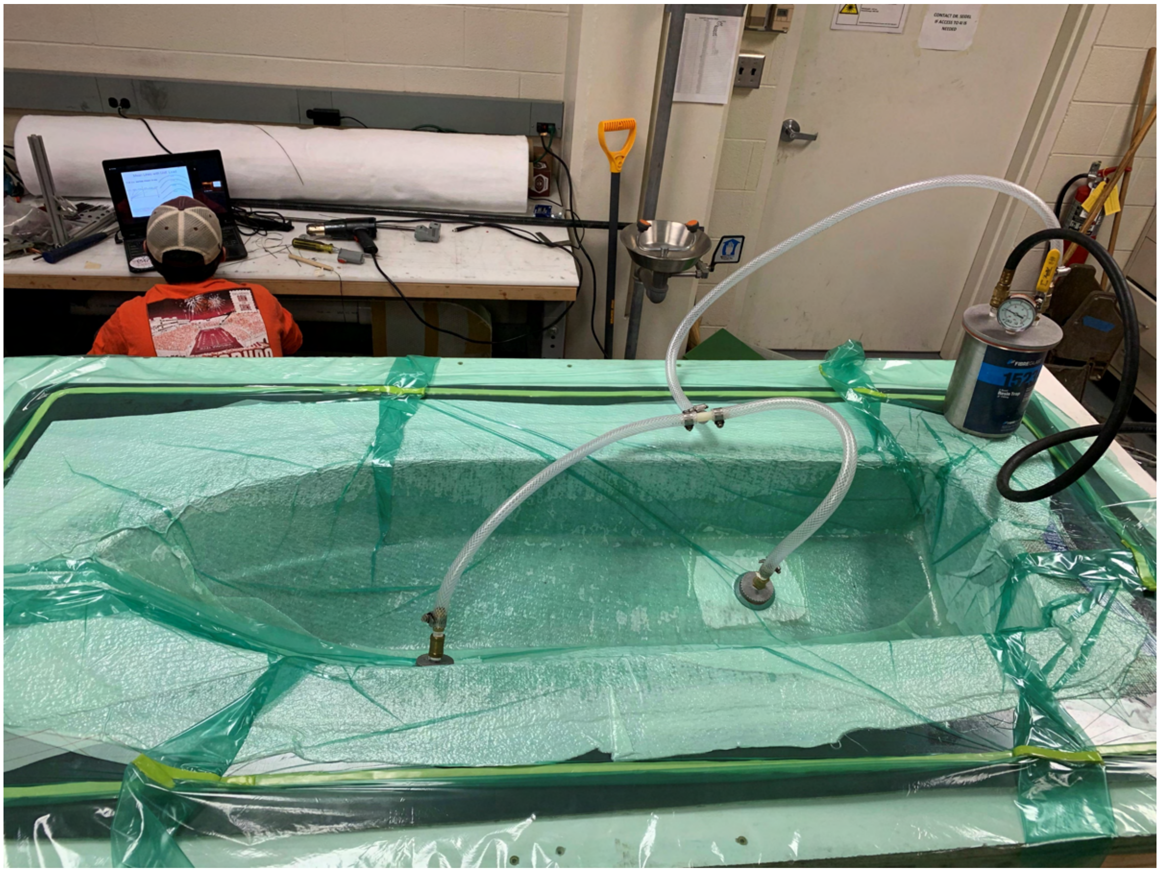

Figure A.11: Perfect vacuum achieved on the model layup

A.5 Model Finishing & Outfitting

Once the model had finished curing it was demolded following the same procedure as the mold. After demolding the flange of the model was trimmed off and the model now looks like a boat. At this point any surface defects in the model surface are repaired with a fairing compound. Holes for pressure sensors are marked and drilled and the aluminum taps adhered to the interior of the model surface by first sanding both parts and then using a five minute epoxy to secure them in place. The mounting block for the heave post was secured into place with epoxy as well. The model was outfitted with pine trim to provide an easy location to mount linear slides and other equipment. The trim was first rough cut to shape with a jigsaw. The joinery was then layed out rough cut with the jigsaw and then paired to the line with a pocket knife. The pieces were then glued together with a waterproof wood glue. The glue joints were allowed to set for half an hour, before nails were placed through the half-lap joints. These nails allowed work to continue while the glue finished curing. The components were then further sanded with a belt sander to have snug fit into the boat. The edge of the boat and trim were then sanded and a layer of epoxy applied to the trim to seal it and prevent it from soaking up excess epoxy when it was finally joined to the boat. The surface coat of epoxy on the trim was then sanded and the trim was glued to the model, clamped and allowed to set overnight.

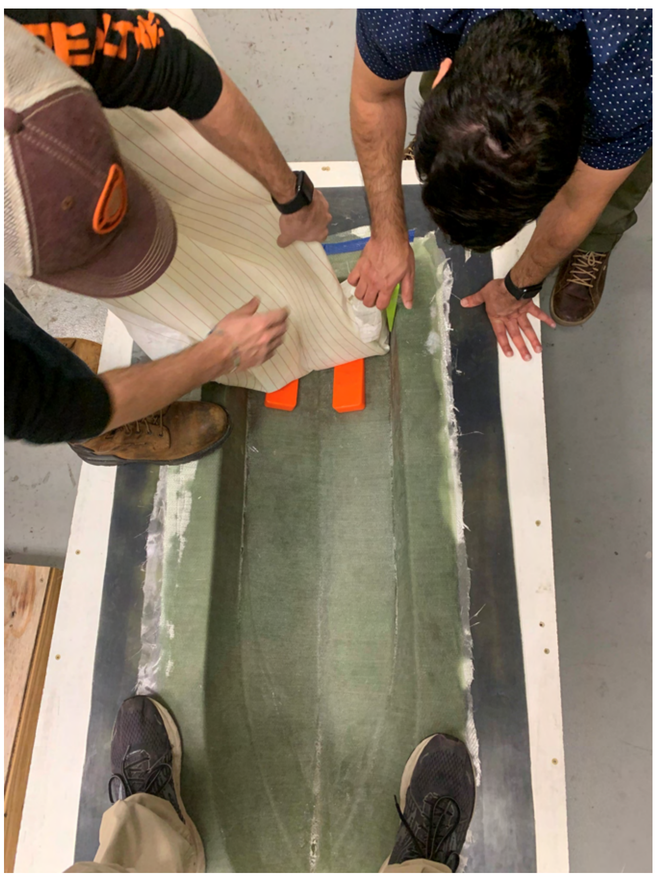

Figure A.12: Model in the process of being demolded

A.6 Resources & References

A list of all of the materials an calculations for the required quantities of resin has been provided here.

Mold Calcs

Molded Length	72	in			
Molded Beam	36	in			
Reinforcements					
2oz Fiberglass Fabric	1	layers	==>	2	yds (38" Wide)
6oz Fiberglass Fabric	2	layers	==>	4	yds (38" Wide)
10oz Fiberglass Fabric	3	layers	==>	6	yds (38" Wide)
20 oz Tooling Fabric	5	layers	==>	10	yds (38" Wide)
Saertex (36 oz/yd^2) Stiched T	0	layers	==>	0	yds (38" Wide)
Resin Calcs					
Total Fabric Weight	19	lbs			
Resin Weight Factor	1.5				Totals:
Total Resin Weight	28.5	lbs			2oz Fiberglass Fabric
Polyester Resin Density	8	lbs/Gal			6oz Fiberglass Fabric
Req. Epoxy	2.671875	Gal			10oz Fiberglass Fabric
Req. Harderner	0.890625	Gal			20 oz Tooling Fabric
					Req Epoxy
Model Calcs					Req Hardender
Molded Length	60	in			
Molded Beam	24	in			
Reinforcements					
Surfacing Veil	1	layers	==>	2	yds (38" Wide)
8.5oz Fiberglass Fabric	1	layers	==>	2	yds (38" Wide)
20 oz Tooling Cloth	4	layers	==>	8	yds (38" Wide)
Resin Calcs (West Systems)					
Total Fabric Weight	12.52153	lbs			
Resin Weight Factor	1.5				
Total Resin Weight	18.78229	lbs			
Polyester Resin Density	8	lbs/Gal			
Req. Epoxy	1.76084	Gal			
Req. Harderner	0.586947	Gal			

==>	0.263889	lbs
==>	1.583333	lbs
==>	3.958333	lbs
==>	13.19444	lbs
==>	0	lbs

4	5.333333	6
4	5.333333	6
8	10.66667	11
18	24	24
4.432714844	5	
1.477571615	1.75	

			t (in)	total t (in)
==>	0.184722	lbs	0.004	0.004
==>	1.78125	lbs	0.009	0.009
==>	10.55556	lbs	0.03	0.12
			T(in)	0.133

Figure A.13: Wooden trim with hand cut joinery being glued up to the model

Figure A.14: Finished model with rounded over wood trim

Appendix B

Tow Tank Operation/Training

Tow Tank Procedures

1

Software Install Procedure

2

Software Install Procedures

1. Download and Install the latest version of SetupEdesignVTCarriage_2022_01_24.exe
2. Download and Install the latest version of Java
3. Drag the Current Control Virginia Tech Carriage Icon onto the desktop
4. Go to Network settings → change adapter options
5. Right Click Ethernet and select properties
6. Select Internet Protocol Version 4 → Properties
7. Ensure that IP address and subnet mask match
8. Open the software in C:\edesign then go to C:\edesign\etc\vt_config
9. Open the vt_carriage.txt file
10. Change belt force to N and make the settings 4000, 1000, 6000
11. Save and Close vt_carriage.txt
12. Open the vt_datachans.txt file
13. Change BeltForceBeach and BeltForceWavemaker to BeltForceWall and BeltForceWalkway respectively
14. Save and Close vt_datachans.txt

3

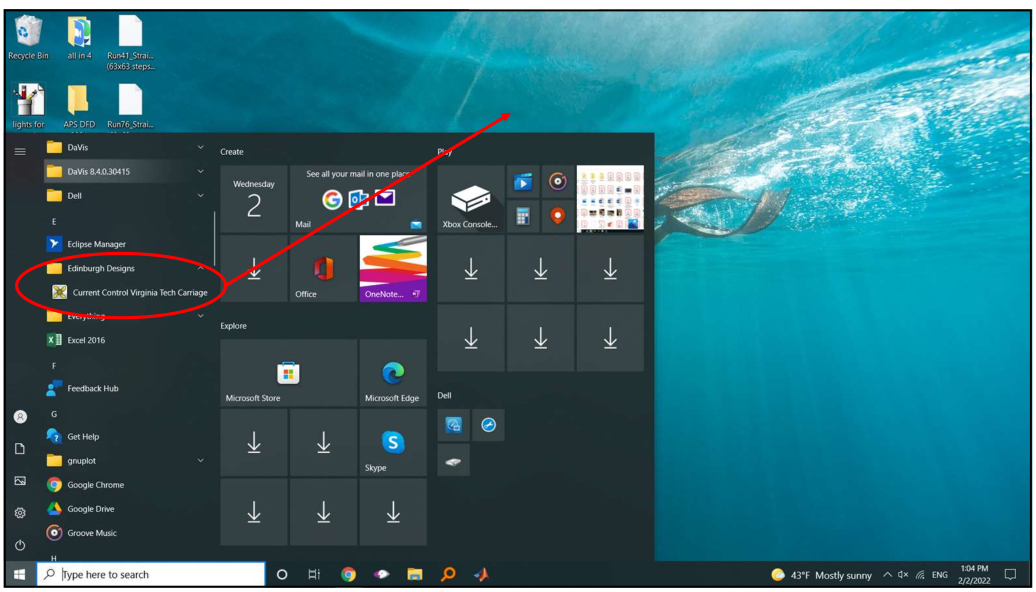

4

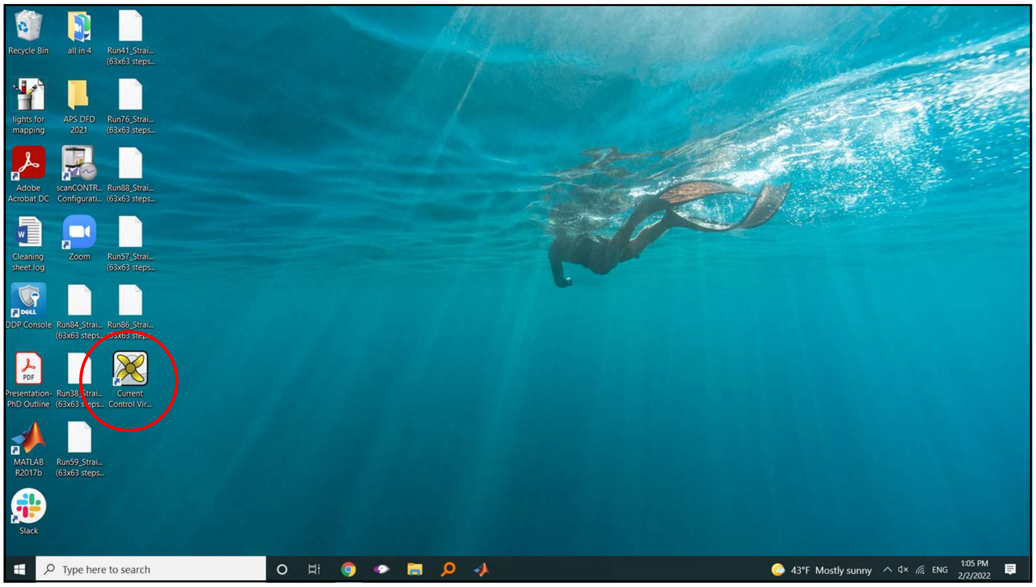
Recycle Bin
all in 4
lights for mapping
APS DFD 2021
Adobe Acrobat DC
Cleaning sheet log
Zoom
DDP Console
Presentation-PhD Outline
Current Control Vir...
MATLAB R2017b
Slack
Type here to search
43°F Mostly sunny
ENG
1:05 PM
2/2/2022

5

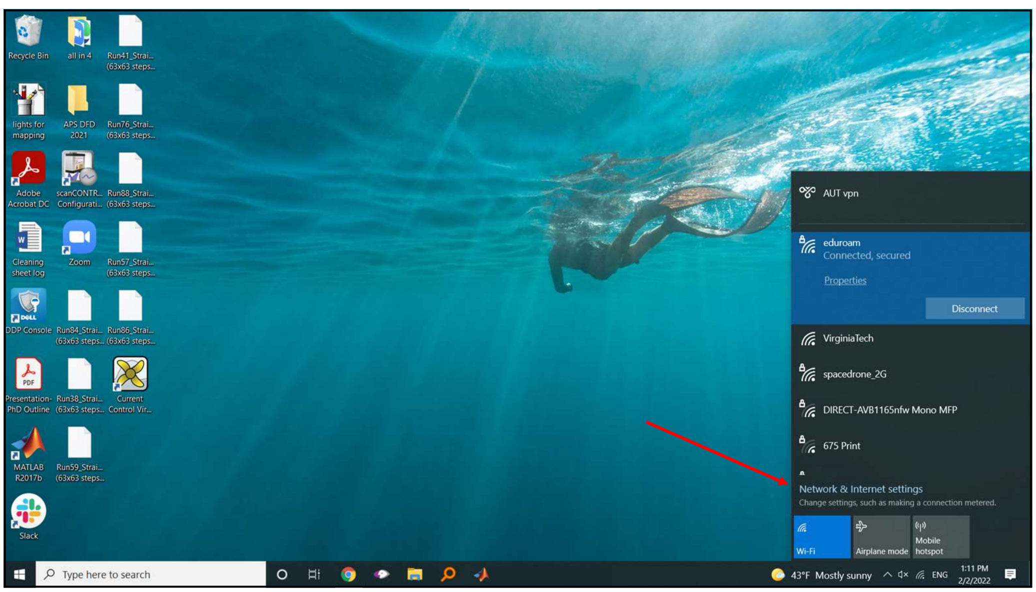
Recycle Bin
all in 4
lights for mapping
APS DFD 2021
Adobe Acrobat DC
Cleaning sheet log
Zoom
DDP Console
Presentation-PhD Outline
Current Control Vir...
MATLAB R2017b
Slack
AUT vpn
eduroam
Connected, secured
Properties
Disconnect
VirginiaTech
spacedrone_2G
DIRECT-AVB1165nfw Mono MFP
675 Print
Network & Internet settings
Change settings, such as making a connection metered.
Wi-Fi
Airplane mode
Mobile hotspot
Type here to search
43°F Mostly sunny
ENG
1:11 PM
2/2/2022

6

4/12/2022

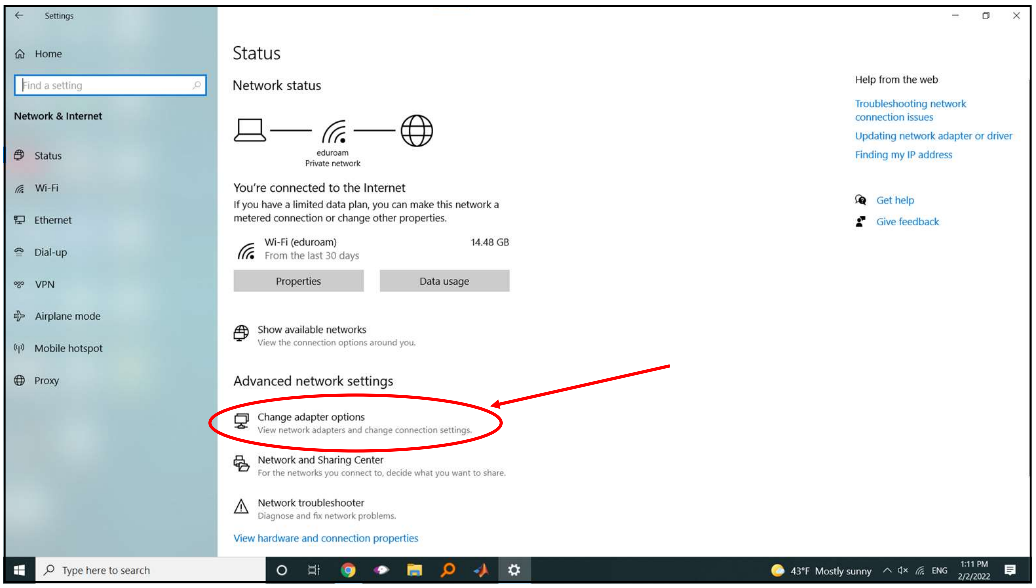
Settings
Home
Find a setting
Network & Internet
Status
Wi-Fi
Ethernet
Dial-up
VPN
Airplane mode
Mobile hotspot
Proxy
Status
Network status
eduroam
Private network
You're connected to the Internet
If you have a limited data plan, you can make this network a metered connection or change other properties.
Wi-Fi (eduroam)
From the last 30 days
14.48 GB
Properties
Data usage
Show available networks
View the connection options around you.
Advanced network settings
Change adapter options
View network adapters and change connection settings.
Network and Sharing Center
For the networks you connect to, decide what you want to share.
Network troubleshooter
Diagnose and fix network problems.
View hardware and connection properties
Help from the web
Troubleshooting network connection issues
Updating network adapter or driver
Finding my IP address
Get help
Give feedback
Type here to search
43°F Mostly sunny
ENG
1:11 PM
2/2/2022

7

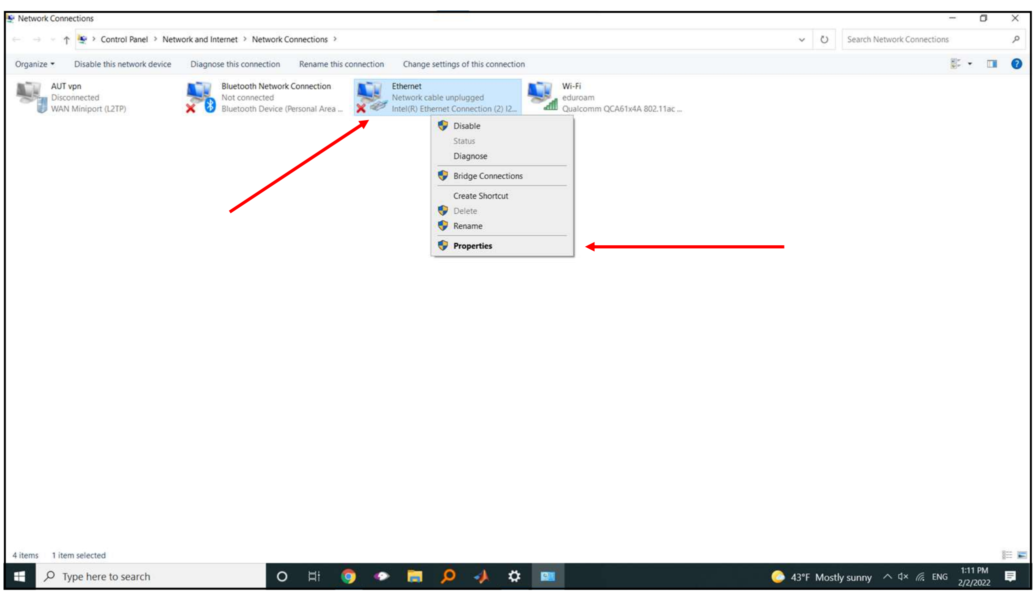
Network Connections
Control Panel > Network and Internet > Network Connections
Search Network Connections
Organize
Disable this network device
Diagnose this connection
Rename this connection
Change settings of this connection
AUT vpn
Disconnected
WAN Miniport (L2TP)
Bluetooth Network Connection
Not connected
Bluetooth Device (Personal Area ...
Ethernet
Network cable unplugged
Intel(R) Ethernet Connection (2) I2...
Wi-Fi
eduroam
Qualcomm QCA61x4A 802.11ac ...
Disable
Status
Diagnose
Bridge Connections
Create Shortcut
Delete
Rename
Properties
4 items
1 item selected
Type here to search
43°F Mostly sunny
ENG
1:11 PM
2/2/2022

8

4

4/12/2022

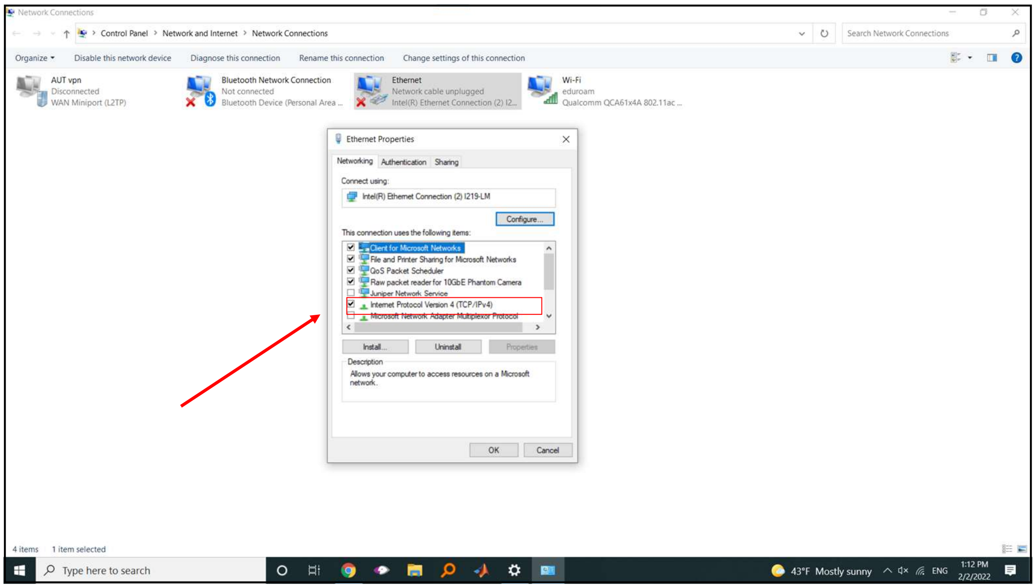
Network Connections
Control Panel > Network and Internet > Network Connections
Search Network Connections
Organize
Disable this network device
Diagnose this connection
Rename this connection
Change settings of this connection
AUT vpn
Disconnected
WAN Miniport (L2TP)
Bluetooth Network Connection
Not connected
Bluetooth Device (Personal Area ...
Ethernet
Network cable unplugged
Intel(R) Ethernet Connection (2) I2...
Wi-Fi
eduroam
Qualcomm QCA61x4A 802.11ac ...
Ethernet Properties
Networking
Authentication
Sharing
Connect using:
Intel(R) Ethernet Connection (2) I219-LM
Configure...
This connection uses the following items:
Client for Microsoft Networks
File and Printer Sharing for Microsoft Networks
QoS Packet Scheduler
Raw packet reader for 10GbE Phantom Camera
Juniper Network Service
Internet Protocol Version 4 (TCP/IPv4)
Microsoft Network Adapter Multiplexor Protocol
Install...
Uninstall
Properties
Description
Allows your computer to access resources on a Microsoft network.
OK
Cancel
4 items
1 item selected
Type here to search
43°F Mostly sunny
ENG
1:12 PM
2/2/2022

9

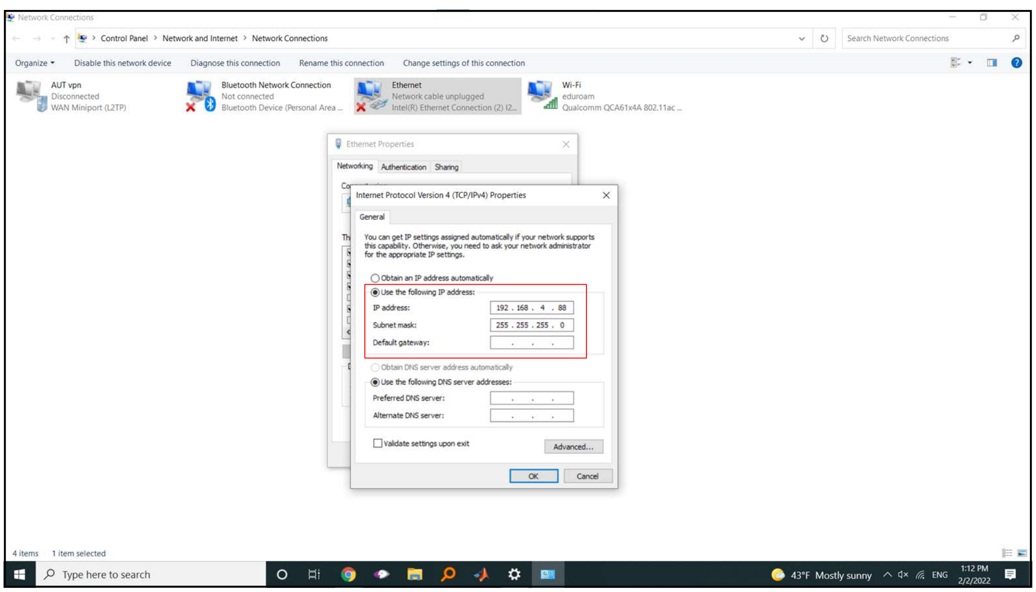
Network Connections
Control Panel > Network and Internet > Network Connections
Search Network Connections
Organize
Disable this network device
Diagnose this connection
Rename this connection
Change settings of this connection
AUT vpn
Disconnected
WAN Miniport (L2TP)
Bluetooth Network Connection
Not connected
Bluetooth Device (Personal Area ...
Ethernet
Network cable unplugged
Intel(R) Ethernet Connection (2) I2...
Wi-Fi
eduroam
Qualcomm QCA61x4A 802.11ac ...
Ethernet Properties
Networking
Authentication
Sharing
Internet Protocol Version 4 (TCP/IPv4) Properties
General
You can get IP settings assigned automatically if your network supports this capability. Otherwise, you need to ask your network administrator for the appropriate IP settings.
Obtain an IP address automatically
Use the following IP address:
IP address:
192 . 168 . 4 . 88
Subnet mask:
255 . 255 . 255 . 0
Default gateway:
Obtain DNS server address automatically
Use the following DNS server addresses:
Preferred DNS server:
Alternate DNS server:
Validate settings upon exit
Advanced...
OK
Cancel
4 items
1 item selected
Type here to search
43°F Mostly sunny
ENG
1:12 PM
2/2/2022

10

4/12/2022

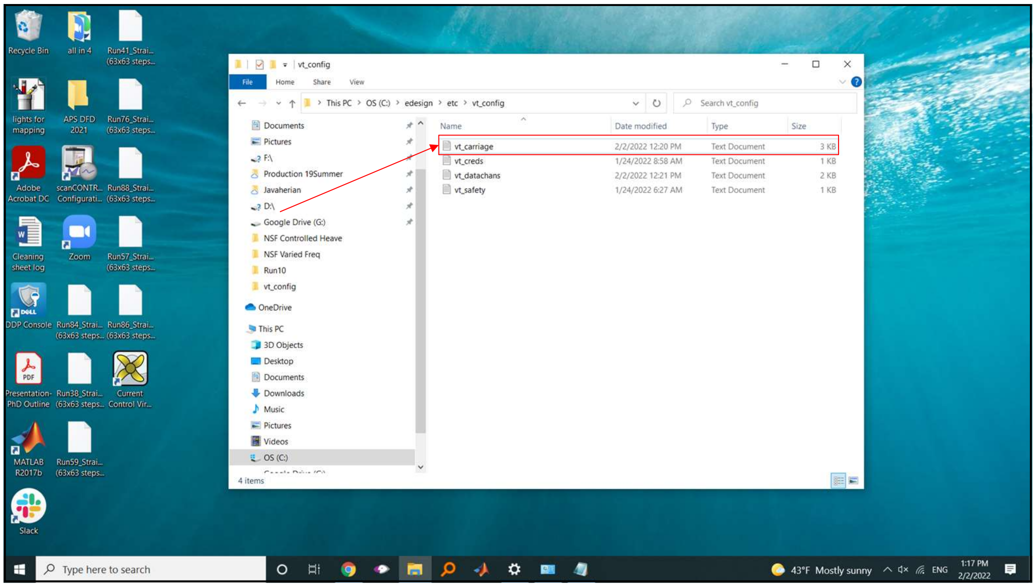

11

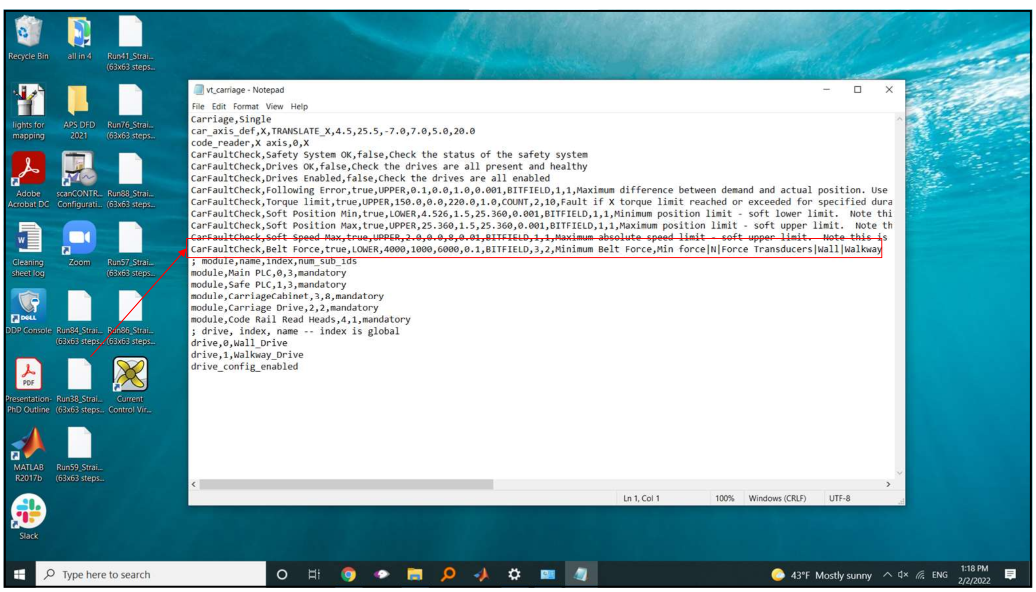

12

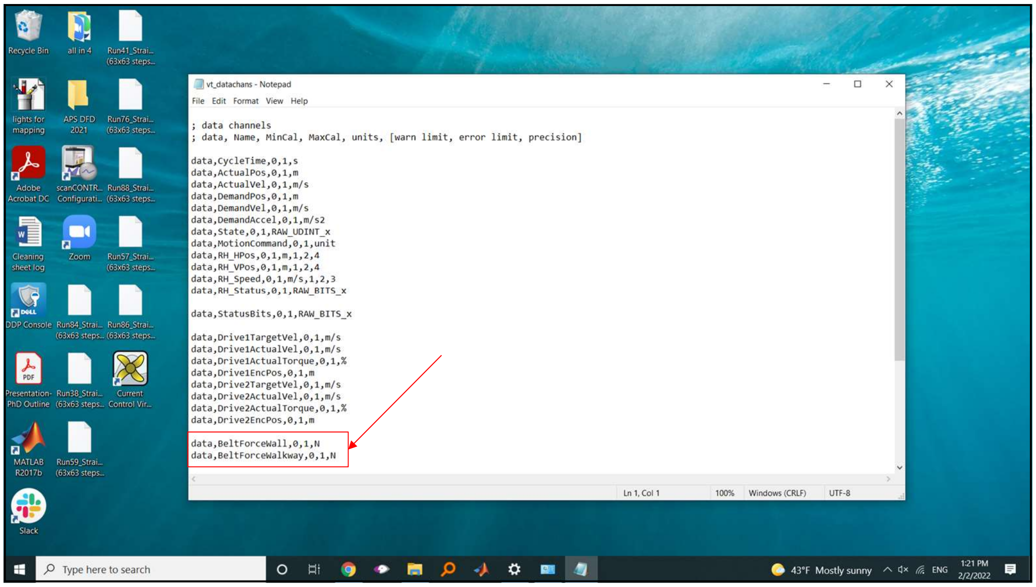

13

Start-Up Procedure

14

Start-Up Procedures

1. Ensure that equipment is fastened tightly and belts are free of debris
2. Energize the system with the large on switch to the right of the electrical cabinet
3. Provide power to the main electrical cabinet followed by the carriage mounted electrical cabinet
4. Ensure that control computer is connected to the main electrical cabinet via ethernet cable
5. Open the Current Control Virginia Tech software
6. Click the Reset button if there is an E-Stop Notification on the Safety Tab (If safe to do so)
7. Go to Carriage Tab
8. At the control station, rotate the key from the OFF to the RUN position. The green light on the carriage and the control station will begin blinking
9. Press the green button
10. Press the Power On Button in the GUI (No Longer Greyed Out)
11. Press the Green button again
12. Carriage Status will be enabled and ready to move

15

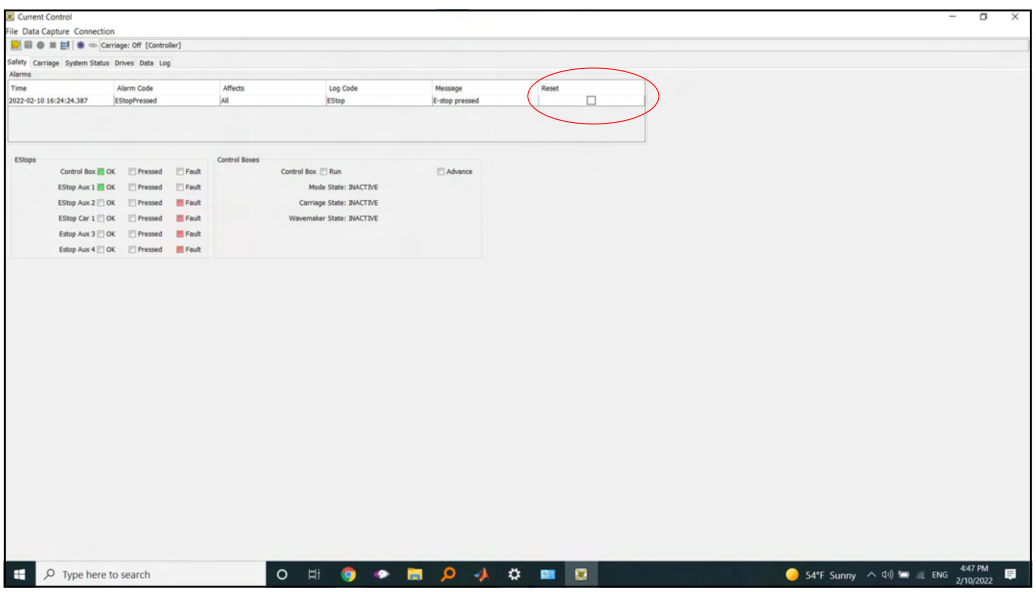

16

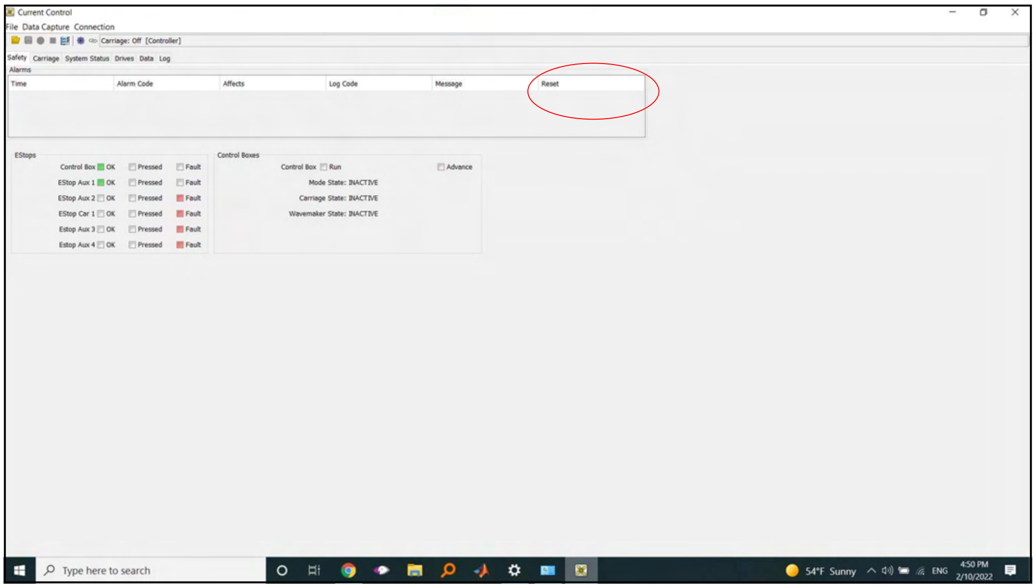
Current Control
File Data Capture Connection
Carriage: Off [Controller]
Safety Carriage System Status Drives Data Log
Alarms
Time
Alarm Code
Affects
Log Code
Message
Reset
EStops
Control Box OK Pressed Fault
EStop Aux 1 OK Pressed Fault
EStop Aux 2 OK Pressed Fault
EStop Car 1 OK Pressed Fault
Estop Aux 3 OK Pressed Fault
Estop Aux 4 OK Pressed Fault
Control Boxes
Control Box Run
Advance
Mode State: INACTIVE
Carriage State: INACTIVE
Wavemaker State: INACTIVE
Type here to search
54°F Sunny
ENG
4:50 PM
2/10/2022

17

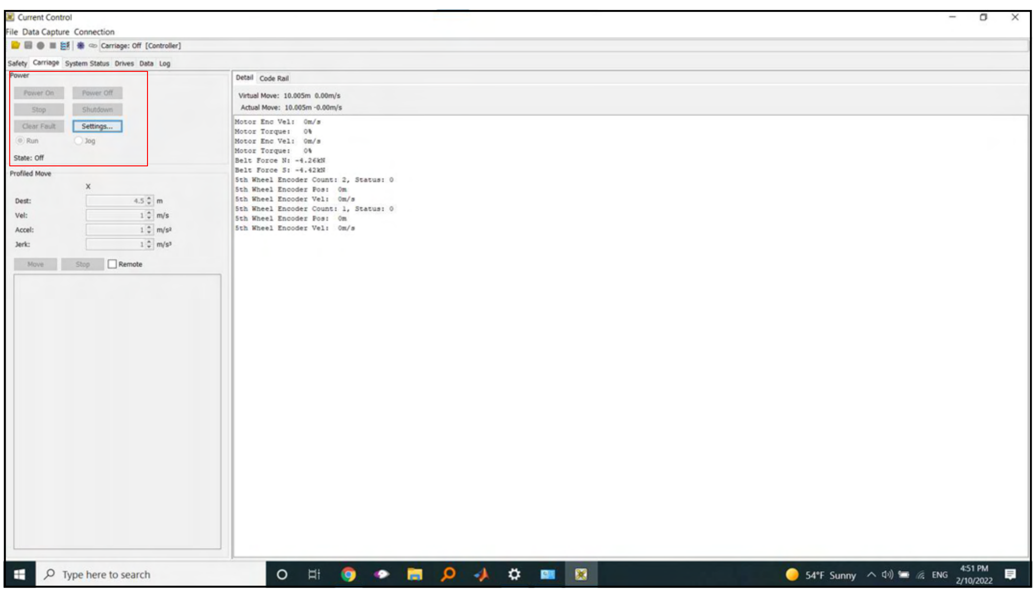
Current Control
File Data Capture Connection
Carriage: Off [Controller]
Safety Carriage System Status Drives Data Log
Power
Power On
Power Off
Stop
Shutdown
Clear Fault
Settings...
Run
Jog
State: Off
Profiled Move
X
Dest:
4.5
m
Vel:
1
m/s
Accel:
1
m/s²
Jerk:
1
m/s³
Move
Stop
Remote
Detail Code Rail
Virtual Move: 10.005m 0.00m/s
Actual Move: 10.005m -0.00m/s
Motor Enc Vel: 0m/s
Motor Torque: 0%
Motor Enc Vel: 0m/s
Motor Torque: 0%
Belt Force N: -4.24kN
Belt Force S: -4.42kN
5th Wheel Encoder Count: 2, Status: 0
5th Wheel Encoder Pos: 0m
5th Wheel Encoder Vel: 0m/s
5th Wheel Encoder Count: 1, Status: 0
5th Wheel Encoder Pos: 0m
5th Wheel Encoder Vel: 0m/s
Type here to search
54°F Sunny
ENG
4:51 PM
2/10/2022

18

4/12/2022

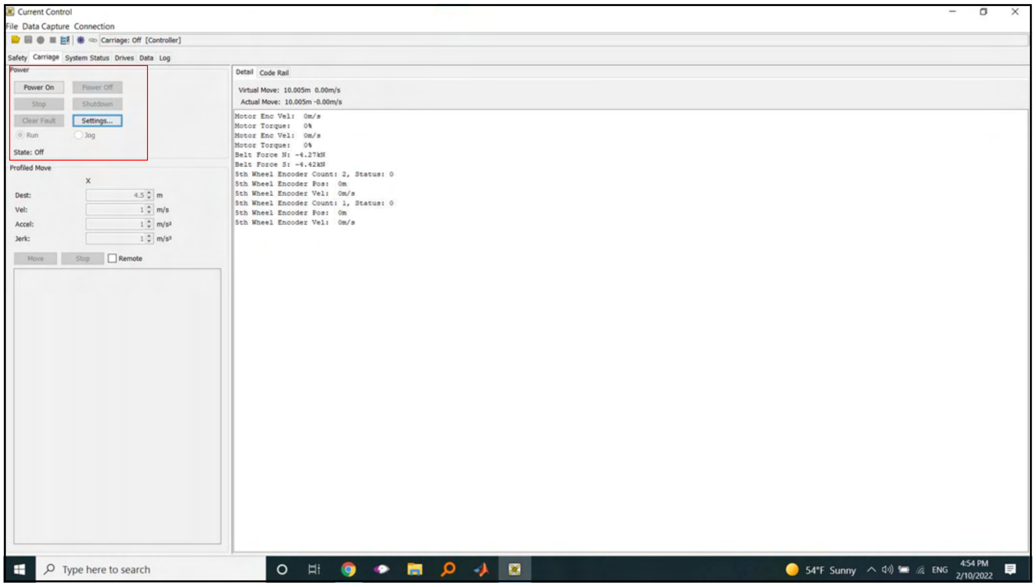

19

Fast Start-Up Procedure

20

FastStart-Up Procedures

1. Open the software
2. At the control station, rotate the key from the OFF to the RUN position. The green light on the carriage and the control station will begin blinking
3. Press the green button
4. Press the Power On Button in the GUI
5. Press the Green button again
6. Carriage Status will be enabled and ready to move

21

Shutdown Procedure

22

Shut Down Procedures

1. Press Power Down on the software
2. Turn key from run position to off position
3. Shut power off at the Carriage
4. Shut power off at the main cabinet
5. Shut power off at the breaker

23

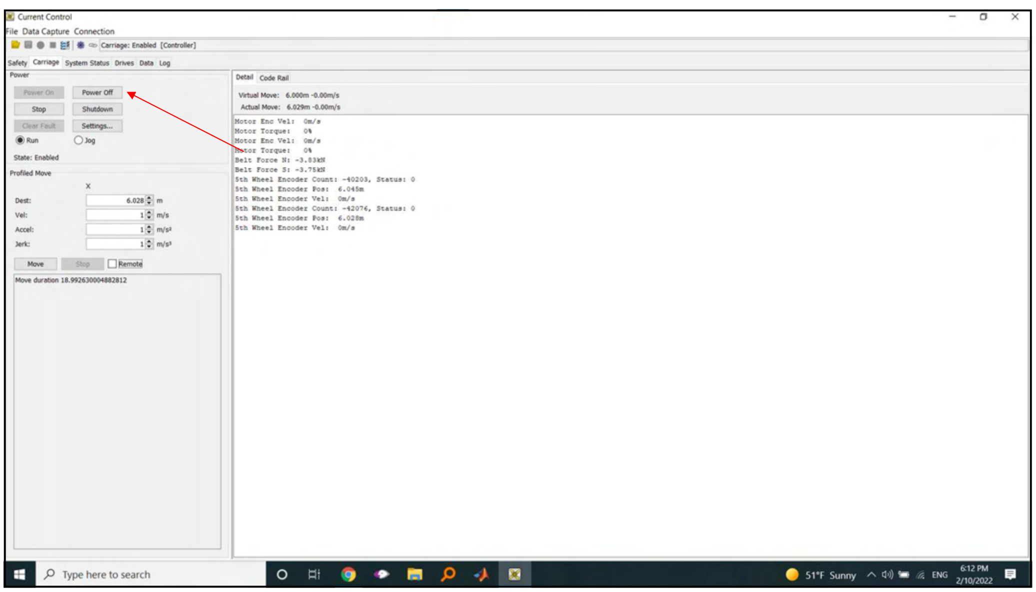

24

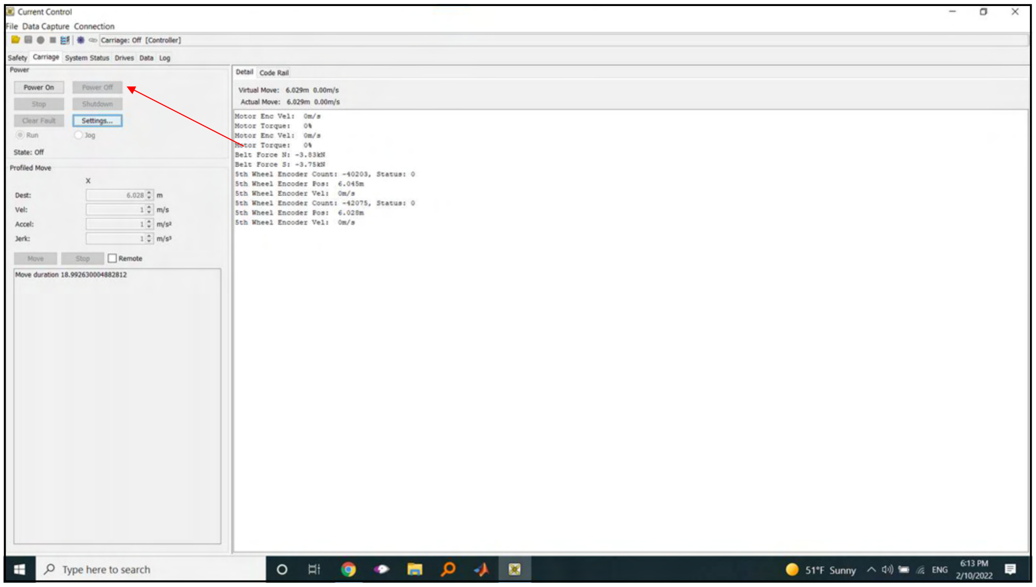

25

Short Shutdown Procedure

26

Shut Down Procedures

1. Press Power Down on the software
2. Turn key from RUN position to OFF position

27

Carriage Specs

28

Carriage Specs

- Maximum Carriage Speed: 7 m/s
- Min Carriage Distance: 6m
- Max Carriage Distance: 24m
- Maximum Acceleration: 5 m/s^2
- Maximum Deceleration: 20 m/s^3
- Maximum Acceleration Jerk: 5 m/s^2
- Max Deceleration Jerk: 20 m/s^3
- Maximum Load: 150 kg

29

Running Procedure

30

Running Procedures

1. Ensure machine status is enabled
2. Set the Destination position of the carriage between (6, 24)m
3. Set the carriage velocity < 7m/s
4. Set carriage acceleration < 5 m/s^2
5. Set carriage jerk <20 m/s^3
6. Announce “STAND BACK THE CARRIAGE IS ABOUT TO MOVE”
7. Announce “MOVING” Press the move button to move the carriage

31

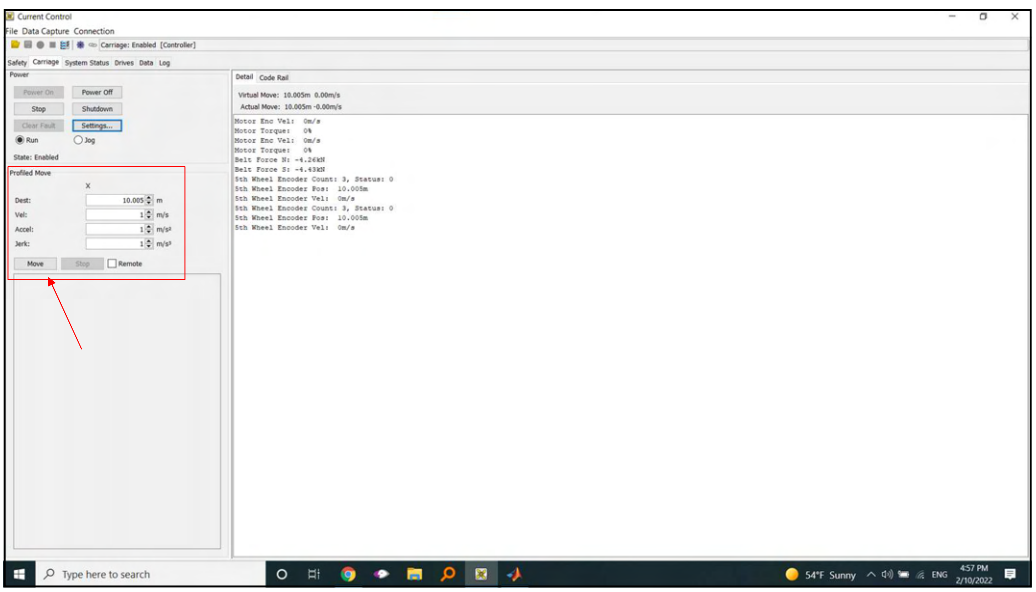

32

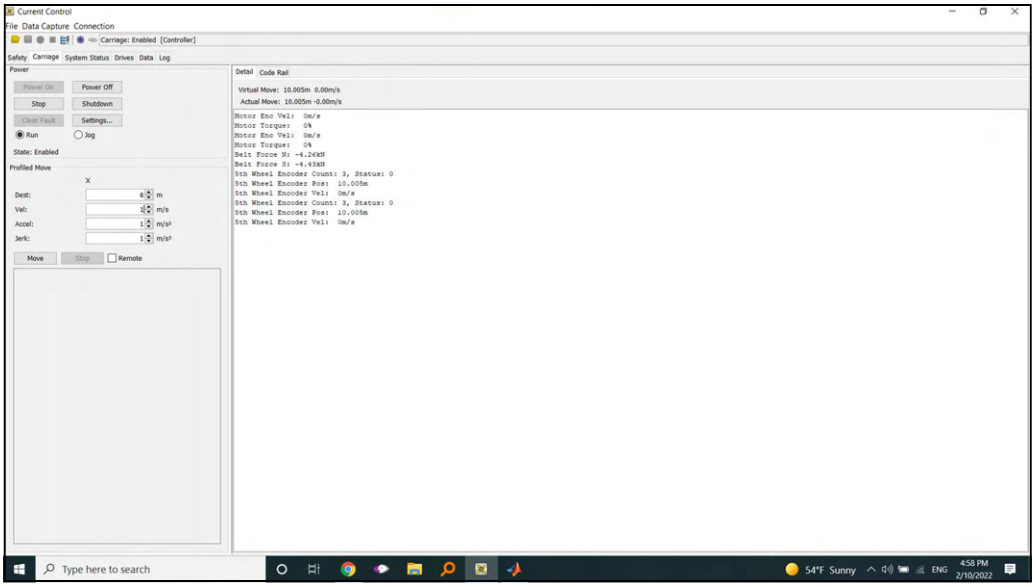

33

E-Stop Procedure

34

E-Stop Procedures

1. If there is any need to stop the carriage immediately PRESS THE E-STOP
2. Carriage will come to an immediate stop
3. Ensure all personnel and equipment are safe and secure
4. When safe to do so close the Fault Window & Release the E-STOP
5. Proceed to the safety tab on the software
6. Press the reset button (Red lights on controller and carriage will switch off)
7. Go to the carriage tab and press the clear fault button
8. Turn Key on controller off then on
9. Press Green Blinking Button
10. Press Power on in GUI
11. Press Green Button again
12. The carriage status will state Enabled and be ready to run

35

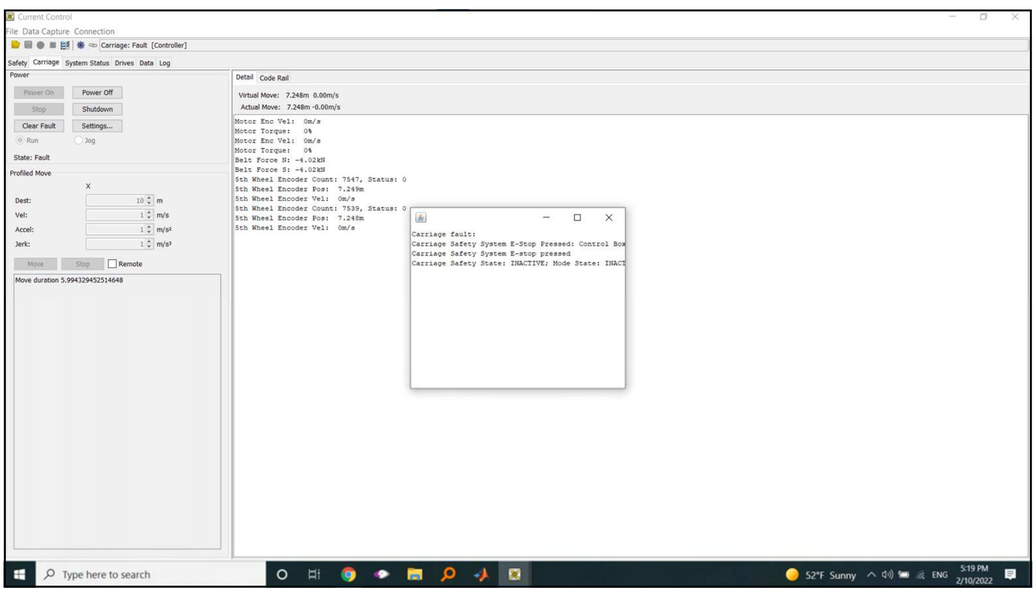

36

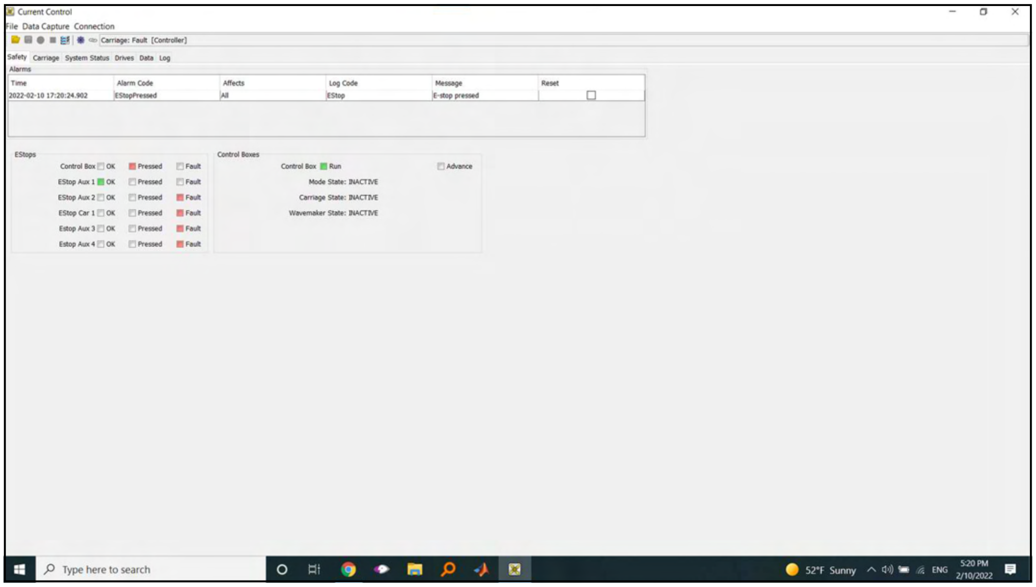
Current Control
File Data Capture Connection
Carriage: Fault [Controller]
Safety Carriage System Status Drives Data Log
Alarms
Time
Alarm Code
Affects
Log Code
Message
Reset
2022-02-10 17:20:24.902
EStopPressed
All
EStop
E-stop pressed
EStops
Control Box OK Pressed Fault
EStop Aux 1 OK Pressed Fault
EStop Aux 2 OK Pressed Fault
EStop Car 1 OK Pressed Fault
Estop Aux 3 OK Pressed Fault
Estop Aux 4 OK Pressed Fault
Control Boxes
Control Box Run
Advance
Mode State: INACTIVE
Carriage State: INACTIVE
Wavemaker State: INACTIVE
Type here to search
52°F Sunny
ENG
5:20 PM
2/10/2022

37

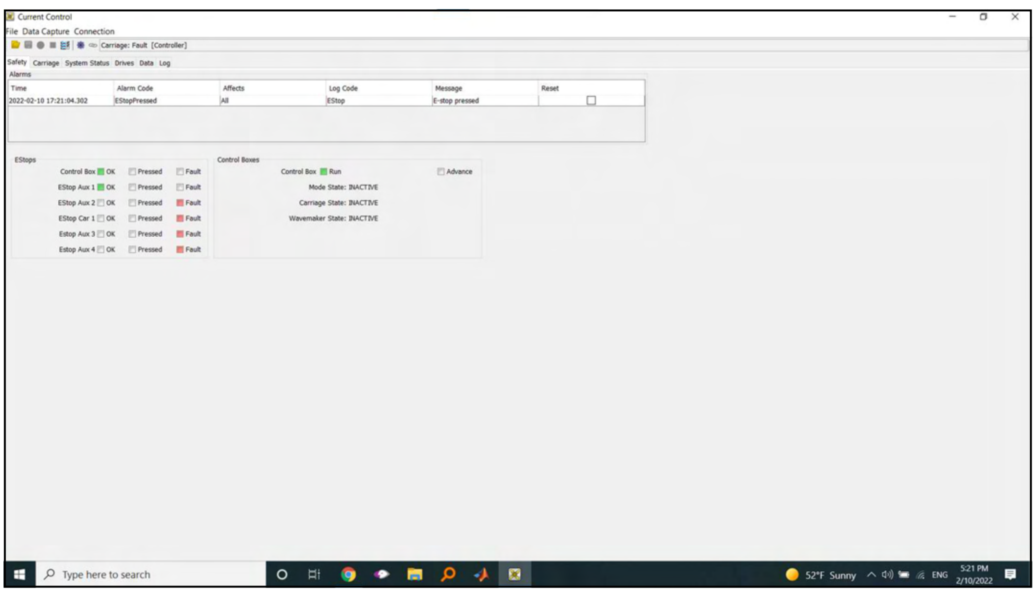
Current Control
File Data Capture Connection
Carriage: Fault [Controller]
Safety Carriage System Status Drives Data Log
Alarms
Time
Alarm Code
Affects
Log Code
Message
Reset
2022-02-10 17:21:04.302
EStopPressed
All
EStop
E-stop pressed
EStops
Control Box OK Pressed Fault
EStop Aux 1 OK Pressed Fault
EStop Aux 2 OK Pressed Fault
EStop Car 1 OK Pressed Fault
Estop Aux 3 OK Pressed Fault
Estop Aux 4 OK Pressed Fault
Control Boxes
Control Box Run
Advance
Mode State: INACTIVE
Carriage State: INACTIVE
Wavemaker State: INACTIVE
Type here to search
52°F Sunny
ENG
5:21 PM
2/10/2022

38

4/12/2022

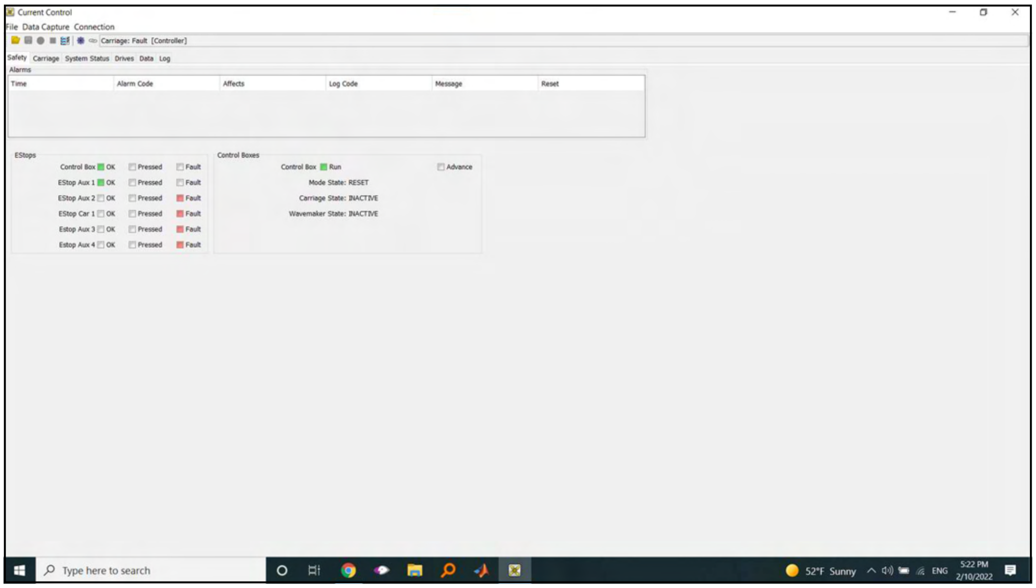

39

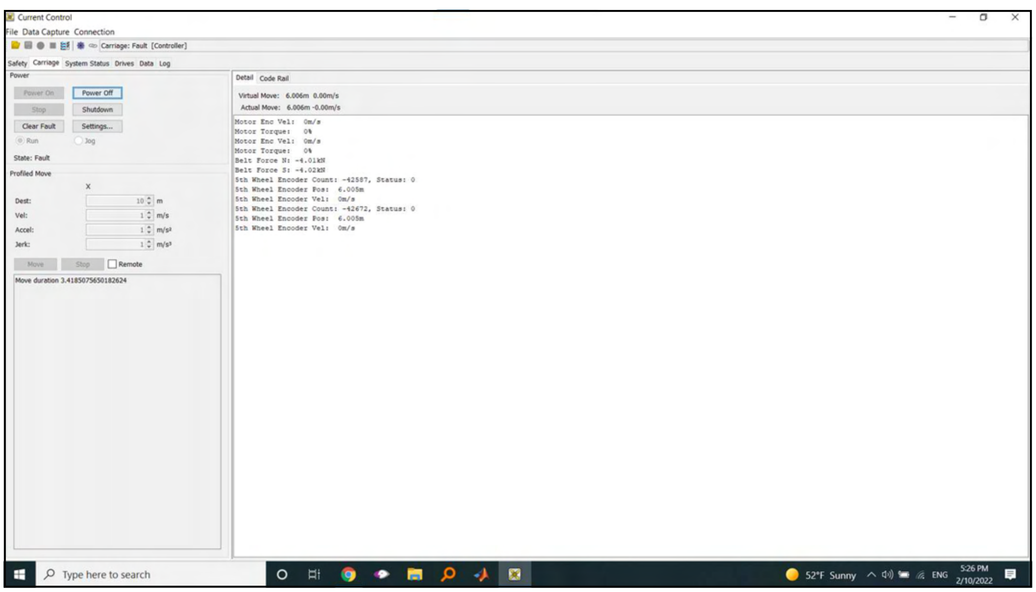

40

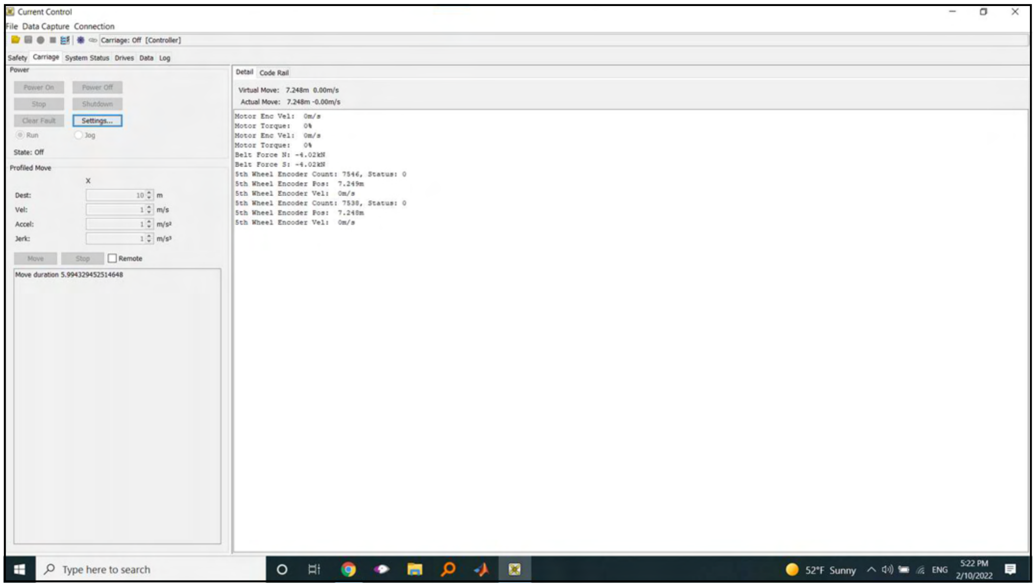
Current Control
File Data Capture Connection
Carriage: Off [Controller]
Safety Carriage System Status Drives Data Log
Power
Power On
Power Off
Stop
Shutdown
Clear Fault
Settings...
Run
Jog
State: Off
Profiled Move
X
Dest: 10 m
Vel: 1 m/s
Accel: 1 m/s²
Jerk: 1 m/s³
Move
Stop
Remote
Move duration 5.994329452514648
Detail Code Rail
Virtual Move: 7.248m 0.00m/s
Actual Move: 7.248m -0.00m/s
Motor Enc Vel: 0m/s
Motor Torque: 0%
Motor Enc Vel: 0m/s
Motor Torque: 0%
Belt Force N: -4.02kN
Belt Force S: -4.02kN
5th Wheel Encoder Count: 7546, Status: 0
5th Wheel Encoder Pos: 7.249m
5th Wheel Encoder Vel: 0m/s
5th Wheel Encoder Count: 7538, Status: 0
5th Wheel Encoder Pos: 7.248m
5th Wheel Encoder Vel: 0m/s
Type here to search
52°F Sunny
ENG
5:22 PM
2/10/2022

41

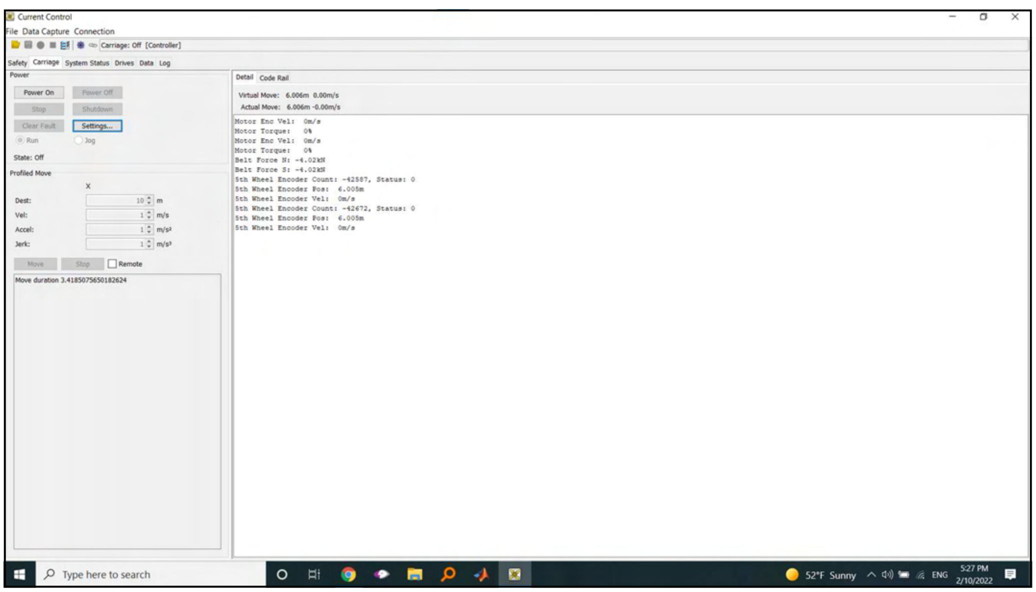
Current Control
File Data Capture Connection
Carriage: Off [Controller]
Safety Carriage System Status Drives Data Log
Power
Power On
Power Off
Stop
Shutdown
Clear Fault
Settings...
Run
Jog
State: Off
Profiled Move
X
Dest: 10 m
Vel: 1 m/s
Accel: 1 m/s²
Jerk: 1 m/s³
Move
Stop
Remote
Move duration 3.4185075650182624
Detail Code Rail
Virtual Move: 6.006m 0.00m/s
Actual Move: 6.006m -0.00m/s
Motor Enc Vel: 0m/s
Motor Torque: 0%
Motor Enc Vel: 0m/s
Motor Torque: 0%
Belt Force N: -4.02kN
Belt Force S: -4.02kN
5th Wheel Encoder Count: -42587, Status: 0
5th Wheel Encoder Pos: 6.005m
5th Wheel Encoder Vel: 0m/s
5th Wheel Encoder Count: -42672, Status: 0
5th Wheel Encoder Pos: 6.005m
5th Wheel Encoder Vel: 0m/s
Type here to search
52°F Sunny
ENG
5:27 PM
2/10/2022

42

4/12/2022

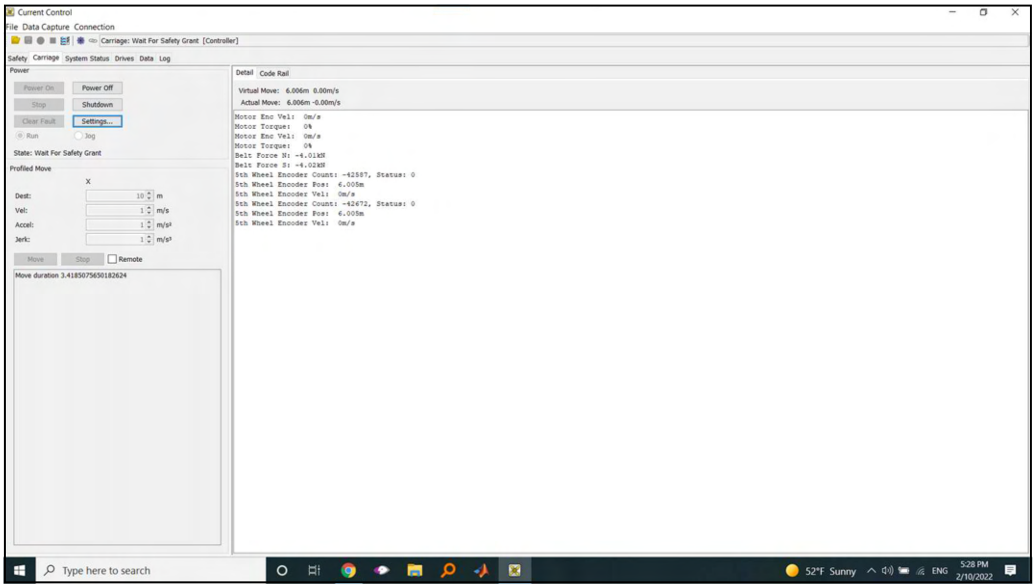

43

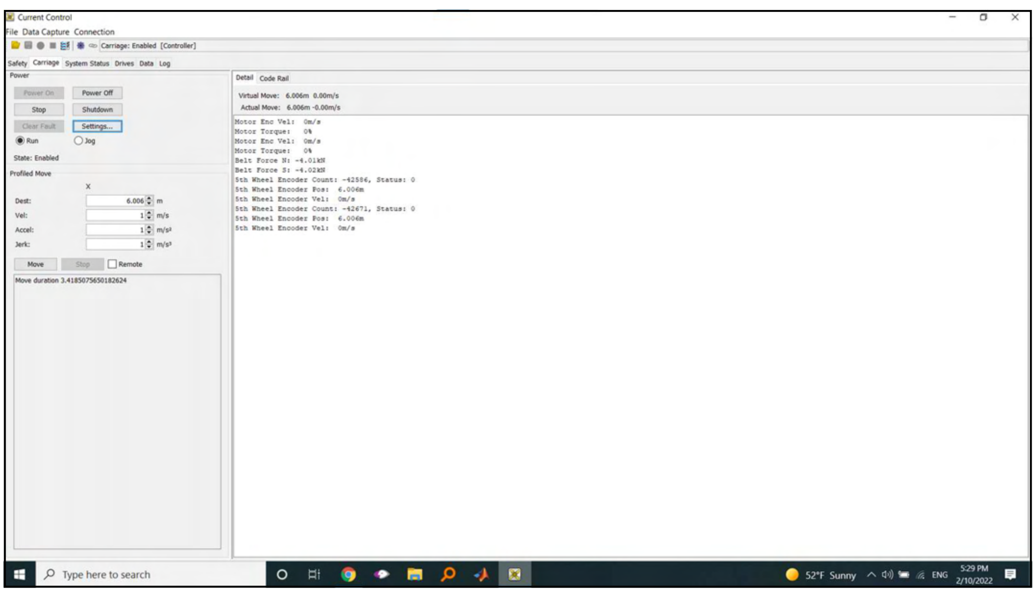

44

Settings

45

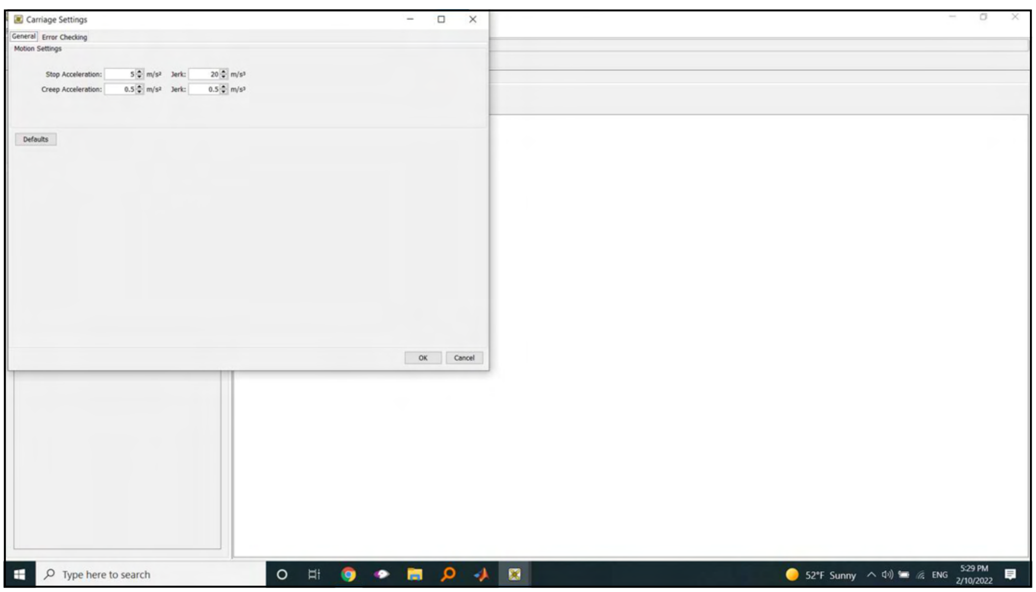

46

4/12/2022

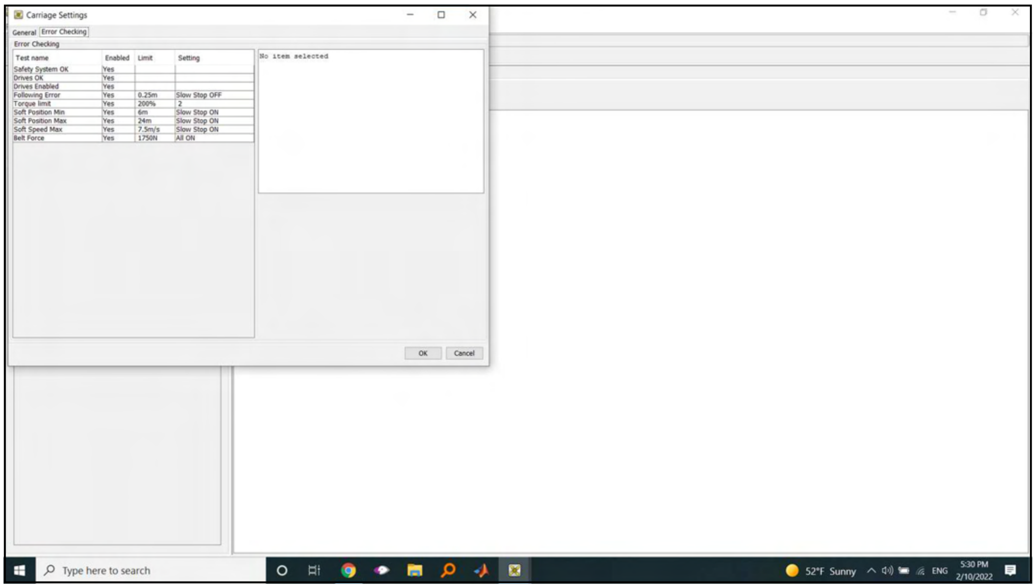

47

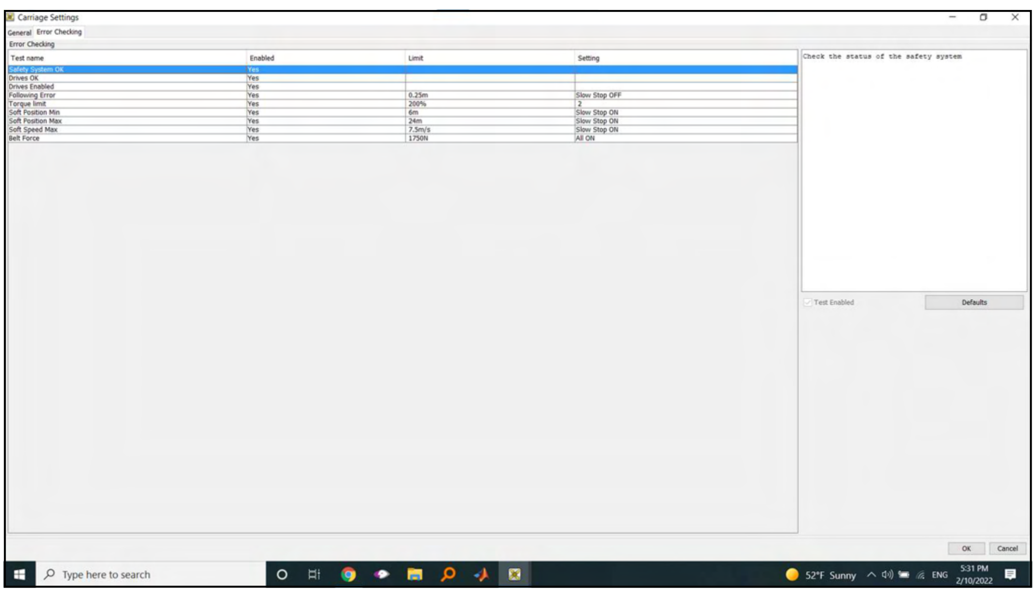

48

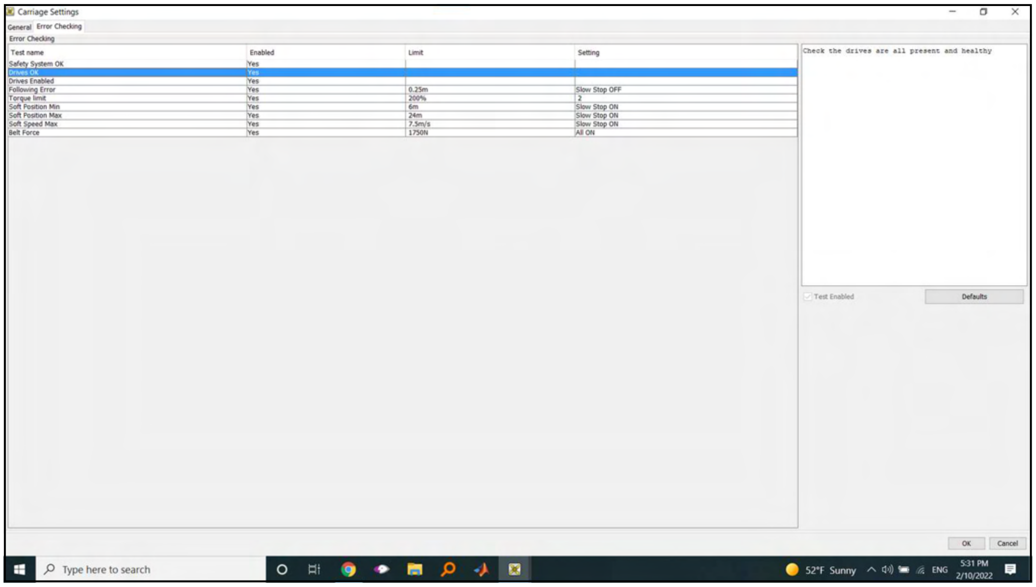
Carriage Settings
General
Error Checking
Error Checking
Test name
Enabled
Limit
Setting
Safety System OK Yes
Drives OK Yes
Drives Enabled Yes
Following Error Yes 0.25m Slow Stop OFF
Torque limit Yes 200% 2
Soft Position Min Yes 6m Slow Stop ON
Soft Position Max Yes 24m Slow Stop ON
Soft Speed Max Yes 7.5m/s Slow Stop ON
Belt Force Yes 1750N All ON
Check the drives are all present and healthy
Test Enabled
Defaults
OK
Cancel
Type here to search
52°F Sunny
ENG
5:31 PM
2/10/2022

49

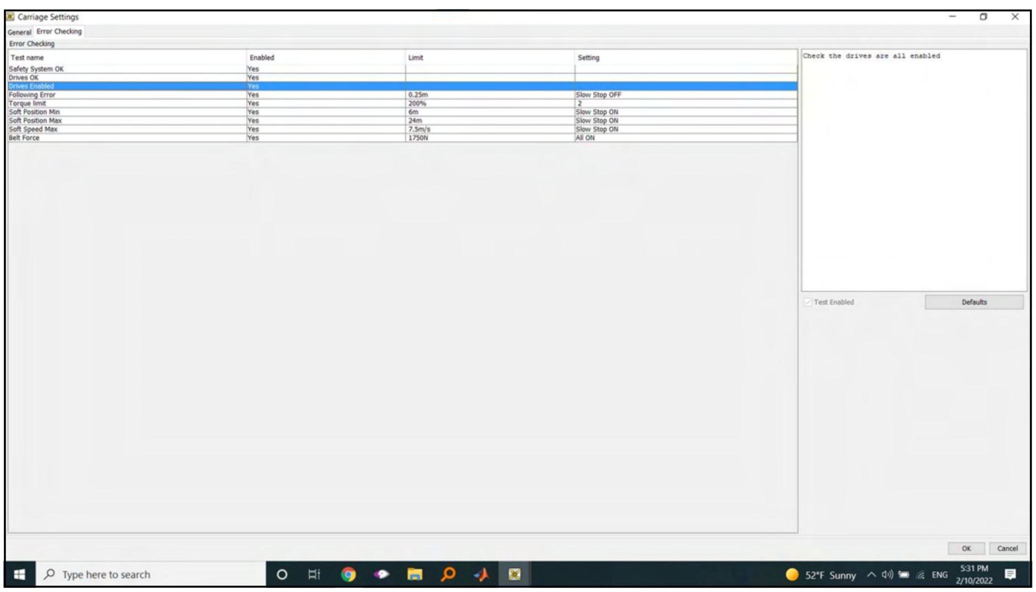
Carriage Settings
General
Error Checking
Error Checking
Test name
Enabled
Limit
Setting
Safety System OK Yes
Drives OK Yes
Drives Enabled Yes
Following Error Yes 0.25m Slow Stop OFF
Torque limit Yes 200% 2
Soft Position Min Yes 6m Slow Stop ON
Soft Position Max Yes 24m Slow Stop ON
Soft Speed Max Yes 7.5m/s Slow Stop ON
Belt Force Yes 1750N All ON
Check the drives are all enabled
Test Enabled
Defaults
OK
Cancel
Type here to search
52°F Sunny
ENG
5:31 PM
2/10/2022

50

4/12/2022

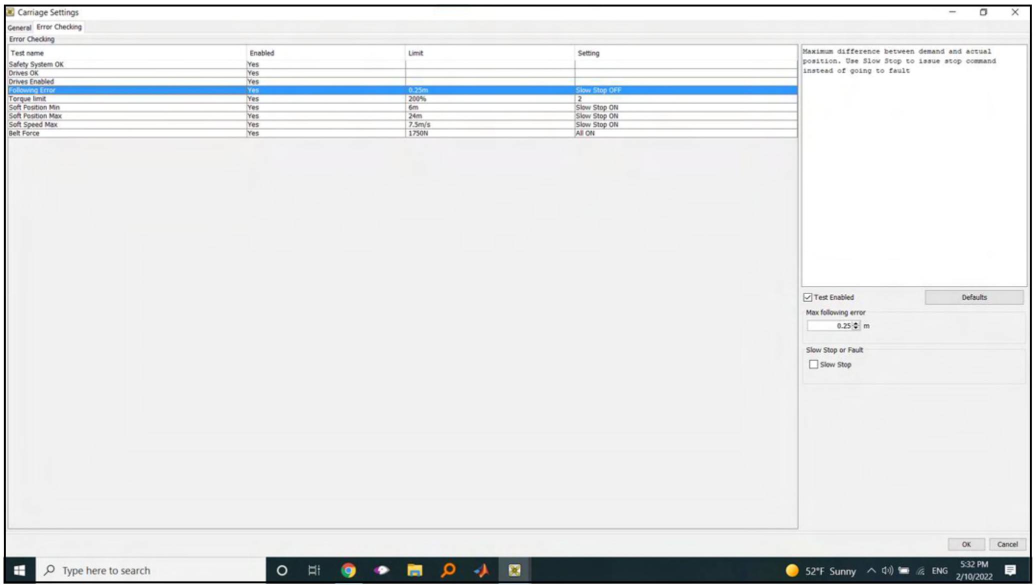

51

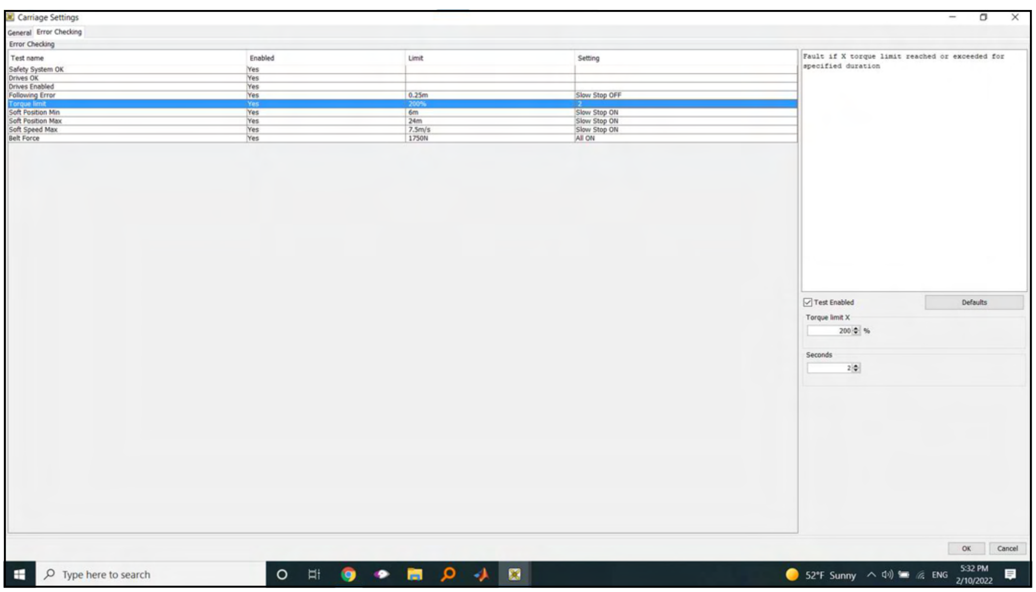

52

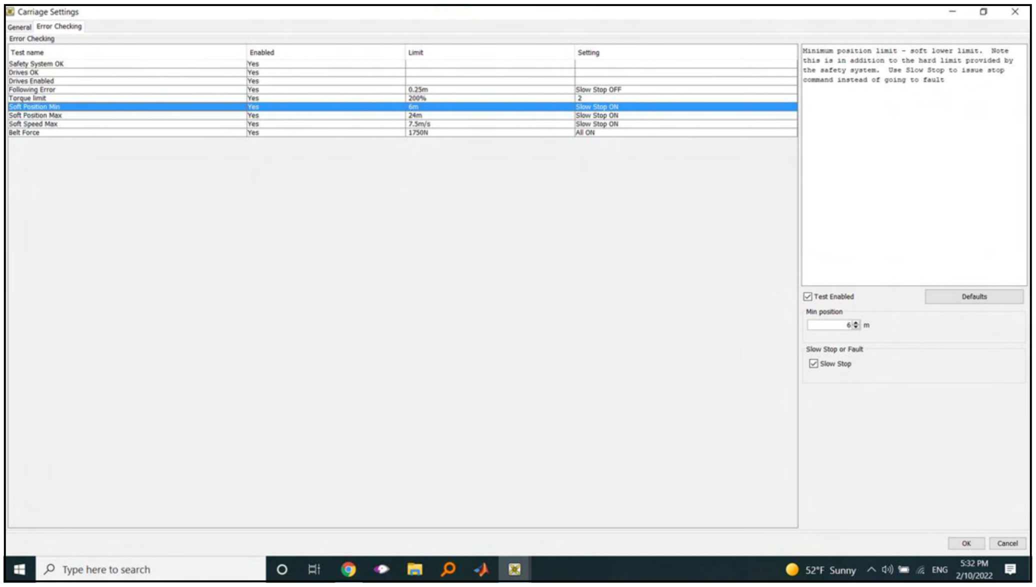
Carriage Settings
General
Error Checking
Error Checking
Test name
Enabled
Limit
Setting
Safety System OK
Yes
Drives OK
Yes
Drives Enabled
Yes
Following Error
Yes
0.25m
Slow Stop OFF
Torque limit
Yes
200%
2
Soft Position Min
Yes
6m
Slow Stop ON
Soft Position Max
Yes
24m
Slow Stop ON
Soft Speed Max
Yes
7.5m/s
Slow Stop ON
Belt Force
Yes
1750N
All ON
Minimum position limit - soft lower limit. Note this is in addition to the hard limit provided by the safety system. Use Slow Stop to issue stop command instead of going to fault
Test Enabled
Defaults
Min position
6
m
Slow Stop or Fault
Slow Stop
OK
Cancel
Type here to search
52°F Sunny
ENG
5:32 PM
2/10/2022

53

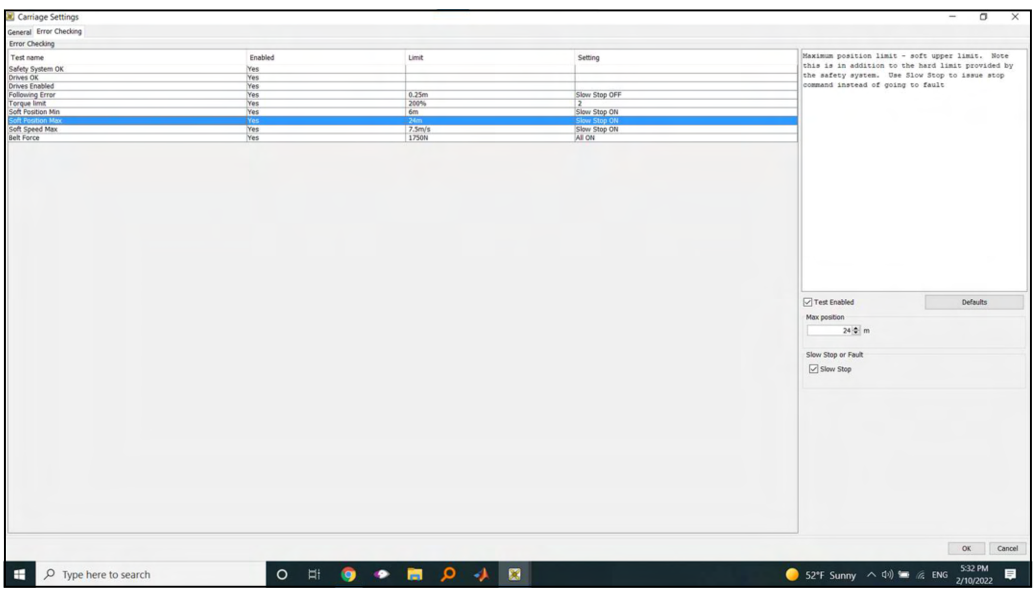
Carriage Settings
General
Error Checking
Error Checking
Test name
Enabled
Limit
Setting
Safety System OK
Yes
Drives OK
Yes
Drives Enabled
Yes
Following Error
Yes
0.25m
Slow Stop OFF
Torque limit
Yes
200%
2
Soft Position Min
Yes
6m
Slow Stop ON
Soft Position Max
Yes
24m
Slow Stop ON
Soft Speed Max
Yes
7.5m/s
Slow Stop ON
Belt Force
Yes
1750N
All ON
Maximum position limit - soft upper limit. Note this is in addition to the hard limit provided by the safety system. Use Slow Stop to issue stop command instead of going to fault
Test Enabled
Defaults
Max position
24
m
Slow Stop or Fault
Slow Stop
OK
Cancel
Type here to search
52°F Sunny
ENG
5:32 PM
2/10/2022

54

4/12/2022

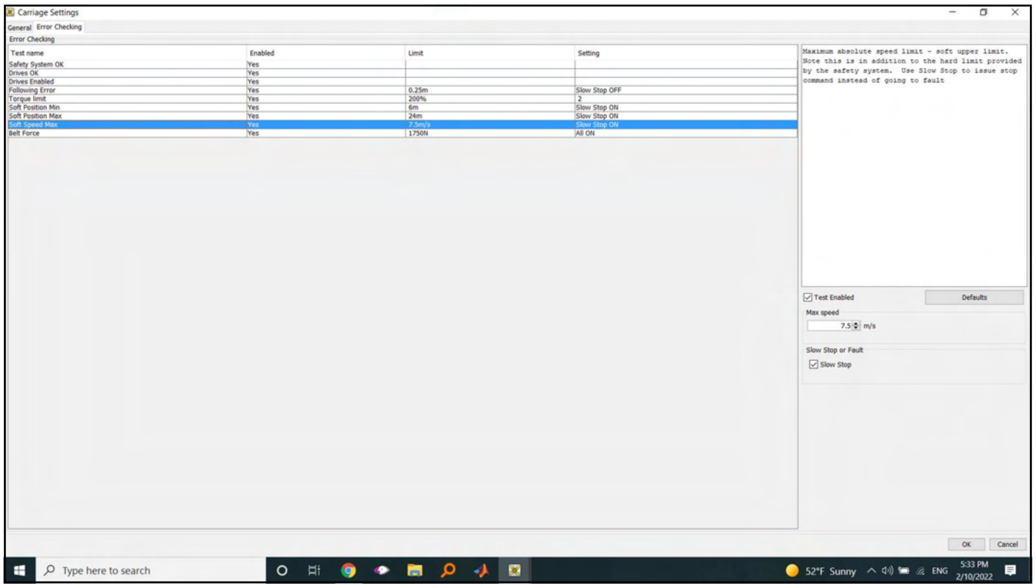

55

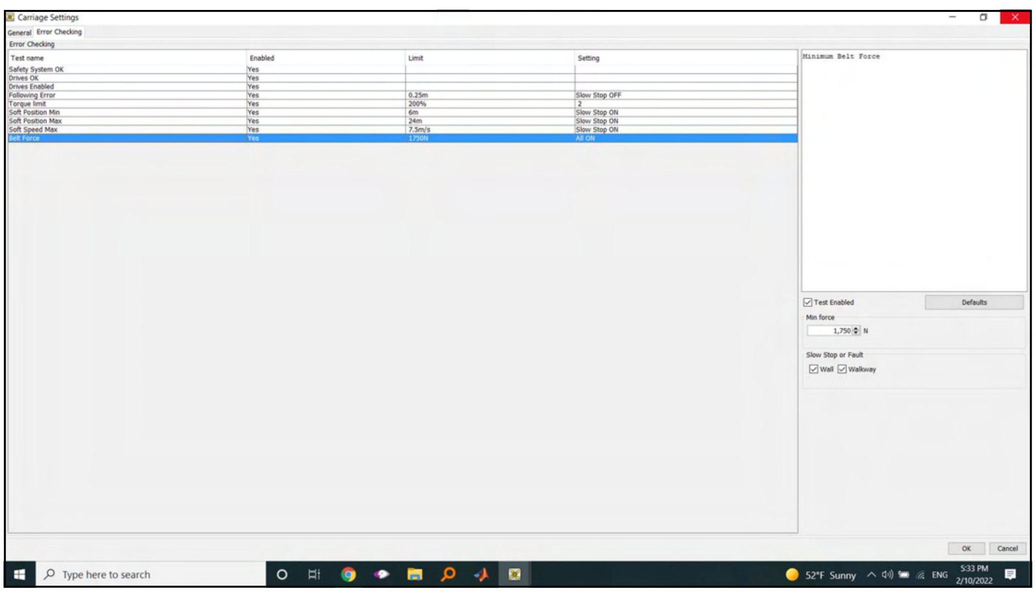

56

Common Errors & Faults

57

Belt Force Error

1. Check Belt Force (should be ~4000N)
2. Tighten Belts if needed or Adjust Setting to lower value (Default 1750N)
3. Once Belts are adjusted Clear the Fault on Carriage Tab
4. Press Power On button in GUI
5. Press Green Button giving Safety Grant

58

4/12/2022

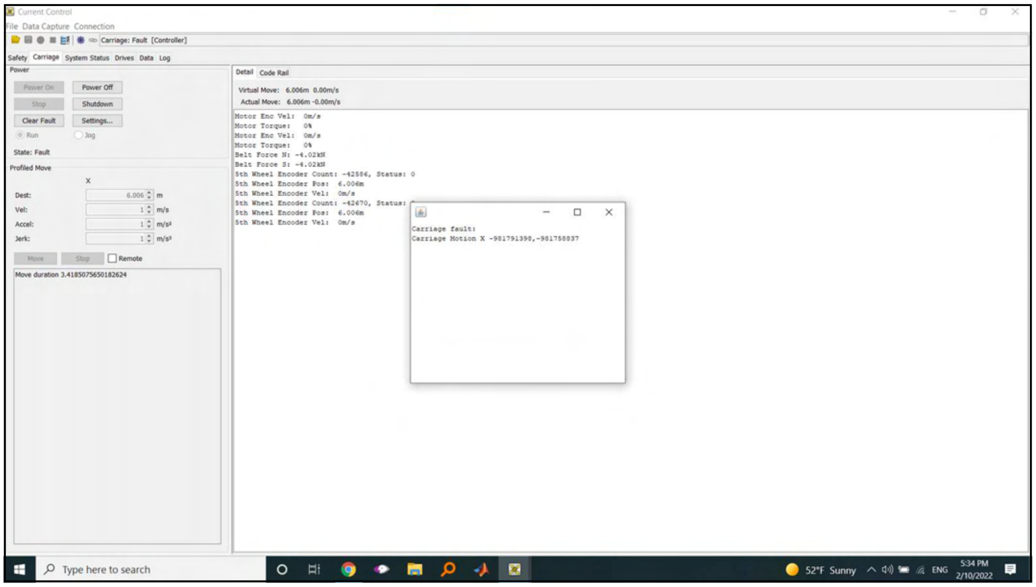

59

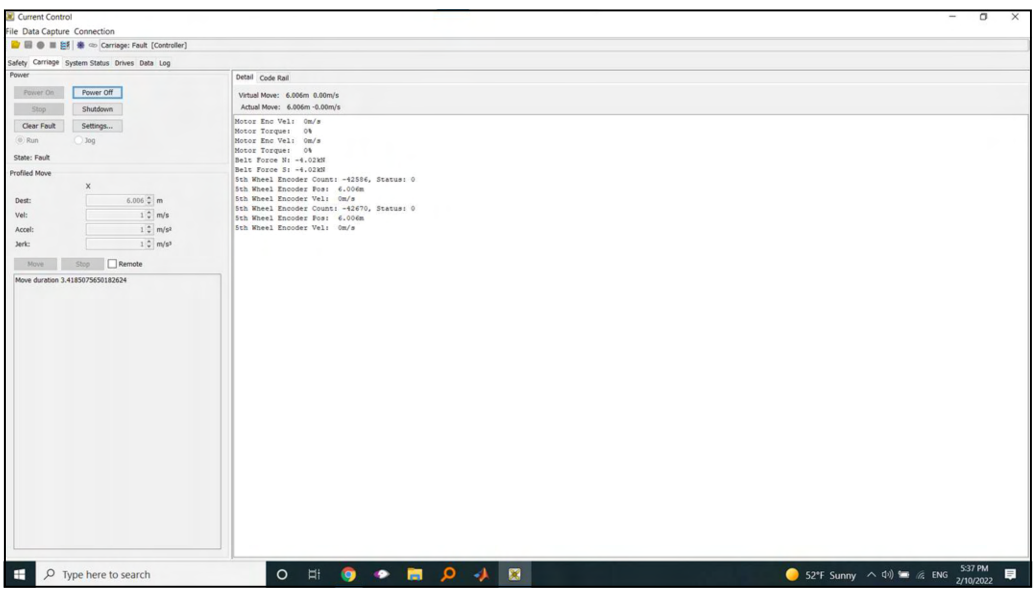

60

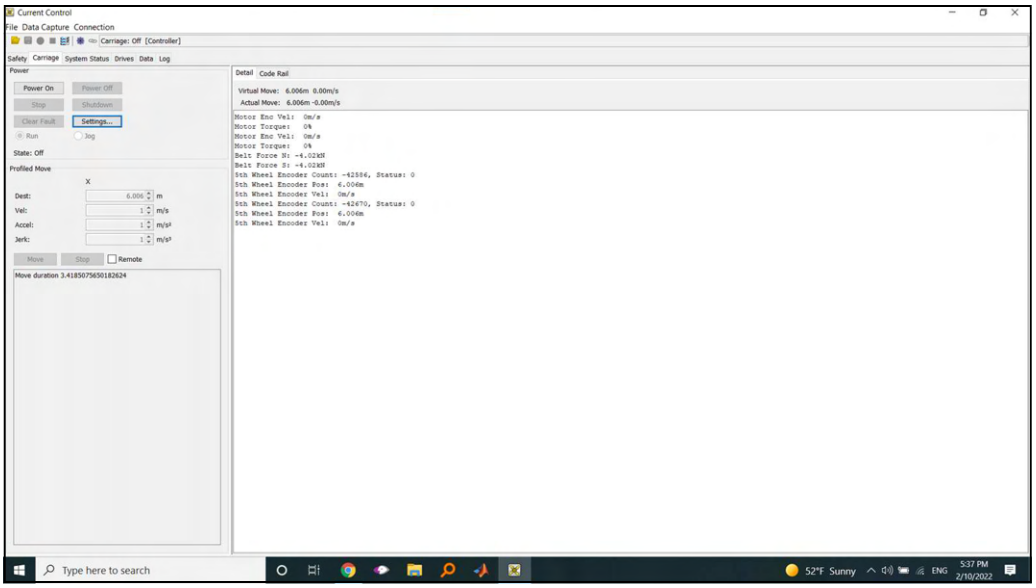

61

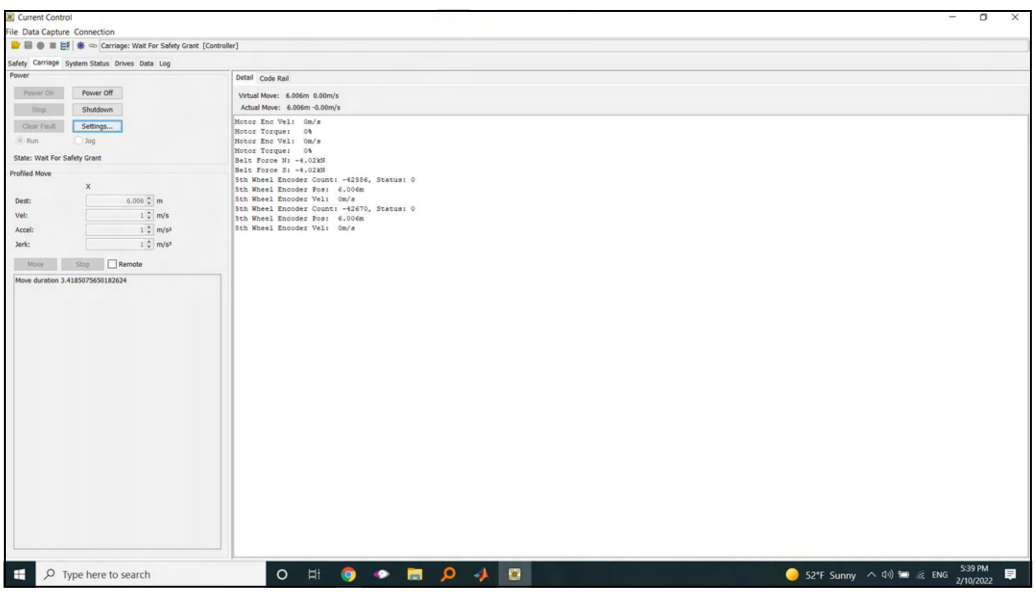

62

FAQs

63

FAQs

- Can I operate the carriage and show it off to my friends?
    - Yes, if properly trained of sound mind, and you do not cause disruption to any on going activities
- What should I do if something breaks?
    - Note in log book and contact Dr. Christine Gilbert immediately
- How do I get the key to the Carriage?
    - Contact Dr. Christine Gilbert to set a time for carriage use and to sign out the keys
- How do I add my experiments to the schedule?
    - Use the Norris Lab 5 calendar. If you do not have access to the calendar contact your lab PI or Dr. Christine Gilbert to schedule a time
- How do I get access to the lab calendar?
    - Contact Dr. Christine Gilbert of Mac McCord
- How do I get access to Norris Lab 5?
    - Fill out the Norris Lab 5 access form and email to Mac McCord
- How do I get trained to use the tow tank?
    - Contact Dr. Christine Gilbert to receive training materials and to schedule a time for in person training
- What equipment can I use as part of the tow tank?

64

FAQs Cont…

- I'm not sure how to do something…who should I talk to?
  - If you have any questions about the tow tank first reference this operations manual and the tow tank manual. If these resources do not contain the answer contact Dr. Christine Gilbert
- How do I mount a model to the carriage?
  - Use the vertical planar motion mechanism or the heave post. Items can be bolted to the ITEM extrusions or new deck plates for mounting can be fabricated.
- How do I get data off of the carriage?
  - Use a daq system, the data capture function in the carriage software or connect an instrument to one of the spare CAT5 cables with the permission of Dr. Christine Gilbert
- I want to modify the carriage for my experiment…who should I talk to?
  - Please contact Dr. Christine Gilbert to have any and all modifications to the carriage approved
- Why is the Tow tank UVA Colors?
  - Good question
- What are the extrusions on the Tow Carriage?
  - The carriage is built from ITEM aluminium extrusions and is compatible with other similar T-slot products
- I want to put in a velocity profile…how do I do that?
  - You can't yet (COMING SOON)

65

Troubleshooting Procedure

66

Troubleshooting

1. Check the Safety Tab ensure all boxes are green
2. Check carriage tab and make sure all faults are cleared
3. Make sure key is in run position and green light is solid
4. Check all E-Stops are not pressed
5. Make sure all components are on
6. Close and reopen the software
7. Shut down machine off and on again (soft shutdown through GUI if possible otherwise turn key to off and then back to run)
8. Hard shutdown machine Turn key to off, turn carriage cabinet and wall cabinet off, turn wall cabinet,then carriage cabinet on, wait ~1 min then turn key to run position
9. If all else fails, save the log and send to ED with description of problem

67

Filling the Tank
(To fill tank contact Mac McCord)

68

Lab Contacts & Resources
(For all tow tank related info contact Dr. Christine Gilbert)

69

Appendix C

VPMM Fabrication

DLBA NAVAL ARCHITECTS
A GIBBS & COX DIVISION

Document: ENGVT3712 - VPMM BOM and Weight Estimate
Project: Virginia Tech Carriage and VPMM
Date: 9/27/2021
Revised: -

Prepared by: TYLER JENKINS
Date: 9/28/2021
Reviewed by: DONALD RICKERSON
Date: 9/28/2021

860 G
Ches
www.

ITEM	QTY	DESCRIPTION	MATERIAL	MANUFACTURER/ VENDOR	PART NO./MODEL	UNIT WEIGHT, LBS	TOTAL WEIGHT, LBS	REMARKS
BILL OF MATERIALS - VPMM								
1	2	VPMM ACTUATOR	VARIES	PARKER / CROSS AUTOMATION	ETH050M20A1K1BFMN0600B	35.05	70.10	-
2	2	VPMM SERVO MOTOR	VARIES	PARKER / CROSS AUTOMATION	MPP1003-KPSB	INC. IN #1	-	-
3	2	VPMM SERVO DRIVE	VARIES	PARKER / CROSS AUTOMATION	S100V2F12I10T10M00	INC. IN #1	-	-
4	2	DOUBLE SIX SLOT RAIL, 80 X 40 MM, 1220 MM LENGTH	ALUMINUM	ITEM	0.0.026.34	8.17	16.34	LONGITUDINAL RAILS
5	2	DOUBLE SIX SLOT RAIL, 80 X 40 MM, 685 MM LENGTH	ALUMINUM	ITEM	0.0.026.34	4.59	9.17	ACTUATOR MOUNTING
6	4	QUAD EIGHT SLOT RAIL, 80 X 80 MM, 880 MM LENGTH	ALUMINUM	ITEM	0.0.265.80	10.33	41.33	TRANSVERSE RAILS
7	4	QUAD EIGHT SLOT RAIL, 80 X 80 MM, 430 MM LENGTH	ALUMINUM	ITEM	0.0.265.80	5.05	20.19	VERTICAL CORNER RAILS
8	16	ANGLE BRACKET, 80 X 80 MM	ZINC	ITEM	0.0.411.23	0.59	9.52	-
9	16	ANGLE BRACKET, 160 X 80 MM	ZINC	ITEM	0.0.436.23	1.17	18.68	-
10	8	ANGLE BRACKET, 40 X 40 MM	ZINC	ITEM	0.0.411.24	0.26	2.10	-
11	8	END CAP, 80 X 80 MM	ZINC	ITEM	0.0.679.73	0.22	1.73	-
12	8	END CAP, 80 X 40 MM	ZINC	ITEM	0.0.679.72	0.11	0.86	-
13	2	FLUORONYLINER BUSHING, 1" CLOSED	VARIES	THOMSON LINEAR	FNYBUPB16	7.8	15.60	CORROSION RESISTANT SEALS
14	2	SHAFT, 1" DIA, 8.5" LENGTH	316 SS	THOMSON LINEAR	1LSS316CTL8.500	1.94	3.87	-
15	4	SHAFT SUPPORT, FOR 1" SHAFT	ALUMINUM	THOMSON LINEAR	ASB16-XS	0.44	1.76	
16	2	VPMM CLEVIS JOINT TOP PLATE, 1", 5" X 2"	AL - 5000 SERIES*	CUSTOM	CUSTOM	0.98	1.95	WITH TAPPED HOLE FOR ACTUATOR SHAFT
17	4	VPMM CLEVIS JOINT SIDE PLATE, 3/4"	AL - 5000 SERIES*	CUSTOM	CUSTOM	0.35	1.42	WITH TAPPED HOLE FOR ITEM #19
18	4	BEARING MOUNTING BRACKET, 1/2"	AL - 5000 SERIES*	CUSTOM	CUSTOM	0.08	0.33	-
19	4	PIN FOR VPMM CLEVIS JOINT, 0.500" DIA, 1.3" length	316 SS	CUSTOM	CUSTOM	0.07	0.30	1/2"-20 THREADED FOR ITEM #17
20	4	SLEEVE BEARING, FOR 1/2" DIA SHAFT	RULON	McMASTER-CARR	6362K304	0.004	0.02	BETWEEN ITEM #17, #18, & #19
21	AR	MISC FASTENERS	-	-	-	-	10.00	-
						Total Weight:	225	
BILL OF MATERIALS - HEAVE STAFF								
22	12	3" X 1.5" U-GROOVE WHEEL	VARIES	SUNRAY INC.	REF QUOTE 56865	1	12.00	ALUMINUM CORE W/SS R4-2RS BEARINGS, 95A BLACK POLYURETHANE
23	24	U-GROOVE WHEEL MOUNTS, 1/2" PLATE	AL - 5000 SERIES*	CUSTOM	CUSTOM	0.21	5.09	-
24	2	HEAVE STAFF TIE BAR, 1" PLATE	AL - 5000 SERIES*	CUSTOM	CUSTOM	1.79	3.58	VERTICAL TUBE SPACERS (TOP AND BOTTOM)
25	2	45" LONG PIPE, 2" OD X 1/8" WALL THICKNESS	AL - 6061 T6	CUSTOM	CUSTOM	3.23	6.46	VERTICAL HEAVE POST TUBES
26	2	TRANSVERSE MOUNTING PLATE, 1/2"	AL - 5000 SERIES*	CUSTOM	CUSTOM	10.71	21.43	TRANSVERSE SPANNER PLATES (2, EA DIFFERENT, SEE MODEL)
27	4	TRIPLE EIGHT SLOT RAIL, 120 X 40 MM, 230 MM LENGTH	ALUMINUM	ITEM	0.0.416.66	2.20	8.81	CONNECTS ITEM #26 TO CARRIAGE
28	12	ANGLE BRACKET, 40 X 40 MM	ZINC	ITEM	0.0.411.24	0.26	3.15	CONNECTS ITEM #27 (LOWER) TO CARRIAGE
29	12	ANGLE BRACKET, 80 X 80 MM	ZINC	ITEM	0.0.411.23	0.22	2.59	CONNECTS ITEM #27 (UPPER) TO CARRIAGE
30	1	PIVOT BOX, SHAFT, 1/2" X 3 1/2"	316 SS	CUSTOM	CUSTOM	0.07	0.07	-
31	AR	PIVOT BOX, BOTTOM AND VERTICAL PLATES, 1/2"	AL - 5000 SERIES*	CUSTOM	CUSTOM	0.78	0.78	-
32	1	PIVOT BOX, TOP PLATE, 1/4"	AL - 5000 SERIES*	CUSTOM	CUSTOM	0.23	0.23	BOLTS TO ITEM #24 (LOWER)
33	2	SLEEVE BEARING, FOR 1/2" DIA SHAFT	RULON	McMASTER-CARR	6362K304	0.004	0.01	-
34	AR	MISC FASTENERS	-	CUSTOM	-	-	2.50	-
						Total Weight:	67	
BILL OF MATERIALS - SUBMERSIBLE ADAPTATION								
35	1	16" LONG PIPE, 3" OD X 1/4" WALL THICKNESS	AL - 6061 T6	CUSTOM	CUSTOM	3.37	3.37	TRANSVERSE TUBE, BOTTOM OF HEAVE STAFF
36	AR	PLATE, 1/2", LOWER HEAVE STAFF	AL - 5000 SERIES*	CUSTOM	CUSTOM	3.27	3.27	BOLTING FLANGES (2) AND CHOCKS (3), SUBMERSIBLE, FILLET WELD SIZE 1/2"
37	1	35" LONG PIPE, 3" OD X 1/4" WALL THICKNESS	AL - 6061 T6	CUSTOM	CUSTOM	7.37	7.37	HEAVE STAFF LOWER TUBE, FILLET WELD SIZE 1/2"
38	2	45" LONG PIPE, 2" OD X 1/4" WALL THICKNESS	AL - 6061 T6	CUSTOM	CUSTOM	6.03	12.06	VERTICAL HEAVE POST TUBES
39	1	HEAVE STAFF TIE BAR, 1" PLATE	AL - 5000 SERIES*	CUSTOM	CUSTOM	1.79	1.79	VERTICAL TUBE SPACER (1)
40	1	PIVOT BOX, SHAFT, 5/8" X 5"	AL - 6061 T6	CUSTOM	CUSTOM	0.15	0.15	TO BE WELDED INSIDE ITEM #35
41	1	PIVOT BOX, BOTTOM AND VERTICAL PLATES, 1/2"	AL - 5000 SERIES*	CUSTOM	CUSTOM	1.23	1.23	-
42	2	SLEEVE BEARING, FOR 5/8" DIA SHAFT	RULON	McMASTER-CARR	6362K307	0.005	0.01	-
43	4	CLEVIS JOINT ROD END, M8 MALE THREADED	SS	NORELEM	27629-08	0.09	0.37	-
44	4	CLEVIS JOINT, M8 FEMALE THREADED	SS	NORELEM	27615-08120820	0.15	0.61	-
45	2	ROD, 3/4" X 30 1/4"	SS	CUSTOM	CUSTOM	3.88	7.75	ROD EXTENSIONS FOR VPMM, TAPPED FOR ITEM #41
46	1	PLATE, 39" X 6 1/2", 1/4" THICK	AL - 5000 SERIES*	CUSTOM	CUSTOM	5.28	5.28	WITH HOLE IN CENTER FOR HEAVE STAFF
47	2	ANGLE, 1" X 1" X 1/4", 39" LONG	AL - 5000 SERIES*	CUSTOM	CUSTOM	1.66	3.33	BOLTED TO ITEM #44
48	AR	MISC FASTENERS	-	-	-	-	1.00	-
						Total Weight:	48	

*AL - 5000 SERIES PARTS TREATED AS ALUMINUM 5086 H112 IN STRENGTH CALCULATIONS, WITH YIELD STRENGTH OF 19 KSI.

DLBA NAVAL ARCHITECTS

Hydroelasticity Lab
VPMM Subsurface Heave Staff

Parts List			
ITEM #	QTY	DESCRIPTION	MATERIAL
1	2	45" LONG PIPE, 2" OD X 1/4" WALL THICKNESS	AL-6061 T6
2	1	16" LONG PIPE, 3" OD X 1/4" WALL THICKNESS	AL-6061 T6
3	1	35" LONG PIPE, 3" OD X 1/4" WALL THICKNESS	AL-6061 T6
4	1	PIVOT BOX, SHAFT, 5/8" X 5"	AL-6061 T6
5	1	FLANGES	$\frac{1}{2}$" AL-5086
6	1	LOWER STAFF TOP PLATE	$\frac{1}{2}$" AL-5086
7	1	ARCH	$\frac{1}{2}$" AL-5086
8	1	ARCH BASE PLATE	$\frac{1}{2}$" AL-5086

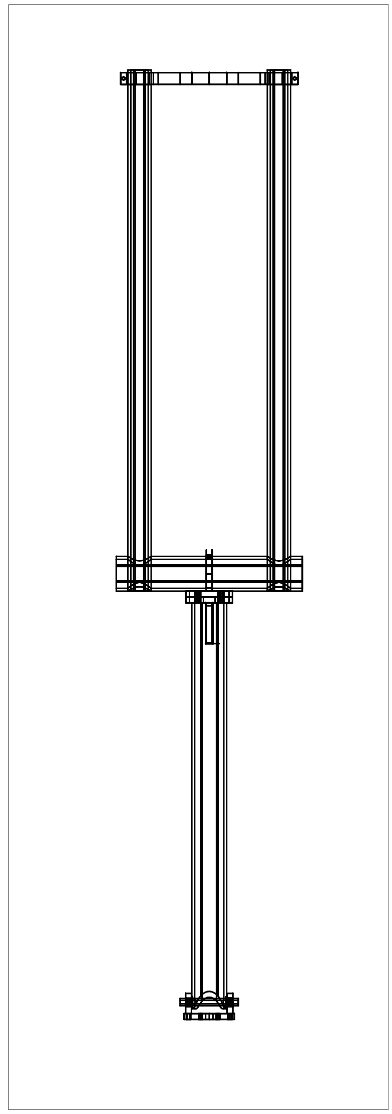

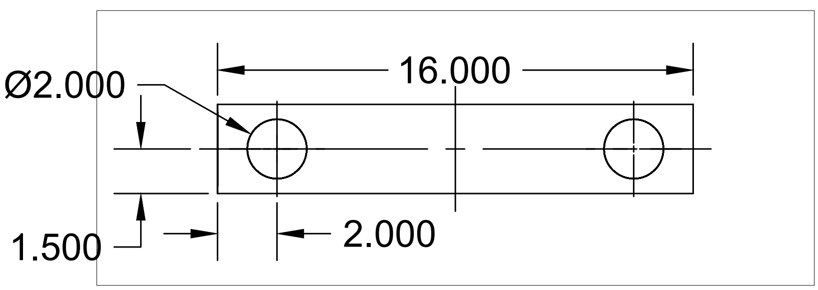

Item # 2

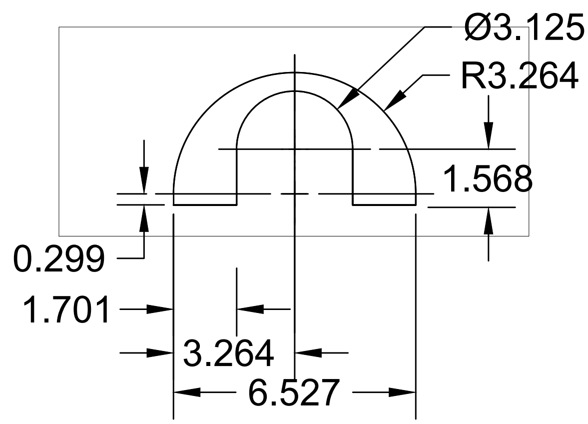

Item # 7

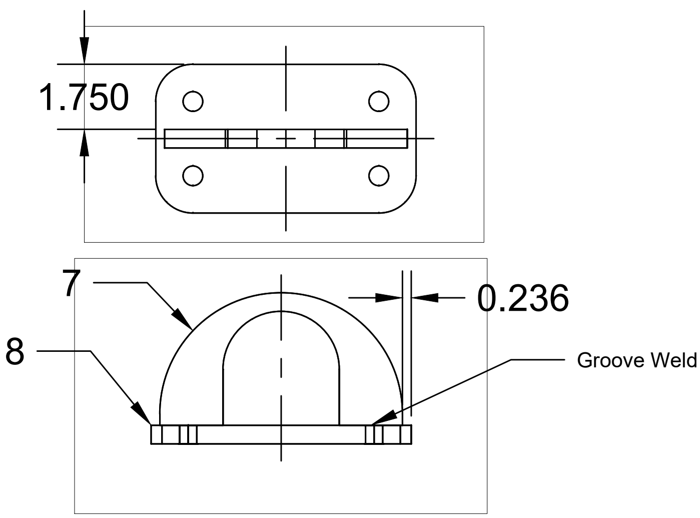

Assembly of
Item # 7 & 8

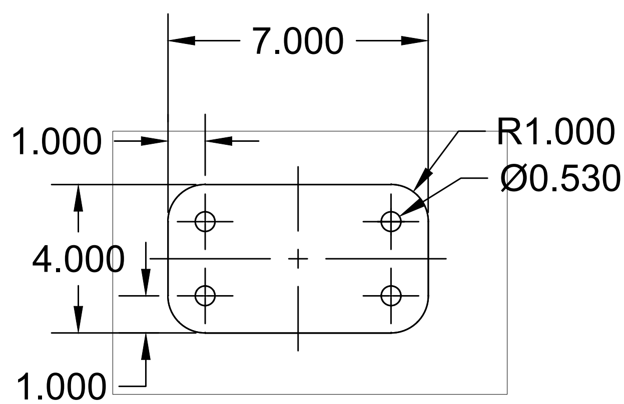

Item # 8

Assembly of Top Portion of Subsurface Heave Staff
Slide the assembly of items 7 & 8 onto item 3, then insert both 45" poles and weld the items 1 to 3 on both sides.

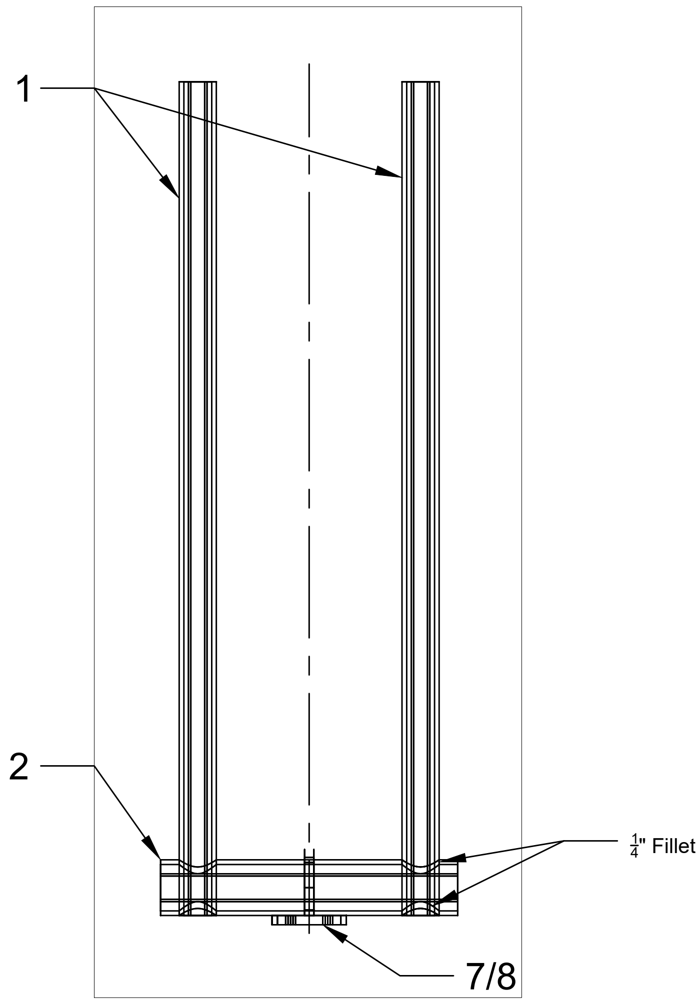

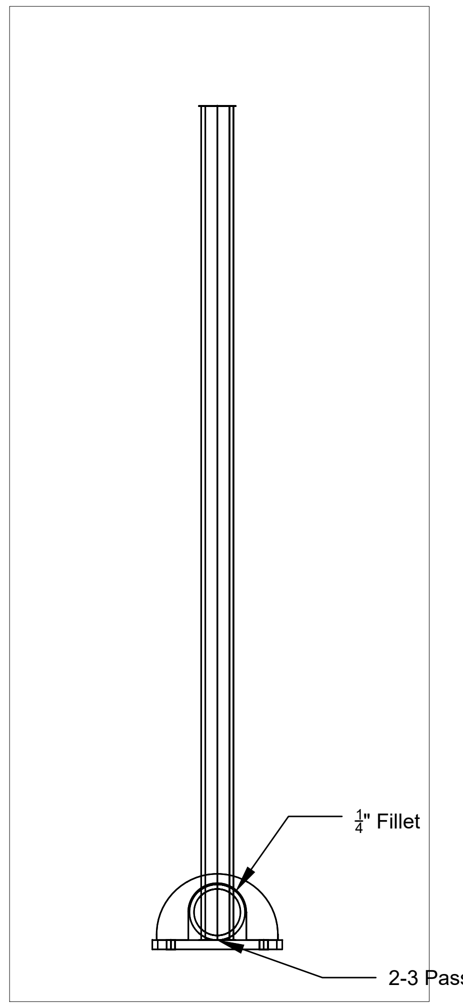

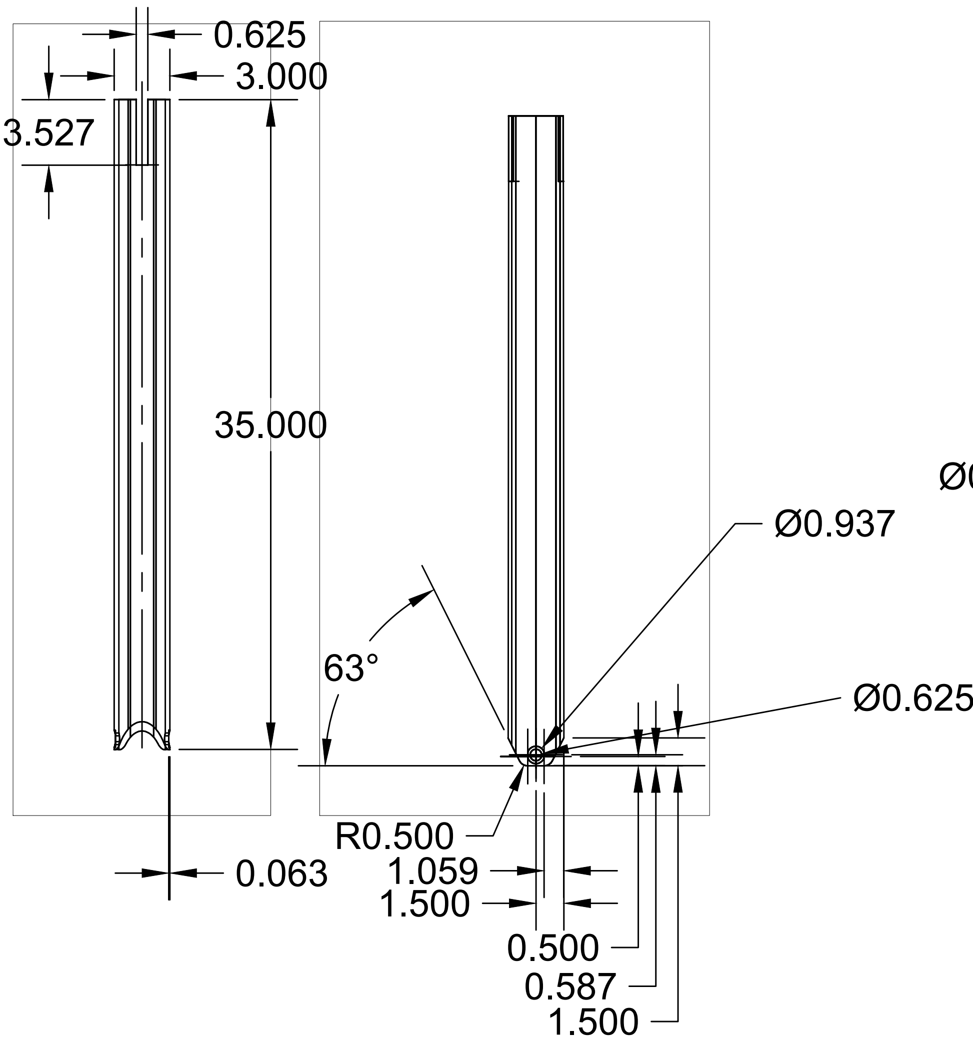

Item #3

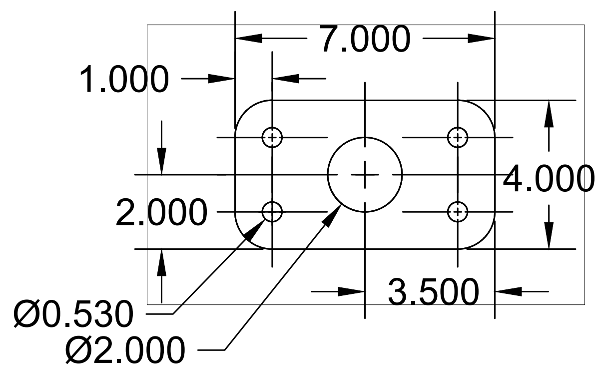

Item #6

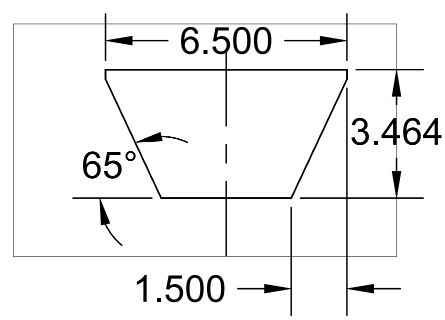

Item #5

Assembly of Bottom Portion of Subsurface Heave Staff
Weld items 5 & 6 to Item 3. Weld item 4 to item 3 on the inside

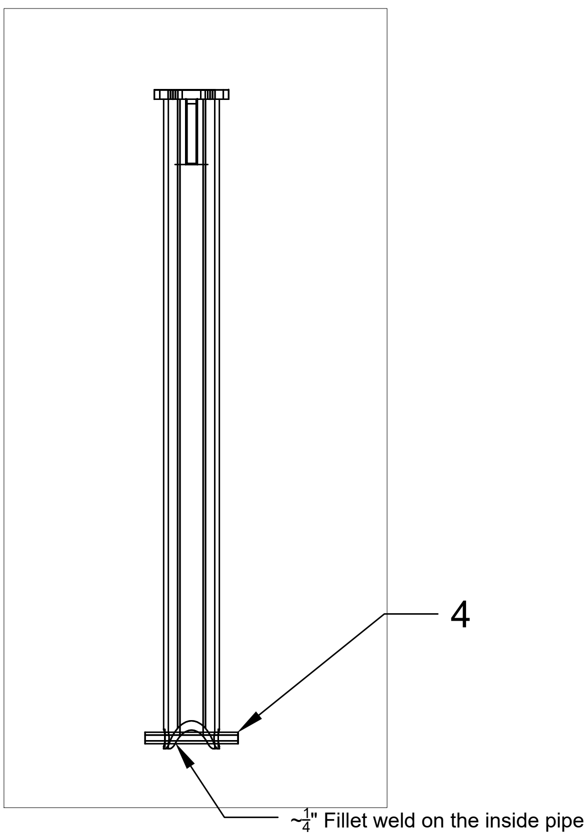

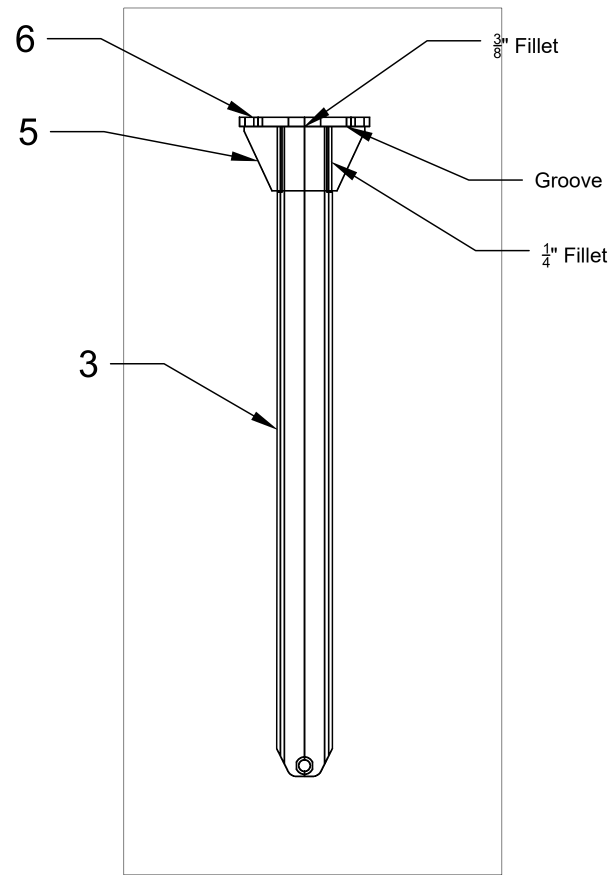

VPMM Clevis Joint Top Plate (2x)
1" AL-5086

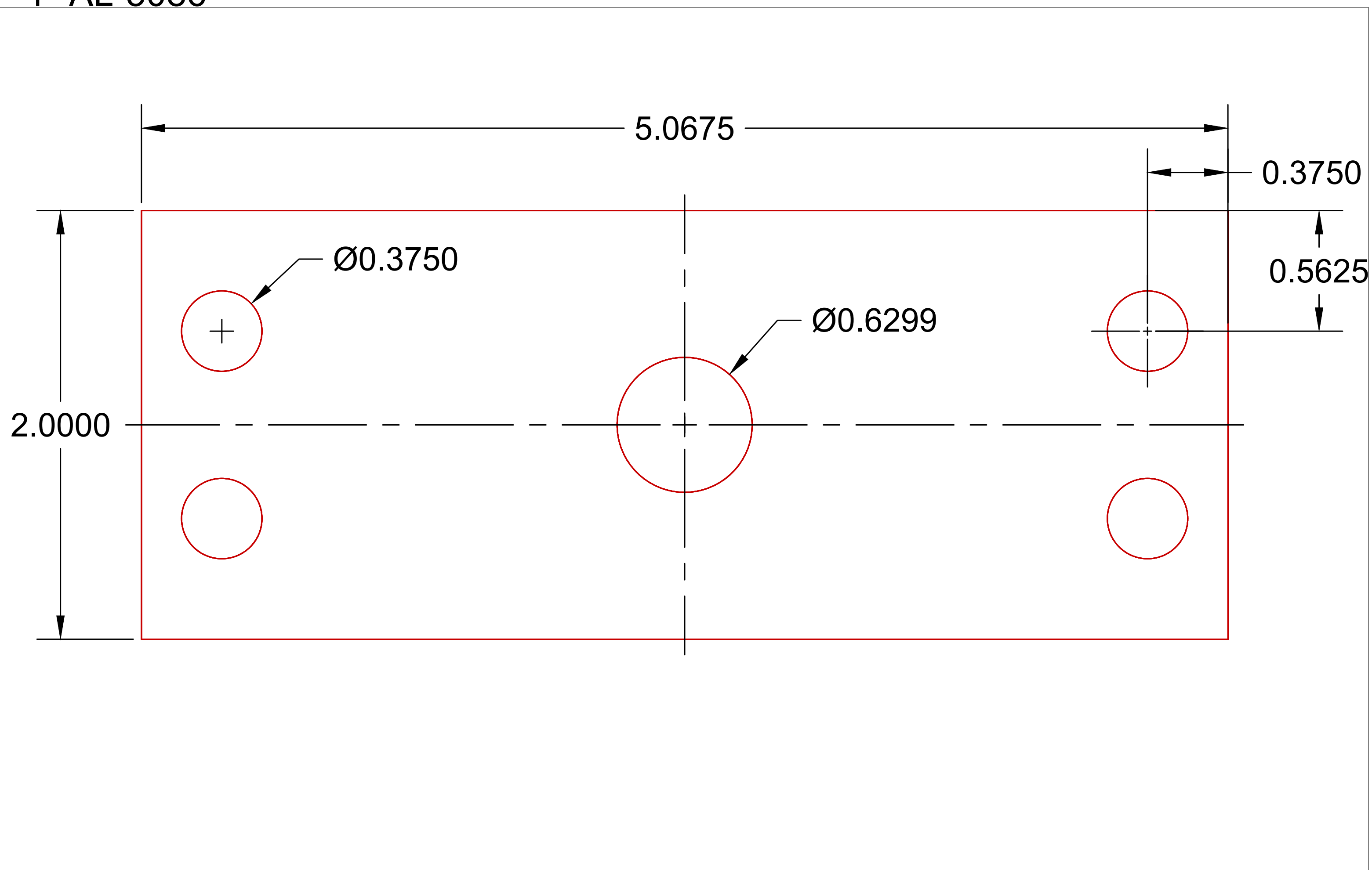

Bearing Mounting Bracket (4x)
$\frac{1}{2}$" Al-5086

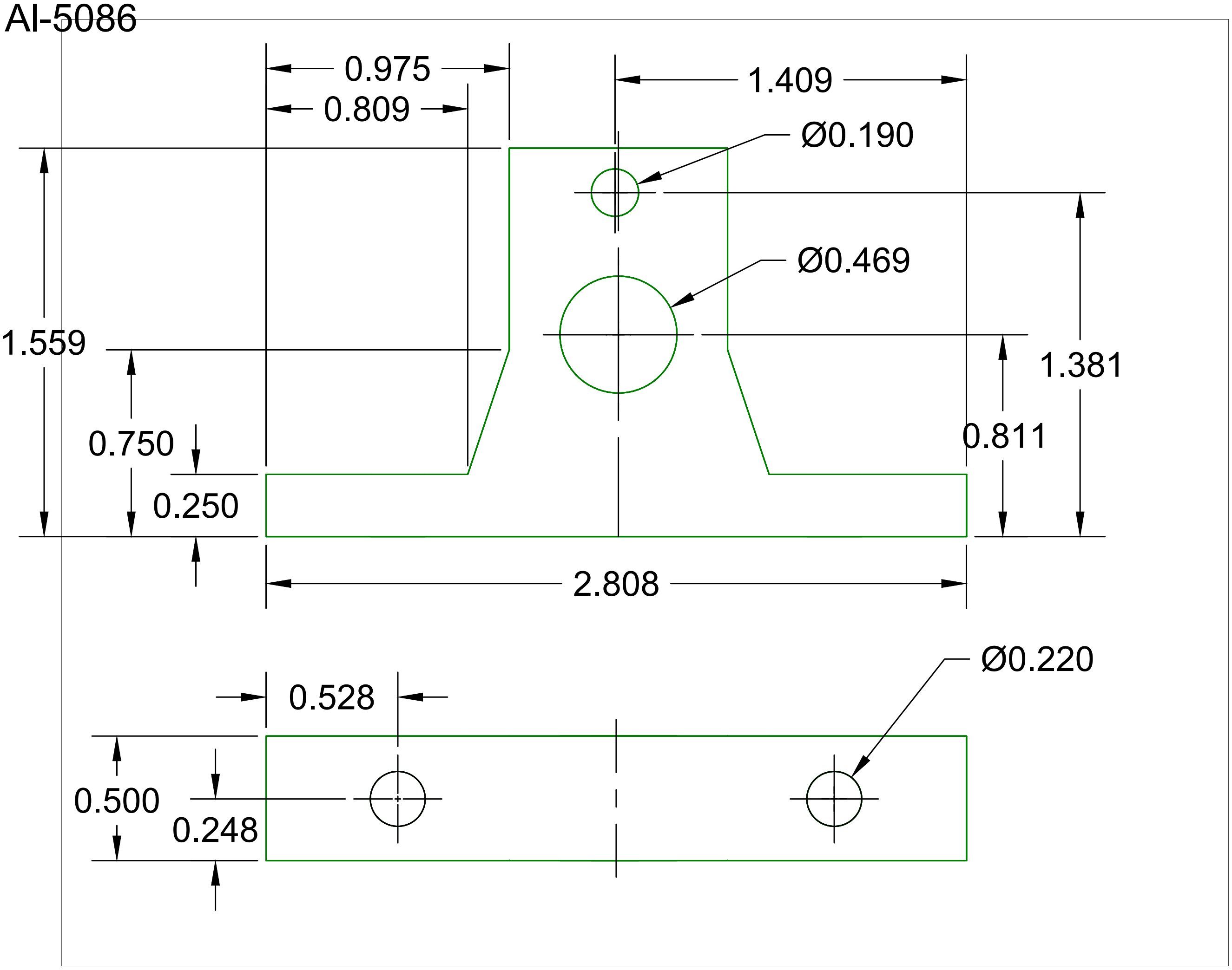

Pivot Box Top Plate (1x)

$\frac{1}{4}$" AL-5086

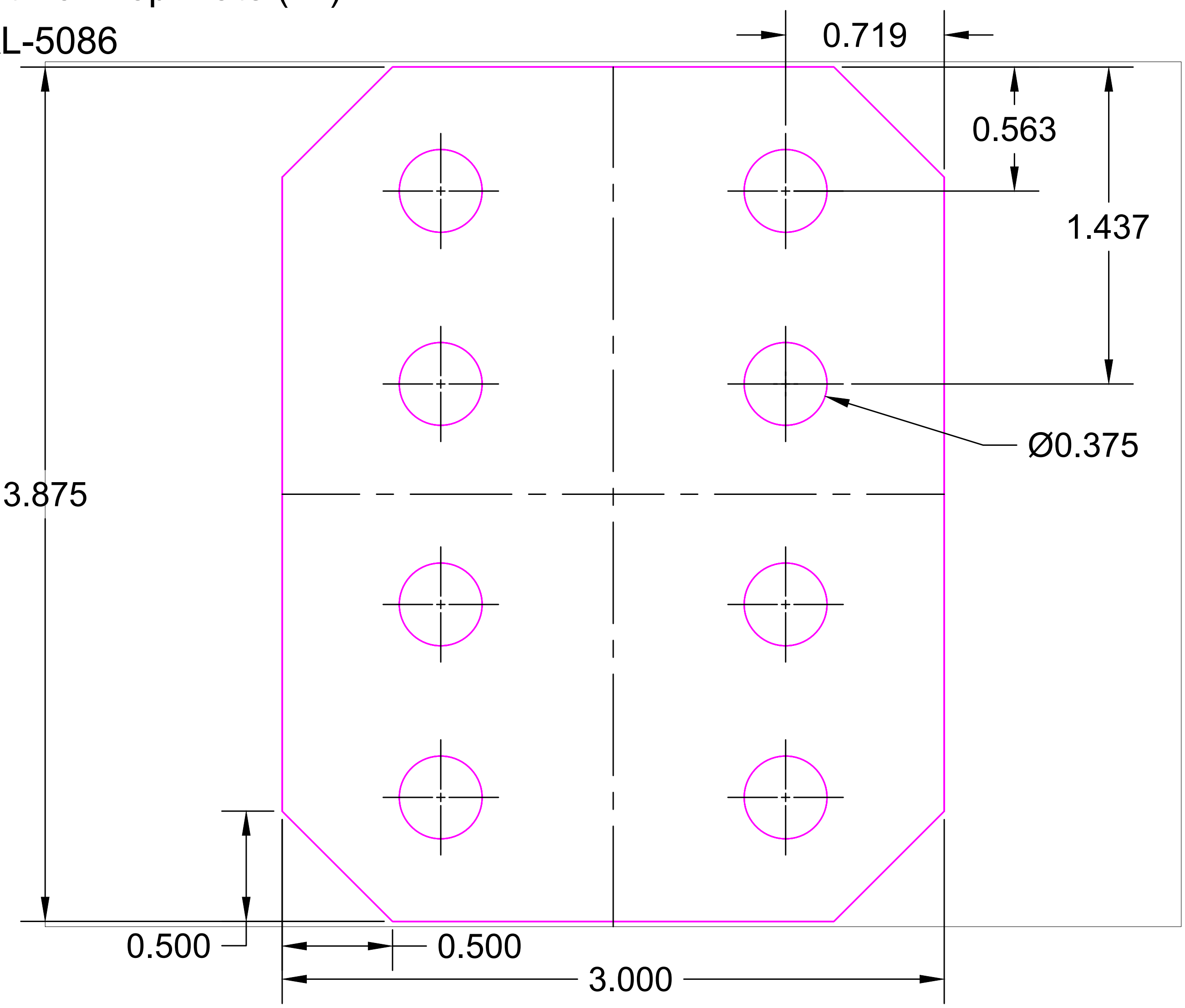

Sub Heave Post Tie Bar (1x)

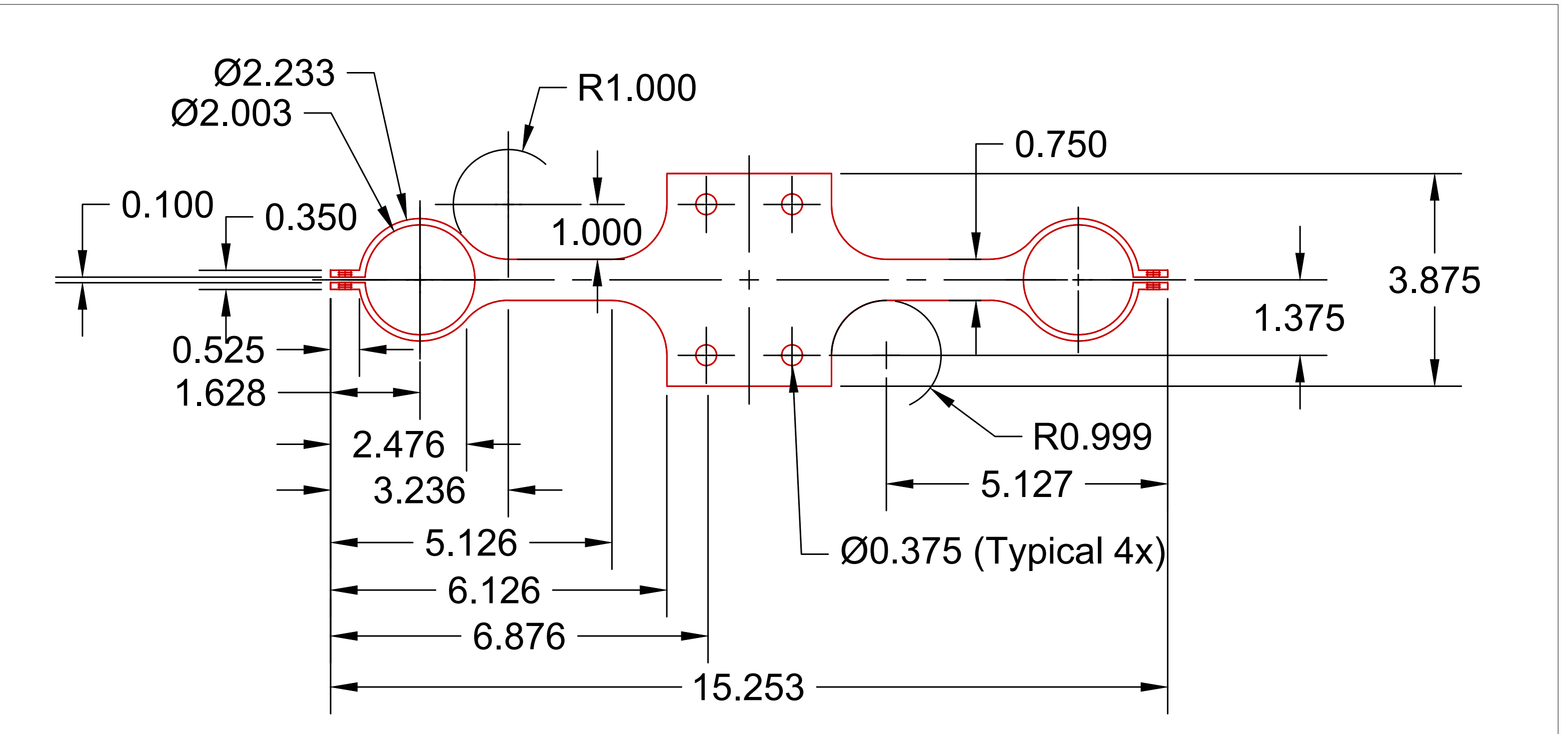

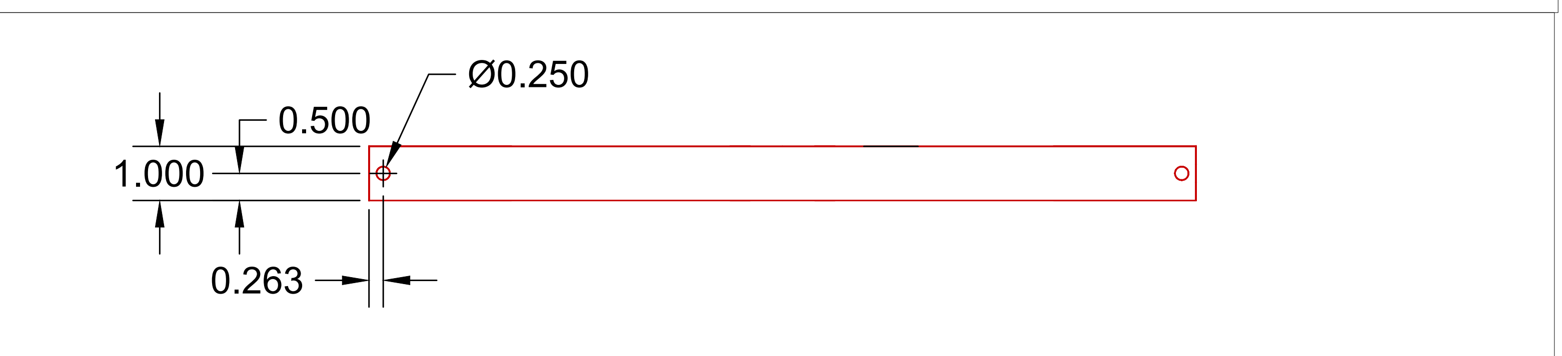

Sub Pivot Box Bottom

1x $\frac{1}{2}$" AL-5086

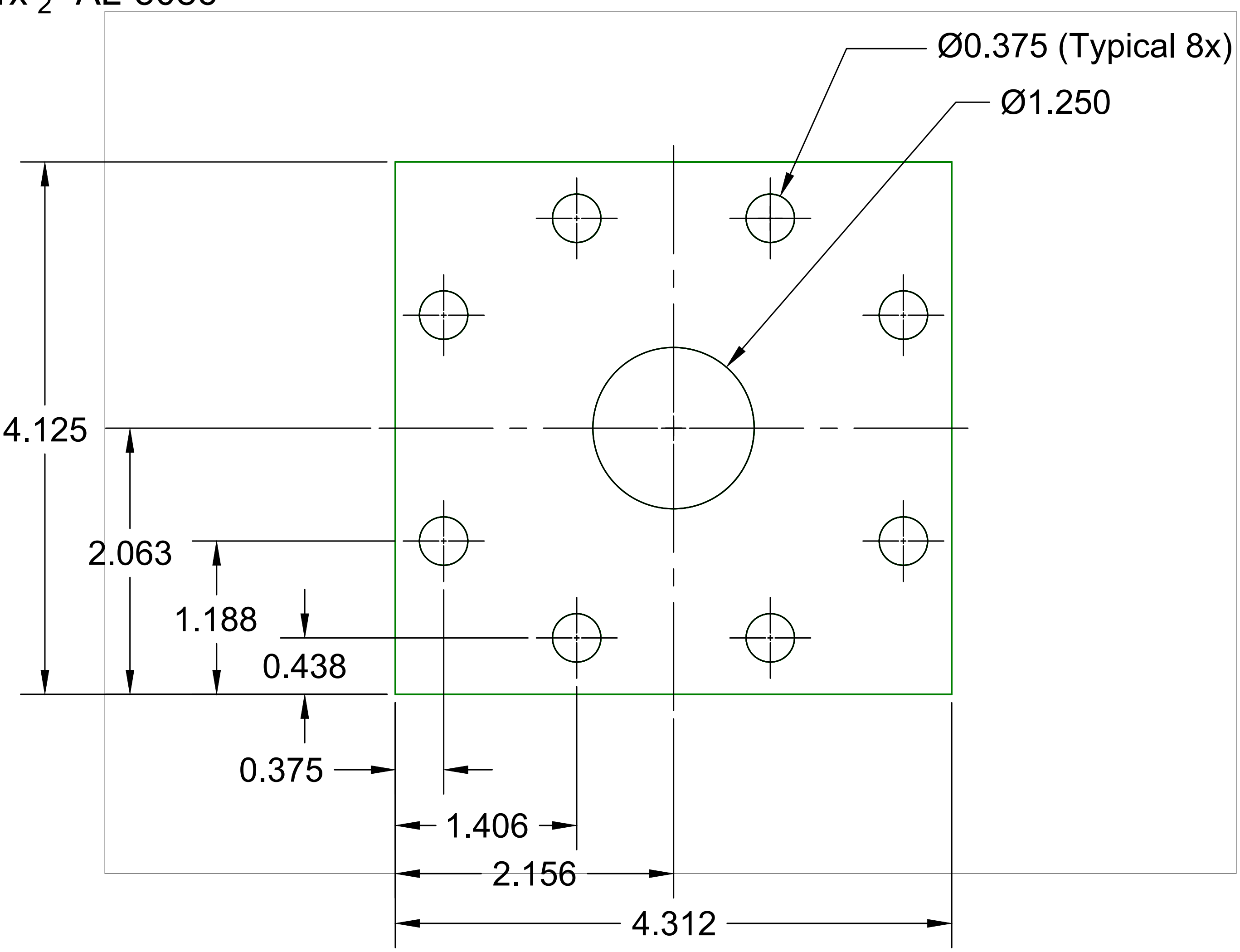

Surface Heave Post Tie Bar (2x)

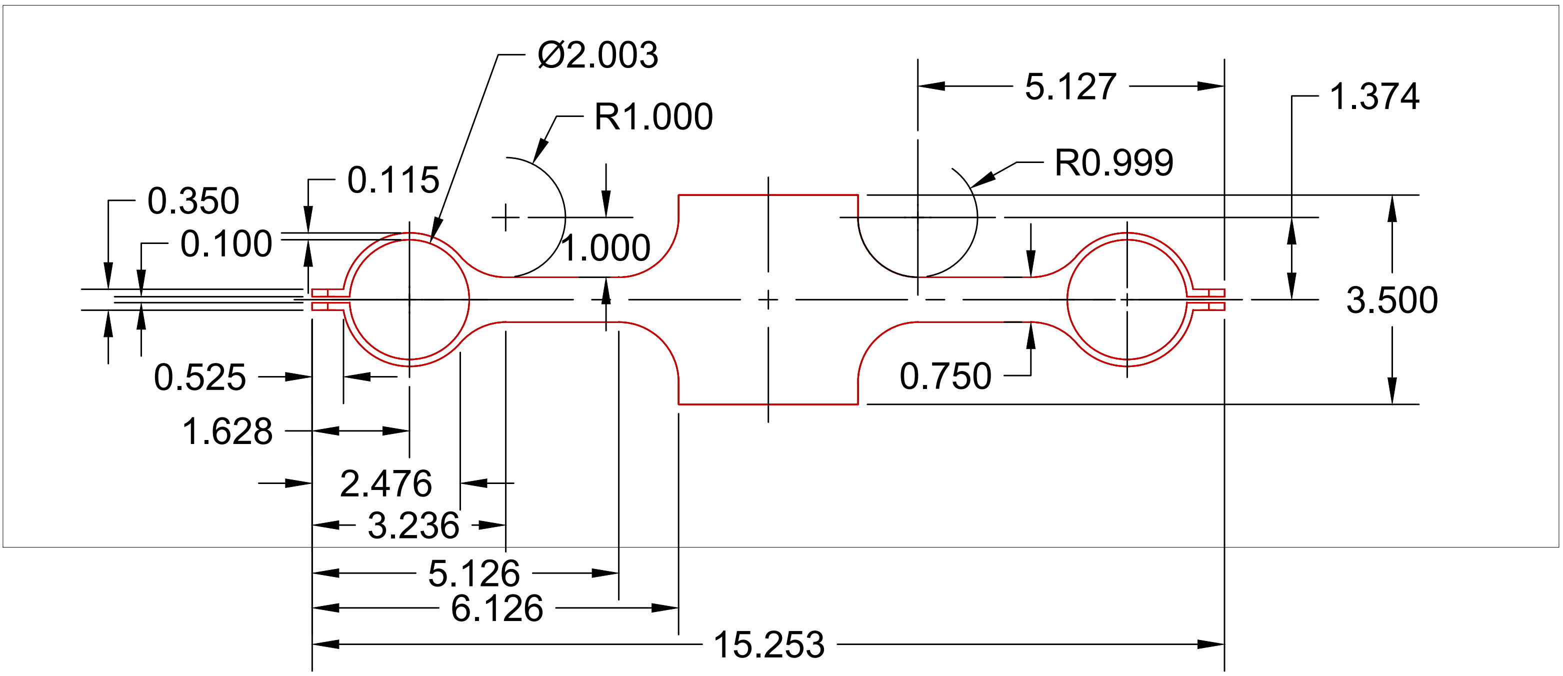

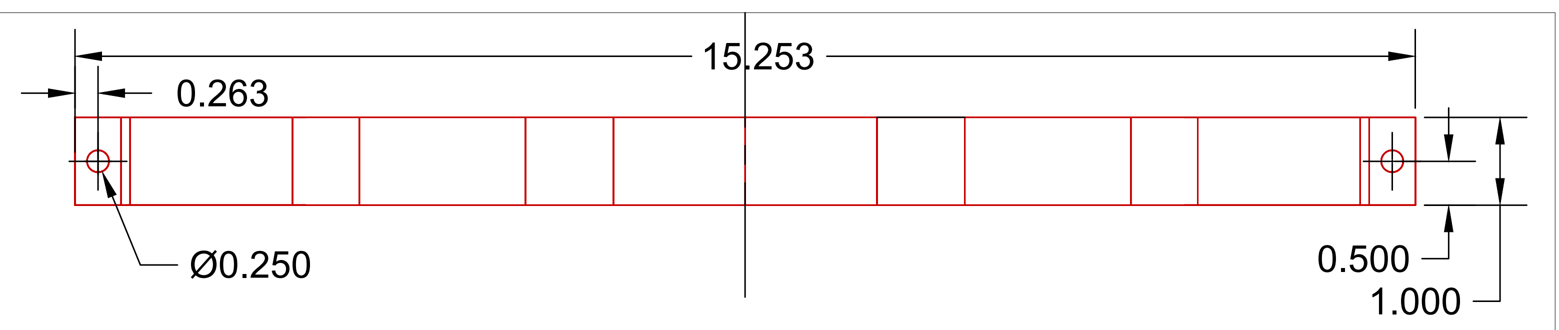

Surface Pivot Box Bottom Plate (1x)

$\frac{1}{2}$" AL-5086

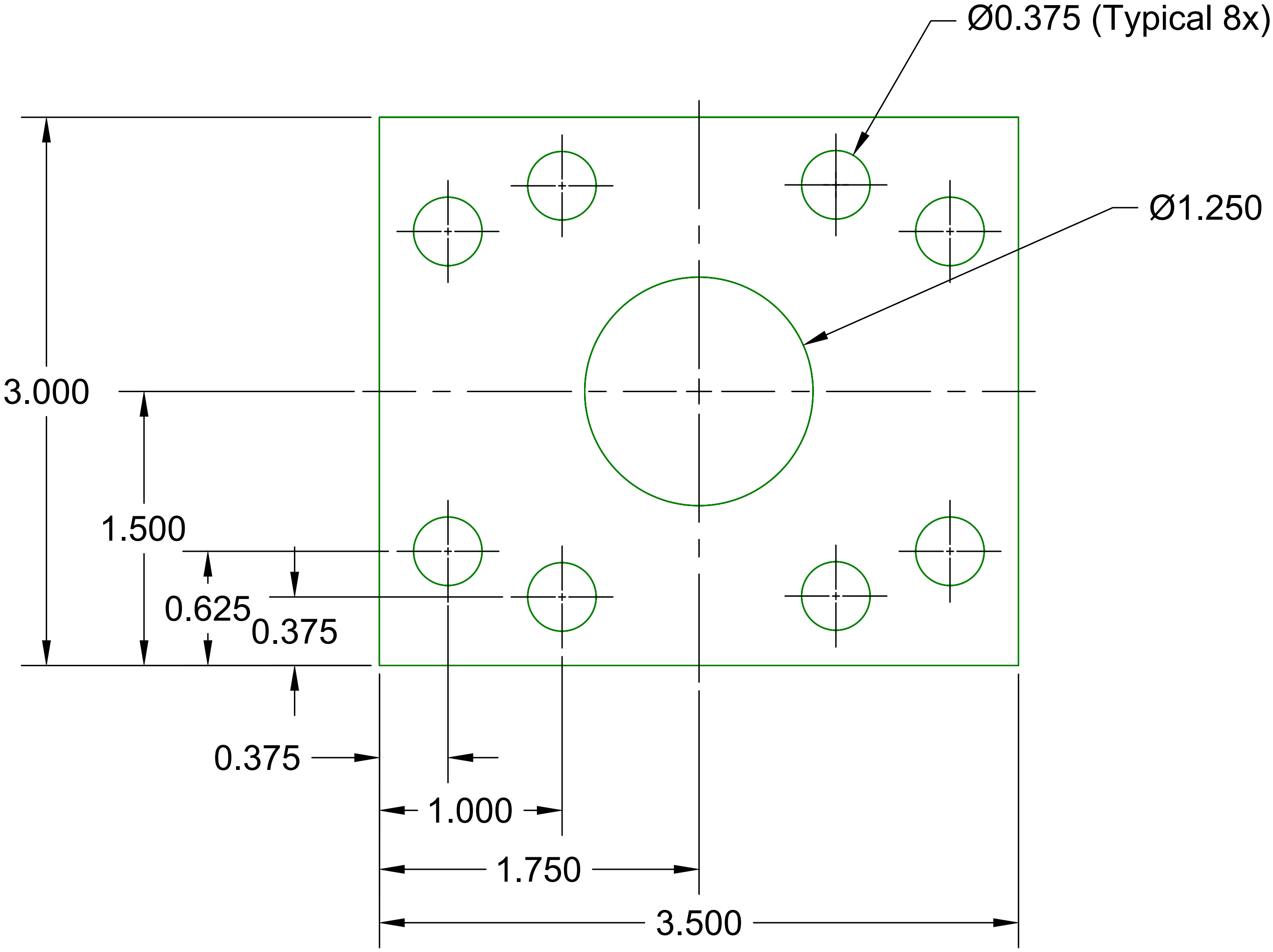

Surface Pivot Box Vertical Plates (2x)

$\frac{1}{2}$" AL-5086

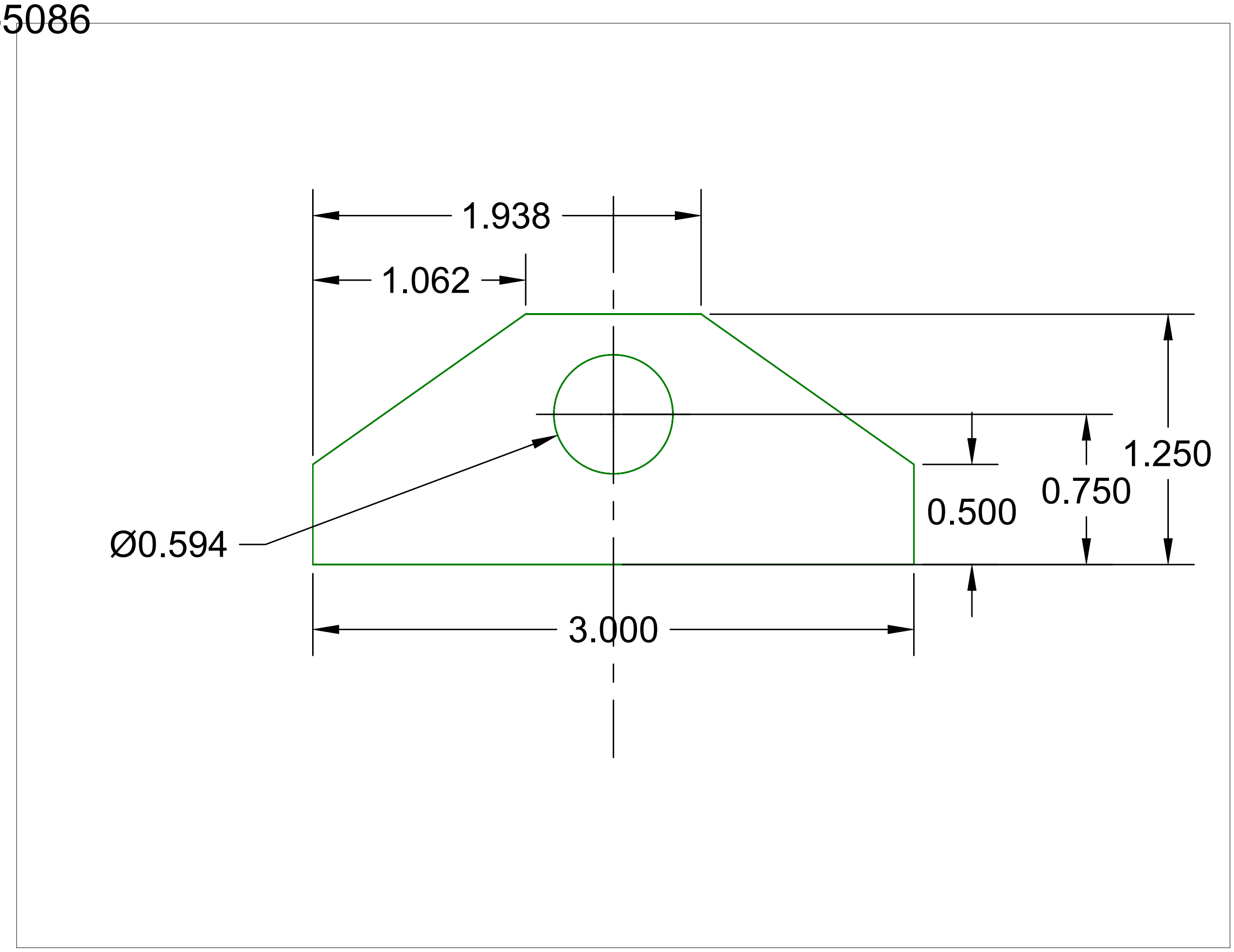

Transverse Mounting Plate - 1

$\frac{1}{2}$" AL-5086 (1x)

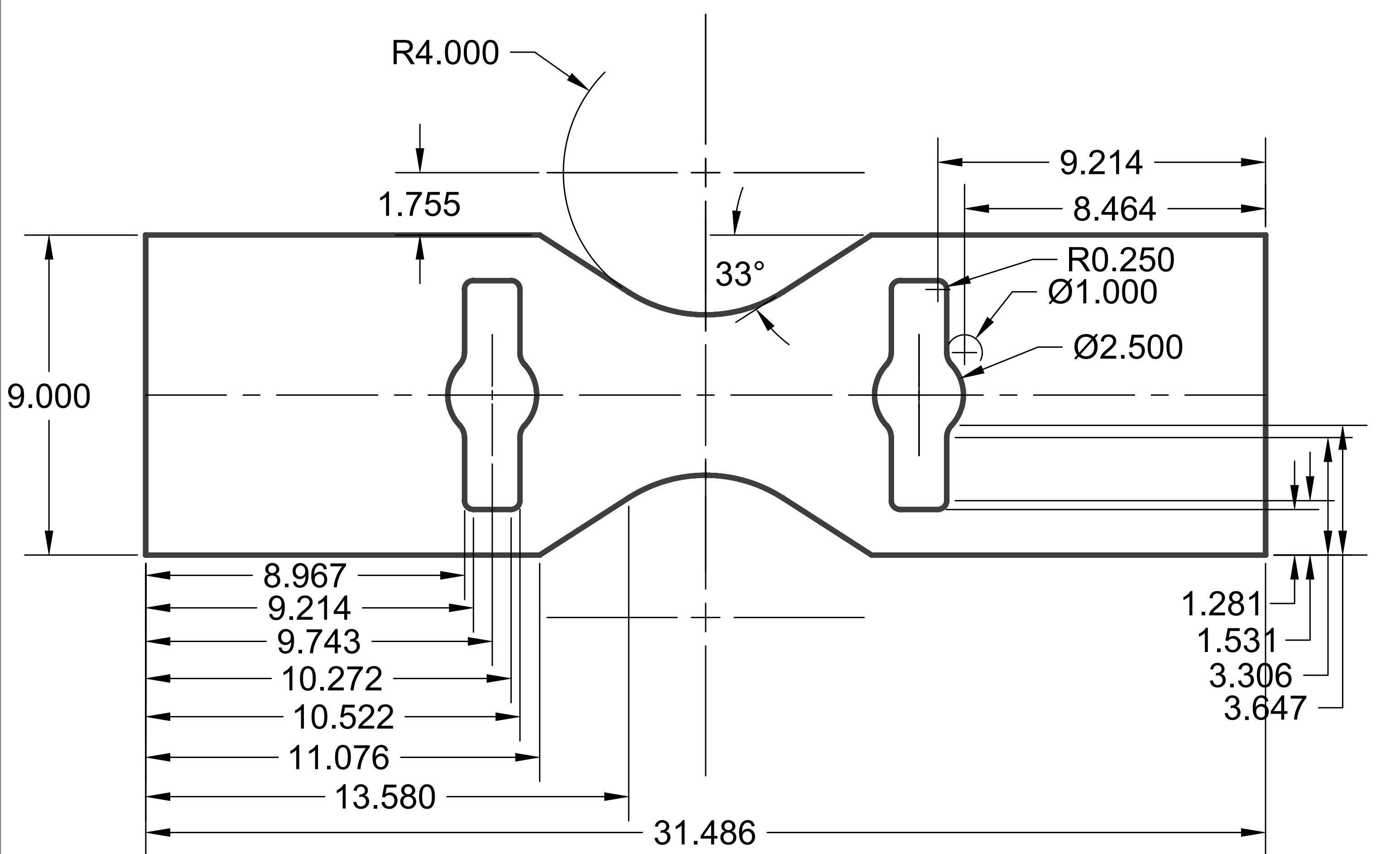

Transverse Mounting Plate - 2

1x ½" AL-5086

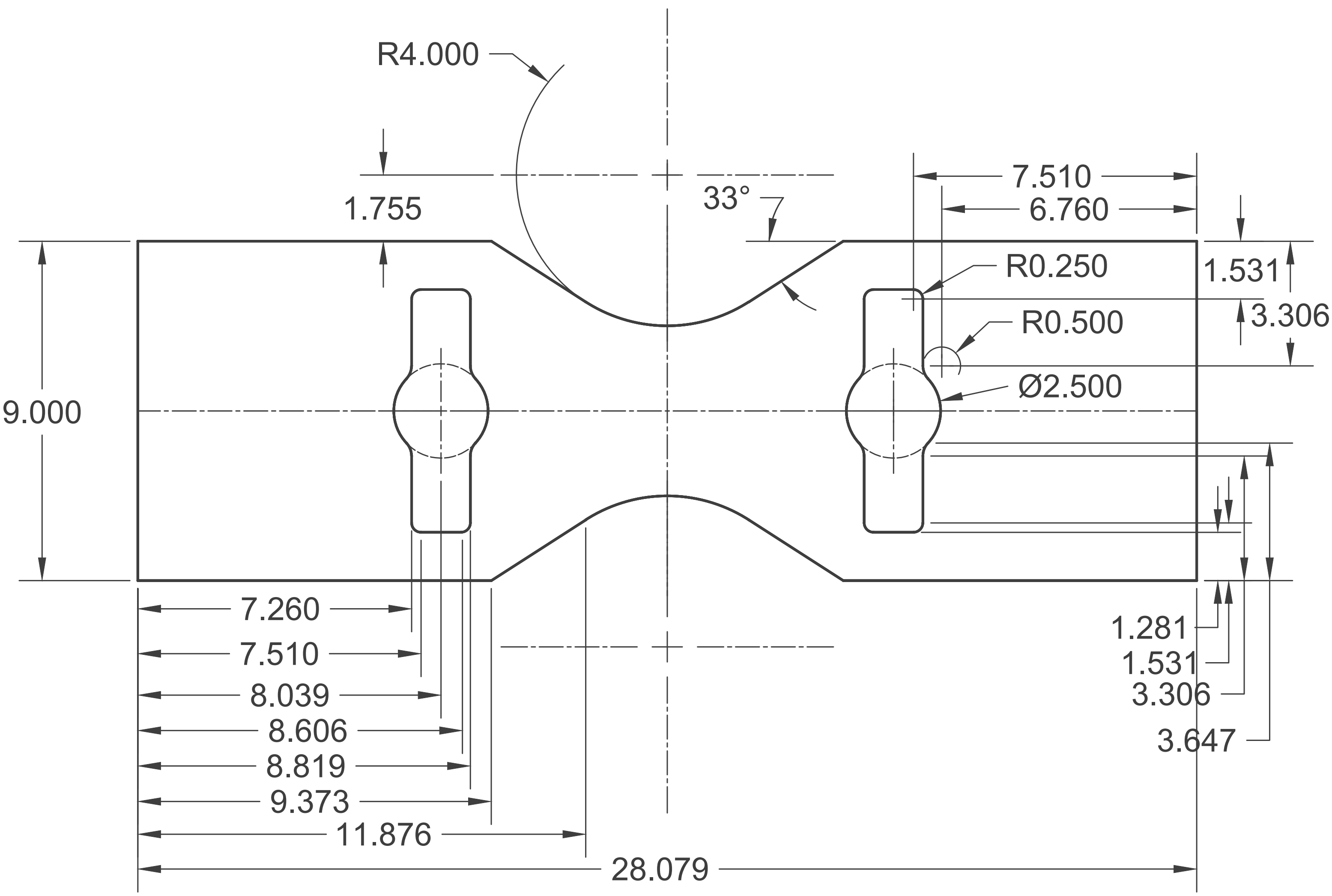

U-Groove Wheel Mount (24x)

$\frac{1}{2}$" AL-5086

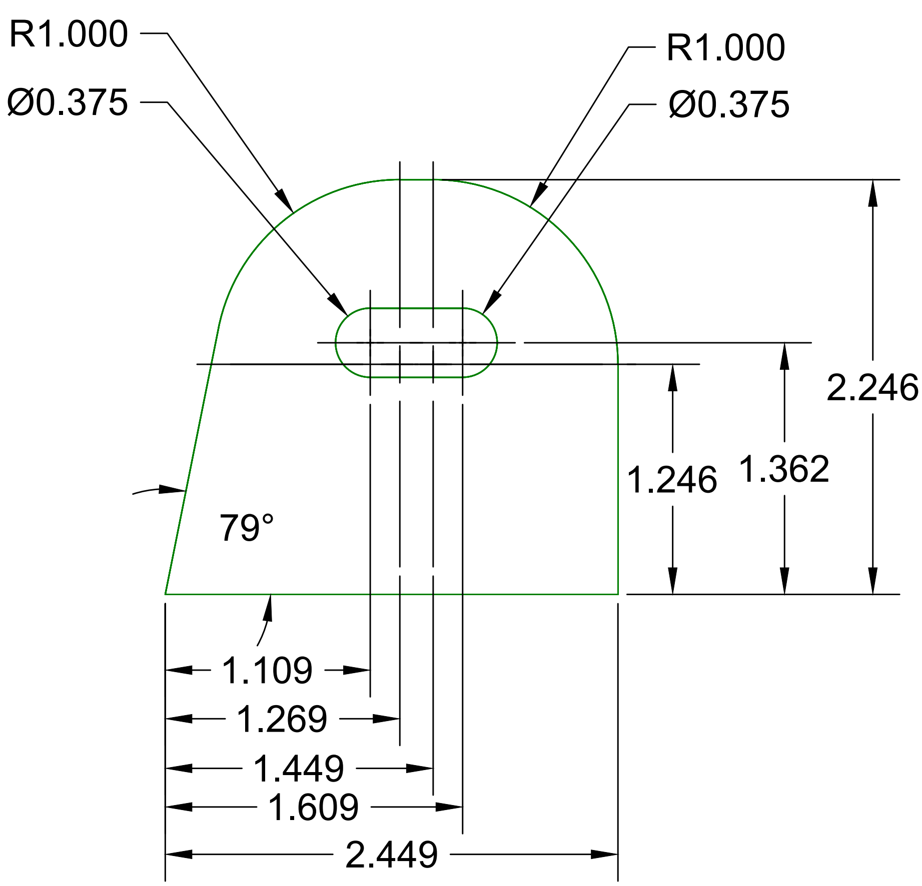

Clevis Joint Side Plate

$\frac{3}{4}$" AL-5086 (4x)

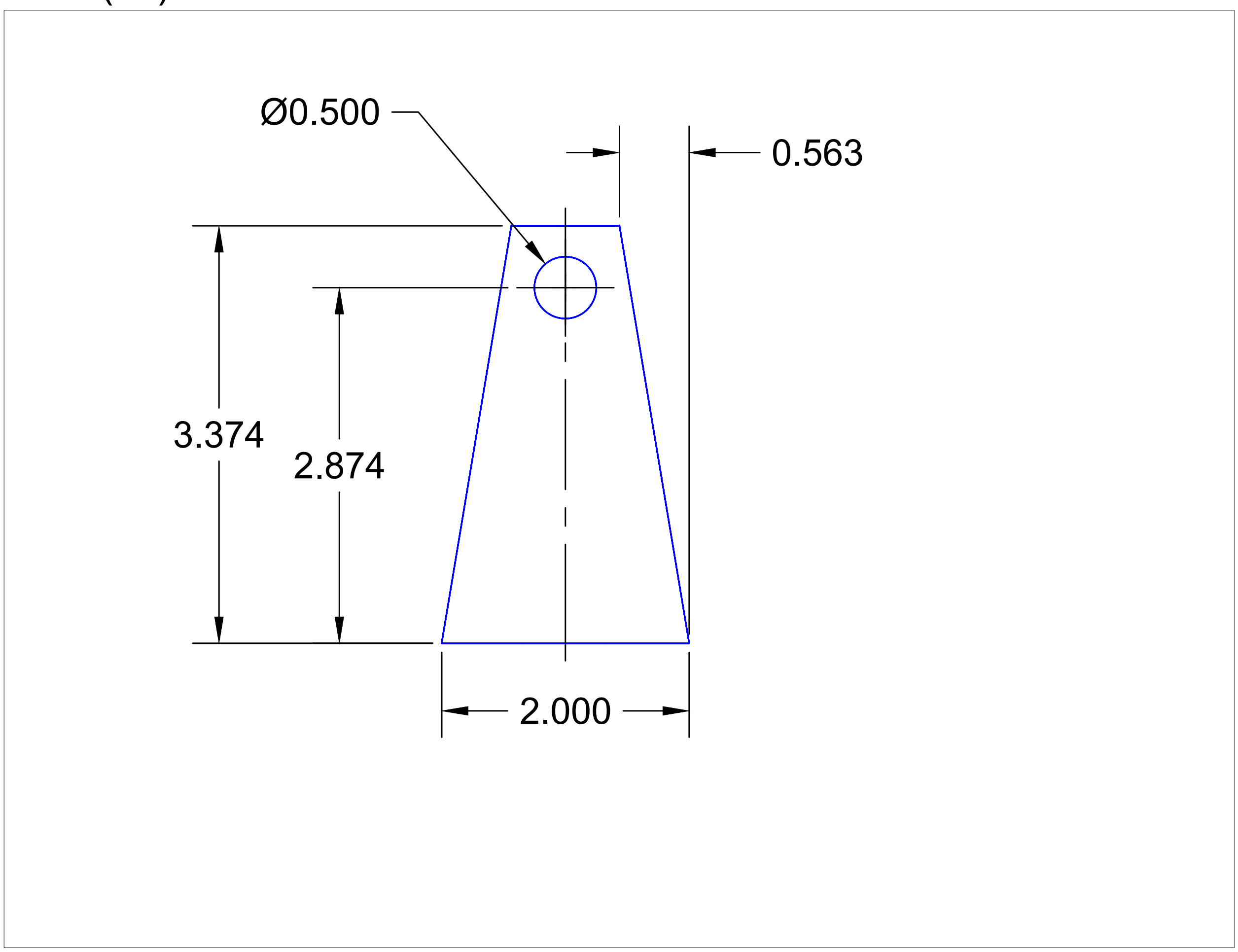

Appendix D

Categorization Code

```
% Individual Impact Similarity Code
% Author: Mark Shepheard
% Date: 12/01/2020
% Desciption: The purpose of this code is to determine what
event an
% unknown slamming event is most similar to
% TASKS:
% - Develop Training Set of Known Types
% - Implement Zeng Method based on SVD Projections to "Slam
Space"


%% Clearing
clear all;
close all;
format compact;
clc;

tic % Used to time the run (tic starts timer, toc ends timer)
%% Setting Up
figIter = 1; % Iterator for Figures
g = 9.81; % Graviational Acceleration (m/s^2)

%Min Acceleration Peak Heights (g)
minBowPeakHeight = 7/g;

% ONLY LOOKING FOR BOW PEAKS
% minMidPeakHeight = 3/g;
% minLCGPeakHeight = 0/g;

%CHANGE THIS
sp=0;   % individual events are lined up so their peak is at
this time for accelerometer

%DONT CHANGE
xlim1=2;    % longer range for plots
xlim2=5;

%CHANGE a little(ranges 0.3)
xlim3=1.75;  % shorter range for plots
xlim4=2.05;

%% Importing Data
cd .. % If file is moved adjust the file path (Goes up one level
to access data)

% This is the normal run number NOT the data Run #
```

```
runnumbers = 25; %[25:28, 42:48, 61:66]; % run numbers to
determine the similarity between
% runnumbers = [28, 29]; % run numbers to determine the
similarity between
% Creating File Paths for Runs
for iter = 1:length(runnumbers)
    DAQ1name(iter)=
convertCharsToStrings(strcat('DAQ1_dataData',num2str(runnumbers(
iter)-1),'.mat'));
    DAQ2name(iter)=
convertCharsToStrings(strcat('DAQ2_dataDAQ2_run',num2str(runnumb
ers(iter)-1),'.mat'));
end

% Loading Data (Structures are used to keep naming simple)
DAQ1 = cell(length((runnumbers)), 1);
DAQ2 = cell(length((runnumbers)), 1);
for iter = 1:length(runnumbers)
    DAQ1{iter} = load(DAQ1name(iter));
    DAQ2{iter} = load(DAQ2name(iter));
end

clc; % Clearing Output from Loading Data
load('InfernoColors');

% Setting Model Length (ft) Based on Run Numbers NOT ACTUALLY
USED ANYWHERE
for iter = 1:length(runnumbers)
    if runnumbers(iter)<78
        modellength(iter) = 8;
    else
        modellength(iter) = 4;
    end
end

%% Syncing DAQ1 & DAQ2
% Finding the trigger index and shifting time to be zero at
trigger
for iter = 1:length(runnumbers)
    [idxTrig1,~]=find(DAQ1{iter}.dataEng1(:,2)>1); % Finding
Index of the Trigger
    timeshift1=DAQ1{iter}.time1(idxTrig1(1),1); % Extracting
Time of trigger

    [idxTrig2,~]=find(DAQ1{iter}.dataEng1(:,2)>1);
    timeshift2=DAQ2{iter}.time2(idxTrig2(1),1);

    % Shifting time for each DAQ
```

```
    time1sync(iter,:) = DAQ1{iter}.time1-timeshift1;
    time2sync(iter, :) = DAQ2{iter}.time2; % TIME NOT SHIFTED IN
INDIVIDUAL IMPACTS CODE WORKS NOT SURE WHY
end

%% Plot Check
% CHANGING FROM g's TO m/s^2 => DECIDED TO KEEP EVERYHING IN g's
% for iter = 1:length(runnumbers)
%     DAQ1(iter).dataEng1(:,6) =
DAQ1(iter).dataEng1(:,6)*9.806;  % unit from $[m/s^2]$ to
[m/s^2](BOW)
%     DAQ1(iter).dataEng1(:,7) =
DAQ1(iter).dataEng1(:,7)*9.806;  % unit from $[m/s^2]$ to
[m/s^2](MID)
%     DAQ2(iter).dataEng2(:,4) =
DAQ2(iter).dataEng2(:,4)*9.806;  % unit from $[m/s^2]$ to
[m/s^2](LCG)
% end

% Plotting Unfiltered Acceleration Data
figure (figIter)
figIter = figIter + 1;

for iter = 1:length(runnumbers)
    subplot(length(runnumbers), 1, iter)
    hold on
    plot(time1sync(iter, :),
DAQ1{iter}.dataEng1(:,6),'color',colors(1,:),'linewidth',1.5) %
Bow

plot(time1sync(iter, :),DAQ1{iter}.dataEng1(:,7),'color',colors(
5,:),'linewidth',1.5) % Mid

plot(time2sync(iter, :),DAQ2{iter}.dataEng2(:,4) ,'color',colors
(7,:),'linewidth',1.5) % LCG A1z
    plot(time1sync(iter, :),DAQ1{iter}.dataEng1(:,4),'--
b','linewidth',1.5) % Pitch
    xlabel('$t$~[s]','interpreter','latex')
    %ylabel('Acceleration [m/s$^2$]','interpreter','latex')
    ylabel('Acceleration [g]');
    title(['Acceleration-from synced Data,
Run=',num2str(runnumbers(iter))])
    legend('Bow', 'Mid', 'LCG', 'Pitch',
'orientation','horizontal','Location','south')
    plotcode
    xlim([xlim1 xlim2])
    hold off
end
```

```
%% Spectral Analysis
% DAQ 1 Analysis
Fs1 = 1/(DAQ1{1}.time1(2)-DAQ1{1}.time1(1)); % Finding Sampling
Frequency of DAQ1

magBow = fft(DAQ1{iter}.dataEng1(:,6));
magMid = fft(DAQ1{iter}.dataEng1(:,7));
magPitch = fft(DAQ1{iter}.dataEng1(:,4));
n = length(DAQ1{iter}.dataEng1(:,6));          % number of
samples
f = (0:n-1)*(Fs1/n);     % frequency range
powerBow = abs(magBow).^2/n;    % power of the DFT
powerMid = abs(magMid).^2/n;
powerPitch = abs(magPitch).^2/n;

% figure(figIter)
% figIter = figIter + 1;
% plot(f,powerBow)
% xlim([0, 50])
% xlabel('Frequency')
% ylabel('Power')
% title('Bow Acceleration Spectral Analysis')
%
% figure(figIter)
% figIter = figIter + 1;
% plot(f,powerMid)
% xlim([0, 50])
% xlabel('Frequency')
% ylabel('Power')
% title('Mid Acceleration Spectral Analysis')

% figure(figIter)
% figIter = figIter + 1;
% plot(f,powerPitch)
% xlim([0, 50])
% xlabel('Frequency')
% ylabel('Power')
% title('Pitch Spectral Analysis')

% DAQ 2 Analysis
Fs2 = 1/(DAQ2{1}.time2(2)-DAQ2{1}.time2(1)); % Finding Sampling
Frequency of DAQ2

magLCG = fft(DAQ2{iter}.dataEng2(:,4));
n = length(DAQ2{iter}.dataEng2(:,4));          % number of
samples
f = (0:n-1)*(Fs2/n);     % frequency range
```

```
powerLCG = abs(magLCG).^2/n;     % power of the DFT

% figure(figIter)
% figIter = figIter + 1;
% plot(f,powerLCG)
% xlim([0, 50])
% xlabel('Frequency')
% ylabel('Power')
% title('LCG Acceleration Spectral Analysis')

%% Filtering
% Cut off frequency nd number of poles
cutoff1 = 80; % Cut off frequency for DAQ1
cutoff2 = 80; % Cut off frequency for DAQ2
% cutoff1 = 10; % Cut off frequency for DAQ1
% cutoff2 = 10; % Cut off frequency for DAQ2
poles = 2;

for iter = 1:length(runnumbers)
    Fs1 = 1/(DAQ1{iter}.time1(2)-DAQ1{iter}.time1(1)); % Finding
Sampling Frequency
    [B1, A1] = butter(poles,cutoff1/Fs1,'low'); % Creating Low
Pass Filter
    % Using Low Pass Filter to create filtered data
    BowAcc(iter, :) = filter(B1,A1,DAQ1{iter}.dataEng1(:,6));
    MidAcc(iter, :) = filter(B1,A1,DAQ1{iter}.dataEng1(:,7));
    Pitch(iter, :) = filter(B1, A1, DAQ1{iter}.dataEng1(:,4));
    Heave(iter, :) = filter(B1, A1, DAQ1{iter}.dataEng1(:, 3));

    Fs2 = 1/(DAQ2{iter}.time2(2)-DAQ2{iter}.time2(1));
    [B2, A2] = butter(poles,cutoff2/Fs2,'low');
    SurgeAcc(iter, :) = filter(B2,A2,DAQ2{iter}.dataEng2(:,2));
    SwayAcc(iter, :) = filter(B2,A2,DAQ2{iter}.dataEng2(:,3));
    LCGAcc(iter, :) = filter(B2,A2,DAQ2{iter}.dataEng2(:,4));


end


%% Calculating Angular Velocity & Acceleration

AngVel = zeros(size(Pitch));
AngAcc = AngVel;

for iter = 1:length(runnumbers)
    AngVel(iter, 2:end) = (Pitch(iter, 2:end) - Pitch(iter,
1:end-1))./(time1sync(iter, 2:end) - time1sync(iter, 1:end-1));
    AngVel(iter, 1) = AngVel(iter, 2);
```

```
    AngAcc(iter, 2:end) = (AngVel(iter, 2:end) - AngVel(iter, 
1:end-1))./(time1sync(iter, 2:end) - time1sync(iter, 1:end-1));
    AngAcc(iter, 1) = AngAcc(iter, 2);
%     AngAcc(iter, :) = AngAcc(iter, :)*pi/180; % Convert to 
(rad/s^2)

    figure
    grid on
    hold on
    plot(time1sync(iter, :), BowAcc(iter, :))
    plot(time1sync(iter, :), Pitch(iter, :))
    plot(time1sync(iter, :), AngVel(iter, :))
    plot(time1sync(iter, :), AngAcc(iter, :))
    xlim([xlim1 xlim2])
    legend('BowAcc', 'Pitch', 'AngVel', 'AngAcc')

end

%% Plotting Filtered Data
figure (figIter)
figIter = figIter + 1;

for iter = 1:length(runnumbers)
    subplot(length(runnumbers), 1, iter)
    hold on
    plot(time1sync(iter, :), 
BowAcc(iter, :),'color',colors(1,:),'linewidth',1.5) % Bow
    plot(time1sync(iter, :), 
MidAcc(iter, :),'color',colors(5,:),'linewidth',1.5) % Mid
    plot(time2sync(iter, :), 
LCGAcc(iter, :),'color',colors(7,:),'linewidth',1.5) % LCG A1z

    xlabel('$t$~[s]','interpreter','latex')
    %ylabel('Acceleration [m/s$^2$]','interpreter','latex')
    ylabel('Acceleration [g]');
    title(['Acceleration-from synced Data, 
Run=',num2str(runnumbers(iter))])
    legend('Bow', 'Mid', 
'LCG','orientation','horizontal','Location','south')
    plotcode
    xlim([xlim1 xlim2])
    hold off
end

% Plotting Triaxial Acceleration
figure(figIter)
figIter = figIter + 1;
for iter = 1:length(runnumbers)
```

```
    subplot(length(runnumbers),1,iter)
    hold on
    plot(time2sync(iter, :),
SurgeAcc(iter, :),'color',colors(1,:),'linewidth',1.5) % Surge
Acceleration
    plot(time2sync(iter, :),
SwayAcc(iter, :),'color',colors(5,:),'linewidth',1.5) % Sway
Acceleration
    plot(time2sync(iter, :),
LCGAcc(iter, :),'color',colors(7,:),'linewidth',1.5) % Heave
Acceleration
    grid on
    box on
    xlabel('Time [s]')
    ylabel('Acceleration [g]')
    title(['Triaxial Acc, Run #', num2str(runnumbers(iter))])
    legend('Surge Acc','Sway Acc','Heave Acc')
    set(gca,'fontsize',10)
    xlim([xlim1 xlim2])
end

%% Spliting Up Individual Slamming Events

for iter = 1:length(runnumbers)
    [a, idx1for1Temp] = min(abs(time1sync(iter, :)-xlim1)); %
finding the bound of time1 (DAQ1) in longer range
    [a, idx2for1Temp] = min(abs(time1sync(iter, :)-xlim2));
    idx1for1(iter) = idx1for1Temp;
    idx2for1(iter) = idx2for1Temp;

    [a, idx3for1Temp] = min(abs(time1sync(iter, :)-xlim3)); %
finding the bound of time1 (DAQ1) in shorter range
    [a, idx4for1Temp] = min(abs(time1sync(iter, :)-xlim4));
    idx3for1(iter) = idx3for1Temp;
    idx4for1(iter) = idx4for1Temp;


    [a, idx1for2Temp] = min(abs(time2sync(iter, :)-xlim1)); %
finding the index of time2 (DAQ2) in longer range
    [a, idx2for2Temp] = min(abs(time2sync(iter, :)-xlim2));
    idx1for2(iter) = idx1for2Temp;
    idx2for2(iter) = idx2for2Temp;

    interval(iter) = idx4for1(iter)-idx3for1(iter);     % No of
samples in shorter range
end

%%%CHANGE THESE
```

```
interval2 = 1350;                    % shorter and final no of 
samples in shorter range
interval3 = 5400;                    % total no of samples in 
shorter range for DAQ 2 (LCG Acc and pressures)
numSampBef2 = 2400;                         % No of samples before 
the max of the event in DAQ 2
numSampAft2 = interval3-numSampBef2;             % No of samples 
after the max of the event in DAQ 2


%Initializing cell array to hold data of different lengths
idxPeaksBow = cell(length(runnumbers), 1);
idxPeaksMid = cell(length(runnumbers), 1);
idxPeaksLCG = cell(length(runnumbers), 1);

% finding indices of the max of accelerations. These points are 
later used to
% extraxt each individual slam (with the help of intervals)
for iter = 1:length(runnumbers)
  % LATER ADD AUTO RANGING OF PEAK HEIGHTS
 [~,idxPeaksBow{iter}] = findpeaks(BowAcc(iter,
idx1for1(iter):idx2for1(iter)),'minpeakheight',minBowPeakHeight,
'minpeakdistance',0.2*DAQ1{iter}.SampleRate1);

 % Defining Events by the peak in Bow Acceleration
 % [~,idxPeaksMid{iter}] = findpeaks(MidAcc(iter,
idx1for1:idx2for1),'minpeakheight',minMidPeakHeight,'minpeakdist
ance',0.2*DAQ1(iter).SampleRate1);
 % [~,idxPeaksLCG{iter}] = findpeaks(LCGAcc(iter,
idx1for2:idx2for2),'minpeakheight',minLCGPeakHeight,'minpeakdist
ance',0.2*DAQ2(iter).SampleRate2);
end

% in all the following loops:
% the first line is the data for the individual events
% the second line is to find the maximum of that individual 
event
% the third line is to choose the limited no of the individuall 
event
% (based on the interval2. 650+700=1350 which is interval2. It 
means we
% choose 650 samples before and 700 samples after the max 
point).

%STRUCTURE OF EVENTS VAR (events{run, index}(time, data, 
event#), where run
%index is the index of the run in runnumbers, data is the col of 
sensor
```

```
%BowAcc, MidAcc, LCGAcc, SurgeAcc, Pitch, and event# is the
index of the
%event in the run
events = cell(length(runnumbers), 1); % Cell Array to hold event
data for  each run

% Each run is composed of a 3D array holding data for each event
for iter = 1:length(runnumbers)
    events{iter} = zeros(interval3, 9,
length(idxPeaksBow{iter})); %Creating number of events in run
end

totalNumEvents = 0;
%STILL NEED TO FIX for iter = 1:length(runnumbers)
for iter = 1:length(runnumbers)
    for i = 1:length(idxPeaksBow{iter})
        bbb = BowAcc(iter, idx1for1(iter) +
idxPeaksBow{iter}(i)-
interval/2:idx1for1(iter)+idxPeaksBow{iter}(i) +interval/2-1);
        [maxx, idxmax1] = max(bbb);
        if idxmax1 > 651
            % BowAccAll(:,i)=bbb(idxmax1-650:idxmax1+700-1);
            events{iter}(1:interval2, 1, i) = BowAcc(iter,
idx1for1(iter) + idxPeaksBow{iter}(i) -
interval2/2:idx1for1(iter) + idxPeaksBow{iter}(i) + interval2/2-
1); % Bow Acceleration
            events{iter}(1:interval2, 2, i) = MidAcc(iter,
idx1for1(iter) + idxPeaksBow{iter}(i) -
interval2/2:idx1for1(iter) + idxPeaksBow{iter}(i) + interval2/2-
1); % Mid Acceleration
            events{iter}(1:interval3, 3, i) = LCGAcc(iter,
idx1for2(iter) + 4*idxPeaksBow{iter}(i) -
interval3/2:idx1for2(iter) + 4*idxPeaksBow{iter}(i) +
interval3/2-1); % LCG Acceleration
            events{iter}(1:interval3, 4, i) = SurgeAcc(iter,
idx1for2(iter) + 4*idxPeaksBow{iter}(i) -
interval3/2:idx1for2(iter) + 4*idxPeaksBow{iter}(i) +
interval3/2-1); % Surge Acceleration
            events{iter}(1:interval2, 5, i) = Pitch(iter,
idx1for1(iter) + idxPeaksBow{iter}(i) -
interval2/2:idx1for1(iter) + idxPeaksBow{iter}(i) + interval2/2-
1); % Pitch Motion

            events{iter}(1:interval2, 6, i) = AngVel(iter,
idx1for1(iter) + idxPeaksBow{iter}(i) -
interval2/2:idx1for1(iter) + idxPeaksBow{iter}(i) + interval2/2-
1); % Angular Velocity
```

```
            events{iter}(1:interval2, 7, i) = AngAcc(iter,
idx1for1(iter) + idxPeaksBow{iter}(i) -
interval2/2:idx1for1(iter) + idxPeaksBow{iter}(i) + interval2/2-
1); % Angluar Acceleration

            events{iter}(1:interval2, 8, i) = Heave(iter,
idx1for1(iter) + idxPeaksBow{iter}(i) -
interval2/2:idx1for1(iter) + idxPeaksBow{iter}(i) + interval2/2-
1); % Heave (in)
            events{iter}(1:interval2, 9, i) =
DAQ1{iter}.dataEng1(idx1for1(iter) + idxPeaksBow{iter}(i) -
interval2/2:idx1for1(iter) + idxPeaksBow{iter}(i) + interval2/2-
1,1); % Carriage Velocity (
            totalNumEvents = totalNumEvents + 1;
        end
    end
end

% UNEEDED CODE
%   for k=1:length(idxPeaksMid)
%       ccc=MidAcc(idx1for1+idxPeaksMid(k)-
interval/2:idx1for1+idxPeaksMid(k)+interval/2-1);
%      [maxx idxmax2]=max(ccc)
%      if idxmax2 > 651 && idxmax2 < 749
%         MidAccAll(:,k)=ccc(idxmax2-650:idxmax2+700-1);
%      end
%   end
%
%   for j=1:length(idxPeaksLCG)-1
%     ddd=LCGAcc(idx1for2+idxPeaksLCG(j)-
interval*4/2:idx1for2+idxPeaksLCG(j)+interval*4/2-1);
%      [maxx idxmax3] = max(ddd)
%      if idxmax3 > aaaa+1
%         LCGAccAll(:,j)=ddd(idxmax3-aaaa:idxmax3+bbbb-1);
%      end
%  end

% Finding the time for the individual impact events.
% In fact, this is the time for only one event. The others are
lined up at this point

timeBowAccAll = (sp-
650*1/DAQ1{iter}.SampleRate1)+(1:interval2)*1/DAQ1{iter}.SampleR
ate1;
timeLCGAccAll =(sp-
numSampBef2*1/DAQ2{iter}.SampleRate2)+(1:interval3)*1/DAQ2{iter}
.SampleRate2;
```

```
%% Marking Peaks
% Marking the peaks on each run for convience
figure (figIter)
figIter = figIter + 1;

for iter = 1:length(runnumbers)
    subplot(length(runnumbers), 1, iter)
    hold on
    plot(time1sync(iter, :),
BowAcc(iter, :),'color',colors(1,:),'linewidth',1.5) % Bow
    plot(time1sync(iter, :),
MidAcc(iter, :),'color',colors(5,:),'linewidth',1.5) % Mid
    plot(time2sync(iter, :),
LCGAcc(iter, :),'color',colors(7,:),'linewidth',1.5) % LCG A1z
    yyaxis right
    plot(time1sync(iter, :), Pitch(iter, :), 'b--', 'linewidth',
1.5) % Pitch Motion

    for i = 1:length(idxPeaksBow{iter})
        plot([time1sync(iter, idxPeaksBow{iter}(i) +
idx1for1(iter)), time1sync(iter, idxPeaksBow{iter}(i) +
idx1for1(iter))], [-2, 6], 'b--')
    end

    xlabel('$t$~[s]','interpreter','latex')
    %ylabel('Acceleration [m/s$^2$]','interpreter','latex')
    yyaxis left
    ylabel('Acceleration [g]');
    yyaxis right
    ylabel('Pitch [deg]')
    title(['Acceleration-from synced Data,
Run=',num2str(runnumbers(iter))])
    legend('Bow', 'Mid', 'LCG',
'Pitch','orientation','horizontal','Location','north')
    plotcode
    xlim([xlim1 xlim2])
    hold off
end


% save('EventSimilarity_v5')

% % %% Starting Zeng's Method
% % Creating Starting Matrix of Known Slamming Types
% % Events in Type 1
% T1 = [1, 4;
%     2, 2];
% M = numel(events{T1(1, 1)}(:, :, T1(1, 2))); % # of Elements
```

```
%
% % Forming Type Event Matrix (T{type#}(data, event #))
% for iter = 1:length(T1(:, 1))
%     T{1}(:,iter) = reshape(events{T1(iter, 1)}(:, :, T1(iter,
2)), M, 1);
% end
% F = mean(T{1}, 2); % 1st Slamming Type average event
% % Events in Type 2
%
% T2 = [1, 2;
%     6, 3];
% for iter = 1:length(T2(:, 1))
%     T{2}(:,iter) = reshape(events{T2(iter, 1)}(:, :, T2(iter,
2)), M, 1);
% end
% F = [F, mean(T{2}, 2)];  % 2nd Slamming Type Average Event
%
%
% N = length(F(1, :)); % # of known faces
% fbar = mean(F, 2); % Average Typical Slamming Event
% A = F - fbar;
% [U, S, V] = svd(A); % Generating SVD of A
% r = length(A(1, :)); % Assuming A is of full rank (Desired #
of Singular Values)
% e1 = 1000; % Error Margin to be a slamming event (1st Guess)
% e0 = 100 % Error Margin to be a Specific Slamming Event (1st
Guess)
%
%
% cd m % Going back to previous folder
% % TestEvent1 = events{T1(2, 1)}(:, :, T1(2, 2));
% % TE2 = [8, 1];
% % TestEvent2 = events{TE2(1)}(:, :, TE2(2));
% % TE3 = [17, 8];
% % TestEvent3 = events{TE3(1)}(:, :, TE3(2));
% % [ef, d, indx, T, A, U, S, V, N, fbar] =
svdRecognition0(TestEvent1, r, N, T, A, U, S, V, fbar, e0, e1);
% % [ef, d, indx, T, A, U, S, V, N, fbar] =
svdRecognition0(TestEvent2, r, N, T, A, U, S, V, fbar, e0, e1);
%
% for iter1 = 1:length(runnumbers)
%     for i = 1:length(idxPeaksBow{iter1})
%         if (iter1 == T1(1, 1) && i == T1(1, 2)) || (iter1 ==
T1(2, 1) && i == T1(2, 2)) || (iter1 == T2(1, 1) && i == T2(1,
2)) || (iter1 == T2(2, 1) && i == T2(2, 2))
%             disp('Event is already in Set')
%         else
```

```
%              TestEvent = events{iter1}(:, i);
%              [ef, dmin, indx, T, F, A, U, S, V, N, fbar] =
svdRecognition0(TestEvent, r, N, T, F, A, U, S, V, fbar, e0,
e1);
%              r = length(A(1, :)); % Assuming A is of full rank
(Desired # of Singular Values)
%              [dmin, indx]
%          end
%      end
% end
%
% %% Finding FaceCoords
% Ur = U(:, 1:r);
% for iter = 1:length(T)
%     for i = 1:length(T{iter}(1, :))
%         ftemp = T{iter}(:, i); % Face of Interest
%         f0 = double(ftemp) - fbar; % Making Normalized Image
%         x{iter}(:, i) = Ur'*f0; % Coordinates of Face
%     end
% end
%
% % Plotting Coordinates
% figure
% hold on
% legendType = []; % Initializing Legend Vector
% for iter = 1:length(x)
%     plot((x{iter})', '.')
%     legendTypes = [legendType, ['Type #' num2str(iter)]];
% end
% grid on
% legend(legendTypes)
% title('Type Scatter Plot')
%
% %% Plotting Results
% % Plot Average Event and Individual Acceleration STDEV
% dim = size(events{T1(1, 1)}(:, :, T1(1, 2)));
% for iter = 1:length(T)
%     avgEvent = reshape(F(:, iter), dim); % Average Event
%     STDEV{iter} =
reshape(std(T{iter}./max(T{iter}(1:interval2, :)), 0, 2),
dim); % Standard Deviation Across normalized Events in Type
%
%     figure (figIter)
%     figIter = figIter + 1;
%
%     subplot(3, 1, 1)
%     grid on
```

```
%     hold on
%     plot(timeBowAccAll,
T{iter}(1:interval2, :)./max(T{iter}(1:interval2, :)), 'r--',
'linewidth', 1.5); % Plotting Average Bow Acceleration Event of
Type
%     plot(timeBowAccAll, T{iter}(dim(1) + 1:dim(1) +
interval2, :)./max(T{iter}(1:interval2, :)), 'b--', 'linewidth',
1.5)
%     plot(timeLCGAccAll, T{iter}(2*dim(1) +
1:3*dim, :)./max(T{iter}(1:interval2, :)), 'g--', 'linewidth',
1.5)
%
%     title({'Average Acceleration',['Type #', num2str(iter)]})
%     xlabel('Time (s)')
%     ylabel('Acc/Peak Bow Acc')
%     legend({'Bow Acc', 'Mid Acc', 'LCG Acc'}, 'Location',
'northwest');
%
%     subplot(3, 1, 2)
%     grid on
%     hold on
%     plot(timeBowAccAll, avgEvent(1:interval2,
1)/max(avgEvent(:, 1)), 'r-', 'linewidth', 1.5); % Plotting
Average Bow Acceleration Event of Type
%     plot(timeBowAccAll, avgEvent(1:interval2,
2)/max(avgEvent(:, 1)), 'b-', 'linewidth', 1.5)
%     plot(timeLCGAccAll, avgEvent(:, 3)/max(avgEvent(:, 1)),
'g-', 'linewidth', 1.5)
%
%     title({'Normalized Average Acceleration',['Type #',
num2str(iter)]})
%     xlabel('Time (s)')
%     ylabel('Acc/Peak Bow Acc')
%     legend({'Bow Acc', 'Mid Acc', 'LCG Acc'}, 'Location',
'northwest');
%
%     subplot(3, 1, 3)
%     grid on
%     hold on
%     plot(timeBowAccAll, STDEV{iter}(1:interval2, 1), 'r-',
'linewidth', 1.5); % Plotting Average Bow Acceleration Event of
Type
%     plot(timeBowAccAll, STDEV{iter}(1:interval2, 2), 'b-',
'linewidth', 1.5)
%     plot(timeLCGAccAll, STDEV{iter}(:, 3), 'g-', 'linewidth',
1.5)
%
```

```
%     title({'Standard Deviation',['Type #', num2str(iter)]})
%     xlabel('Time (s)')
%     ylabel('STDEV')
%     legend({'Bow Acc', 'Mid Acc', 'LCG Acc'}, 'Location',
'northwest');
%
%
%
% % Plot Average Event and Individual Acceleration STDEV
%
%     avgEventDim = reshape(F(:, iter), dim); % Average Event
%     STDEVdim{iter} = reshape(std(T{iter}, 0, 2), dim); %
Standard Deviation Across normalized Events in Type
%
%     figure (figIter)
%     figIter = figIter + 1;
%
%     subplot(3, 1, 1)
%     grid on
%     hold on
%     plot(timeBowAccAll, T{iter}(1:interval2, :), 'r--',
'linewidth', 1.5); % Plotting Average Bow Acceleration Event of
Type
%     plot(timeBowAccAll, T{iter}(dim(1) + 1:dim(1) +
interval2, :), 'b--', 'linewidth', 1.5)
%     plot(timeLCGAccAll, T{iter}(2*dim(1) + 1:3*dim, :), 'g--',
'linewidth', 1.5)
%
%     title({'Average Acceleration',['Type #', num2str(iter)]})
%     xlabel('Time (s)')
%     ylabel('Vertical Acceleration (g)')
%     legend({'Bow Acc', 'Mid Acc', 'LCG Acc'}, 'Location',
'northwest');
%
%     subplot(3, 1, 2)
%     grid on
%     hold on
%     plot(timeBowAccAll, avgEventDim(1:interval2, 1), 'r-',
'linewidth', 1.5); % Plotting Average Bow Acceleration Event of
Type
%     plot(timeBowAccAll, avgEventDim(1:interval2, 2), 'b-',
'linewidth', 1.5)
%     plot(timeLCGAccAll, avgEventDim(:, 3), 'g-', 'linewidth',
1.5)
%
%     title({'Average Acceleration',['Type #', num2str(iter)]})
%     xlabel('Time (s)')
```

```
%     ylabel('Vertical Acceleration (g)')
%     legend({'Bow Acc', 'Mid Acc', 'LCG Acc'}, 'Location',
'northwest');
%
%     subplot(3, 1, 3)
%     grid on
%     hold on
%     plot(timeBowAccAll, STDEVdim{iter}(1:interval2, 1), 'r-',
'linewidth', 1.5); % Plotting Average Bow Acceleration Event of
Type
%     plot(timeBowAccAll, STDEVdim{iter}(1:interval2, 2), 'b-',
'linewidth', 1.5)
%     plot(timeLCGAccAll, STDEVdim{iter}(:, 3), 'g-',
'linewidth', 1.5)
%
%     title({'Standard Deviation',['Type #', num2str(iter)]})
%     xlabel('Time (s)')
%     ylabel('STDEV')
%     legend({'Bow Acc', 'Mid Acc', 'LCG Acc'}, 'Location',
'northwest');
%
% end

%% Saving Figures
% FolderName = "G:\.shortcut-targets-by-
id\0BwrZneK4SrCnblhhTUlaOW85WUE\Gilbert Research
Group\Individual Researchers Folder\Shepheard\Tow Tank
Plots\Facial Recognition Trials";   % Your destination folder
% FigList = findobj(allchild(0), 'flat', 'Type', 'figure');
% for iFig = 1:length(FigList)
%   FigHandle = FigList(iFig);
%   FigName   = num2str(get(FigHandle, 'Number'));
%   set(0, 'CurrentFigure', FigHandle);
%   savefig(fullfile(FolderName, [FigName '.fig']));
% end



%% Similarity

% CREATING BASE SPACE OF SLAMMING EVENTS
%



% % Identifiying which events are wanted to compare MANNUAL
% E1 = [1, 5]; % Event #1 [runnumber, event#]
% E2 = [2, 2]; % Event #2 [runnumber, event#]
%
```

```
% Computing entire SVD (Has been simplified)
% [U1, S1, V1] = svd(events{E1(1)}(:, :, E1(2)));
% [U2, S2, V2] = svd(events{E2(1)}(:, :, E2(2)));
%
% sig1 = zeros(max([length(diag(S1)), length(diag(S2))]), 1);
% sig2 = zeros(max([length(diag(S1)), length(diag(S2))]), 1);
% sig1(1:length(diag(sig1))) = diag(S1);
% sig2(1:length(diag(sig2))) = diag(S2);

% Creating cosPhi Cell Array
% tic
% cosPhi = cell(length(runnumbers));
% for iter1 = 1:length(runnumbers)
%     for iter2 = 1:length(runnumbers)
%         cosPhi{iter1, iter2} =
zeros(length(idxPeaksBow{iter1}), length(idxPeaksBow{iter2})); %
Empty Comparison Matrix
%     end
% end
% toc
% tic
% for iter1 = 1:length(runnumbers)
%     for i = 1:length(idxPeaksBow{iter1})
%         for iter2 = iter1:length(runnumbers)
%             if iter2 == iter1
%                 k1 = i + 1;
%             else
%                 k1 = 1;
%             end
%
%             for k = k1:length(idxPeaksBow{iter2})
%
%                 % Identifiying which events are wanted to
compare
%                 E1 = [iter1, i]; % Event #1 [runnumber,
event#]
%                 E2 = [iter2, k]; % Event #2 [runnumber,
event#]
%                 % Extracting Vector of singular values for
each event
%                 sig1 = svd(events{E1(1)}(:, :, E1(2)));
%                 sig2 = svd(events{E2(1)}(:, :, E2(2)));
%
%                 % Finding the cosine of the angle btw the
singular values
%                 cosPhi{iter2, iter1}(k, i) = dot(sig1,
sig2)/(norm(sig1)*norm(sig2));
```

```
%             end
%         end
%     end
% end
% toc

%% Identifiying which events are wanted to compare MANNUAL
% E1 = [2, 2]; % Event #1 [runnumber, event#]
% E2 = [1, 5]; % Event #2 [runnumber, event#]
% % Plotting an overlay of the data from each event
% figure (figIter)
% figIter = figIter + 1;
% hold on
% grid on
% %Bow Acceleration
% plot(timeBowAccAll, events{E1(1)}(1:interval2, 1,
E1(2))/max(events{E1(1)}(1:interval2, 1, E1(2))), 'r-',
'linewidth', 1.5)
% plot(timeBowAccAll, events{E2(1)}(1:interval2, 1,
E2(2))/max(events{E2(1)}(1:interval2, 1, E2(2))), 'r--',
'linewidth', 1.5)
% % title('Normalized Bow Accelration')
% % xlabel('Time (s)')
% % ylabel('Bow Acc/Peak Bow Acc')
%
% %Mid Acceleration
% plot(timeBowAccAll, events{E1(1)}(1:interval2, 2,
E1(2))/max(events{E1(1)}(1:interval2, 1, E1(2))), 'b-',
'linewidth', 1.5)
% plot(timeBowAccAll, events{E2(1)}(1:interval2, 2,
E2(2))/max(events{E2(1)}(1:interval2, 1, E2(2))), 'b--',
'linewidth', 1.5)
% % title('Normalized Mid Accelration')
% % xlabel('Time (s)')
% % ylabel('Mid Acc/Peak Bow Acc')
%
% %LCG Acceleration
% plot(timeLCGAccAll, events{E1(1)}(:, 3,
E1(2))/max(events{E1(1)}(1:interval2, 1, E1(2))), 'g-',
'linewidth', 1.5)
% plot(timeLCGAccAll, events{E2(1)}(:, 3,
E2(2))/max(events{E2(1)}(1:interval2, 1, E2(2))), 'g--',
'linewidth', 1.5)
% % title('Normalized LCG Accelration')
% % xlabel('Time (s)')
% % ylabel('LCG Acc/Peak Bow Acc')
%
```

```
% title({'Normalized Acceleration',['E1 = Run#',
num2str(runnumbers(E1(1))), ', Slam#', num2str(E1(2))], ['E2 =
Run#', num2str(runnumbers(E2(1))), ', Slam#', num2str(E2(2))]})
% xlabel('Time (s)')
% ylabel('Acc/Peak Bow Acc')
% legend({'Bow Acc (E1)', 'Bow Acc (E2)', 'Mid Acc (E1)', 'Mid
Acc (E2)', 'LCG Acc (E1)', 'LCG Acc (E2)'}, 'Location',
'northwest');
%
% tolTime = toc % Ending the timer

%% Comparison to Cosine Wave
% % Identifiying which events are wanted to compare MANNUAL
% E1 = [1, 2]; % Event #1 [runnumber, event#]
% % w = 2*pi/(timeBowAccAll(end)-timeBowAccAll(1));
% tstart = -0.025;
% tend = 0.075;
% preVec = -0.2*ones(1, int64((tstart - timeBowAccAll(1))*Fs1));
% postVec = -0.2*ones(1, int64((timeBowAccAll(end) -
tend)*Fs1));
% midVec = tstart:1/Fs1:tend;
% w = 2*pi/(tend - tstart); % Attempting to Match Peak
% delta = (tstart + tend)/2;% Phase Shift
% E2 = [preVec, 0.6*cos(w.*(midVec - delta)) + 0.4, postVec]'; %
Cosine Wave
% E11 = events{E1(1)}(1:interval2, 1, E1(2));
% % Computing entire SVD (Has been simplified)
% sig1 = svd(events{E1(1)}(1:interval2, 1, E1(2)));
% sig2 = svd(E2);
%
% cosPhi = dot(sig1, sig2)/(norm(sig1)*norm(sig2))
% cosPhi1 = dot(events{E1(1)}(1:interval2, 1, E1(2)),
E2)/(norm(events{E1(1)}(:, 1, E1(2)))*norm(E2))
%
% % Plotting an overlay of the data from each event
% figure (figIter)
% figIter = figIter + 1;
% hold on
% grid on
% %Bow Acceleration
% plot(timeBowAccAll, events{E1(1)}(1:interval2, 1,
E1(2))/max(events{E1(1)}(1:interval2, 1, E1(2))), 'r-',
'linewidth', 1.5)
% plot(timeBowAccAll, E2, 'r--', 'linewidth', 1.5)
%
```

```
% title({'Normalized Acceleration',['E1 = Run#',
num2str(runnumbers(E1(1))), ', Slam#', num2str(E1(2))], ['E2 =
Run# Cosine']})
% xlabel('Time (s)')
% ylabel('Acc/Peak Bow Acc')
% legend({'Bow Acc (E1)', 'Bow Acc (E2)', 'Mid Acc (E1)', 'Mid
Acc (E2)', 'LCG Acc (E1)', 'LCG Acc (E2)'}, 'Location',
'northwest');

toc % Ending the timer
```

```
%%
% Zengs Method Recognition v5
% Author: Mark Shepheard
% Date: 12/01/2020
% Description: The purpose of this code is to determine what
event an unknown slamming event is most similar to
% TASKS:
% - Develop Training Set of Known Types
% - Implement Zengs Method based on SVD Projections to "Slam
Space"

%%
clear all;
close all;
clc;


%%
cd ..
load('EventSimilarity_v5.mat')


%% Just Messing w/ Data
E = zeros(totalNumEvents, 17);
row = 0;
for iter = 1:length(runnumbers)
    for i =  1:length(idxPeaksBow{iter})
        row = row + 1;
        % Matrix of Events and Properties
        % run#/slam#/Bow Peak Amplitude/Mid Peak Amplitude/Mid
Peak Time/LCG Peak
        % Amplitude/LCG Peak Time/Bow Acceleration @ t=-
0.05s/Pitch @
        % t=0/Impact Time/Bow Acceleration @ Impact/Trim @
Impact/Angular
        % Vel @ Impact/Angular Acc @ Impact/Heave Velocity @
Impact/Total
        % Velocity @ Impact/Velocity Angle @ Impact


        % NEW CODE
        % Finds changes in slope
        TF = ischange(squeeze(squeeze(events{iter}(1:650, 1,
i))), 'linear', 'MaxNumChanges', 1);
        TF = [TF; zeros(interval2-650, 1)];

        [~, idxImpact] = max(TF); % Gives aproximate index of
vessel impact
```

```
        % Plotting Impact Location for Verification
%         if iter == 1 && i == 1
            figure
            grid on
            hold on
            plot(timeBowAccAll, [5*TF(1:interval2),-
5*TF(1:interval2)])
            plot(timeBowAccAll,
squeeze(squeeze(events{iter}(1:interval2, 1, i))))
            plot(timeBowAccAll,
squeeze(squeeze(events{iter}(1:interval2, 5, i))))
%             plot(timeBowAccAll,
squeeze(squeeze(events{iter}(1:interval2, 6, i))))
%             plot(timeBowAccAll,
squeeze(squeeze(events{iter}(1:interval2, 7, i))))

            legend('Impact', 'BowAcc', 'Trim')%, 'AngVel',
'AngAcc
%         end

        % Heave Velocity (ft/s)
        if idxImpact > 1
            Vh = (events{iter}(idxImpact + 1, 8, i) -
events{iter}(idxImpact - 1, 8, i))...
                /(time1sync(iter, idxImpact + 1) -
time1sync(iter, idxImpact - 1))/12;
        else
            Vh = (events{iter}(idxImpact + 1, 8, i) -
events{iter}(idxImpact, 8, i))...
                /(time1sync(iter, idxImpact + 1) -
time1sync(iter, idxImpact))/12;
        end

        % Total Velocity & Angle
        Vtotal = sqrt(Vh^2 + (events{iter}(idxImpact, 9, i))^2);
        Vang = atand(Vh/(events{iter}(idxImpact, 9, i)));
        %%%%%%%

        [maxMov, idxMax] = max(squeeze(events{iter}(:, :, i)));
        E(row, 1:17) = [iter, i, maxMov(1), maxMov(2),
timeBowAccAll(idxMax(2)),...
            maxMov(3), timeLCGAccAll(idxMax(3)),
squeeze(squeeze(events{iter}(400, 1, i))),...
            squeeze(squeeze(events{iter}(650, 5, i))),
timeBowAccAll(idxImpact), ...
            squeeze(squeeze(squeeze(events{iter}(idxImpact, 1,
i)))), ...
```

```
            squeeze(squeeze(squeeze(events{iter}(idxImpact, 5,
i)))),...
            squeeze(squeeze(squeeze(events{iter}(idxImpact, 6,
i)))),...
            squeeze(squeeze(squeeze(events{iter}(idxImpact, 7,
i)))),...
            Vh, Vtotal, Vang];
    end
end

% Time at t=-0.05s vs Max Bow Peak
figure
scatter(E(:, 8), E(:, 3), '.')
grid on
xlabel('Bow Acc (g) @ t=-0.05s')
ylabel('Peak Bow Acc (g)')

% Time at t=-0.05s vs Max Bow Peak
figure
scatter(E(:, 8), E(:, 3), '.')
grid on
xlabel('Bow Acc (g) @ t=-0.05s')
ylabel('Peak Bow Acc (g)')

% Heave Velocity vs Max Bow Peak
figure
scatter(E(:, 15), E(:, 3), '.')
grid on
xlabel('Heave Velocity @ Impact (ft/s)')
ylabel('Peak Bow Acc (g)')

% Total Velocity vs Max Bow Peak
figure
scatter(E(:, 16), E(:, 3), '.')
grid on
xlabel('Total Velocity @ Impact (ft/s)')
ylabel('Peak Bow Acc (g)')

% Velocity Ang vs Max Bow Peak
figure
scatter(E(:, 17), E(:, 3), '.')
grid on
xlabel('Velocity Angle @ Impact (deg)')
ylabel('Peak Bow Acc (g)')

% Time @ Impact vs Max Bow Peak
figure
scatter(E(:, 11), E(:, 3), '.')
```

```
grid on
xlabel('Bow Acc (g) @ Impact')
ylabel('Peak Bow Acc (g)')

figure
scatter(E(:, 9), E(:, 3), '.')
grid on
xlabel('Pitch @ t=0')
ylabel('Peak Bow Acc (g)')

figure
scatter(E(:, 12), E(:, 3), '.')
grid on
xlabel('Pitch @ Impact')
ylabel('Peak Bow Acc (g)')

figure
scatter(E(:, 13), E(:, 3), '.')
grid on
xlabel('AngVel @ Impact')
ylabel('Peak Bow Acc (g)')

figure
scatter(E(:, 14), E(:, 3), '.')
grid on
xlabel('AngAcc @ Impact')
ylabel('Peak Bow Acc (g)')


%% Starting Zeng's Method
% Creating Starting Matrix of Known Slamming Types
% Events in Type 1
T1 = [1, 4;
    2, 2];
M = numel(events{T1(1, 1)}(:, :, T1(1, 2))); % # of Elements
E(4, end)  = 1; % Setting Event to Type #1
E(9, end) = 1;
% Forming Type Event Matrix (T{type#}(data, event #))
for iter = 1:length(T1(:, 1))
    T{1}(:,iter) = reshape(events{T1(iter, 1)}(:, :, T1(iter,
2)), M, 1);
end
F = mean(T{1}, 2); % 1st Slamming Type average event
% Events in Type 2

T2 = [1, 2;
    6, 3];
E(2, end)  = 2; % Setting Event to Type #2
```

```
E(35, end) = 2;

for iter = 1:length(T2(:, 1))
    T{2}(:,iter) = reshape(events{T2(iter, 1)}(:, :, T2(iter,
2)), M, 1);
end
F = [F, mean(T{2}, 2)];  % 2nd Slamming Type Average Event


N = length(F(1, :)); % # of known faces
fbar = mean(F, 2); % Average Typical Slamming Event
A = F - fbar;
[U, S, V] = svd(A); % Generating SVD of A
r = length(A(1, :)); % Assuming A is of full rank (Desired # of
Singular Values)

e1 = 1000; % Error Margin to be a slamming event (1st Guess)
e0 = 12225; % Error Margin to be a Specific Slamming Event (1st
Guess)


cd m % Going back to previous folder
% TestEvent1 = events{T1(2, 1)}(:, :, T1(2, 2));
% TE2 = [8, 1];
% TestEvent2 = events{TE2(1)}(:, :, TE2(2));
% TE3 = [17, 8];
% TestEvent3 = events{TE3(1)}(:, :, TE3(2));
% [ef, d, indx, T, A, U, S, V, N, fbar] =
svdRecognition0(TestEvent1, r, N, T, A, U, S, V, fbar, e0, e1);
% [ef, d, indx, T, A, U, S, V, N, fbar] =
svdRecognition0(TestEvent2, r, N, T, A, U, S, V, fbar, e0, e1);

tol = 0; % Tolerance for Convergence

% Convergence Loop
for iter = 1:10
    fprintf('Starting Iteration #%1.0f\n\n\n', iter)
    row  = 0;
    for iter1 = 1:length(runnumbers)
        for i = 1:length(idxPeaksBow{iter1})
            row = row + 1;
            if iter == 1 && ((iter1 == T1(1, 1) && i == T1(1,
2)) || (iter1 == T1(2, 1) && i == T1(2, 2)) || (iter1 == T2(1,
1) && i == T2(1, 2)) || (iter1 == T2(2, 1) && i == T2(2, 2)))
                disp('Event is already in Set')
            else
                TestEvent = events{iter1}(:, :, i);
```

```
                [ef, dmin, indx, T, F, A, U, S, V, N, fbar] =
svdRecognition0(TestEvent, r, N, T, F, A, U, S, V, fbar, e0, e1,
iter);
                r = length(A(1, :)); % Assuming A is of full
rank (Desired # of Singular Values)
                E(row, end) = indx; % Setting Event Type #
                [dmin, indx]
            end
        end
    end
    Ahist{iter} = A;

    if iter > 1 && norm(Ahist{iter} - Ahist{iter -
1})/norm(Ahist{iter}) < tol % Convergence Criteria for
Clustering Algorithm
        break
    end



    EventTable{i} = array2table(E(:, 3:end), 'VariableNames',
{'BowPeakAcc', 'MidPeakAcc', ...
        'MidPeakTime', 'LCGPeakAcc', 'LCGPeakTime', 't05',
'Pitch', 'ImpactTime',...
        'BowImpact', 'TrimImpact', 'AngVel', 'AngAcc', 'Type'});
    % SVD recognition Scatters
    % Time at t=-0.05s vs Max Bow Peak
%     figure
%     gscatter(EventTable{i}.t05, EventTable{i}.BowPeakAcc,
EventTable{i}.Type)
%     grid on
%     xlabel('Bow Acc (g) @ t=-0.05s')
%     ylabel('Peak Bow Acc (g)')
%
%     figure
%     gscatter(EventTable{i}.LCGPeakAcc,
EventTable{i}.BowPeakAcc, EventTable{i}.Type)
%     grid on
%     xlabel('Peak LCG Acc (g)')
%     ylabel('Peak Bow Acc (g)')
%
%
%     figure
%     gscatter(EventTable{i}.BowPeakAcc,
EventTable{i}.LCGPeakTime, EventTable{i}.Type)
%     grid on
%     xlabel('Peak Bow Acc (g)')
```

```
%     ylabel('Time LCG Peak (s)')
%
%     figure
%     gscatter(EventTable{i}.Pitch, EventTable{i}.BowPeakAcc,
EventTable{i}.Type)
%     grid on
%     xlabel('Pitch (deg)')
%     ylabel('Peak Bow Acc (g)')
%
%     figure
%     gscatter(EventTable{i}.TrimImpact,
EventTable{i}.BowPeakAcc, EventTable{i}.Type)
%     grid on
%     xlabel('Trim @ Impact (deg)')
%     ylabel('Peak Bow Acc (g)')
%
%     figure
%     gscatter(EventTable{i}.AngVel, EventTable{i}.BowPeakAcc,
EventTable{i}.Type)
%     grid on
%     xlabel('AngVel @ Impact (deg/s)')
%     ylabel('Peak Bow Acc (g)')
%
%     figure
%     gscatter(EventTable{i}.AngAcc, EventTable{i}.BowPeakAcc,
EventTable{i}.Type)
%     grid on
%     xlabel('AngAcc @ Impact (deg/s^2)')
%     ylabel('Peak Bow Acc (g)')

    fprintf('\n\n\nEnding Iteration #%1.0f\n\n\n', iter)
end

 figure
    gscatter(EventTable{i}.t05, EventTable{i}.BowPeakAcc,
EventTable{i}.Type)
    grid on
    xlabel('Bow Acc (g) @ t=-0.05s')
    ylabel('Peak Bow Acc (g)')

    figure
    gscatter(EventTable{i}.LCGPeakAcc, EventTable{i}.BowPeakAcc,
EventTable{i}.Type)
    grid on
    xlabel('Peak LCG Acc (g)')
    ylabel('Peak Bow Acc (g)')
```

```
    figure
    gscatter(EventTable{i}.BowPeakAcc,
EventTable{i}.LCGPeakTime, EventTable{i}.Type)
    grid on
    xlabel('Peak Bow Acc (g)')
    ylabel('Time LCG Peak (s)')

    figure
    gscatter(EventTable{i}.Pitch, EventTable{i}.BowPeakAcc,
EventTable{i}.Type)
    grid on
    xlabel('Pitch (deg)')
    ylabel('Peak Bow Acc (g)')

    figure
    gscatter(EventTable{i}.TrimImpact, EventTable{i}.BowPeakAcc,
EventTable{i}.Type)
    grid on
    xlabel('Trim @ Impact (deg)')
    ylabel('Peak Bow Acc (g)')

    figure
    gscatter(EventTable{i}.AngVel, EventTable{i}.BowPeakAcc,
EventTable{i}.Type)
    grid on
    xlabel('AngVel @ Impact (deg/s)')
    ylabel('Peak Bow Acc (g)')

    figure
    gscatter(EventTable{i}.AngAcc, EventTable{i}.BowPeakAcc,
EventTable{i}.Type)
    grid on
    xlabel('AngAcc @ Impact (deg/s^2)')
    ylabel('Peak Bow Acc (g)')

    figure
    gscatter(EventTable{i}.BowImpact, EventTable{i}.BowPeakAcc,
EventTable{i}.Type)
    grid on
    xlabel('Bow Acc @ Impact (m/s^2)')
    ylabel('Peak Bow Acc (g)')

% knnmodel = fitcknn(EventTable{iter}, 'Type',
"NumNeighbors",3);

% %% Finding FaceCoords
% Ur = U(:, 1:r);
% for iter = 1:length(T)
```

```
%     for i = 1:length(T{iter}(1, :))
%         ftemp = T{iter}(:, i); % Face of Interest
%         f0 = double(ftemp);% - fbar; % Making Normalized Image
%         x{iter}(:, i) = Ur'*f0; % Coordinates of Face
%     end
% end
%
% % Plotting Coordinates
% figure
% hold on
% legendType = []; % Initializing Legend Vector
% for iter = 1:length(x)
%     plot((x{iter})', '.')
%     legendTypes = [legendType, ['Type #' num2str(iter)]];
% end
% grid on
% legend(legendTypes)
% title('Type Scatter Plot')
%

%% Plotting Results
% Plot Average Event and Individual Acceleration STDEV
dim = size(events{T1(1, 1)}(:, :, T1(1, 2)));
for iter = 1:length(T)
    avgEvent = reshape(F(:, iter), dim); % Average Event
    STDEV{iter} =
reshape(std(T{iter}./max(T{iter}(1:interval2, :)), 0, 2),
dim); % Standard Deviation Across normalized Events in Type

    figure

%     subplot(3, 1, 1)
    grid on
    hold on
    plot(timeBowAccAll,
T{iter}(1:interval2, :)./max(T{iter}(1:interval2, :)), 'r--',
'linewidth', 1.5); % Plotting Average Bow Acceleration Event of
Type
    plot(timeBowAccAll, T{iter}(dim(1) + 1:dim(1) +
interval2, :)./max(T{iter}(1:interval2, :)), 'b--', 'linewidth',
1.5)
    plot(timeLCGAccAll, T{iter}(2*dim(1) +
1:3*dim, :)./max(T{iter}(1:interval2, :)), 'g--', 'linewidth',
1.5)

    title({'Average Acceleration',['Type #', num2str(iter)]})
    xlabel('Time (s)')
    ylabel('Acc/Peak Bow Acc')
```

```
    %legend({'Bow Acc', 'Mid Acc', 'LCG Acc'}, 'Location',
'northwest');
%
%     subplot(3, 1, 2)
%     grid on
%     hold on
%     plot(timeBowAccAll, avgEvent(1:interval2,
1)/max(avgEvent(:, 1)), 'r-', 'linewidth', 1.5); % Plotting
Average Bow Acceleration Event of Type
%     plot(timeBowAccAll, avgEvent(1:interval2,
2)/max(avgEvent(:, 1)), 'b-', 'linewidth', 1.5)
%     plot(timeLCGAccAll, avgEvent(:, 3)/max(avgEvent(:, 1)),
'g-', 'linewidth', 1.5)
%
%     title({'Normalized Average Acceleration',['Type #',
num2str(iter)]})
%     xlabel('Time (s)')
%     ylabel('Acc/Peak Bow Acc')
%     legend({'Bow Acc', 'Mid Acc', 'LCG Acc'}, 'Location',
'northwest');
%
%     subplot(3, 1, 3)
%     grid on
%     hold on
%     plot(timeBowAccAll, STDEV{iter}(1:interval2, 1), 'r-',
'linewidth', 1.5); % Plotting Average Bow Acceleration Event of
Type
%     plot(timeBowAccAll, STDEV{iter}(1:interval2, 2), 'b-',
'linewidth', 1.5)
%     plot(timeLCGAccAll, STDEV{iter}(:, 3), 'g-', 'linewidth',
1.5)
%
%     title({'Standard Deviation',['Type #', num2str(iter)]})
%     xlabel('Time (s)')
%     ylabel('STDEV')
%     legend({'Bow Acc', 'Mid Acc', 'LCG Acc'}, 'Location',
'northwest');



% Plot Average Event and Individual Acceleration STDEV

    avgEventDim = reshape(F(:, iter), dim); % Average Event
    STDEVdim{iter} = reshape(std(T{iter}, 0, 2), dim); %
Standard Deviation Across normalized Events in Type

    figure
%     subplot(3, 1, 1)
```

```
    grid on
    hold on
    plot(timeBowAccAll, T{iter}(1:interval2, :), 'r--',
'linewidth', 1.5); % Plotting Average Bow Acceleration Event of
Type
    plot(timeBowAccAll, T{iter}(dim(1) + 1:dim(1) +
interval2, :), 'b--', 'linewidth', 1.5)
    plot(timeLCGAccAll, T{iter}(2*dim(1) + 1:3*dim, :), 'g--',
'linewidth', 1.5)
    ylim([-2, 9])
    title({'Composite Acceleration',['Type #', num2str(iter)]})
    xlabel('Time (s)')
    ylabel('Vertical Acceleration (g)')
    %legend({'Bow Acc', 'Mid Acc', 'LCG Acc'}, 'Location',
'northwest');
    grid on; box on
    set(gca,'fontsize',10)
    set(gcf,'PaperPosition',[0 0 4 3]);
    set(gcf,'PaperSize',[4 3]);


    figure
%     subplot(3, 1, 2)
    grid on
    hold on
    plot(timeBowAccAll, avgEventDim(1:interval2, 1), 'r-',
'linewidth', 1.5); % Plotting Average Bow Acceleration Event of
Type
    plot(timeBowAccAll, avgEventDim(1:interval2, 2), 'b-',
'linewidth', 1.5)
    plot(timeLCGAccAll, avgEventDim(:, 3), 'g-', 'linewidth',
1.5)
    ylim([-2, 8])
    title({'Average Acceleration',['Type #', num2str(iter)]})
    xlabel('Time (s)')
    ylabel('Vertical Acceleration (g)')
    legend({'Bow Acc', 'Mid Acc', 'LCG Acc'}, 'Location',
'northwest');
    grid on; box on
    set(gca,'fontsize',10)
    set(gcf,'PaperPosition',[0 0 4 3]);
    set(gcf,'PaperSize',[4 3]);


    figure
%     subplot(3, 1, 3)
    grid on
    hold on
```

```
    plot(timeBowAccAll, STDEVdim{iter}(1:interval2, 1), 'r-',
'linewidth', 1.5); % Plotting Average Bow Acceleration Event of
Type
    plot(timeBowAccAll, STDEVdim{iter}(1:interval2, 2), 'b-',
'linewidth', 1.5)
    plot(timeLCGAccAll, STDEVdim{iter}(:, 3), 'g-', 'linewidth',
1.5)
    ylim([0 2])
    title({'Standard Deviation',['Type #', num2str(iter)]})
    xlabel('Time (s)')
    ylabel('STDEV')
    legend({'Bow Acc', 'Mid Acc', 'LCG Acc'}, 'Location',
'northwest');
    grid on; box on
    set(gca,'fontsize',10)
    set(gcf,'PaperPosition',[0 0 4 3]);
    set(gcf,'PaperSize',[4 3]);

end

%% Saving Figures
% FolderName = "G:\Shared drives\Hydroelasticity Laboratory -
Gilbert Research Group\Personnel\Shepheard\Master's
Research\Experimental Matrix Development\Figures3";   % Your
destination folder
% FigList = findobj(allchild(0), 'flat', 'Type', 'figure');
% for iFig = 1:length(FigList)
%   FigHandle = FigList(iFig);
%   FigName   = num2str(get(FigHandle, 'Number'));
%   set(0, 'CurrentFigure', FigHandle);
%   savefig(fullfile(FolderName, [FigName '.fig']));
% end
```

```
%
% svdRecognition0
% Author: Mark Shepheard
% Date: 12/01/2020
% Description: Performs the Linear Algebra for Zengs Method

function [ef, dmin, indx, T, F, A, U, S, V, N, fbar] =
svdRecognition0(fnew, r, N, T, F, A, U, S, V, fbar, e0, e1,
rnum)
    % INPUTS:
    % fnew: New Image
    % r: # of sv chosen
    % T: Event Data for Slamming Types
    % A: Known Face Matrix - Average Face
    % N: # of known faces
    % U: Left Singular Vectors
    % S: Singular Value Matrix
    % V: Right Sigular Vectors
    % fbar: Average Face
    % e1: Error Margin to be a Face
    % e0: Error Margin for Specific Face
    % faceCoords: Coordinates of face in facespace

    % OUTPUTS:
    % ef: Error of Normalized Face to Face Space
    % d: Distance to all known faces
    % indx: Index of Type of Slamming Event
    % A: Updated Know Slamming Events
    % U, S, V: Updated Singular Value Decomposition
    % x: Coordinates of Face in Facespace

    Ur = U(:, 1:r);
    X = Ur'*A;
%     fnew = imread(newName);
%     fnew = imresize(fnew, [112, 92]);
    f = reshape(fnew, numel(fnew), 1); % Reshaping Image Matrix
to Vector
    f0 = double(f) - fbar; % Making Normalized Image
    x = Ur'*f0;
    fp = Ur*x;
    ef = norm(f0 - fp);

%     if ef < e1
        D = X - x*ones(1, N);
        d = sqrt(diag(D'*D));
        [dmin, indx] = min(d);
        if dmin < e0
            fprintf(['Event is Type #', num2str(indx), '\n']);
```

```
            T{indx} = [T{indx}, f]; % Updated Type Data
            F(:, indx) = mean(T{indx}, 2); % Updating Type
Average Event
            fbar = mean(F, 2); % Mean Event
            A = double(F) - fbar; % Updated A Matrix
            [U, S, V] = svd(A, 'econ');
        elseif rnum == 1 % If statement ensures that types can
only be added during the first run...
            fprintf('Unknown Event Type \n');
            % Adding New Face to Set of Known Faces
            T{N + 1} = f; % Creating New Event Type
            F = [F, T{N + 1}];
            fbar = mean(F, 2); % Mean Event
            A = double(F) - fbar; % Updated A Matrix
            [U, S, V] = svd(A, 'econ');
            indx = N + 1;
            N = N + 1;
        end
% %     else
% %         fprintf('The input image is not a Slamming
Event\n');
% %     end
end
```